

INVESTIGATION OF OBJECTIVE-DRIVEN SLICING IN  
MULTI-AXIS EXTRUSION BASED ADDITIVE  
MANUFACTURING PROCESSES

A thesis submitted for the degree of Doctor of Philosophy

by

Marko Chorbikj

Department of Design, Brunel University London

October, 2020

## Abstract

---

This Doctoral Research has been dedicated towards the advancement of multi-axis Material Extrusion (ME) technology where the manufacturing of parts involves the orthogonal deposition of material along freeform, 3-dimensional layers, conversely to conventional 3-axis Material Extrusion where the part is approximated through a plurality of only horizontal, planar layers. This transition from 2D to 3D space in which the layers span, enables for a vast increase in freedom in the spatial arrangement of layers that constitute a part, and consequently, its final properties. While in conventional ME the control a user has over the layer generation process is largely represented by the choice of part orientation and layer height, in multi-axis ME the shape of each and all layers themselves can also be controlled. However, with the increase in liberty of the process design, is there a direct necessity in understanding how to select a certain layer arrangement over another? How does one pick a specific slicing strategy if there is conceptually infinite possible solutions to manufacture the same part?

It is exactly this curiosity that represents the core of this Doctoral Research; it hypothesises that desired part characteristics can be treated as objectives in the slicing process so that they help define a suitable layer arrangement.

The design and planning of this research study have been defined following a detailed and systematic literature review with a wide research horizon of prior works that cover relevant multi-axis Additive Manufacturing (AM) topics not only in the family of Material Extrusion (ME), but also in a variety of other AM techniques dealing with metals, hybrid systems and novel, unconventional approaches. This resulted in the formulation of two research questions aimed at revealing the governing mechanism between the choice of a multi-axis slicing strategy and its effect on part's accuracy and functionality accordingly.

Case-study based research methodology was applied as a general, enveloping research approach. The obtained case-studies were then investigated combining qualitative and quantitative analysis ranging from observing part's build and layer formation to an in-depth examination of numerical measurements data of a variety of part's characteristics.

The lack of a suitable processing tool required to practically implement layer-based, multi-axis ME by elaborating multi-axis slicing, toolpath formation and guidance of the manufacturing process, has prompted that an initial phase of this research addresses the development of such processing tool and its associated algorithms. Such a conglomerate of digital processing steps

and a suitable manufacturing equipment were analysed in detail, developed, applied on a pilot study and ultimately established as a suitable framework for conducting the case-studies.

The key research consisted in two parallel branches dedicated on investigating potential answers to the two research questions. Each of them included a two-step analysis method where first an isolated study provided the basis for establishing a slicing strategy aimed at part's accuracy and functionality accordingly. In a second step, both of the established slicing strategies were applied on a fixed cross-comparative geometry, thus leaving the slicing strategy as the only independent variable in the studies. A total of eight case-studies were examined, with resulting evidence and data formulated in conclusions with respect to the research questions and hypothesis elaborated in this research.

## Attestation of Authorship

---

I hereby declare that the work presented in this dissertation is my own original work unless otherwise cited or referenced within the writing. The contents of the presented thesis have not been submitted, neither in full nor in part, to any other institution of higher learning for the purpose of obtaining another degree or diploma.

# Table of Contents

<b>Abstract</b> .....	<b>i</b>
<b>List of Figures</b> .....	<b>vi</b>
<b>List of Tables</b> .....	<b>x</b>
<b>List of Abbreviations</b> .....	<b>xi</b>
<b>List of Symbols</b> .....	<b>xii</b>
<b>1. Introduction</b> .....	<b>1</b>
1.1. Technology background .....	2
1.2. Shortcomings of Material Extrusion technologies .....	7
1.3. Curved Layer paradigm: a potential improvement vector .....	10
1.4. Aim and objectives of the research .....	11
1.5. Scope of the thesis .....	13
<b>2. Prior Knowledge and Research Plan</b> .....	<b>14</b>
2.1. Literature review .....	15
2.1.1. Method and execution .....	15
2.1.2. Analysis and discussion.....	21
2.2. Defining research plan.....	26
2.2.1. Hypothesis and research questions .....	26
2.2.2. Research methods .....	31
<b>3. Development of a Multi-axis ME Processing Tool and the Associated Algorithms</b> .....	<b>35</b>
3.1. Introduction.....	36
3.2. Defining specifications for the ME system .....	37
3.3. Slicing procedure.....	39
3.4. Toolpath development.....	44
3.5. Extrusion data management and instruction list .....	48
3.6. Overview of processing framework.....	51
3.7. Conclusions.....	53
<b>4. Prelude to Experiments</b> .....	<b>55</b>
4.1. Multi-axis manufacturing system and process parameters .....	56
4.2. Pilot test.....	58
4.3. Assumptions and considerations .....	61

<b>5. Non-planar Slicing Driven by Part Accuracy .....</b>	<b>65</b>
5.1. How to slice for improved accuracy.....	66
5.1.1. Introduction .....	66
5.1.2. Methodology .....	67
5.1.3. Single surface slicing.....	68
5.1.4. Multiple surface slicing through volume sub-division.....	72
5.1.5. Results and conclusion .....	74
5.2. Applying multiple surface slicing method through volume sub-division.....	82
5.3. Accuracy driven non-planar slicing: observations and conclusions .....	86
<b>6. Non-planar Slicing Driven by Functionality of Conductive Materials .....</b>	<b>89</b>
6.1. How to slice for improved conductivity .....	90
6.1.1. Introduction .....	90
6.1.2. Post-printing functional analysis .....	91
6.1.3. Post-printing physical characterisation .....	96
6.1.4. Results and conclusion .....	100
6.1.5. Postulates for expansion in 3D space .....	104
6.2. Applying single layer conductive tracks method .....	106
6.3. Comparing and combining function driven with accuracy driven slicing: results..	111
6.4. Function driven non-planar slicing: observations and conclusions .....	117
<b>7. Conclusions .....</b>	<b>119</b>
7.1. Summary, discussion and feedback to research questions .....	120
7.2. Contributions.....	126
7.2.1. Contributions to knowledge.....	126
7.2.2. Contributions to tools .....	129
7.3. Limitations and risks to validity.....	131
7.4. Research implications.....	133
<b>References.....</b>	<b>136</b>
<b>Appendix A: Supplementary manufacturing images.....</b>	<b>146</b>
<b>Appendix B: Complete data of resistivity measurements.....</b>	<b>154</b>

## List of Figures

<i>Figure 1.1 Basic conceptual process flow behind Additive Manufacturing technologies</i> .....	2
<i>Figure 1.2 Schematic diagram of material extrusion adopted from [7]. Key elements: 1-support structure, 2-build platform and elevator, 3-heated nozzle, 4-feedstock supply, 5-product</i> .....	4
<i>Figure 1.3 Typical process planning for AM, adopted from [8]. From left to right: digital geometry generation, tessellation, slicing and machine instructions</i> .....	5
<i>Figure 1.4 An illustration of the staircase effect in the case of manufacturing of a spherical feature with different level of approximation as a consequence of layer height. Adopted from [18]</i> .....	9
<i>Figure 1.5 The basic concept behind Curved Layer and non-planar ME in general: a) Planar, conventional, 3-axis slicing and b) CLFDM slicing</i> .....	10
<i>Figure 2.1 Graphical representation of query formation necessary for literature review</i> ...	18
<i>Figure 2.2 Graphical depiction of hypothesis through examples of different slicing strategies related to the same part geometry, potentially resulting in different post-printing characteristics of the part: b) top-down slicing, c) bottom-up slicing, d) waved based slicing, e) side slicing and f) combined slicing strategy</i> .....	28
<i>Figure 2.3 Overview of research methods schematics in the context of the entire research.</i>	33
<i>Figure 3.1 An example of slicing approach and layer formation in: a) Conventional, 3-axis slicing, and b) non-planar slicing</i> .....	39
<i>Figure 3.2 An exemplary NURBS surface represented by: a) Its geometric shape and control points, b) parametric domain depiction</i> .....	40
<i>Figure 3.3 Orthogonal (normal) uniform distance offset of a surface</i> .....	41
<i>Figure 3.4 Intersection between offset of slicing surface and part volume for layer identification (red)</i> .....	42
<i>Figure 3.5 Insufficient geometrical data when slicing with surfaces from CAD model: a) No intersection between orthogonal offset and part model, b) proposed solution by smooth surface extension (dark brown)</i> .....	43
<i>Figure 3.6 Example of freeform slicing on a uniform thickness part. Dark blue: slicing surface, light blue: obtained layers, transparent grey: part model a) Using surface from part model b) using surface not belonging to part's model</i> .....	43
<i>Figure 3.7 Flowchart of the implemented steps for generating both intra-layer infill and inter-layer toolpaths</i> .....	46
<i>Figure 3.8 Toolpath algorithm applied to a variety of freeform layers with different shape. Intra-layer infill toolpaths represented in red and blue in a)-d), while inter-layer safety movements shown in green in a)</i> .....	47
<i>Figure 3.9 Snippet of a 3-axis g code generated by CURA [31], post processed to fit manufacturing system</i> .....	49
<i>Figure 3.10 Procedure for point extraction from curves for linear interpolation: a) Sampling of source NURBS curve for linear segment poly-line b) Surface evaluation in</i>	

point $p_{(u,v)}$ and extraction of unit normal vector and its projections along X, Y and Z axis of coordinate system .....	49
Figure 3.11 Snippet of the 5axis g-code instruction list sent to manufacturing system.....	51
Figure 3.12 An overview of the processing framework and flow of information through it	52
Figure 3.13 Different phases of data processing: a) 3D part model, b) Layers, output of slicing phase, c) process planning simulation based on layers only, d) process planning simulation based on toolpaths with alternating orientation .....	53
Figure 4.1 Description of the manufacturing system: a) Kinematic schematics and b) photograph of the multi-axis manufacturing system used for the study .....	56
Figure 4.2 Conical shape design of extruder's nozzle: a) 3D model and b) a close-up photograph of the nozzle during manufacturing of one case study.....	57
Figure 4.3 Progressive steps through processing pipeline of the pilot case study: a) 3D model, b) Layers as outcome of slicing, c) Alternating toolpaths between red and blue orientation d) Simulation of extrudate (contours removed for clarity).....	59
Figure 4.4 Several views of the Pilot case study printed with multi-axis software tools, framework and manufacturing system.....	60
Figure 4.5 Examples of different manufacturing systems used in various prior art: a) Adopted from [58], b) Adopted from [99], c) Adopted from [75], d) Adopted from [52].....	62
Figure 5.1 Problem of accuracy with respect to the ideal geometrical shape in a case of a) planar and b) non-planar layers. Red arrows point presence (low accuracy) while green lack of staircase effect (improved accuracy).....	66
Figure 5.2 Part A geometry: a) Transparent model, b) the model with emphasised principle surfaces for different slicing: top (gold) surface propagated downwards or bottom (red) surface propagated upwards .....	69
Figure 5.3 Combined slicing using both top and bottom surface: a) top 3 layers and remaining volume b) remaining volume sliced with bottom surface (right) .....	72
Figure 5.4 Mapping of process parameters during deposition: a) and b): Model and length distance variations of layer height; c) and d): Nozzle axis (orange lines) and normal vectors of substrate (green arrows) for angle angular deviation analysis.....	77
Figure 5.5 Simulated and experimental samples displaying varying staircase effect features as a result of varying layer arrangement: a) and b): Case_Atop, c) and d): Case_Asan, e) and f): Case_Abot .....	79
Figure 5.6 Deviations measurements between real and ideal layer formation due to fall of material under gravity: a) Case_Atop, b) Case_Asan.....	80
Figure 5.7 Part B geometry: a) Transparent model, b) the model with emphasised principle surfaces for different slicing: top surface (gold), side surface (green) and bottom surface (red). Dimensional units – [mm] .....	82
Figure 5.8 Slicing sequence of two different layer arrangements: a), c) and e) Case_Btop and b), d) and f) Case_Bside.....	83
Figure 5.9 Concept for an ideal, theoretical layer spanning across entire part model for slicing strategy aimed at optimising accuracy.....	88



<i>Figure 6.1 Design of sample shape for experiment: a) A schematics in top view, b) From the top: a CAD model of single, double and triple slicing strategy of a sample with an equal total height</i> .....	92
<i>Figure 6.2 Images of the in-house 3D printer used to manufacture the samples: a) Front view of the 3D printer, b) A deposited sample of a conductive track</i> .....	93
<i>Figure 6.3 Images of deposited conductive tracks: a) Microscope image of 3 segments of 0.6mm conductive tracks with 3 different deposition strategies, b) Image of 5 samples used in the experiment</i> .....	95
<i>Figure 6.4 Resistivity measurements and equipment: a) Open Hirschmann safety probe prior to contact, b) Agilent device used to measure resistivity</i> .....	95
<i>Figure 6.5 An illustration of the sample holder design with 6 cross sections mounted and submerged in resin</i> .....	97
<i>Figure 6.6 Sample preparation for cross section analysis: a) An example of two random sections cut away from the mid-zone of a conductive track sample b) a polished sample revealing 6 cross sections for microscopy imaging</i> .....	98
<i>Figure 6.7 An example of image analysis process of one cross section of a conductive track sample with a total height of 0.7mm made by triple layer strategy: a) 32 bit grayscale image, b) extracted outline for surface area measurement</i> .....	99
<i>Figure 6.8 Increase in resistance between samples made by ProtoPasta material according to total sample height and number of layers used to fabricate the samples</i> .....	100
<i>Figure 6.9 Increase in resistance between samples made by AlphaOhm material according to total sample height and number of layers used to fabricate the samples</i> .....	101
<i>Figure 6.10 Increase in resistance between samples of equal height when comparing 3 Vs. 2 layer strategies</i> .....	101
<i>Figure 6.11 An example of shape of cross section according to different slicing in the case of 0.6mm height samples with greatest variation in surface area a) single layer strategy b) double layer strategy c) triple layer strategy</i> .....	102
<i>Figure 6.12 Visual description of Postulate 1 – freeform conductive tracks in space would exhibit the same phenomenon of resistance increase by multi-layered manufacturing instead of single-layer one</i> .....	104
<i>Figure 6.13 Visual description of Postulate 2 – smooth, continuous conductive track will have lower resistance than a counterpart with equal geometry constituting sections manufactured by multi-layer slicing</i> .....	105
<i>Figure 6.14 Design of case study with embedded conductive tracks: a) Part B with required functionality of 3 conductive tracks between edge T, M and top surface; b) definition of a new surface N that could be used to guide slicing for optimised conductivity</i> .....	106
<i>Figure 6.15 Creation of a new surface N that does not appertain from the part’s model to guide slicing oriented towards optimised functionality of conductive tracks Ct1, Ct2 and Ct3</i> .....	107
<i>Figure 6.16 Different views of simulated transparent (a),c),e)) and physical (b),d),f)) printed samples with slicing for the purpose of embedding single-layer conductive tracks within a part</i> .....	108

*Figure 6.17 A split model for improved visual validation of the single-layered conductive tracks manufactured for optimised post-printing functionality ..... 109*

*Figure 6.18 Comparison between accuracy driven slicing (left and centre) and function driven one (right)..... 112*

*Figure 6.19 Simulated overview of Case\_Btop slicing strategy with cut-out sections for implementation of segmented conductive tracks ..... 113*

*Figure 6.20 Case\_Bx slicing strategy: a)-g): ordered manufacturing steps for a multi-objective slicing aimed at benefiting both part's accuracy and the conductivity of embedded conductive tracks, h) frontal view ..... 115*

*Figure 7.1 Sub-volume slicing method exemplified on Case\_Bx. a) colours relate sub-volumes with respective slicing surfaces b) obtained layers from slicing operations ..... 127*

*Figure 7.2 An overview of the processing framework and flow of information through it 131*

## List of Tables

---

<i>Table 2.1 List of attributes and carriers .....</i>	<i>16</i>
<i>Table 2.2 Further defined form of queries with generated results in terms of prior work... 19</i>	
<i>Table 4.1 Process parameters used throughout all of the studies .....</i>	<i>58</i>
<i>Table 5.1 Case_Abot study info table.....</i>	<i>70</i>
<i>Table 5.2 Case_Atop study info table.....</i>	<i>71</i>
<i>Table 5.3 Case_Asan study info table .....</i>	<i>73</i>
<i>Table 5.4 Accuracy data per case study extracted from digital processing parameters .....</i>	<i>75</i>
<i>Table 5.5 Case_Btop study info table.....</i>	<i>84</i>
<i>Table 5.6 Case_Bside study info table.....</i>	<i>85</i>
<i>Table 6.1 Slicing Strategies applied to conductive tracks samples with different height .....</i>	<i>93</i>
<i>Table 6.2 3D Printer Specifications .....</i>	<i>94</i>
<i>Table 6.3 Process Parameters applied throughout the experiment .....</i>	<i>94</i>
<i>Table 6.4 Measured and processed data from the functional analysis experiment.....</i>	<i>96</i>
<i>Table 6.5 Cross section analysis of ProtoPasta samples (left half) and mass measurements of all samples (right half) .....</i>	<i>99</i>
<i>Table 6.6 Case_Bcon study info table .....</i>	<i>110</i>
<i>Table 6.7 Case_Bx study info table.....</i>	<i>116</i>
<i>Table 7.1 Summary of case studies and analysis conducted for this Doctoral Research....</i>	<i>122</i>

## List of Abbreviations

---

*ABS – Acrylonitrile Butadiene Styrene*

*AM – Additive Manufacturing*

*ASTM – American Society for Testing and Materials*

*BS – British Standard*

*CAD – Computer Aided Design*

*CAM – Computer Aided Manufacturing*

*CLFDM – Curved Layer Fused Deposition Modeling*

*CNC – Computer Numerically Controlled*

*DED – Direct Energy Deposition*

*EB – Extrusion Based*

*EBAM – Extrusion Based Additive Manufacturing*

*FDM – Fused Deposition Modeling*

*ISO – International Organization for Standardization*

*LOM – Laminated Object Manufacturing*

*ME – Material Extrusion*

*NURBS – Non-Uniform Rational Basis Splines*

*PLA – Polylactic Acid*

*PP – Polypropylene*

*RSD – Relative Standard Deviation*

*STL – Stereolithography*

## List of Symbols

---

$R_1, R_2$  – research questions

$M_1 .. M_4$  – research methods

$E_1, E_2$  – crucial elements of theoretical framework

$O_1 .. O_7$  – objectives for development of processing framework

$S_{(u,v)}$  – a generic NURBS surface. Mathematical model and internal variables defined locally.

$u$  – parametric dimension of a generic NURBS surface

$u_{min}$  – curve containing all parametric points with  $v = 0$

$v$  – parametric dimension of a generic NURBS surface

$v_{min}$  – curve containing all parametric points with  $u = 0$

$l_h$  – layer height

$n_{(u,v)}$  – normal vector of a NURBS curve at point  $(u, v)$

$L_k$  – all layers constituting a part

$I_i$  – iso-curves of a given NURBS surface

$Y_{ti}$  – infill toolpaths

$C_{ti}$  – contour toolpaths

$T_{ti}$  – unified toolpath

$T_{tsi}$  – safety toolpath

$s_d$  – safety distance

$P_{ss}$  – starting safety point

$P_{es}$  – ending safety point

$p_i$  – sampled points from a toolpath

$l_s$  – linear segments resulting from toolpath sampling

$e$  – extrusion quantity

$e_{max}$  – maximum permitted error during sampling

$W$  – width of deposited filament strand

$d$  – nozzle diameter

$n_d$  – distance of extruded filament at nozzle end

$X$  –  $X$  cartesian coordinate

$Y$  –  $Y$  cartesian coordinate

$Z$  –  $Z$  cartesian coordinate

$A$  – rotation around  $X$  axis

$B$  – rotation around  $Y$  axis

$\vec{i}$  – projection of normal vector  $\vec{n}$  along  $X$  axis

$\vec{j}$  – projection of normal vector  $\vec{n}$  along  $Y$  axis

$\vec{k}$  – projection of normal vector  $\vec{n}$  along  $Z$  axis

$f_d$  – diameter of filament as raw material

$f_l$  – travel length of filament as raw material

$SS$  – slicing surface

$SO$  – slicing operation

$S_s$  – safety surface

$F$  – feedrate

$V, V_{total}, V_{bot}, V_{top}, V_{side}$  – volume of an entire part or a specific slicing operation

$P_1, P_2$  – first and second postulate

$M, T$  – edges of Part B geometry

$N$  – user defined slicing surface

$Ct_1, Ct_2, Ct_3$  – conductive tracks of Case\_Bcon

# 1

## Introduction

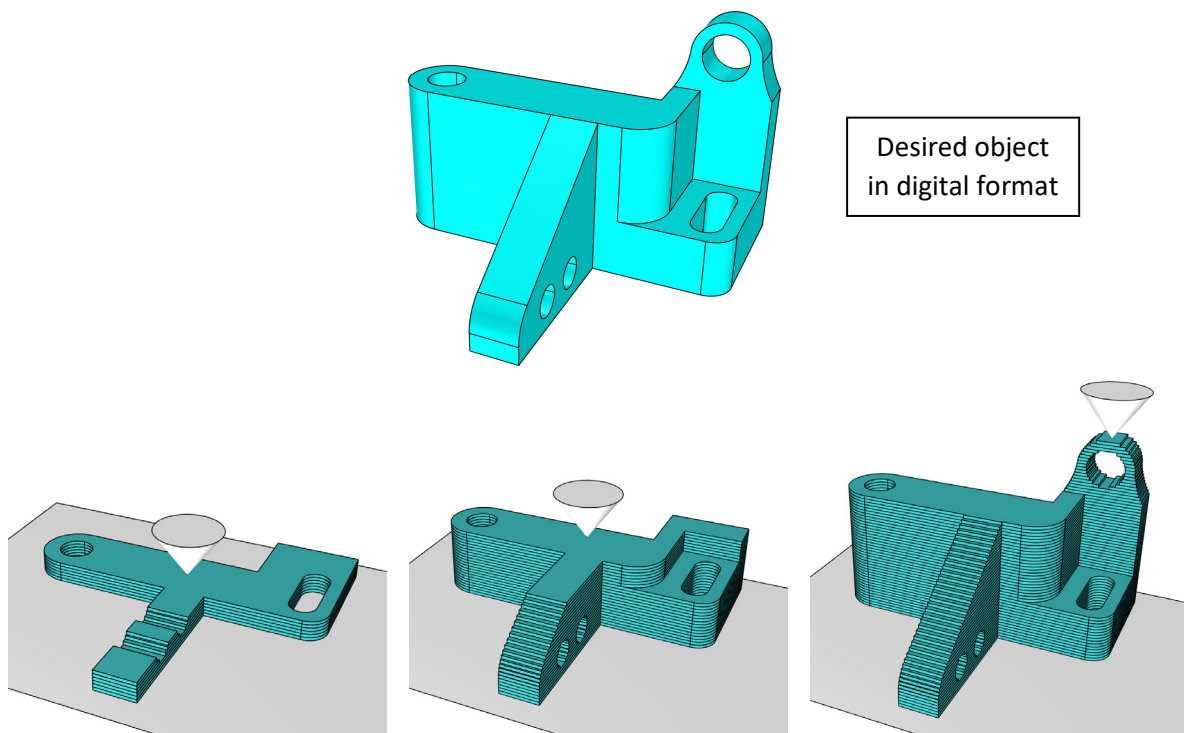
Opening Chapter 1 will provide a brief context into where this research is placed and what it intends to achieve.

The objective is to provide the basis for the technology, which Additive Manufacturing process will be investigated, terminology, current modus operandi and shortcomings, and what subfield has been identified as a potential improvement vector for further technological advancement.

---

## 1.1. Technology background

Additive Manufacturing (AM) is a term used to describe a family of technologies that use a similar fabrication principles of successive material inclusion in order to obtain an object. The process would usually start from either an empty machine workspace or within a container filled with the raw material, where the desired object (or a near net shape of it) is obtained by adding or solidifying small quantities of material wherever needed according to the digital shape of the desired object. Such characteristics makes the family of AM technologies fundamentally different from other conventional forming or subtractive manufacturing processes. The material addition is usually done in a layer-by-layer fashion where a digital, Computer Aided Design (CAD) model gets processed and based upon the digital data obtained from it, a manufacturing system is actuated to fabricate said CAD model, in most cases without the need of part specific tooling equipment. The material and machines can vary greatly, however, the principle idea behind all AM techniques can be obtained from Figure 1.1 depicting the manufacturing flow of a general AM process.



*Figure 1.1 Basic conceptual process flow behind Additive Manufacturing technologies*

The beginnings of AM have been marked by the appearance of Stereolithography in 1987, a process where the object is realised by solidifying liquid resin through the use of a laser [1]. Since then, many other AM techniques have emerged and new or hybrid ones are constantly



being invented, with some such processes even challenging the typical layered nature, as it will be noted later on in Section 2.1 by the literature review. Each of the various AM technologies uses a different combination of physical phenomena on how to include, deposit or otherwise add precise quantities of material, different energy sources or stimuli, different materials, machines and processing parameters. Some of the materials that are used include plastics, paper, metal, gel and the machines used to manufacture objects can have various embodiments making use of light, temperature, chemicals, pressure etc. depending on the specific AM process. More detailed insight into the world of AM can be obtained through [2]. The spread of AM has also prompted the activity of competent bodies related to standardisation and regulation of this family of manufacturing processes. Their definition according to the BS ISO/ASTM 52900:2015 [3] standard is:

*“process of joining materials to make parts from 3D model data, usually layer upon layer, as opposed to subtractive manufacturing and formative manufacturing methodologies”*

Over its three decades of development, other terms such as: additive techniques, layered manufacturing, freeform solid fabrication and others have also been used to denote the same idea. Research on AM technologies in general has been vast and increasing with every following year as more and more topics such as technological development, materials, manufacturing systems, supply chain management, product design, environmental aspects, strategic challenges, manufacturing frameworks, business and social impacts and economics of AM are gaining rising attention [4]. Positive industrial growth is also discussed in [5] and a Strategic Research Agenda can be found in [6] discussing the developments of AM from different technological and economic aspects. Even though this family of technologies are not solving all of the manufacturing issues and in certain manufacturing application are not the most suitable fabrication method, a global overall growing image full of positive prospect can be obtained based on the research, industrial and funding initiatives displayed today.

The technologies that fall under the umbrella of AM can be grouped in seven basic categories based on rudimentary parts of machine’s functionality. As indicated in the referenced source, it should be noted that this list is not and cannot be exhaustive due to the ongoing developments of new AM techniques. These categories as defined in BS ISO/ASTM 17296-2:2016 [7] are:

- Vat Photopolymerization
- Material Jetting

- Binder Jetting
- Powder Bed Fusion
- Material Extrusion
- Directed Energy Deposition
- Sheet Lamination

This Doctoral Research puts focus on Material Extrusion (ME) category of technologies that can be done with both planar, 2-dimensional layers (hence, 3-axis process context) or with freeform, 3-dimensional layers, in multi-axis process context. ME is one of the most widespread techniques in both commercial and academic realms due to its relatively low cost and simplicity in use. Occasional references however to other AM technologies might be encountered in this work in order to distinguish or present in a better way the rationale of undertaken activities or to relate to certain overarching elements valid through the entire scope of AM. The definition of ME technologies according to BS ISO/ASTM 17296-2:2016 [7] is:

*“additive manufacturing process in which material is selectively dispensed through a nozzle or orifice”*

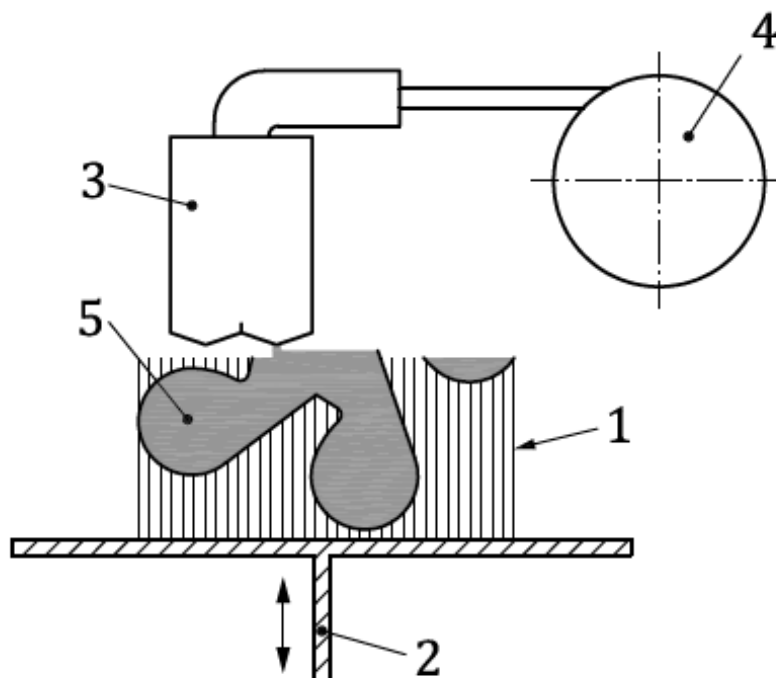


Figure 1.2 Schematic diagram of material extrusion adopted from [7]. Key elements: 1-support structure, 2-build platform and elevator, 3-heated nozzle, 4-feedstock supply, 5-product

Schematic diagram of Material Extrusion with the key features is presented in Figure 1.2. It consists of extruding feedstock material (4) through an opening and depositing it wherever needed according to the model of the part (5). Most commonly, the material is a thermoplastic polymer that is melted in the extruder (3) and is then deposited on a platform (2) layer-by-layer. In certain occasions, depending on the geometric shape of the desired part, there is also the need to build up a supporting structure (1) that serves the sole purpose of physically sustaining the part model that would otherwise collapse due to gravity; after the fabrication process is over, the support material is removed and disposed of since it does not contribute towards the final part's geometry.

The fundamental process chain will be briefly explained below while making reference to the steps depicted in Figure 1.3. The reader can refer to [8] for a detailed recent review on the overall picture of Processing Pipeline extending from digital file all up to the manufacturing of the part in general Additive Manufacturing structure.

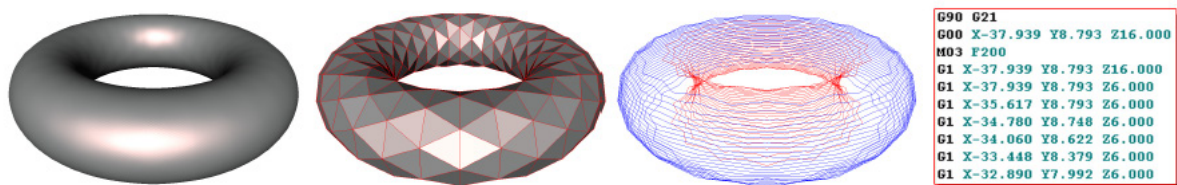


Figure 1.3 Typical process planning for AM, adopted from [8]. From left to right: digital geometry generation, tessellation, slicing and machine instructions

It begins with the intake of a digital 3D model of the shape that is to be obtained. While there are initiatives from both standardization bodies [9], industrial consortia [10] and reports on research efforts delivering a 3D model through alternative formats [11], STL remains one of the most active means of data format. An STL file describes the geometric shape by a plurality of triangles (planar facets) and their normal vectors. The geometry of the digital model described can be reached by either direct data preparation or data acquisition and can be either directly created to a triangular mesh or obtained by a process of tessellation of a different CAD format. Tessellation is a common step in the AM process pipeline and it decides the first level of approximation that is done on the digital geometry as it is a discretised way of representing a closed volume. An increased number of triangles would generate smoother surfaces closer to the ideal desired one, but would increase the size of the digital model and increase the time needed for subsequent procedures involved the process pipeline. Hence, in certain cases of more complex geometry or shapes including small features, depending on the

desired outcome on the accuracy of the final part, what is aimed for is a compromise between the number of triangles included in the mesh and the difficulty in processing the data. It should also be noted that while the tessellation as a step is very common in ME and AM in general, it is not an absolutely necessary one as other forms of geometrical data can also be used to extract part model information to guide the production phase [11].

Given that traditionally both ME and AM technologies in general are most often fabricating objects by a successive deposition of planar layers, a procedure is needed where the geometric volume needs to be divided to a plurality of layers, so-called slicing. In order for slicing to take place, a selection of a slicing direction and layer height are necessary. This direction is given by a particular orientation of the digital model. It is usually left as a user's choice or can be obtained through optimization methods that are able to locate a building direction aimed at satisfying a set objective [12], such as minimizing the volume of support structure needed. The layer height is a parameter that indicates the physical thickness of a single layer once deposited. The choice of this parameter directly then dictates the total number of layers that will be deposited successively, in order to arrive at an approximation of the desired shape. Once the build (slicing) direction and layer height are known, an automatic procedure of support generation takes place. The following step involves the use of a slicing algorithm that intersects the digital geometry of both the model and the support structure with a number of parallel planes, each a layer height distance from the previous one. The obtained contours on each of the layers represent the cross section of the 3D model at that specific height.

Different AM techniques fulfil the layers with material in a different way with various dimensional span. According to the classification by Pham discussed in [2], ME technologies have been developed as systems that use a single point source to include material, that is, a single nozzle or orifice through which a filament with a specific width is extruded and deposited. So far technological developments and physical constraints have limited the introduction of a 1D (line, or array of single points) or 2D (plane) method of delivering the material in ME. This in turn means that the orifice which extrudes the material needs to be controlled in a way so that it infills all of the internal surface of a specific layer. This process is known as infill, scanning or hatching. There are a number of different strategies that can be used in order to fill the needed surface with a single point extrusion delivery system. One of the most common ones is a combination of external contours with a linear zig-zag pattern on the inside. The selection of a specific strategy carries heavy impact on the meso-structure of the final product [13]. Furthermore, the choice of infill parameters such as raster angle, road width and fill gap give additional degrees of freedom that can be controlled as process parameters in order to better control geometric accuracy, structural performance and

manufacturing time of the part. Internal porosity as a parameter is also dictated by this phase as it specifies the level of volumetric infill the produced part is going to have. A complete infill would generate the most structurally sound part but would increase processing time dramatically and cost of the print. Therefore, a usual practice is to find a suitable compromise between these two objectives by fabricating the part with, for example, 30% – 70% of porosity on the internal structure and deposit full layers with no gaps in the sections where the outer shell of the part is being manufactured as to preserve the desired geometry. The outcome of this phase is a toolpath trajectory for each of the layers.

The following step in the process chain is the preparation of code list for the machine of interest. This is an operation that is taking as input the toolpath trajectory from the preceding stage and it creates a list of codes that are to be executed by an AM system. This code list can be proprietary, executable on a specific firmware or it can be in the form of a more open/standardised format structure such as G-code, typically used for similar instruction lists and control of Numerically Controlled machines [14]. This list describes every movement of the machine required to manufacture the desired part and would typically also contain certain information concerning the process parameters such as: nozzle temperature, potential heated bed or heated chamber temperature, velocity of deposition, process specific movements (filament retraction) and so on.

Finally, the instruction list is sent to the AM system for execution and the part is being manufactured by successive deposition of layers where a combination of build and support material results in a physical approximation of the digital model. In the general case where the finished part has been manufactured by a combination of both build and support material, there is the need of a secondary (post processing) operation where the support material is removed whether manually or by submerging the piece in a solution designed to dissolve the support material. Removing the support closes the fabrication process, leaving a physical approximation of the model geometry as a final part.

## 1.2. Shortcomings of Material Extrusion technologies

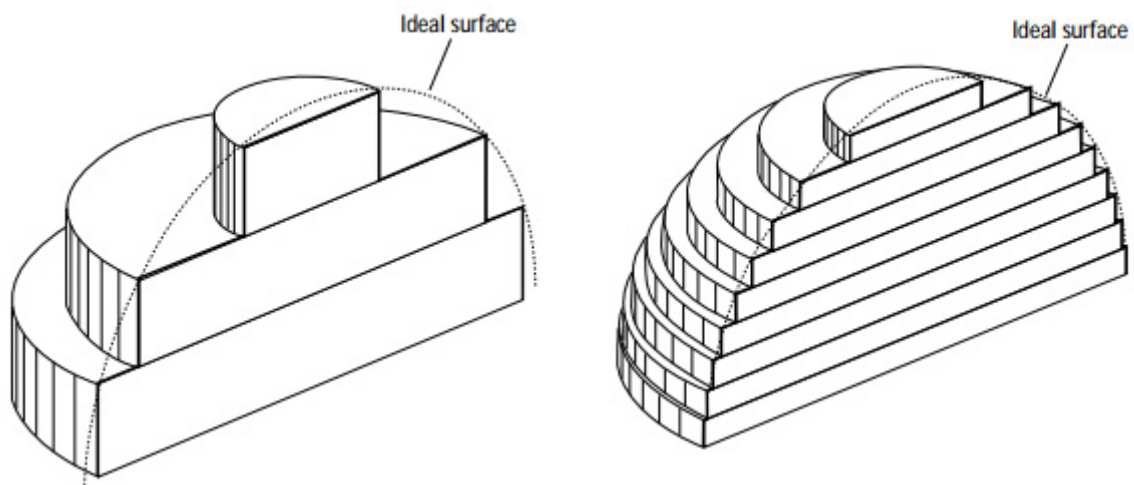
In order to paint a picture of the current technological drawbacks of a conventional ME category of AM methodologies, reference will be made to Fused Deposition Modeling™ (FDM), a technology initially developed by the company Stratasys Ltd. Since the name Fused Deposition Modeling is trademarked by the company [15], this technology is also known under the term Fused Filament Fabrication (FFF). This fabrication method is selected as the

best representative for the category of ME technologies as it has had the longest period of development and the highest level of diffusion in popularity and use with both industry and academia. Since the cost of both the manufacturing system and operation is among the lowest ones in AM in general, this technology has seen a surge in popularity over the last decade which brought about the development of a variety of manufacturing systems with a broad range of price, quality and materials.

When approaching a specific manufacturing technology from the perspective of further development, it is vital to understand the intrinsic characteristics of it, as they indicate both the strong and weak traits crucial for its implementation. From the advantages point of view, as almost all of the technologies from additive nature, FDM is characterised with a large enough design freedom, especially in the case where the manufacturing system is equipped to handle both build and support material, giving the possibility to manufacture geometries that would otherwise be unobtainable by conventional subtractive or forming techniques. Further to this it is also relatively cheap, easy and safe to implement, manufactured parts can be functional products and offers an ever increasing range of materials for implementation, some of which are composite blends with fine-tuned functional traits. Some of the most crucial drawbacks on the other hand will be looked at with a more in-depth analysis in the following:

*Anisotropy:* one of the principal problems that many of the AM technologies are facing but especially evident in the case of ME, is the mechanical characteristics of the final object. Namely, parts produced by FDM have been heavily investigated in terms of their strength and often compared to parts produced by injection moulding. Numerous tests have been performed on this since the emergence of FDM [16] that have all shown consistency in the results that the FDM made parts have inferior mechanical properties, related directly with two parameters: building orientation and intra-layer infill strategy. This anisotropic behaviour (more evident in the tensile and bending tests than compression) has immediate implications on the functionality of the finished product which in turns limit the application of the technology in different industrial sectors. The core concept behind the results of mechanical properties analysis of FDM made parts can be summarised by concluding that the strength along the axial length of a deposited filament is superior to the bonding strength between two adjacent filaments or between adjacent layers [17]. Even though research data performed on FDM technology only is used to describe the presence and severity of anisotropy, it is hypothesised that this phenomena is transversal and active to some extent throughout the entire family of Extrusion Based (EB) technologies due to the nature on how material is deposited and solidified, at least within the scope where temperature is used to liquefy the material being deposited from the nozzle.

*Geometrical accuracy – staircase effect:* this phenomenon follows directly from the fact that the digital 3D model used as input for the manufacturing process chain, undergoes an inevitable approximation by being recreated by a plurality of planar layers. The staircase effect has been extensively studied in the literature [18], [19]. Its major characteristic is the discretised step-like surface that introduces accuracy errors and has a high aesthetics impact due to the non-smooth surface finish, especially evident on inclined or curved surfaces. An illustration adopted from [18] of the staircase effect is presented in Figure 1.4.



*Figure 1.4 An illustration of the staircase effect in the case of manufacturing of a spherical feature with different level of approximation as a consequence of layer height. Adopted from [18]*

While this is an unavoidable element in the conventional process setup, the technology itself provides an intuitive method for decreasing the staircase effect: by lowering the layer height. However, this approach would directly increase the total number of layers necessary to build the part which subsequently affects the building time heavily. Consequently, researchers have proposed other methods as a solution to this compromise such as adaptive layer height slicing [20] and sub-layer thickness changes [21]. Yet another way to eliminate the stair-case effect is post-processing of the finished product, via for instance, a chemical method as described in [22] that besides the roughness impacts the strength of polylactic acid (PLA) parts as well.

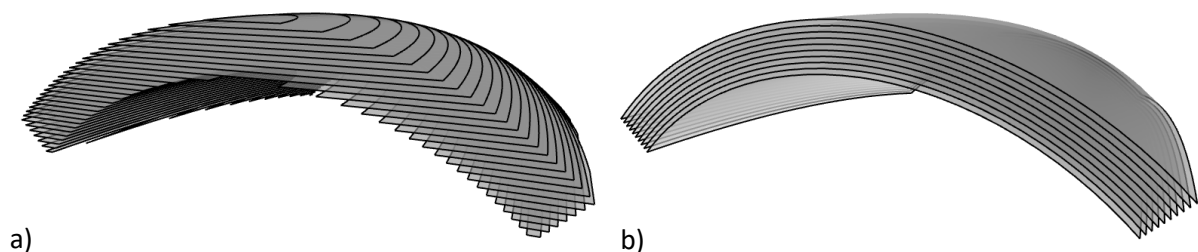
*Processing time:* due to the fact that the material extrusion system is a single point orifice through which a filament with a certain diameter is dispensed, a lot of time is spent for filling out the internal segments of every single layer with the desired infill strategy. Furthermore, the infill should follow the instructions for a possible multi-material deposition on layer basis,

which leads to dead times for switching between for ex. build and support material. It should be also noted that the time issue is affected greatly with the size of the object, geometrical characteristics of the parts (if it includes support structure), the percentage of porosity with which the material volume is filled, orientation and as well as other process parameters [23].

While the above shortlist of crucial drawbacks of the ME technologies captures some of the weakest links that hinder the capacity of the process itself, it is certainly not an exhaustive, definitive list of all matter that could be further improved or studied within the process of ME. Other problems such as process resolution [24], or how that translates in feature quality [25] also exist and have been confronted by researchers.

### 1.3. Curved Layer paradigm: a potential improvement vector

In order to try and limit the effect of the afore-mentioned shortcomings, this research looks at Curved Layer Fused Deposition Modelling (CLFDM) as the core vector towards improvement; a mean of passing from conventional ME process to a newly developed one that might provide solutions to the current technological problems. Even though curved layers in AM processes were discussed as early as 1997 ([26], [27]), it is widely recognised that the basis of CLFDM has been set by Chakraborty et al. in 2008 [28]. It has been the first work where the primary concept of CLFDM has been brought forward specifically for FDM, together with the inherent potential of this method to increase mechanical performance, geometrical accuracy and productivity by depositing layers that span in three-dimensional, freeform shape following the curvature of the part itself. It is hypothesised that high equipment and system development costs however, has slowed down the advancement of CLFDM over time, with the majority of the research (experimental results in particular) being done over the last 5 years. The state-of-the-art of CLFDM will be analysed in depth in the critical literature review.



*Figure 1.5 The basic concept behind Curved Layer and non-planar ME in general: a) Planar, conventional, 3-axis slicing and b) CLFDM slicing*



The essential idea behind it, illustrated in Figure 1.5, is to create and deposit layers that are non-planar and follow the shape of the object, achieving so longer filament continuity, improved accuracy and decreased manufacturing times. CLFDM has had a limited implementation in the fabrication of parts by ME technologies, focused principally in the research and academic realms. However, it is based on a proven theory that slicing an object along a curved surface following the shape of the object itself instead of a horizontal plane, does have great effect on all of the principle drawbacks pointed out earlier [29]. Most of previous works [28], [30] point out the fact that ideally, the practical execution of CLFDM would be done on a multi-axis system while keeping an orthogonal orientation between the extruder nozzle and the deposition surface, even though this can be approximated with a 3-axis system for cases where the curvature of the non-planar layer is restricted to small amounts. Regardless of the level of approximation in the execution of the process, the non-planar concept changes the slicing procedure, including new degrees of freedom that are now accessible on process planning level, which could enable a more effective fabrication approach.

While this opens a window of opportunities for a new process planning design, it clearly poses challenges in how those degrees of freedom will be managed in a complex setup where a number of crucial interlacing areas are present such as: geometrical design, mechatronic AM systems, extrusion based tools and materials available for processing. So far, in the conventional planar-layer approach of ME technologies, these disciplines have been connected according to certain design rules, process chain, data flow and corresponding manufacturing systems with certain mechatronic and material dispensing architectures. Bringing changes to some of these aspects, for example the planarity (dimensionality) of the layers, will certainly have an effect on the other related areas.

#### 1.4. Aim and objectives of the research

Current manufacturing process chain used in ME, as described in Section 1.1 is reasonably mature, reliable and relatively simple. This is also shown by the high availability of different software packages (a number of them free-to-use and open source) that currently exist, such as [31]. It can be argued that a probable future trend would be for the AM processing tools to follow a similar development path as the one historically witnessed by the subtractive Computer Numerically Controlled (CNC) machines; moving towards a more complex machine architecture with multi-axis synchronous motion for an improved process or part quality. When this retrospective view is combined with the relatively novel approach of non-planar layers described in Section 1.3, it can be hypothesised that expansion of ME into multi-axis

realm is both crucial for its improvement and inevitable. Clearly, it should also be acknowledged that such a scenario is not always merely a conversion or re-application of solid principles already used and tested in the multi-axis subtractive realm. In fact, as the names themselves suggest, additive and subtractive manufacturing technologies have highly different intrinsic attributes and these distinctions have to be accounted for in a suitable way.

As a consequence, the work in this thesis will be organised around the goal of further improvement of the ME technology in the direction of multi-axis paradigm. In a more philosophically-oriented context, the intent is to dedicate this Doctoral Research effort towards a clearer understanding of what can be achieved when ME process is extended into a multi-axis space, how can this be used to improve existing ME disadvantages and how to guide its implementation. Since ME is a manufacturing technology where the process and product outcome are intrinsically interlinked, another dimension of this study is to directly apply multi-axis ME for the fabrication of objects, in order to inspect and practically demonstrate, how can we improve the quality of manufactured parts, or endow them with a certain feature or characteristics. It is hoped that the findings of this study regarding the manufacturing process, reflected by the exhibited qualities of obtained parts, will ultimately help accelerate the evolution of multi-axis ME towards a more sophisticated method of manufacturing of objects.

Content-wise on the other hand, this will be reflected by putting focus and contributing towards the following research objectives:

- Understanding of how does the introduction of curved layer slicing change the conventional process chain from design to manufacturing in terms of logical procedure/sequence.
- Developing of a flexible software tool able to perform curved layer slicing and populate the layers with certain infill strategy.
- Analysing the possible interactions between curved layer and a multi-material aspect of a part.
- Investigating possible correlation between non-planar layers arrangement and final qualities obtained in a finished product; in a situation of many slicing possibilities, how do we select one?
- Practical execution of freeform, layer-based, orthogonal, multi-axis Material Extrusion using a multi-axis manufacturing system.

These objectives will serve as a guide during the critical literature review, will help base a criteria for the selection of inclusion of previously done work and will ultimately assist the formation of specific research questions.

It should be noted that this research has been conducted in partial correlation with the MovAiD project that is a part of European Union's Horizon 2020 research and innovation programme, funded under grant agreement No 680754 [32]. This project has a goal of developing the enabling technologies for the manufacturing of intelligent and passive movement assistive devices.

### 1.5. Scope of the thesis

In order to reach the above objectives this thesis will address the following:

- An extensive and systematic literature review of prior works around the key topic of “non-planar Material Extrusion” to serve as basis in formulating a hypothesis and research questions for this thesis. It should be noted that the core concept of non-planar, layer-based AM has been present also in other categories of technologies apart from ME, therefore the span of interest regarding non-planar, layer-based concepts will not be limited to ME only. This approach will be reflected also during the definition of the scope and inclusion criteria of the literature review in the next chapter.
- Formulation of an overview of the processing tools and respective data-flow for non-planar slicing and their associated algorithms, necessary to implement the technology such as slicing and toolpath generation algorithms. This will help in identifying ready-to-use processing tools that can be adopted for this study, or will serve as the base for a development of such processing tool in case of lack thereof.
- Design and execution of studies that practically implement multi-axis ME technology in the fabrication of samples, oriented towards providing answers to the research questions and hypothesis. Consequently, creating a portfolio of samples manufactured by multi-axis ME technology, demonstrating a certain application, is also within the scope of this thesis.
- Measurement, analysis and formulation of conclusions based on the matter observed.

# 2

## Prior Knowledge and Research Plan

Sections 1.4 and 1.5 have established the broader research intent of this work, its focus and direction of desired advancements to which it aims, but even the more detailed research objectives do not yet represent clear and concise research questions required for Doctoral Research planning. In order to better define them, in Section 2.1 this work initially goes through a retrospective analysis of published literature that has recorded previous research attempts oriented towards similar intentions or aims as the ones put forward here. Having a better understanding of previous and recent developments then leads to defining specific hypothesis and research questions as goals of this Doctoral Research, and methods on how to hopefully arrive to answers in Section 2.2.

---

## 2.1. Literature review

With an objective to utilise this research effort effectively, possibly also leading towards outcomes with significant impact and extent, a thorough overview of published works regarding this topic has been done. This allows for a better understanding of previous and recent developments done towards the advancement of multi-axis ME, contributes towards locating research space scarcely populated with data from prior studies and provides vision of research objectives and methods used by previous researchers.

### 2.1.1. Method and execution

As it can be observed in the objectives set out in the previous section, Curved Layers Fused Deposition Modeling plays a central role which is why it has been the topic of a systematic and more rigorous literature review. The general intention of this review is to obtain a solid understanding of the current state and level of adoption of the CLFDM paradigm for the manufacturing of functional parts by using ME. This was carried out through the following steps:

- *Keyword selection*: an initial phase of selection of terms that best describe the concept of Curved Layer Fused Deposition Modeling.
- *Scope limitations*: definition of boundaries within which the literature review will be performed for obtaining both a clear, well-defined research area and a realistic, reasonably sized horizon.
- *Inclusion criteria*: a set of posed regulations, or rationale in general, by which results generated by the search engine will be either included or disregarded in the literature review.
- *Execution*: the carrying out of the literature review by selecting suitable syntax operators.
- *Post-analysis classification*: once evaluated, the publications were grouped based on common characteristics that help deliver a better literature overview and organise the publications in smaller sets for easier future reference.

*Keyword selection:* since the CLFDM is neither a standardised term nor it has had an extended historical presence, but is rather a term introduced by pioneering researchers in the area, a structured terminology related to the idea of it does not exist. In order to minimise the probability of missing a conceptually relevant publication with a different nomenclature, effort was made to select several different key words that when combined among themselves in search queries would create sufficient search scope.

The selection of these keywords was done by first splitting the term “Curved Layer Fused Deposition Modeling” into two parts: “Curved Layer” and “Fused Deposition Modeling”. It was noted that the latter one is depicting a certain Material Extrusion technology while the former one is rather an explanation of the special attributes/characteristics exhibited by the technology. This led to the creation a shortlist of synonyms for the phrase “Curved Layer” called *attributes*, and a shortlist of synonyms for the phrase “Fused Deposition Modeling” called *carriers* that would later be used for creating combinations for search queries. By using this method, especially the inclusion of the carriers, a widening of the spectrum of technologies has been obtained where similar concepts might have already been researched. The lists of the selected keywords is shown in Table 2.1.

Attributes	Carriers
Curved Layer	Fused Deposition Modeling
multi-axis	Additive Manufacturing
multi-direction	3d printing
5 axis	Fused Filament Fabrication
6 axis	Material Extrusion

*Table 2.1 List of attributes and carriers*

*Scope limitation:* the following list of boundaries was taken in consideration when limiting the scope of the literature review:

- Only publications in English Language have been considered.
- Limitation on the year of publication has been evaluated as unnecessary since all of the developments on non-planar deposition in Additive Manufacturing are inherently recent.
- All results in the form of conference proceedings have been excluded.
- The literature review was performed using Scopus as it is a human curated search engine that manages one of the largest databases for accurate retrieval of previous work using advanced searching methods.
- Search within the title, abstract and key words has been used.

*Inclusion criteria:* arguably the most critical point in the design of such a review since a suitable model for inclusion does not and cannot exist in the literature due to the unique objectives of this research. In the following a list of criteria that were considered is presented:

- All publications dealing with the process of Curved Layer Fused Deposition Modeling in any way or form have been included.
- All publications dealing with multi-axis machine architecture for use with ME technologies have been included. A particular subset of the publications in this category are the ones relying on robotics based systems instead of machines for execution of the process. These have been judged additionally also on the application: while functional product applications have been included, architecture and design applications were deemed as lower priority and included only if they present some focus on process pipeline (data treatment, slicing etc.).
- Publications concerning Hybrid Manufacturing that consider ME technologies in any way or form have been included.
- Publications concerning ME technologies within the bio-extrusion sector have generally been excluded with the exception of research involving multi-axis extrusion or manufacturing system.
- Publications concerning Direct Energy Deposition (DED) or Hybrid Manufacturing of metals have been included if at least some portion of the publication is dealing with the process pipeline. Conversely, publications of this group focusing on material properties or technology parameters have been omitted due to their intrinsic difference to ME.
- All publications dealing with non-conventional extrusion technologies have been included. Same judgement principles apply as stated above regarding cases where robotic based manufacturing systems have been used.
- Duplicating publications resulting from one single search query (one specific combination of an attribute and a carrier) have not been included.

- Duplicating publications resulting from different search queries have been included with the intention of removing the effect of the order in which different search queries were conducted.
- All of the above considerations were judged evaluating the title, abstract and key words sections.

*Execution:* the review was carried out by performing 25 different search queries resulting from the combination of each of the carriers and attributes using Scopus as a search platform. Furthermore, special characters from Scopus' search syntax were used to compensate for varying terminology or spelling. A graphical representation of the review is shown in Figure 2.1 while queries and results are shown in Table 2.2.

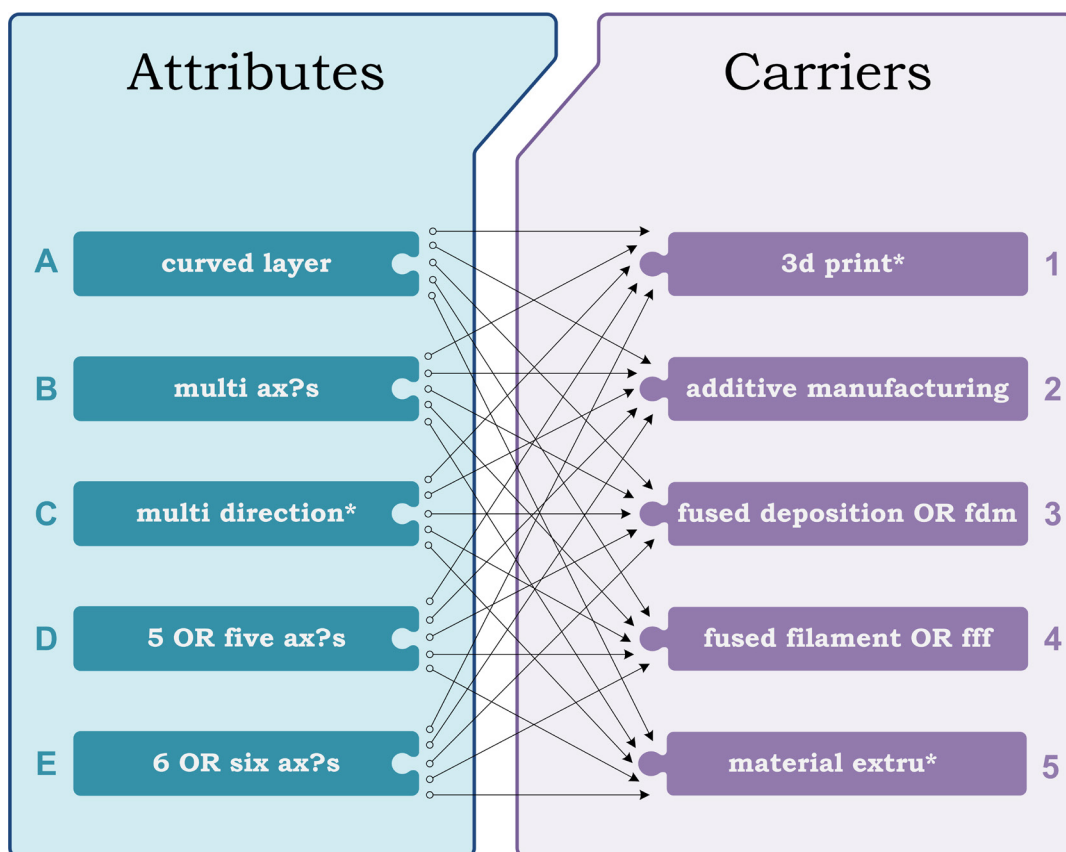


Figure 2.1 Graphical representation of query formation necessary for literature review



<b>Query ID</b>	<b>N. of generated results</b>	<b>N. of selected results</b>
<i>A1</i> – curved layer 3d print*	40	13
<i>A2</i> – curved layer additive manufacturing	36	9
<i>A3</i> – curved layer (fused deposition OR fdm)	21	12
<i>A4</i> – curved layer (fused filament OR fff)	9	7
<i>A5</i> - curved layer material extru* )	22	3
<i>B1</i> – multi ax?s 3d print*	71	16
<i>B2</i> – multi ax?s additive manufacturing	52	17
<i>B3</i> – multi ax?s (fused deposition OR fdm)	16	6
<i>B4</i> – multi ax?s (fused filament OR fff)	7	1
<i>B5</i> - multi ax?s material extru*	47	2
<i>C1</i> – multi direction* 3d print*	119	13
<i>C2</i> – multi direction* additive manufacturing	53	15
<i>C3</i> – multi direction* (fused deposition OR fdm)	41	5
<i>C4</i> – multi direction* (fused filament OR fff)	3	0
<i>C5</i> - multi direction* material extru*	89	4
<i>D1</i> – (5 OR five) ax?s 3d print*	96	15
<i>D2</i> – (5 OR five) ax?s additive manufacturing	57	10
<i>D3</i> – (5 OR five) ax?s (fused deposition OR fdm)	58	7
<i>D4</i> – (5 OR five) ax?s (fused filament OR fff)	49	1
<i>D5</i> - (5 or five) ax?s material extru*	106	4
<i>E1</i> – (6 OR six) ax?s 3d print*	52	8
<i>E2</i> – (6 OR six) ax?s additive manufacturing	34	9
<i>E3</i> – (6 OR six) ax?s (fused deposition OR fdm)	42	4
<i>E4</i> – (6 OR six) ax?s (fused filament OR fff)	51	1
<i>E5</i> - (6 or six) ax?s material extru*	71	3

Table 2.2 Further defined form of queries with generated results in terms of prior work

The review resulted in 66 unique publications, 3 of which were not available for access at the time of writing which left a final count of 63 publications originating from the systematic review. The publishing time window is between 1997 and 2017 with approximately half of the previous works done since 2015 onwards. The critical review was finalised with a phase of citation search of the publications selected as most crucial background. This resulted in the addition of 15 publications that increased the total number of analysed works to 78. After their examination, 10 publications were characterised with low relevance or with focus on subjects that are too far from the scope of this research and were therefore removed from both literature review and bibliography in general. The literature review was continuously updated throughout this Doctoral Research in order to stay up to date with relevant studies being done in parallel with this work, enabling the correlation with similar research done in the field. 28 other publications were added to their respective group of relevant prior work following this method. Additionally, dedicated reviews of previous knowledge are also included in the introduction of Chapters 3,5 and 6, relevant to their corresponding contents.

*Classification:* after studying the selected publications they were grouped into several classes with a common characteristics. The following clusters of publications were created: *CLFDM focus* – research that introduced the term, specific to FDM or ME in general and has proposed slicing and infill algorithms. In other words, this group would best represent the core of CLFDM; *Extrusion Based Manufacturing Systems* – research with a heavy focus on developing hardware for EB technologies for non-conventional, curved layer or in-space approach with both machine and robotics based equipment. *Metal and Hybrid Additive Manufacturing* – non-extrusion technologies included due to the high technical development of robust algorithms for multi-directional slicing and toolpath generation. *Novel emerging technologies and methods* – technologies or methods involving non-conventional principles that often challenge the concepts of standard planar layer deposition.

It should be noted that this classification was not performed using a strictly defined model or classification system but rather on the author's perception on both common characteristics and relevance on the publications in relation with the research proposed here. The objective of this is to have a better classified vision on different aspects of research focus that have been done in the past and a better clustering system for future reference. In the following, a detailed analysis on each of these groups has been done with discussion on their corresponding publications.

### 2.1.2. Analysis and discussion

#### *CLFDM focus.*

Manufacturing time and surface quality of parts with curved surfaces made by AM technology has been addressed by [33] by developing slicing algorithms for use with a five-axis waterjet machine and introducing a slope on the cutting edges. A later study with a similar focus on bevelled-edge slicing has been done by [34]. However, the first research effort on building an object by using a concept of non-planar layers that follow the curvature of the object itself, has been noted in [27] where a modified process planning and hardware has been developed for Laminated Object Manufacturing (LOM) technology. Later this concept has been introduced specifically for FDM technology by [28], where also toolpath generation algorithm and the possible hypothetical benefits of such CLFDM method were discussed. An experimental approach involving slicing and toolpath development algorithms were used by [35] obtaining the first results consistent with the hypothesis that CLFDM improves the mechanical strengths of parts made by ME. Further experimental tests were performed in order to understand the effect of raster angle and fill gap by [36] and [37]. A study on combining the CLFDM with flat conventional layers is presented in [38]. Further developments involving elaborate algorithms of both conventional and adaptive flat and curved layers slicing is reported in [39]. The focus has been kept on the slicing approach of CLFDM with detailed analysis on development of suitable algorithms while evaluating their effectiveness primarily in a software environment on different part or hypothetical digital geometry, with limited cases of experimental work. Another study focusing also on the process of CLFDM is [40], where an approach of modifying the toolpath for a more suitable implementation on 3-axis machines has been done, enhanced with an improved modelling of the filaments obtained by CLFDM. The approach was evaluated by implementing it in a software environment.

An in-depth investigation of the CLFDM process and its practical implementation has been conducted by [30] and [41], where initially software tools have been developed for slicing and toolpath generation which have later been practically implemented by using a 3-axis Delta manufacturing system. The experimental data on processing time and quality of the obtained products show the potential of CLFDM approach. Furthermore, important auxiliary areas concerning multi-material aspect and collision avoidance have also been discussed.

Other related research efforts have kept a focus more oriented towards the concept of multi-material implementation in combination with non-planar layers for different purposes. [42] discussed the potential of CLFDM in implementing conductive electronic tracks during fabrication of the part, while [43] investigated the potential of involving non-planar layers

where composite materials are deposited in order to increase the mechanical performance of a part made by ME (FDM in specific). While a proposal for design of such applications has been stated and a prototype of tool embedding composite materials developed, the study does not present experimental data of the overall approach. [44] on the other hand has approached the mechanical improvement issue by involving special features called stiffeners performed by non-planar layers suitable for manufacturing with multi-axis manufacturing systems.

A particular subgroup of research has put emphasis on the creation and mechanical testing of lattice structures that span along freeform layers [45]–[48]. This direction of work demonstrates the outreach potential that can be achieved by transitioning from 2D to 3D layers, particularly regarding the freedom in control over mechanical properties of parts printed by non-planar layers.

Some of the most recent studies involving CLFDM in either 3-axis [49], [50] or 5-axis setup [51]–[53] have been done with a holistic view of the overall framework and process planning required for implementing the technology. This envelops the methodologies for slicing, toolpath generation and manufacturing by using a suitable manufacturing system. These works will be discussed further in Section 3.1 dedicated on the multi-axis ME framework development.

#### *Extrusion Based Manufacturing Systems.*

Starting from 3-axis manufacturing systems, the earliest interest in research for a manufacturing system that would enable specifically Curved Layer FDM was encountered in the work of [54]. It consisted of modifying a Fab@Home machine, developing slicing and toolpath algorithms for CLFDM and performing experiments. [55] on the other hand modified an industrially graded Stratasys 3000 FDM machine enabling it to print on different surfaces, including non-planar ones. Another manufacturing system based on Automatically Programmed Tools has been proposed by [56] while focusing more on extrusion tool and overall flexible, multi-material framework. An interesting research focused on large-scale application with a 3-axis machine has been presented in [57] by extruding cement while using the concept of CLFDM. The work also approached the problem of slicing algorithms and developed a software tool based on the software environment of Rhinoceros®. This work can be seen as one of the studies that expand the CLFDM concept outside of a smaller scale, polymer based application, proving that similar concepts might be transversally applicable throughout the entire family of Extrusion Based technologies.

Regarding multi-axis manufacturing systems, there has been a considerable number of publications since 2013 onwards taking mainly two directions: machine and robotic manufacturing systems. One of the initial machine attempts presented in [58] designed and tested a 6-axis parallel manipulator as a stage on which the extruder is mounted, giving it movement capability for both position and orientation. A study aimed at designing and testing a 5-axis hybrid stage using FDM as the additive technology has been done by [59] and [60]. Their work also touches on the subject of using the additional axis to orient the tool and deposit on already pre-manufactured parts. [61] have designed a four-axis FDM printer as the first step towards a five-axis one, applied slicing and toolpaths methods and tested their manufacturing system while also discussing the effect of inclination of the deposition nozzle on the process. Another novel manufacturing system for used with EB technology of metals and ceramics has been disclosed in [62] and [63]. The concept of the manufacturing system is a combination of a parallel manipulator and an Agile Eye mechanism, with ongoing physical realisation. More recently, a 5-axis ME system has been used in research aiming for improvement of strength properties of parts in [64].

Many researchers have also focused on the implementation of robotic equipment for the application of extrusion deposition. The work presented in [65] and [66] can be considered as a good representative for the research done in this subfield. Their methods involved development of slicing and toolpath generation algorithms and mounting of an extrusion tool on an industrial 6-axis robot. Furthermore aspects of pre-manufacturing simulation and integration with the manufacturing system were considered, as well as practical experiments of functional products as a platform for verification. [67] has also used a 6-axis industrial robot with a specifically developed process procedure for conformal deposition on a given freeform surface in a medical application. Similar hardware setup has been considered for structural improvement application where the deposition is done along the principle stress lines of the object in [68], and more recently [69] while [70] investigated an application of architectural structural components and fabrication of multi-functional walls. Compound Manufacturing has been proposed as a novel manufacturing paradigm in [71] where robot equipment interacts with different tools from additive, subtractive and forming manufacturing for an integrative manufacturing approach whereas focus on different extrusion tools, materials development and sustainability aspects have been addressed in [72] and [73]. Robotic setup has also been used in [74] in an investigation aimed at improving the strength of parts, while two robotic arms have been used in [75] to demonstrate independence between surface roughness and orientation with respect to gravity. Additionally, hybrid approach in robotic setup has been addressed in [76] while motion control aspects regarding smoothness of path and feedrate have been studied in [77].

### *Metal and Hybrid Additive Manufacturing.*

Research on multi-directional Additive (referred to also as Layered) Manufacturing in general has had a slightly longer historical development when compared to ME systems and processes. A recent review outlines some of the most important developments and aspects crucial for the technological development of advanced hybrid manufacturing [78]. The extensive work of D. Dutta et al., some of which is presented in [79] and [80] has been widely recognised as one of the pioneering ones in this field that has established certain basis regarding geometrical volume division, multi-directional slicing and path planning algorithms, touching also on the subject of a suitable manufacturing system for use in such occasions. [81] has worked on and tested a procedure for overhang analysis and implementation on a Hybrid Plasma Deposition system, while [82] has applied similar manufacturing approaches for use with a Hybrid Laser Metal Deposition process and have investigated the ordering of slices and later collision check methods for successful implementation with a manufacturing system. [83] have proposed a general simulation framework to use with virtually any 5-axis manufacturing technology whereas [84] studied the potential of a robust algorithm for automatic volumetric sub-division of the part. Another direction of research has been more oriented towards the advancements in Wire and Arc Additive Manufacturing where the ample research done by Donghong Ding et al. is highly present. Ranging from introducing some of the most critical elements of such a process planning framework in [85], his work extends to multi-directional slicing algorithms [86], gap free generation of toolpaths specifically developed for that type of technology [87], involving neural networks for bead modelling and pre-manufacturing predictive simulations [88] and an overall automated process starting from part's digital geometry up to manufacturing process [89].

An active area of research in non-planar metal AM is organised around Direct Energy Deposition (DED) techniques. While inherently different than ME in many aspects ranging from bead formation to used equipment, research concepts regarding slicing, toolpath generation and overall process planning offer valuable insight. One such research focusing on Laser-based Metal Deposition is presented in [90] where an in-depth process analysis has been explored in combination with a complex 8-axis manufacturing system. Other recent studies have described non-planar slicing and toolpath generation from both parametric and mesh models [91], have proposed slicing models that address the issue of collision-free toolpaths [92], implemented advanced algorithms for deposition of overhangs, infill toolpaths [93] and layers with varying layer height [94]. A summary of some of the most recognised slicing and infill strategies for this cluster of Hybrid Metal Manufacturing research is presented in [95].

### *Novel emerging technologies and methods.*

Different types of research, often exploratory ones directed away from optimisation of standard conventional concepts, have led to the emergence of new technologies, many of which challenge the standard planar deposition principle in ME. One such research is presented in [96] and [97] that has focused on the in-air fabrication of low fidelity wireframe models of the objects that has later been adopted for implementation on a 5-axis ME system, accompanied with ordering and collision avoidance algorithms. Also, *RevoMaker* was introduced as a novel extrusion 3D printer in [98] for building on and around an object with increased functionality. A more recent study with a similar concept of building an object starting from a cylindrical core using spiral toolpaths for improving the strength has been described by [99]. [21] on the other hand have worked out a new method that improves geometric accuracy of final objects by varying the layer thickness during deposition and is applicable as a pre-manufacturing filtering script on different kinds of manufacturing systems. In [100] a novel system for printing Dielectric Elastomer Actuators onto an inflatable air-permeable mandrel has been developed.

On a different note, analysing multi-material integration within a 3D printed part, [101] has investigated the selection of build orientation in a case of multi-material parts. Other studies such as [102] have introduced a process planning framework for an integrative process of electronics embedding within an object manufactured with stereolithography, while [103] have introduced technology suitable for integration with additive ones in order to precisely embed conductive traces even on curved surfaces. Yet another example of research directed in a similar way is [104] where conductive patterned layers have successfully been embedded in additively manufactured parts. The topic of combining topology optimization with the internal material structure of the parts has been discussed in [105] for a possible application not specific for a certain AM technology. A novel fabrication technique called Hybrid Deposition Manufacturing has been introduced by [106] in a study combining FDM with casting towards multi-material final products.

Lastly, the work of Yong Chen and Chi Zhou has been reported in a number of publications regarding advancements on a novel layerless AM process based on CNC accumulation. The technology has been proposed in [107] and [108] together with hardware development and initial experimental tests. Further assessment of suitability of this technology for use in cases of curved surfaces and building around inserts have been reported in [109] and [110] correspondingly.

## 2.2. Defining research plan

The analysis of prior work done in Section 2.1 has been used here to identify distinct hypothesis and research questions to be addressed by a research study and research methods on how to hopefully reach answers or conclusions.

### 2.2.1. Hypothesis and research questions

With a solid background information and an overview of the literature available up to date, it can be concluded that CLFDM as a paradigm is still at its infancy when it comes to its implementation as a standard technique for functional parts. While the core theory behind it has been proven as an effective method in overcoming some of the drawbacks present in ME, previous work has been more local, addressing problems like slicing and toolpath generation with methods and software tools that vary from research to research. In general, while certain technicalities of implementing CLFDM have been investigated, some of the elements that can be noted as missing from the current literature are the following:

- *Process understanding and guidelines.* There is currently very little understanding on how can the curved layer slicing be guided and how different curved layer slicing affects the process and part quality. In other words, the inclusion of non-planar layer increases immensely the process design freedom, but currently there is no understanding on how to guide all that freedom and how to select from the many possibilities available. Instead, current research only shows isolated, sporadic, non-systematic case studies without an analysis of how different slicing strategies affect the part's final quality.
- *Curved layer software processing tool (also known as slicer).* This is missing as a tool currently in both academic and commercial areas and is a presumably a considerable barrier towards a more regular adoption of the curved layer paradigm and towards a higher research presence.
- *Practical implementation of orthogonal curved layer slicing in multi-axis manufacturing system setup.* Relatively high number of previous Curved Layer research activities have been limited in the case of 3-axis systems with clear barriers



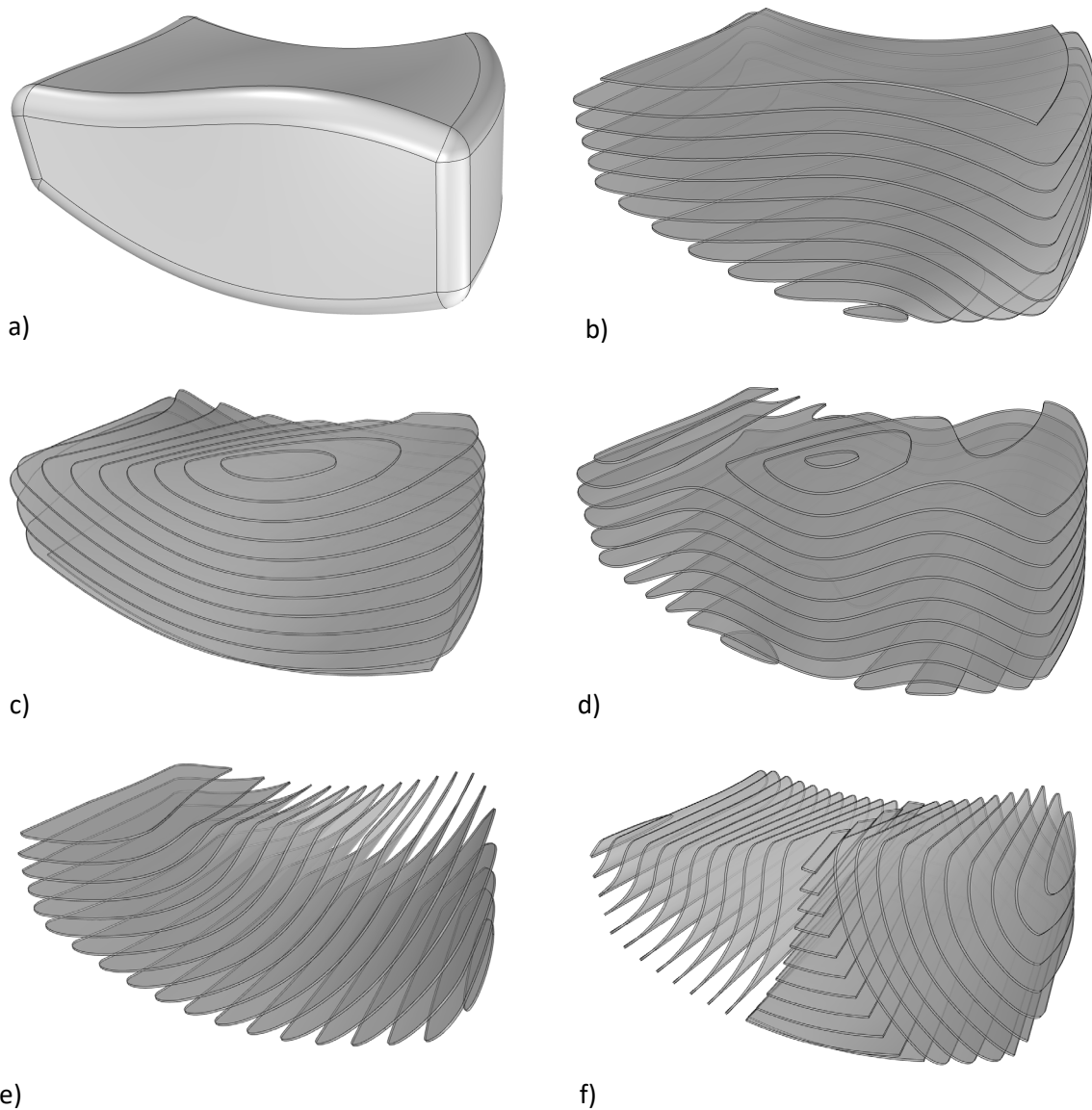
for unlocking the full potential of multi-axis extension of ME, remaining therefore in a subset of possibilities with regards of what could potentially be achieved by multi-axis ME process. With the exception of few instances, 5-axis cases are most prominent in design and architecture context where ad-hoc toolpaths have been developed rather than a manufacturing context with focus on understanding process and outcome.

- *Analysis of the relationship of curved layer slicing with multi-material aspect.* All previous case studies have been focused on a deposition of single material. An interesting hypothesis of potential advantage of curved layers put forward in [111] and functional materials (conductive materials in specific) has not yet been tested nor practically executed.
  
- *Curved layer layout with respect to the entire part.* Majority of research has looked into enabling the manufacturing of a single curved surface, an isolated surface of an object or an object with simple geometrical shape.

The literature review performed as described in this chapter provides evidence that there is a general need of research effort towards multi-axis ME technologies with many open questions for investigation and analysis, giving the impression that researchers are just starting to reveal both its full potential and the necessary guidance for execution. In other words, it appears that it is still not fully understood what this technology can offer as a benefit if used as a manufacturing method, nor how to define all of its necessary processing parameters. All of the different previous works done close to this topic, especially under the umbrella of the CLFDM terminology, have made use of different freeform layers spanning in space in terms of different surface topology. Some of them have employed non-planar layers also in a combination with conventional 3-axis slicing, or have even had them combined with adaptive slicing paradigms, pointing towards the idea that non-planar slicing could be done using many different surfaces. Nevertheless, besides this immense apparent increase of freedom in guiding the layers in freeform space instead of being restricted to the planar domain, it seems that no previous research has attempted to relate different slicing strategies to different outcomes in terms of part quality, leaving us with deficiency in understanding on how to guide the multi-axis slicing process; how to potentially pick between these numerous possibilities, supposing they exist.

Therefore, this Doctoral Research has put forward a hypothesis that will attempt to investigate:

- ***Hypothesis:*** Extension into multi-axis space allows for many different slicing strategies of the same part, each with given impact on the outcome. If so, understanding the relationship between the slicing strategies and their outcome on part's quality can consequently allow for slicing tailored for a specific objective.



*Figure 2.2 Graphical depiction of hypothesis through examples of different slicing strategies related to the same part geometry, potentially resulting in different post-printing characteristics of the part: b) top-down slicing, c) bottom-up slicing, d) waved based slicing, e) side slicing and f) combined slicing strategy.*

To further describe, the idea behind the hypothesis is that, much like how the choice of orientation of part model in conventional planar ME has an impact on both the process (cost, manufacturing time, use of material etc. [112]) and the part's quality (strength, accuracy, feasibility etc. [113]), the choice of slicing strategy in multi-axis ME technologies impacts part's quality. If supported, this could suggest that the slicing can be guided according to desired characteristics of the final part. The main idea behind the hypothesis is that there could be multiple ways of slicing a given object, (Figure 2.2 a) with different post-printing characteristics obtained as a direct result of how the layers have been arranged (Figure 2.2 b)-f), is represented also visually in Figure 2.2. This could potentially mean that, for example, top-down slicing strategy b) offers a better resistance to compression with respect to side slicing strategy e) that instead enables the printing without support in a certain orientation. Or that bottom-up slicing c) optimises for bottom surface accuracy, waved based slicing d) for elasticity and maximum inter-layer surface area for inclusion of continuous functional materials while combined slicing strategy f) allows for a controlled fracturing after excessive compression.

In order to investigate this hypothesis however, besides the evident need for multiple slicing strategies of an identical part model, there is also the need for a certain benchmark in terms of part quality. As it can be noticed from Figure 2.2, the Hypothesis is heavily oriented towards spatial redistribution or arrangement of the layers w.r.t. the part model generated as a result from certain slicing, rather than being correlated to the material itself used to manufacture the part. In other words, it puts focus on how the slicing is done, rather than which material has been used or the toolpaths used for infill.

The two most commonly emphasised benefits of the use of non-planar slicing in previous works have been improved structural integrity of parts and improved accuracy, also identified with lack of the staircase effect as described in Section 1.2. While of very high importance and potential impact, structural integrity is a direct function of the material used to build the part. Also, it is foreseen that any research effort in relating different slicing strategies and strength of obtained part will inevitably be highly influenced by the toolpath generation methods used within the study, since these software operations would heavily impact the material distribution within the part i.e. its meso-structure. It can thus be argued that such tests would involve substantial risk of reporting data that is, to some extent, dependent on the algorithms used for toolpath generation. In order to avoid such risk, the strength of the obtained part will not be considered as one of the quality characteristics used in this study.

The latter benefit of improved part accuracy has been shown only on some selected surfaces instead of the entire part or parts with a geometry obtained by offsetting a single surface by a uniform thickness. There is the necessity for further tests in order to understand the

relationship between slicing strategy and the accuracy of the entire part, and since accuracy is mostly affected by how the slicing is done (the arrangement of layers) instead of the toolpaths used for infill or the material used to manufacture it, there is limited risk for data impacted by the software tools developed for this study. For these reasons accuracy will be considered as one of the quality characteristics used as a benchmark for this study, formulated in the shape of a specific research question R1:

R1: How do different non-planar slicing strategies affect part's accuracy? Is there a generic slicing method that can be used to optimise the post-printing accuracy of the part?

In an optimal setup, a research into the above defined hypothesis would have at least two different quality benchmarks in order to better demonstrate potential slicing strategies oriented towards one or the other quality characteristics. As previously mentioned, it has been theorised by other researchers that non-planar slicing could bring forward benefits regarding the implementation of functional materials inside a given part, referring to fibre-reinforced composite materials [43] or conductive materials [111] as examples of embedding of functional materials. Due to their uncorrelation to strength of the part as a function, and independency of part build material, conductive polymer blends will be considered in this research as a representative of functional materials. Also, neither 3-axis nor 5-axis ME experiments that support the theory behind non-planar layer benefiting the embedding of conductive materials have been encountered throughout the literature review, expending the potential impact of such research in both of these realms. For these reasons, post-printing functionality of conductive materials has been selected as the second quality characteristics used as a benchmark for this study, formulated in the shape of a specific research question R2:

R2: How do different non-planar slicing strategies affect the part's conductivity? Is there a non-planar slicing method that can be used to optimise the post-printing functionality of conductive materials?

It is acknowledged that absolute, complete understanding of the above curiosities within all of its limits and conditions will be difficult to achieve as it can be realistically expected from a research effort with limited time and resources. However, it is assumed that through an effort in answering these two distinct research questions, some evidence of different non-planar

slicing strategies each with different impact regarding the accuracy and functionality of conductive materials will be presented that either support or contrast the set hypothesis to a certain extent.

### 2.2.2. Research methods

As shown by the literature review, very small number of multi-axis ME applications have effectively been done all through the manufacturing point, limiting our perception of what can be effectively achieved through this technology. Moreover, the hypothesis set out for this research proposes the concept of many possible slicing strategies that can be applied to a given part model, so investigating a variety of part-to-slicing combinations appears to be beneficial in demonstrating the high number of technological possibilities. Therefore, research approach based on case studies has been identified as a suitable method for exploring different possible applications of multi-axis ME, by creating a considerable number of practically manufactured samples with defined process parameters.

However, two necessary elements have been identified in order to guide a high quality explorative research that will result in informative objective data obtained with significant rigour:

#### E1. A fixed processing framework.

As established previously in this work, there is currently an absence of standards, academic or industrial software tools and a fixed framework for this technology. It also lacks a historically extended period of use and numerous literature sources that could be used to deduct most common overlapping principles. Yet, the use of some processing framework is an inevitable element since it is the algorithmic embodiment of the technology itself. Consequently, all case studies in this research will be processed by an unvarying processing framework developed for this study. In order to eliminate ambiguity and justify its form, the flow of its requirements, design and development will be analysed in detail. A pilot case study will be used to effectively demonstrate the application of the framework that implements multi-axis ME technology, from digital geometry all through manufacturing of a given part, as a way to validate it is fit-for-purpose as a tool for testing multi-axis ME technology. Finally, in order to avoid that some framework elements impact the final case studies, all parameters within the framework will be kept fixed throughout all case studies.

E2. Case study design driven by evidence.

While qualitative research based on case studies can indeed be beneficial in showcasing one possible combination of an applied principle, the design and selection of the case studies needs to be systematically guided and justified through some form of a measurement data. In this Doctoral Research, two quality characteristics were set as benchmark parameters that could potentially serve as objectives in multi-axis ME technology: accuracy of obtained part and post-printing functionality of conductive materials. Given the scale at which the technology will be implemented in this study, much of the accuracy quality can be verified visually through inspection, similarly to previous research works in the field. Microscope images will be used as non-destructive measurement techniques that due to their digital nature can be directly compared to simulated outcomes. While accuracy as a part characteristic has already been shown to benefit from the application of non-planar layers, no previous data relates post-printing functionality of conductive materials (tracks) with slicing strategies. Therefore, a dedicated quantitative study will be done in order to test the theory of multi-axis slicing for optimised conductivity, measured through the electrical resistance they exhibit.

The above noted considerations provide arguments that a combination of qualitative and quantitative research could provide for an effective methodology suitable for analysing the hypothesis and research questions set in the previous section. Putting all of the aspects together: the two quality characteristics used as a benchmark, the need for a fixed framework, qualitative approach for the use of case studies and the need for measured data, an overview of the research methods applied for this Doctoral Research can be summarised in the following steps, represented graphically in Figure 2.3:

M1. Design and development of a processing framework (including software tools for slicing and toolpath development and hardware tools for execution) able to apply multi-axis ME technology on a given geometry and manufacture it into a tangible part. Pilot testing for verification of fitness-for-purpose and establishment of fixed process parameters. Elaborated in Chapters 3 and 4.

M2. Design of case studies, application of different slicing strategies and measurement of impact on accuracy through characterisation of the staircase effect, quantification of accuracy data from digital models and non-destructive image metrology (Section 5.1). Application of observations and findings on a fixed geometry serving as a common input parameter for comparison across different case studies (Section 5.2).

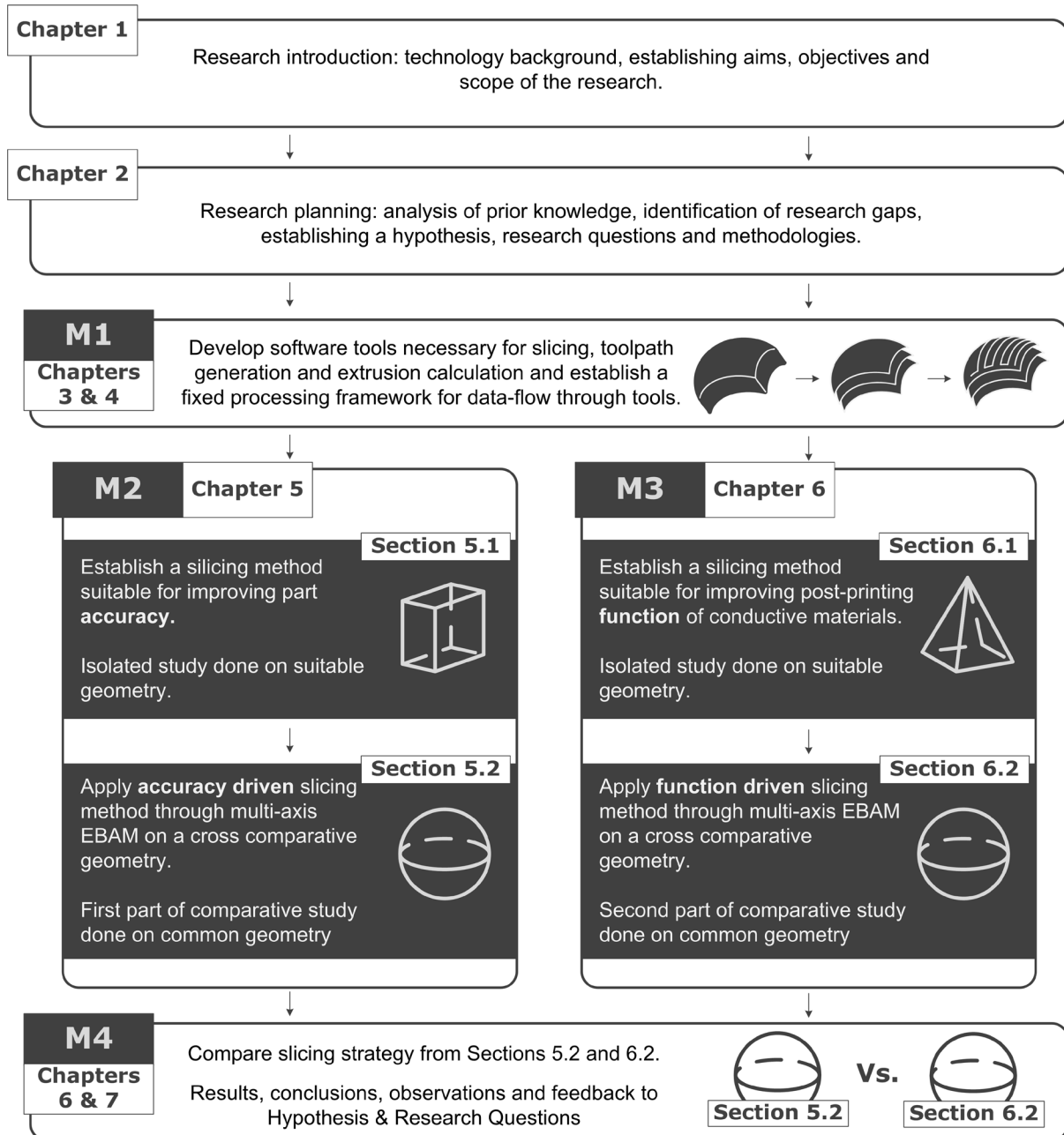


Figure 2.3 Overview of research methods schematics in the context of the entire research

M3. Design of case studies, application of different slicing strategies and measurement of impact on post-printing functionality of conductive materials measured through the

exhibited resistance of conductive tracks (Section 6.1). Application of observations and findings the same fixed geometry serving as a common input parameter for comparison across different case studies (Section 6.2).

M4. Comparison of slicing strategy dedicated on part accuracy vs. slicing strategy dedicated on post-printing functionality of conductive materials, applied on a common part geometry. Conclusions, observations and answers to set hypothesis and research questions. Elaborated in Chapters 6 and 7.



# 3

## Development of a Multi-axis ME Processing Tool and the Associated Algorithms

In Section 1.1, the conceptual steps of a process pipeline for regular 3-axis ME technology were described. Such processing pipeline is extensively used for enabling planar ME technologies in manufacturing products and it has been proven to be a valid, robust way of transferring the process information from the digital model to the manufacturing system. Therefore, it is postulated that the same high-level, conceptual phases could provide for a good starting point when creating a processing tool and pipeline for multi-axis non-planar ME technologies. However, given the multi-axis nature of manufacturing systems envisioned to execute the process and the liberty for a layer to now extend into three-dimensional space, existing 3-axis software solutions available nowadays are unfit for multi-axis ME process. Consequently, it is inevitable that some form of a processing tool and processing steps list is established whenever one aims to research non-planar ME technologies, especially so if there is the intent for an empirical aspect of it.

In this chapter, an in-depth explanation of the processing tool and pipeline established and developed for this research is provided.

---

### 3.1. Introduction

Other researchers have addressed the topic of ME framework or process planning pipeline of non-planar layers. Reference to previous works with CLFDM focus can be made in Section 2.1.2. for an overview of prior work on process implementation. In studies with emphasis on a framework aspect [114], [49] the process planning with the outcome of generating collision-free curved layers suitable for 3-axis printers has been addressed. Other computational frameworks for multi-axis ME volume printing have been described and implemented by [51] and [53]. Higher emphasis has been put on analysing the latter group of prior work since the framework developed here is aiming for the realisation of multi-axis ME manufacturing using 5 axis. An additional study [52] has developed and applied a framework with an aspect on freeform layers with variable layer height.

Investigating previous research on non-planar layered ME framework, high number of different proposals for solution can be noted. It can be argued that this comes from the fact that this topic contains a high degree of design decisions when developing a framework and as such it can not be easily expressed or approached as an exact, deterministic science subject. Instead, it appears that framework design research has generated an assortment of different framework and process planning approaches; a current situation in the research ambience aided also by the very high grade of interdisciplinarity in the topic. Also, many of the framework design approaches have been organised around different objectives, even though the goal of support-free printing appears to be dominating the research direction. While analysing previous works has contributed towards an improved perception of what qualities a multi-axis ME tool would have to possess, it did not reveal such an available software tool suitable for the requirements of this Doctoral Research. Consequently, a non-planar ME processing pipeline is developed for the needs of this study, capable of processing a given part model through the phases of slicing, toolpath generation and physical process realisation.

Tool development was initiated by specifying a list of processing goals that would serve as requirements which if satisfied would be sufficient for the needs of the study. Algorithms were then established in an effort to meet said requirements and ultimately result in an instrument for multi-axis ME implementation. A further benefit for an internal development of a processing framework is the in-depth knowledge and control of all aspects of its function: from computational geometry algorithms to communication with the manufacturing system.

### 3.2. Defining specifications for the ME system

Each processing stage was either inherited from a conventional processing pipeline of a 3-axis context, or an added one arising from the conceptual difference between 3-axis and multi-axis ME technology. It should be acknowledged that even though this list is based on the conventional planar process and supported by extensive previous research on multi-axis ME and CLFDM, its contents are a result of one plausible design specification approach; it does not result from any optimisation procedure or reflect any largely agreed framework in neither industry nor academia. It is instead a list of objectives set within this study that is seen as necessary and that if satisfied, would enable the functionality required to do this study. This approach was considered satisfactory due to the fact that the quality of such a tool, according to any benchmark, is not the primary focus of this Doctoral Research nor this chapter, but rather its sufficient operation as an instrument for non-planar slicing implementation. Furthermore, the case studies have been designed in a way that the design and development choices explained in this chapter have minimal impact on the reported results since the major outcome being analysed here is the slicing i.e. the shape and arrangement of non-planar layers rather than specific details related to their meso-structure or toolpath generation. The order of the following objectives list also reflects the order in which these stages would execute.

*Q1: Intake of a digital geometry.* The very first requirement seen for the processing pipeline and tool development - that coincides also with the first step in a conventional file processing - is the capacity to input a digital geometry in some format. Previous research has had examples of using both tessellated [39] and parametric B-spline [115] CAD representation. For this research, non-uniform rational B-spline (NURBS) geometry was used, eliminating the passage of tessellation and therefore geometrical approximation.

*Q2: Intake of a freeform slicing surface.* Conventional ME process planning builds up the object as a plurality of planar, horizontal layers that approximate the digital geometry. This process can be seen as having a slicing surface that is a planar, horizontal  $X - Y$  plane, and all of the layers are obtained as intersections between the object's geometry and multiple instances of the  $X - Y$  planar slicing surface offset in  $Z$  direction by some distance. In this context, conventional ME technology always uses a planar horizontal plane as a slicing surface.

Contrary to conventional 3-axis ME, previous research on non-planar ME technology documented in Section 2.1.2 has deposited along a variety of non-planar layers that have been obtained in different ways according to the method established in the corresponding research. So it would appear that freeform layer shape could be virtually any freeform surface. In this

research, the term *slicing surface* as described above will depict any non-planar surface that will subsequently be offset in order to find intersections with the digital geometry in the slicing operation. This was defined as a requirement specification since it was seen as a crucial capability that would endow the tool with flexibility in manipulating the non-planar layer arrangement within a part.

Q3: Orthogonal surface offset and slicing. Given that the research keeps a focus on orthogonal 5-axis CLFDM process, an algorithm that performs a uniform orthogonal offset for a given distance of a given freeform surface, is imperative. The offset is required to work for both planar and non-planar surfaces. Finally, in order to locate the trimmed surface that would represent a non-planar layer, the tool needs to have the capability of locating the set of three-dimensional curves obtained by the intersection of a non-planar surface and the volume of the object.

Q4: Intra-layer infill toolpath generation. Following the steps present also in conventional processing protocol, the subsequent phase is to generate a toolpath based on a certain infill strategy. The term toolpath in this research is intended as the ordered array of curves, lines or points that represent the relative positioning between the extrusion nozzle and the substrate. The majority of prior research within the CLFDM scope has been focused on this topic. In this research the aim is put on equipping the software tool with a stable and robust, serpentine-style (zig-zag), toolpath generation algorithm that can generate approximately equidistant trajectories along a freeform surface and alternate the raster orientation between adjacent layers. The computational time of such algorithm was also taken into account due to its impact on practicality and therefore applicability to tests/case studies.

Q5: Inter-layer toolpath generation. In order to generate the entire set of toolpaths for a desired geometrical model, also the movements between consecutive layers needs to be defined, particularly in the aspect of multi-axis ME technologies where collision avoidance is not an issue that can be solved with simple strategies as in the case of conventional, 3-axis process. Therefore this objective requires that the tool generates also the trajectories that define the movement of the machine during the passage from one layer to the next one.

Q6: Extrusion quantity. Another requirement for developing a non-planar tool is for it to eventually be used in a practical environment where the generated output data will be used to control a given manufacturing system through multi-axis ME process. Hence, another necessary information is the amount of material required for extrusion during fabrication. This is modelled as a linear function of the relative distance between the extrusion nozzle and the substrate on top of which material is extruded.

*Q7: Generation of instruction list.* Finally, the last requirement defined for a multi-axis ME tool is the capacity to generate an instruction list that contains the information necessary for guiding the manufacturing process of a given digital geometry and according to the parameters selected through the pipeline. There is no requirement set on the specific format or standard of the file, but rather its effective functionality in interfacing to the manufacturing system.

### 3.3. Slicing procedure

This research adopts the approach of layer-based multi-axis ME. In other words, it adopts the conventional approach of approximating a given geometry by its decomposition in layers. In a general sense, that would also define the slicing process: the operation where the geometrical model is represented by a plurality of surface-like sections that when superimposed, would result in a close approximation of the geometrical model.

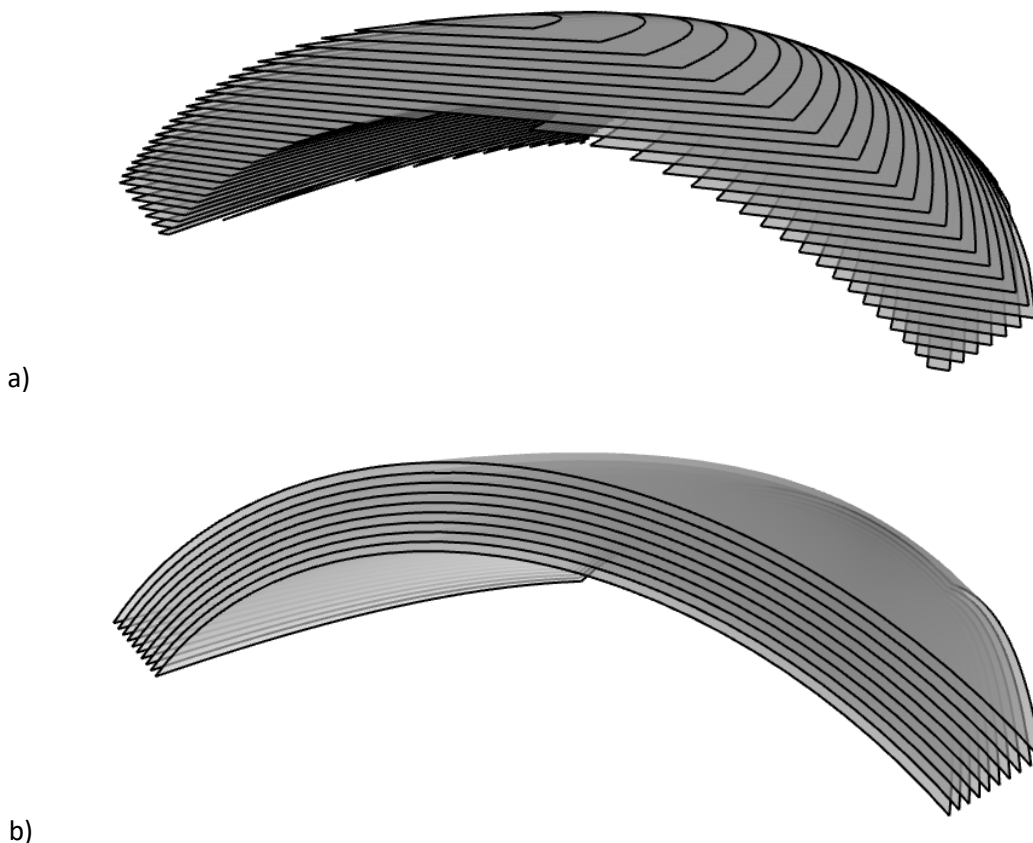


Figure 3.1 An example of slicing approach and layer formation in: a) Conventional, 3-axis slicing, and b) non-planar slicing

In a planar, 3-axis ME context, this converges to the particular case of always approximating the digital geometry with planar layers, becoming so a plurality of cross sections obtained between the digital geometry and a multitude of horizontal planes on a different Z height. In a non-planar, multi-axis ME context, the layers can take any three-dimensional, freeform shape, allowing for the slicing to be done through the intersection between the digital geometry and a plurality of non-planar, freeform surfaces. Re-iterating the comparison between planar and non-planar slicing on an example geometry can be seen in Figure 3.1.

The mathematical modelling and operations necessary for manipulating freeform surfaces is significantly different and computationally more demanding as opposed to planar surfaces. In this work, Rhinoceros® graphical suite [116] and its functions have been used for the computational geometry processing of all geometrical elements encountered throughout this study. Parametric geometries and processing algorithms were used based on Non-uniform rational B-splines (NURBS); an effective mathematical model for creating and representing curves and surfaces through parameters such as control points (vertices), weights and nonrational B-spline basis function of a specific degree [117]. A NURBS surface is characterised with its parametric domain, usually denoted as a square with one dimension designated as the  $U$  direction and the other as the  $V$  direction. An example NURBS surface with its control points is shown in Figure 3.2a) while its parametric domain is depicted in Figure 3.2b).

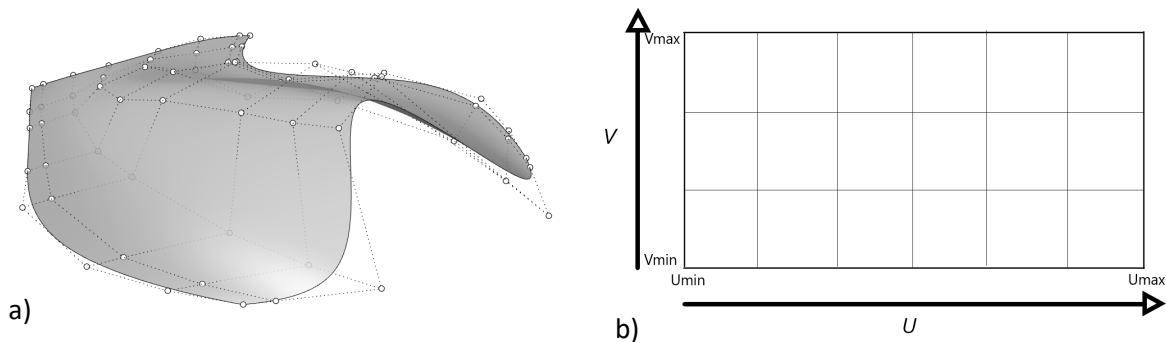


Figure 3.2 An exemplary NURBS surface represented by: a) Its geometric shape and control points, b) parametric domain depiction

Each point of the parametric domain corresponds to a point on the actual geometrical shape of the surface, but correlation might not always be intuitive in that, for instance, the mid point of the parametric space might not correspond to the midpoint of the surface itself. A generic NURBS surface can be expressed as:

$$S_{(u,v)} = \frac{\sum_{i=0}^t \sum_{j=0}^s P_{i,j} w_{i,j} N_{i,p}(u) N_{j,q}(v)}{\sum_{i=0}^t \sum_{j=0}^s w_{i,j} N_{i,p}(u) N_{j,q}(v)} \quad Eq. (1)$$

Where  $P_{i,j}$  represents the net of control vertices with  $t$  and  $s$  number of vertices in  $u$  and  $v$  direction respectively,  $w_{i,j}$  are the weights appointed to those vertices,  $N_{i,p}(u)$  and  $N_{j,q}(v)$  are the B-spline basis functions of order  $p$  in the  $u$  direction and order  $q$  in the  $v$  direction. In this work, all nominal geometric shapes have consisted of NURBS surfaces of order no greater than 3, created from NURBS curves representing their edges of order no greater than 3. Also, nominal surface shapes such as a cone or a sphere, which might lead to a singularity in the parametric domain were not used.

In order to generate a non-planar slicing with a uniform layer thickness, a normal (orthogonal) offset has been used of the selected slicing surface, by a fixed distance throughout the entire span of the surface. This distance is referred to as the layer thickness  $l_h$ . The newly generated offset surface depicted in Figure 3.3 can be represented by [114]:

$$S_{1(u,v)} = S_{(u,v)} \pm l_h * n_{(u,v)} \quad Eq. (2)$$

Where  $n_{(u,v)}$  is the unit normal vector of  $S_{(u,v)}$  at  $(u, v)$ . The topic of offsetting NURBS surfaces and methodologies on how to avoid self intersection has been extensively addressed in prior works, such as by [118].

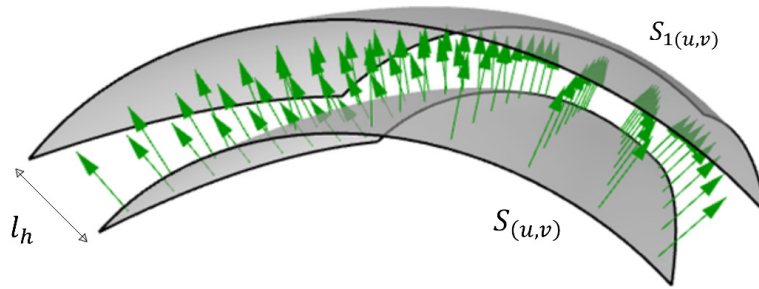


Figure 3.3 Orthogonal (normal) uniform distance offset of a surface

As already mentioned, the offset alone as a step in the slicing algorithm is not sufficient in locating the required layers that would constitute the part. Another necessary step is locating the intersection of offset surfaces and the digital geometry that needs to be manufactured. This in turn generates the trimmed section of the offset surfaces that falls within the enclosed volume of the desired part, describing effectively the portion of the surface where material

would later need to be deposited in order to build up the part. Such trimmed section would only relate to a smaller subset or region of the parametric space of its nominal surface. An example of trimmed surface is shown in Figure 3.4. Therefore, an algorithm has been developed that iteratively performs normal offset as described in Eq. 2 and trims the offset surface to the part's model volume, in order to find the set of all  $k$  necessary layers to build up the part,  $L_k$ .

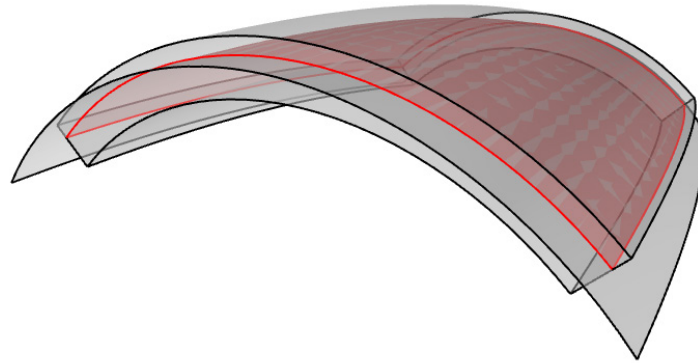


Figure 3.4 Intersection between offset of slicing surface and part volume for layer identification (red)

Throughout the development of slicing and trimming algorithms, this research concluded that if a surface from the geometry of the part model is used as a nominal slicing surface which is subsequently offset a number of times to locate the freeform layers, it is not guaranteed that the newly generated offset surfaces will intersect with the enclosed volume of the part model. This is particularly common at the edges of the surfaces where, depending on the topology of the surface, the local normal vectors and the geometry of the part model, the normal offset generates a new surface that does not extend enough to intersect the part model. Therefore, it would appear that orthogonal slicing by using the surfaces from the CAD model can result in insufficient amount of geometric information, since some form of additional geometric data needs to be added to enable the slicing procedure. This problem is shown in Figure 3.5a) and the solution adopted for this research consisting in the smooth extension of the edges in Figure 3.5b).

This issue of a lack of intersection between the part's model and the offset surface has also been briefly noted by [114] where enlargement coefficient has been used, albeit with little detail of the exact methodology. With intentions on maintaining the perpendicular offset intact, the methodology developed here avoided the use of enlargement coefficients that could modify or distort the nominal orthogonal offset. Instead, it involved a surface extension along the edges, that is, the curves corresponding to  $u_{min}$ ,  $u_{max}$ ,  $v_{min}$  and  $v_{max}$  of the slicing surface,



in order for the newly generated surfaces to intersect the CAD model, as shown in Figure 3.5b). The extension is done for a predefined length that varied based on the part model and preserved the local surface curvature. No other studies were encountered in the literature review that analyse the lack of geometrical data necessary for performing an optimal non-planar slicing or methodologies on how to deal with this issue.

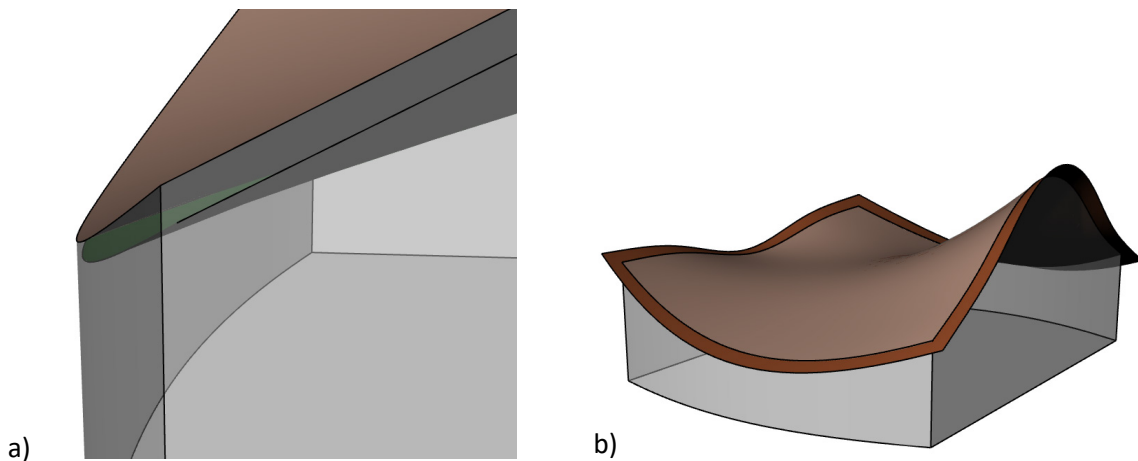


Figure 3.5 Insufficient geometrical data when slicing with surfaces from CAD model: a) No intersection between orthogonal offset and part model, b) proposed solution by smooth surface extension (dark brown)

The above described steps and basis of the slicing algorithm were considered satisfactory in terms of reaching objectives O1, O2 and O3 described in the list of Section 3.2. The described method enables the slicing of any CAD geometry with theoretically any NURBS surface, regardless if it is a surface extracted from the part's model or a different one, as long as its necessary offsets required for slicing are fully defined and not self-intersecting.

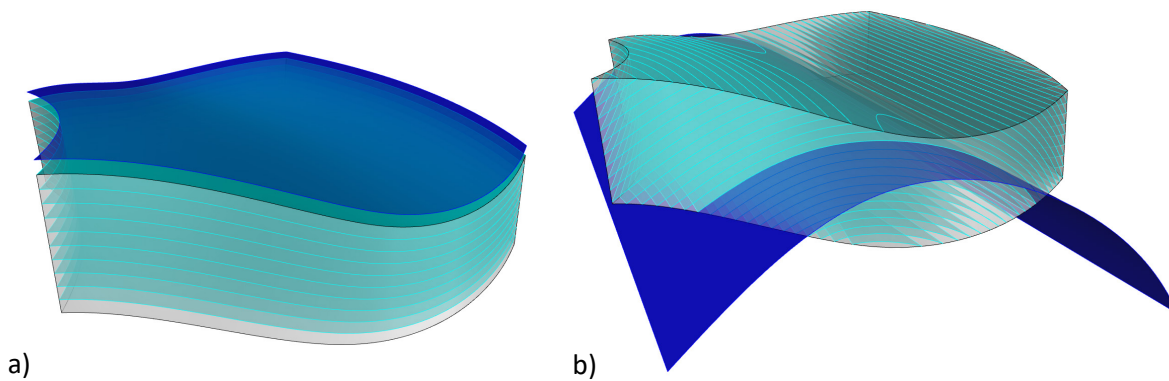


Figure 3.6 Example of freeform slicing on a uniform thickness part. Dark blue: slicing surface, light blue: obtained layers, transparent grey: part model a) Using surface from part model b) using surface not belonging to part's model

Figure 2.2 graphically depicting the Hypothesis set forward for this research, also shows the diversity of the slicing algorithm developed here. Additional cases of slicing using a surface from the part model (a) and user defined surface (b) on an exemplary model are represented in Figure 3.6.

### 3.4. Toolpath development

Toolpath generation is a step where critical differences can be noted between conventional and non-planar ME technologies. One reason for this is the geometrical space in which the toolpaths need to span. Namely, in planar ME technologies, the layers are maintained horizontal and described with a plurality of planar curves that designate some enclosed space where eventually build material would be deposited, whereas the rest of the surface area on the other hand might potentially contain toolpaths for deposition of support material. Regardless of whether build material or support material toolpaths are deposited within a layer, in conventional flat ME process, they always infill a limited 2D planar space.

Contrary to this, and with reference to Section 3.2 and the slicing operation, in non-planar, multi-axis ME setup the toolpaths need to be generated as a plurality of ordered curves that belong to the specific non-planar layer surface. Following this approach, the equidistance between two consecutive non-planar layers guaranteed by the orthogonal offset during the slicing operations, can now be transferred as a characteristics to the generated toolpaths. This in turn defines a uniform layer thickness and hence, a uniform theoretical filament height along the entire layer. The aspect of generating toolpaths has been the biggest focus of prior research with numerous of publications dealing with varying methods, each with a different set of assumptions and approximations [40], [52]. One feature that has often been pointed out is the necessity of these toolpaths to be equidistant in order to enable a controlled contact line between consecutive filament strands [28]. In that work the authors argue that due to the equidistant characteristics, CLFDM toolpaths need to sway away from iso-parametric toolpaths and instead be more similar to iso-scallop toolpaths developed in previous works on subtractive technology.

In this work, an algorithm that developed non-planar, multi-axis ME toolpaths based on the parametric values of a freeform surface was created. Trimmed surfaces representing the non-planar layers generated previously in the slicing step are used as input. Infill strategy is limited to parallel zig-zag pattern and the direction of the toolpaths follows one of the  $u_{min}$  or  $v_{min}$  surface edges for a given layer  $i$ , which then alternates for the subsequent layer  $i + 1$  for an

improved structural integrity of the practical case studies [36]. In order to make sure that the toolpath span over the entirety of the required layer, the information of its untrimmed surface was extracted and used as a guide for the  $u_{min}$  or  $v_{min}$  direction. In the following, a list of operations that summarise the flow and operation of the toolpath generation algorithm:

1. Intake of  $k$  non-planar layer surfaces from the set of all layers necessary to build a given part  $L_k$ , and extraction of their untrimmed mathematical models  $S_{1...k}$ , as described by Eq. 1.
2. Selection between  $u_{min}$  or  $v_{min}$  of a starting parametric direction for toolpath orientation of first layer. This direction is then alternated for adjacent layers to obtain a deposition with a varying raster angle.
3. Extraction of  $x$  iso-curves  $I_{1...x}$  parallel to parametric direction selected in step 2. Iso-curves parametrically parallel to  $u_{min}$ , and spanning between  $u_{min}$  and  $u_{max}$  parametric space, are obtained by solving Eq. 1 for a constant  $u$  parameter. Same analogy can be applied for iso-curves spanning between  $v_{min}$  and  $v_{max}$ .
4. Division of each iso-curve  $I_{1...x}$  into segments with equal, pre-set length:  $I_{11}, I_{12}, \dots, I_{1a}, I_{21}, I_{22} \dots I_{2b}, I_{31}, I_{32} \dots I_{3c} \dots$ , where  $a, b, c \dots$  represent the number of segments of equal length created for each iso-curve based on their respective length.
5. Interpolating  $y$  open 3<sup>rd</sup> degree NURBS curves on corresponding layer surface as follows: all end points of all first segments  $\sum_{i=1}^x I_{i1}$  interpolated into a first curve, all end points of all second segments  $\sum_{i=1}^x I_{i2}$  interpolated into a second curve etc., until the completion of all segments' end points.
6. Trimming  $y$  curves obtained in step 5 according to the trimmed region of the layer or its offset, generating  $Y_t$  which denotes the set of all raw equidistant toolpaths of said layer.
7. Extracting trimmed layer edge data and using it to construct 1 suitable contour toolpath  $C_t$  per layer.
8. Joining contour toolpath  $C_t$  to set of infill toolpaths  $Y_t$  into a single toolpath per layer  $T_t$ .
9. Repetition of steps 2-8 for each layer from the set of all layers required to build a given part  $L_k$ .

This algorithm was used on a layer level for generating toolpaths that first deposited a contour filament that defined the borders of the layer, followed by an internal infill serpentine-like

toolpath that deposited the surface of the freeform layer. In addition to taking freeform layers as input, toolpath algorithms were also designed for intake of curves as input, in which case they would simply follow the provided curve for toolpath generation, combined with the safety movements. This feature was necessary for the realisation of some of the case studies in this research that are designed in a multi-material context. The above described steps and basis of the intra-layer toolpath generation algorithm were considered satisfactory in terms of reaching objective O4 described in the list of Section 3.2.

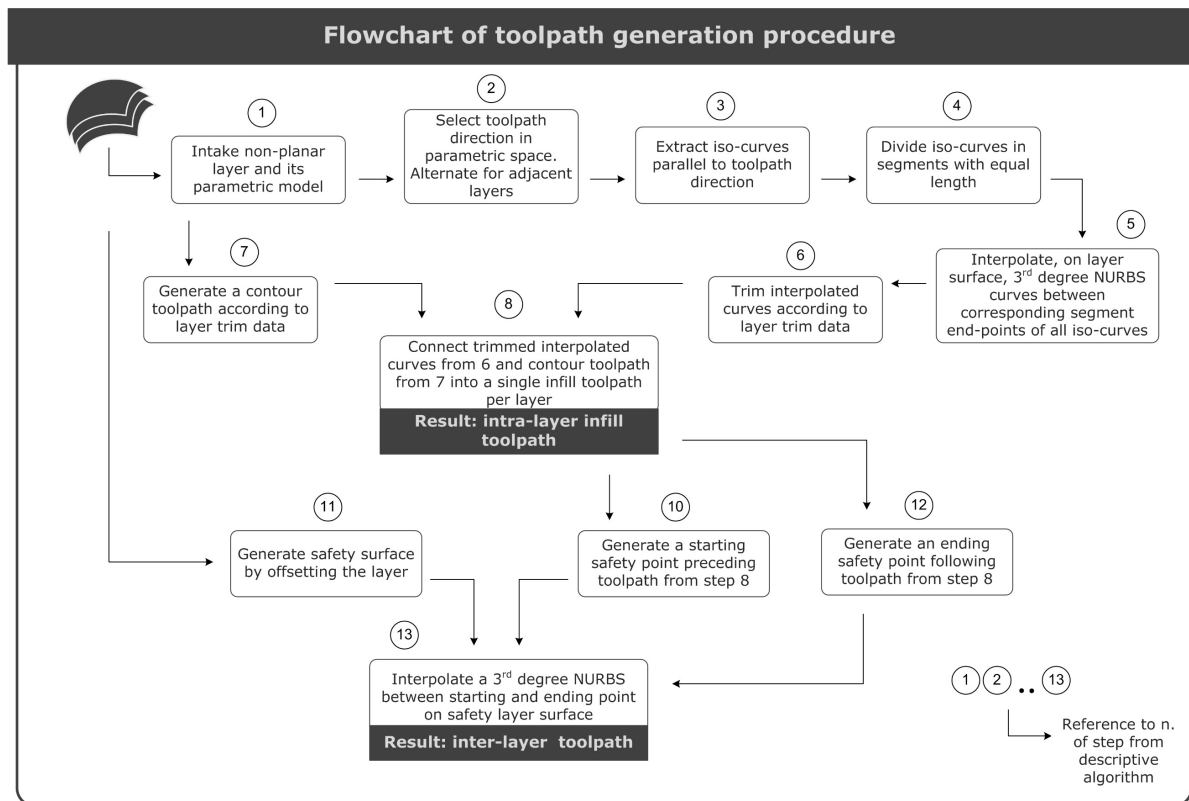


Figure 3.7 Flowchart of the implemented steps for generating both intra-layer infill and inter-layer toolpaths

With the intention for efficient tool that will enable the automatic toolpath generation for an entire part model, an additional algorithm was developed for inter-layer toolpath generation. Namely, once the deposition of a single isolated layer has been fulfilled, a passage to the following layer needs to be done. In conventional 3-axis ME, due to the planarity of the layers and their perpendicularity to the Z axis, a relatively simple movement in Z axis is sufficient to increase the distance between the deposition nozzle and the deposited layer, so that the movements for the following layer can be initiated, effectively eliminating in great deal the danger of collisions. However, in multi-axis ME technology, simply employing a movement in Z axis does not guarantee that a subsequent linear move to the starting point of the next layer

will not cause collision between the deposition head and the already deposited layers. Therefore, an additional algorithm for inter-layer toolpath generation was developed that involved the following steps:

10. Generation of a starting safety point  $P_{ss}$  for  $T_{ti}$  toolpath of layer  $i$ , by translating the end point of  $T_{ti}$  by a distance  $s_d * l_h$  along  $n_{si}$ , where  $l_h$  is the layer height and  $n_{si}$  is the normal vector of the layer surface at end point of  $T_{ti}$ , and  $s_d$  is a safety distance parameter.
11. Generation of a safety surface  $S_{si(u,v)} = S_{i(u,v)} + S_d * l_h * n_{i(u,v)}$ , where  $S_{i(u,v)}$  is the surface of layer  $i$ .
12. Generation of an ending safety point  $P_{es}$  for  $T_{ti}$  toolpath of layer  $i$ , by translating the start point of  $T_{ti+1}$  by a distance  $(s_d - 1) * l_h$  along  $n_{si+1}$ , where  $l_h$  is the layer height and  $n_{si+1}$  is the normal vector of the layer surface at start point of  $T_{ti+1}$ .
13. Interpolating a 3<sup>rd</sup> degree open NURBS curve on surface  $S_{si(u,v)}$  between points  $P_{ss}$  and  $P_{es}$  in order to generate a safety toolpath  $T_{tsi}$  between adjacent layers  $i$  and  $i + 1$ .
14. Repetition of steps 10-14 for each layer  $i$ , for  $i = 1, 2, \dots, k$ , and generate  $k - 1$  safety toolpaths.

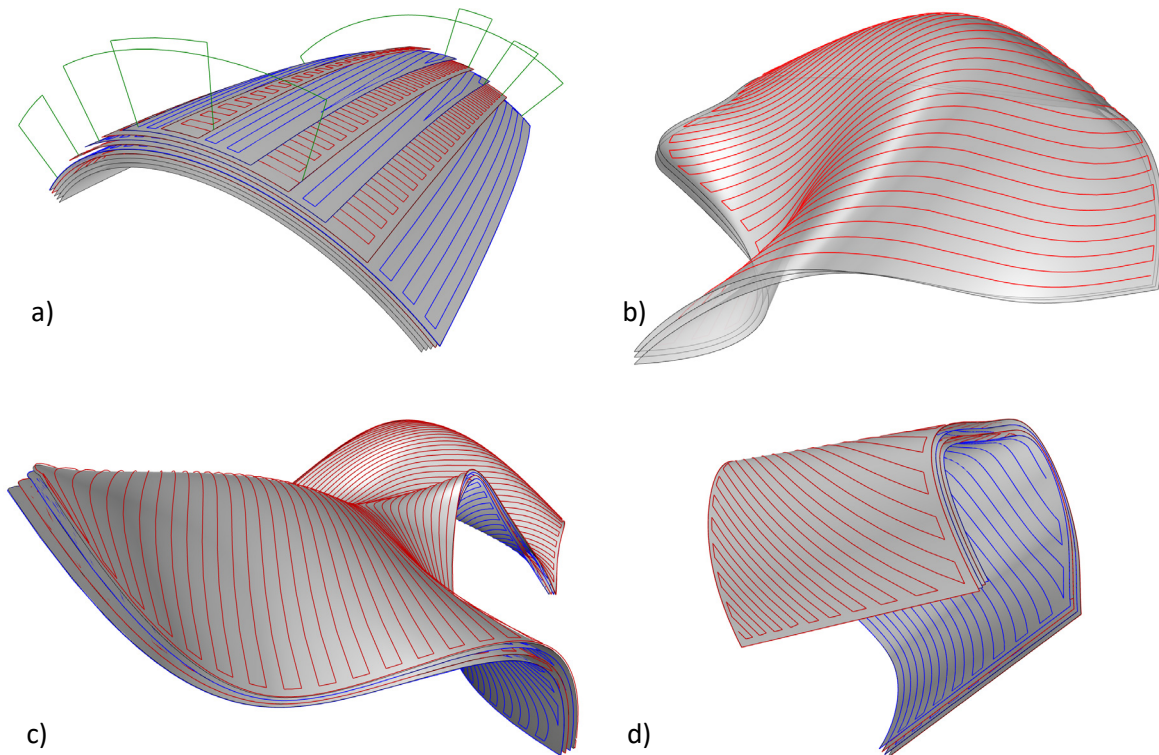


Figure 3.8 Toolpath algorithm applied to a variety of freeform layers with different shape. Intra-layer infill toolpaths represented in red and blue in a)-d), while inter-layer safety movements shown in green in a)

The above described steps and basis of the intra-layer toolpath generation algorithm were considered satisfactory in terms of reaching objective O5 described in the list of Section 3.2. Integrating both the intra-layer and inter-layer toolpath generation algorithms as described above and in the flowchart in Figure 3.7, resulted in an ordered, continuous array of curves that explained all motion aspects required for a multi-axis ME process. Figure 3.8 shows several examples of the toolpath algorithm applied to different non-planar layer surfaces of varying topology, complexity and scale.

### 3.5. Extrusion data management and instruction list

ME processing software tools generate output files that are heavily based on many variations of the ISO 6983-1:2009 standard [14] and also known as G-code. G-code is a set of instructions regulations that describe a format, or a way, of transmitting data from digital processing stage to a manufacturing system. Chronologically, it was initially used for other technologies such as machining and was later introduced in the AM environment. Historically extended presence and considerable use has led G-code to envelop many variations, even within the limited scope of non-proprietary software tools for planar ME [119]. It should be acknowledged that using G-code as a way to transmit data to a manufacturing system has its limitations [120], and due to its conception decades ago, it can be regarded as an outdated method in some aspects and the bottleneck for the next generation manufacturing systems. However, noting it is currently the dominating output format of non-proprietary software tools for conventional 3-axis ME, many of which are used in academic research, g-code can be considered as an effective vector of data transmission for a multi-axis ME process. It has recently been adopted also by other researchers in a multi-axis ME context [52].

G-code files used in the area of ME technologies contain instructions that explain the 3D printing process. It can be grouped in two categories: instructions that control process parameters or particular machine behaviour such as extrusion temperature, activity of cooling fans, homing procedures etc., and motion instructions that point by point describe the movement and quantity of material to be extruded during the movements. The first category commonly require definition only in a few distinct instances during the printing process, while the latter category of instructions are what provides for most of the contents of the document and are specified on a point-to-point basis, in order to accurately describe the motion and material extrusion of the printing process. The point-to-point characteristic comes from the fact that toolpaths are most commonly described by discretising, or rather, sampling of points, in order to be recreated by the manufacturing system by means of linear interpolation.

```

G0 F300 X36.178 Y-1.656 Z0.25
;TYPC:SKIRT
G1 F480 X36.196 Y-1.439 C0.01811
G1 X36.931 Y8.602 C0.85525
G1 X36.945 Y8.831 C0.87433
G1 X37.498 Y20.303 C1.82934

```

Figure 3.9 Snippet of a 3-axis g code generated by CURA [31], post processed to fit manufacturing system

As described in previous Section 3.4, open, 3<sup>rd</sup> degree NURBS curves were used during the toolpath generation phase. A discretising algorithm was then used in order to approximate those NURBS curves ( $t_i$ ) by the lowest number of linear segments ( $l_{sij}$ ) that would result in a poly-line with a maximum allowed dimensional deviation  $e_{max} = 0.02$  [mm] with respect to the respective source NURBS curve (Figure 3.10a)). The extreme points ( $p_{ij}$ ) of those segments were then analysed as a function of the parametric space of the corresponding layer surface for subsequent creation of the instruction list, since they represent the carrier of all geometric information that will be streamlined down the process chain.

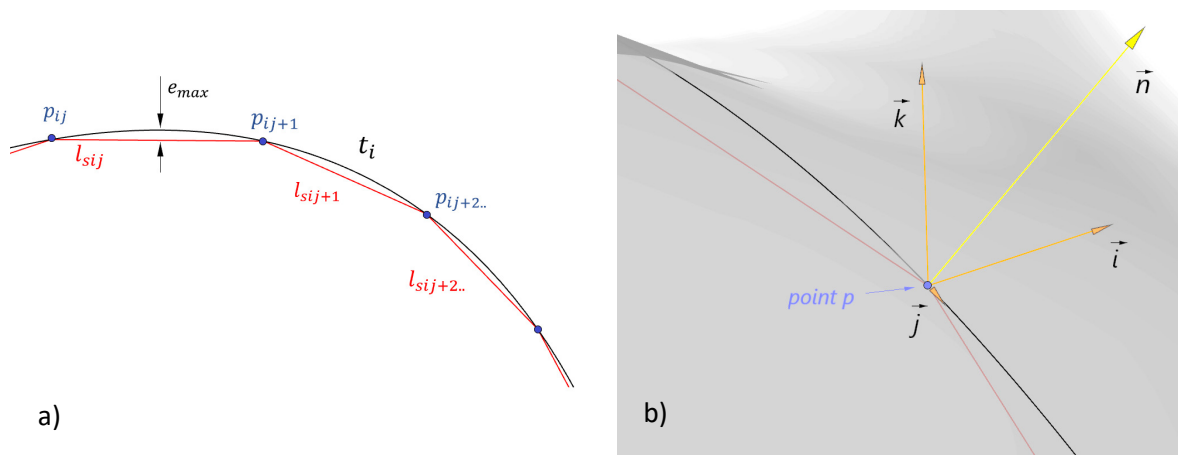


Figure 3.10 Procedure for point extraction from curves for linear interpolation: a) Sampling of source NURBS curve for linear segment poly-line b) Surface evaluation in point  $p_((u,v))$  and extraction of unit normal vector and its projections along X, Y and Z axis of coordinate system

In a conventional 3-axis ME setup, in order to explain the motion aspect of the manufacturing system, the coordinates of these points in the correct sequence would be sufficient. However, in the case of a multi-axis context, besides the need to control the relative positioning between the substrate and the deposition nozzle, it is also required to maintain a perpendicular orientation between the local deposition surface and the deposition nozzle. Hence, additional information needs to be retrieved from the points which consists in the  $\vec{i}$ ,  $\vec{j}$  and  $\vec{k}$  projections

of the surface normal unit vector in the corresponding point along the  $X$ ,  $Y$  and  $Z$  axis of the part model coordinate system, as shown in Figure 3.10b). Three variables are collected from the points in order to understand the orientation of the normal vector and therefore the relative orientation between the part and the extrusion nozzle, however, 2 rotary axes on a machine are sufficient to reach the desired orientation, through the application of the inverse kinematics of the manufacturing systems used. Consequently, five variables were reported in the instruction list regarding the motion aspect of the machine:  $X$ ,  $Y$ ,  $Z$ ,  $A$  and  $B$ , where  $A$  and  $B$  describe the movement of two rotary axis, mutually perpendicular to each other. The manufacturing system used for this study is explained in detail in Chapter 4.

Lastly, the quantity of extruded material needs to be controlled synchronously with the rest of the motion axes in order to accurately execute the manufacturing process. Similarly to the case of conventional 3-axis ME technologies where the extrusion quantity is reported with every point in the toolpath, much like a motion axis itself, the same approach was maintained in this study. The quantity of extrusion  $e$  [ $mm^3$ ] was approximated as a volume of a parallelepiped where the length is represented by the distance between each two consecutive points, the width  $W$  [ $mm$ ] is represented as 120% of the nozzle diameter  $d$  and the height  $l_h$  [ $mm$ ] is the selected layer thickness. Therefore, the quantity of material to be extruded, in  $mm^3$ , during a movement between point  $i$  and  $i + 1$ , is calculated as:

$$e = \sqrt{(X_{i+1} - X_i)^2 + (Y_{i+1} - Y_i)^2 + (Z_{i+1} - Z_i)^2} \times W \times l_h \quad Eq. (3)$$

Due to mass conservation principle, the same quantity of material has to be extruded through the nozzle of the extruder with a nozzle diameter  $d$  [ $mm$ ] and distance of cylindrical extrudate relative to the extruder nozzle, referred to here as nozzle distance  $n_d$  [ $mm$ ]:

$$e = \frac{\pi d^2}{4} \times n_d \quad Eq. (4)$$

Also, the same material quantity needs to equal the mass input in the extrusion system in the form of a filament with a specific diameter  $f_d$  [ $mm$ ]. The material is then fed into the system by actuating a motor that pushes the filament for a given filament length  $f_l$  [ $mm$ ].

$$e = \frac{\pi f_d^2}{4} \times f_l \quad Eq. (5)$$

By manipulating Eq. 1 – 3, it is possible to relate the quantity of material extruded during movement to the actuation system used to feed it, or in other words, solve for the  $f_l$  variable



according to the specific hardware used. The extrusion was then added as a 6<sup>th</sup> variable C that was reported on a point-to-point basis in the G-code based instruction list. A snippet from this instruction list is shown in Figure 3.11.

```
G92 C3  
G92 C0  
G01 X6.074 Y-23.832 Z46.479 A-12.97039 B37.40186 C0.44279 F300  
G01 X5.720 Y-23.774 Z46.731 A-12.97039 B34.88735 C0.89215  
G01 X5.349 Y-23.719 Z46.971 A-12.97039 B32.33769 C1.34779
```

*Figure 3.11 Snippet of the 5axis g-code instruction list sent to manufacturing system*

The g-code instruction list was completed with additional control for material extrusion (retraction and compensation) before and after all movements generated by the inter-layer toolpath generator. This was done to obtain an improved quality in the experimental phase.

### 3.6. Overview of processing framework

The above algorithms outlined in Sections 3.3, 3.4 and 3.5 provide the details on how specific multi-axis implementation aspects have been affronted in the phase of software tool development. In this section, an ordered summary of all steps taken to arrive to a g-code file executable on a multi-axis manufacturing system starting from the 3D part model is presented and discussed. Graphical representation of the processing framework with its dataflow down the processing pipeline is presented in Figure 3.12.

The processing framework defined and developed for this work can be identified as having three main distinct phases. In an initial slicing phase, starting from an input that is the 3D part geometry, the goal is to arrive to all of the layers which would reconstruct the part. This initial phase would cover the developments in Section 3.3. The layers therefore are represented by plurality of freeform, 3-dimensional surfaces that once deposited would approximate the part geometry to a high extent. It can be noted that as depicted in the Figure 3.12, it is foreseen that more than one slicing procedure can be performed on a single part model. Examples of such multi-surface slicing can be seen later in Chapter 5 and 6.

The second and most elaborate phase would cover the remaining steps towards reaching all of the motion and process data required for guiding the manufacturing of the desired part, also known as Computer Aided Manufacturing (CAM) data.

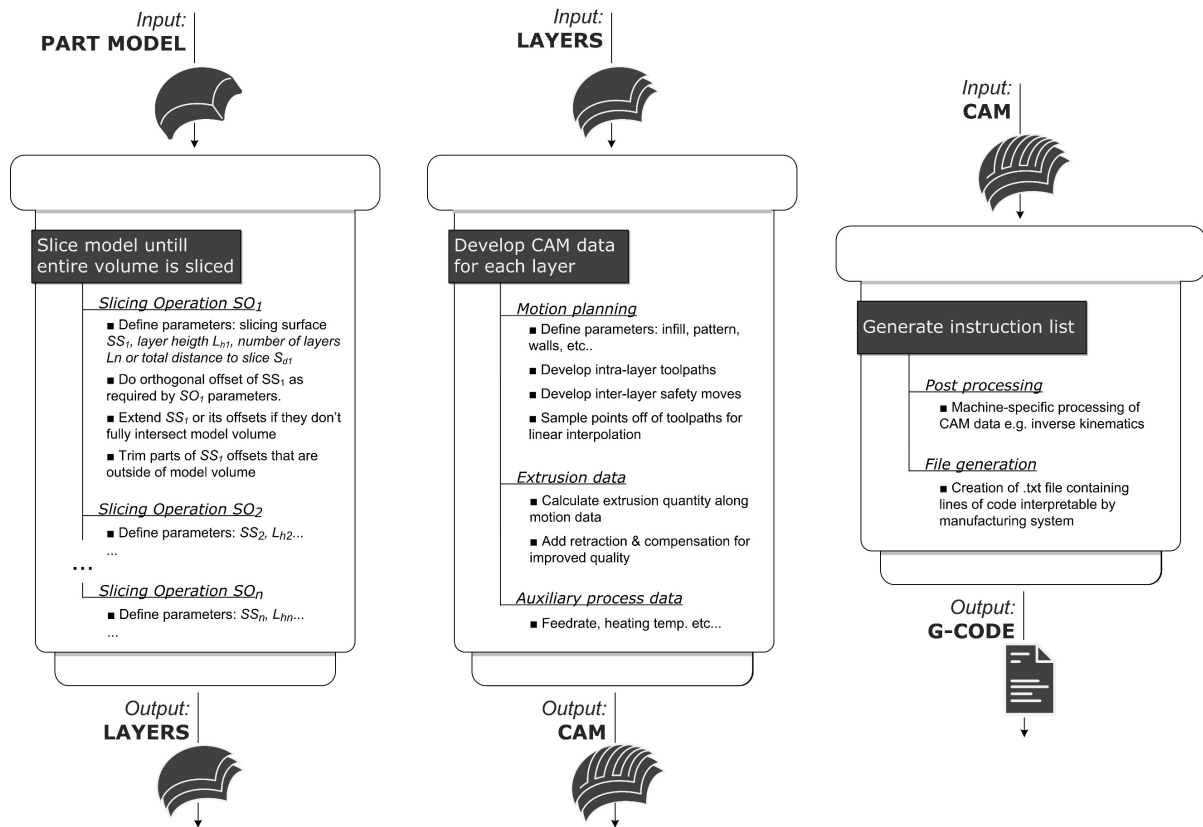


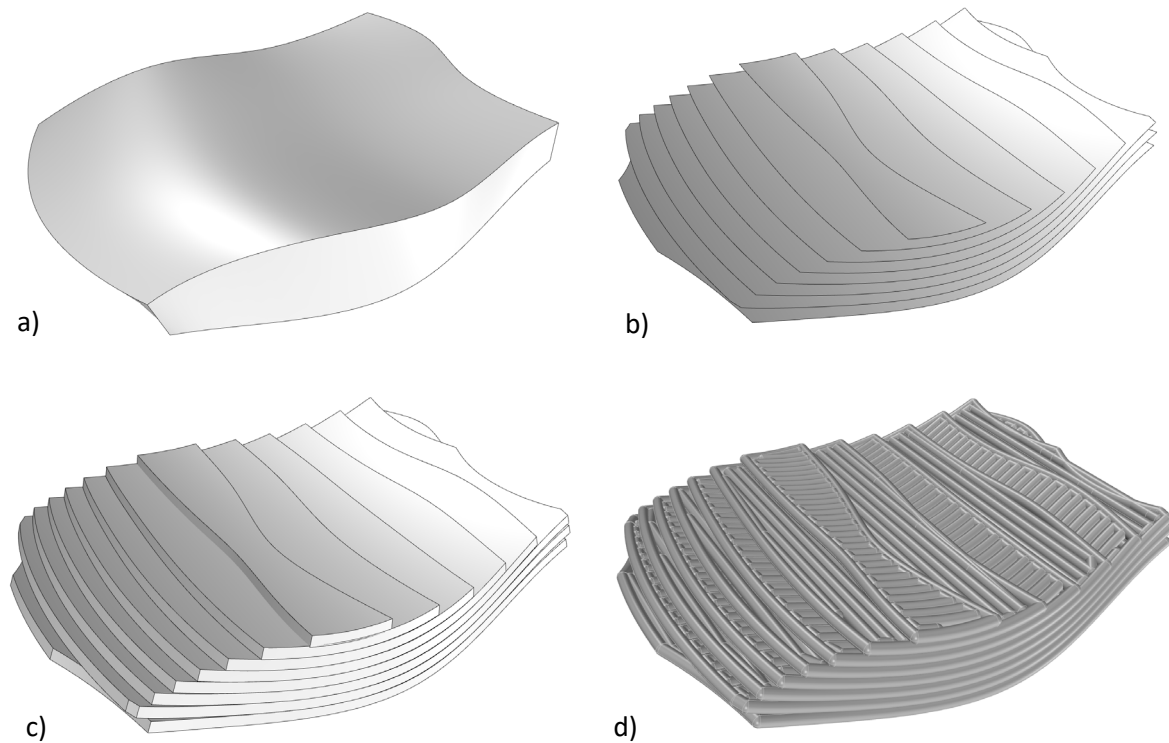
Figure 3.12 An overview of the processing framework and flow of information through it

It uses the layers developed in the preceding slicing phase as input and generates the CAM data, that in this work, is represented by plurality of geometrical points densely sampled from the toolpaths, with process data associated to some of them e.g. quantity of material to be extruded, velocity at which manufacturing would take place, extruder temperature etc. Therefore, all of the information theoretically necessary for the manufacturing of the part is known and defined at the end of this phase.

The third and final phase represents the application of CAM data to an actual manufacturing system through an instruction list in a form of a file. It is at this point that the data is adjusted according to the real-world multi-axis machine that will produce the part. Finally, a text file is generated and run by the control system installed on the machine with the purpose of guiding it through the manufacturing process as described by the CAM data.

The shape of this processing framework as summarised here has been maintained throughout this study. One aspect worth noting is that it does not need to be implemented all the way to the end for useful information to be generated. Partially processed data across the pipeline can be selectively picked out and used for simulation or process planning. In one example in Figure 3.13c), the layers generated after the slicing phase can be used to recreate also their thickness

and provide an idea about the upcoming process planning, before undergoing the computational burden of CAM data. In another example in Figure 3.13d), the CAM data itself can be used for a detailed simulation of the mesostructured of the obtained part since both the motion planning and process data are known.



*Figure 3.13 Different phases of data processing: a) 3D part model, b) Layers, output of slicing phase, c) process planning simulation based on layers only, d) process planning simulation based on toolpaths with alternating orientation*

All of the algorithms and procedures falling under the scope of computational geometry, or in any case, digital processing up to the manufacturing of the part were implemented using the Rhinoceros® software suite [116]. It should be acknowledged that the processing framework defined and used in this work represents one embodiment of many imaginable varieties for multi-axis ME technology implementation methods or data formats.

### 3.7 Conclusions

A processing tool for multi-axis ME technology represents a conglomerate of digital algorithms and procedures, interconnected in a defined protocol for elaborating digital data with the purpose of enabling the practical execution of said technology for the scope of

manufacturing desired objects. This research concluded that a defined consensus for how such processing tool needs to be organised does not yet exist, neither in academic nor in industrial realm. One possible reason could be that the high number of algorithms that need to be addressed, each with its own set of possible approaches to solution, leads to high variety of processing tool outcomes.

Throughout the analysis of Chapter 3, this research has established a processing tool and framework for layer-based multi-axis ME technology, where multiple slicing operations can be implemented in order to provide the flexibility to guide the slicing strategy for the manufacturing of a desired object, thus reaching the objective of developing a suitable framework for conducting the studies of this research. Furthermore, it has identified three core phases of the data processing:

- Slicing phase: a phase where the passage is made from the part's model to the layers through the definition of slicing operations.
- CAM phase: a phase where each of the identified layers is further elaborated for the development of toolpaths that define the motion aspect of the manufacturing procedure, coupled with auxiliary manufacturing data for process execution.
- Instruction list phase: a phase where the CAM information is used to construct a digital file for a suitable manufacturing system.

An additional important aspect that has been identified during the development of the processing tool is the need for additional geometrical information in certain slicing operations as mentioned in section 3.3. Namely, when the slicing is done using geometry information from the part model itself, there is a possibility that normal orthogonal offset does not result in a surface that intersects the parts volume. In such occasions there is a need for extrapolating additional geometry information that will enable the suitable generation of necessary layers. In this research, this issue has been addressed by extending the slicing surface along its edges, by following the curvature, but other methods could provide a suitable solution as well.

Lastly, it is worth noting that other elements or algorithms can be incorporated within similar processing tools for multi-axis ME technology, such as for example an advanced collision detection algorithm or various simulations of the motion aspect, process measurement and execution or part quality, that can augment the use and efficiency of the processing tool as a whole. These additional elements can also be directly related to a particular manufacturing system design as described in [121] such as the on-board control or sensorics sub-systems.

# 4

## Prelude to Experiments

Chapter 4 is intended to serve as a brief prelude to the empirical phase of this work. It aims to describe the multi-axis manufacturing system and its primary hardware aspects, the process parameters selected for the rest of the experiments and the manufacturing of a pilot case with multi-axis ME technology. The pilot case manufacturing is seen as a validation of operation for the entire chain of tools and processing sequences as it helped in relating the entire framework developed here with previous work done in this field.

It is acknowledged that the aspects elaborated in this chapter have a limited academic potential. Yet, their reporting was seen a key element in enabling transparency, reproducibility and integrity of the undertaken research work. This is also enhanced by the fact that orthogonal, layer-based, multi-axis ME manufacturing requires the integration of several different fields, for instance: computational geometry, process planning, multi-axis mechatronic systems, multi-axis motion and process control. This could arguably be one of the reasons why its practical implementation is still relatively rare with only a handful of instances in previous studies. Therefore, it was considered that a holistic overview of the technology could provide the reader with a better understanding of how these different pieces could fit together, impact each other and potentially, through this comprehensive perspective, stimulate future, more specific, research endeavours.

---

## 4.1. Multi-axis manufacturing system and process parameters

The multi-axis manufacturing system used in the experimental procedures for this Doctoral Research was a 5-axis machine with an  $X - Z$  configuration on the extrusion tool, and a  $Y, A$  and  $B$  configuration on the deposition platform. The kinematics setup and a picture of the system are shown in Figure 4.1.

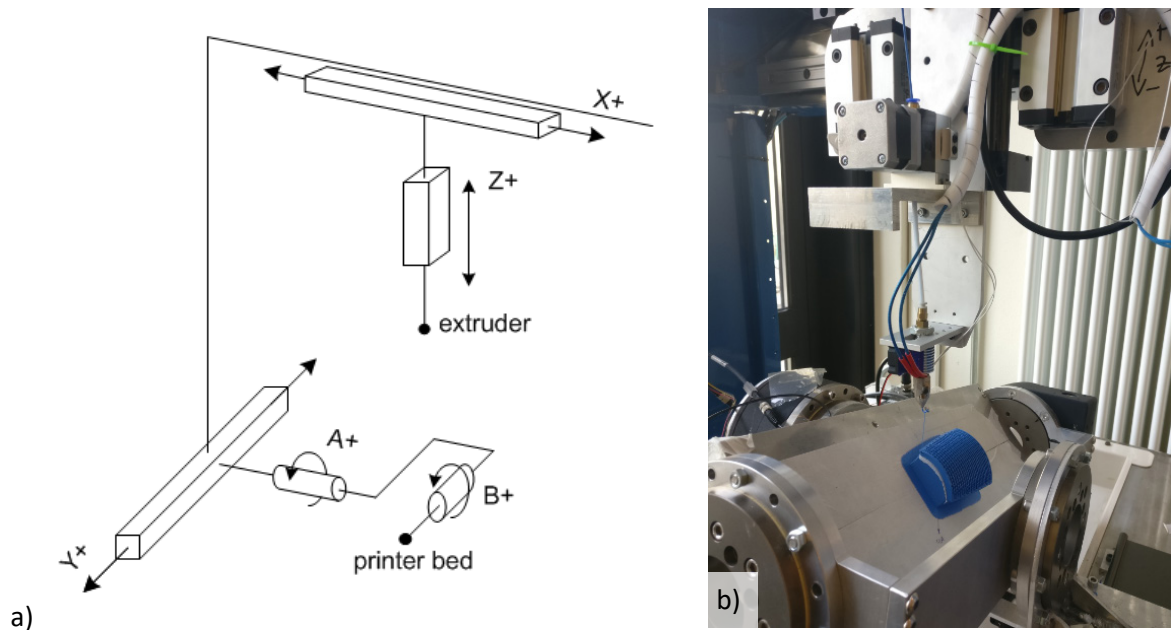


Figure 4.1 Description of the manufacturing system: a) Kinematic schematics and b) photograph of the multi-axis manufacturing system used for the study

The multi-axis system is equipped with 5 NEMA 23 stepper motors joined in 3 linear and 2 rotary motion assemblies from *IGUS*. Both the motion control module and the rest of the control system was based on *LinuxCNC* [122] platform and control was done in open-loop without the use of any type of positional or velocity feedback. The machine was equipped with 5 proximity sensors that were used to establish a repetitive homing sequence. Mechanical backlash errors were measured with a comparator and an average value for each axis was used for software backlash compensation. After homing, the planarity of the deposition platform was reported within  $\pm 0.035\text{mm}$ .

The manufacturing system featured an extrusion subsystem comprising *Bulldog XL* filament extruder and a modified *E3D v6* hot-end, in a Bowden setup with  $8\text{cm}$  of filament distance between them. *MKS Gen L V1.0* electronics board was used to control the temperature. One  $12\text{V}$  cooling fan was used to cool down the hot-end and no other cooling fans aimed at the

deposited filaments were used. The modification of the hot-end consisted in implementing an in-house developed aluminium extrusion nozzle, with an integrated cone-shaped heat block, that enabled a higher liberty in relative movement between the nozzle and deposition substrate without physical collisions as shown in Figure 4.2. The inclination of the heat block was designed as to enable  $\pm 60$  degrees of clearance angle.

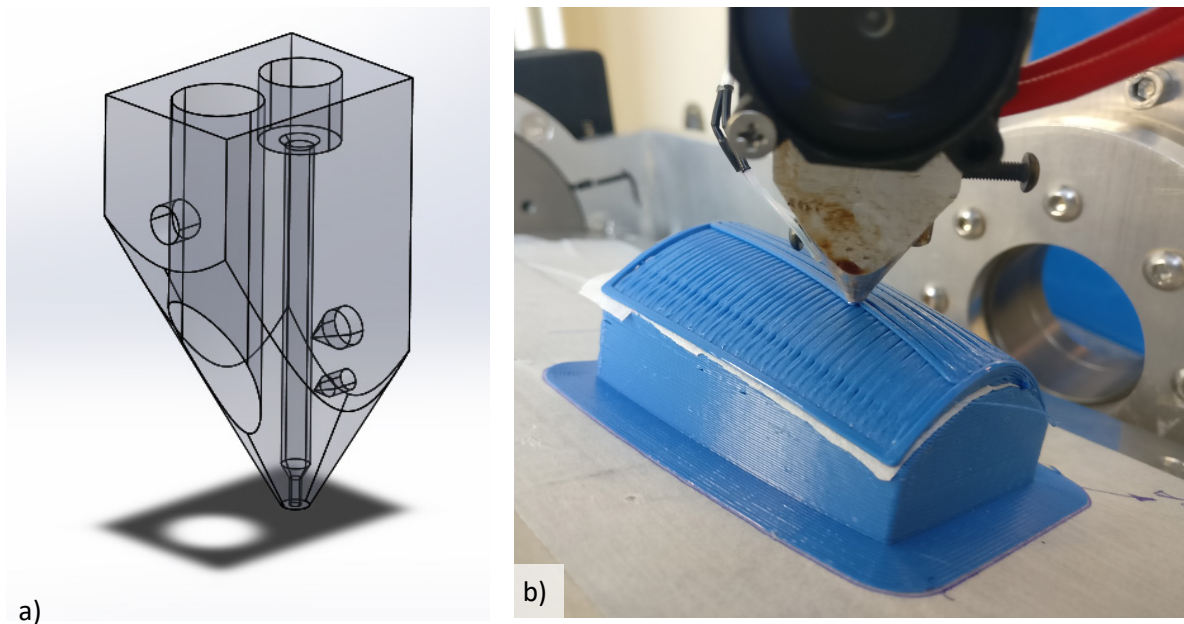


Figure 4.2 Conical shape design of extruder's nozzle: a) 3D model and b) a close-up photograph of the nozzle during manufacturing of one case study

As it has been noted in previous research on this topic, freeform layered deposition requires a suitable shaped support that will physically sustain the deposition of layers. In this research, the support was created by conventional 3-axis ME technology with a build file generated through *CURA* software [31]. Multiple case studies shared the geometry of the bottom-most surface, so multiple case studies were able to be deposited on the same support structure; yet another observation characteristic of multi-axis as opposed to planar layer ME. A single layer of paper tape was placed on top of the support structure before each multi-axis print. Paper tape is a common practice in ME, but while it is mostly used for an improved adhesion between the printing bed and the newly deposited material, in this work it was primarily done for a facilitated separation between the support and part structure after printing, in order to avoid plastically deforming the case studies samples during removal. All case studies have been processed with the toolpath generation algorithms described in Chapter 3, with a desired distance between adjacent toolpaths of  $1.5\text{ mm}$ , while the nominal width of deposited filament was  $1.1\text{ mm}$  varying  $\pm 10\%$ . The material used for all studies for both the support structure

and the build materials was *PLA+* from *Sunlu*. It was selected due to its ability to maintain its form after being deposited without warping and good adhesion properties to paper tape.

The processing parameters selected for all of the case studies are reported in Table 4.1 below.

<b>Material</b>	PLA+ from <i>Sunlu</i>	<b>Extrusion temp</b>	200 °C
<b>Nozzle diameter</b>	0.8 mm	<b>hot environment, bed</b>	No, no
<b>Printing speed</b>	F300 mm/min	<b>Layer height</b>	0.6mm, 75% of nozzle diameter

*Table 4.1 Process parameters used throughout all of the studies*

The above described setup and processing parameters were not modified throughout the experimental work of multi-axis ME.

## 4.2. Pilot test

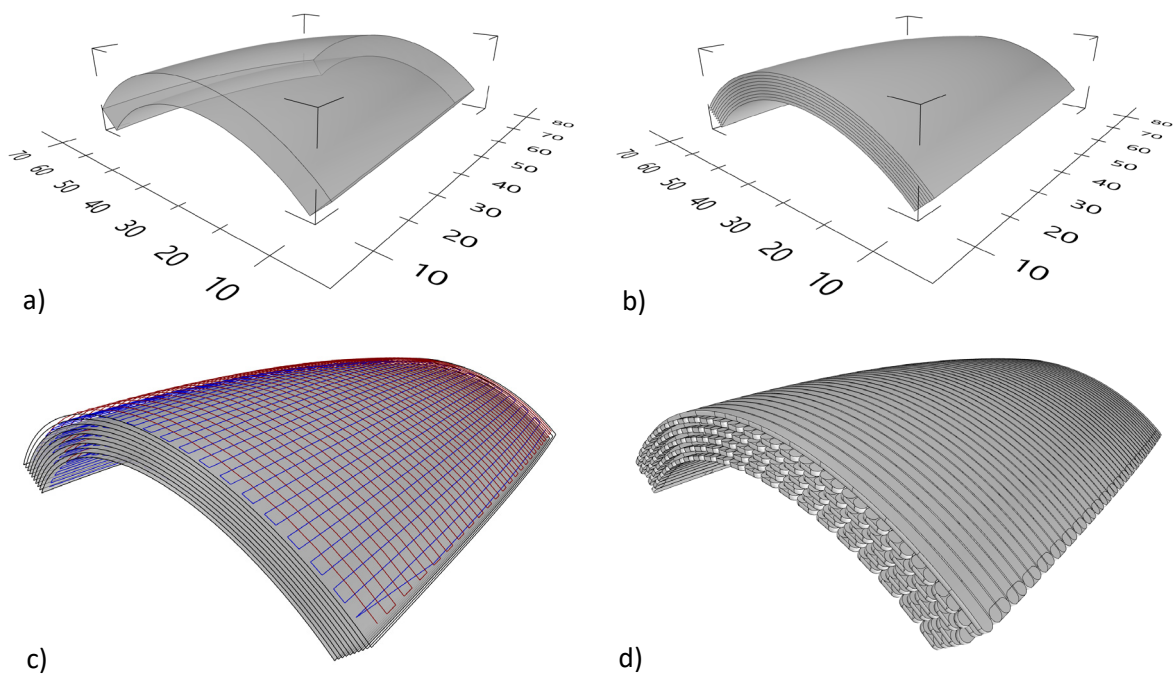
Before proceeding to investigate the hypothesis and research questions established for this Doctoral Research in Chapter 2, a pilot case study was processed and manufactured by multi-axis ME, using the software tools, processing framework and manufacturing system described above. The objective with this pilot case study was twofold:

- to apply all of the elements in the processing chain (Figure 3.12), down to the physical realisation of a desired part, demonstrating the level of capacity for this framework to process multi-axis ME. In other words, demonstrate if the combination of software tools described in Chapter 3 together with the manufacturing system are fit for purpose.
- to give an example with high similarities to work done in previous research, so that it establishes a form of benchmark, connection, or in other words, a starting reference point delivered through a multi-axis orthogonal deposition.

The part model resembled the geometries commonly used in previous multi-axis ME or CLFDM research: a uniform thickness part with smooth double curvature. Normal vectors of the two most prominent freeform surfaces constituting the part model spanned within  $\pm 45$



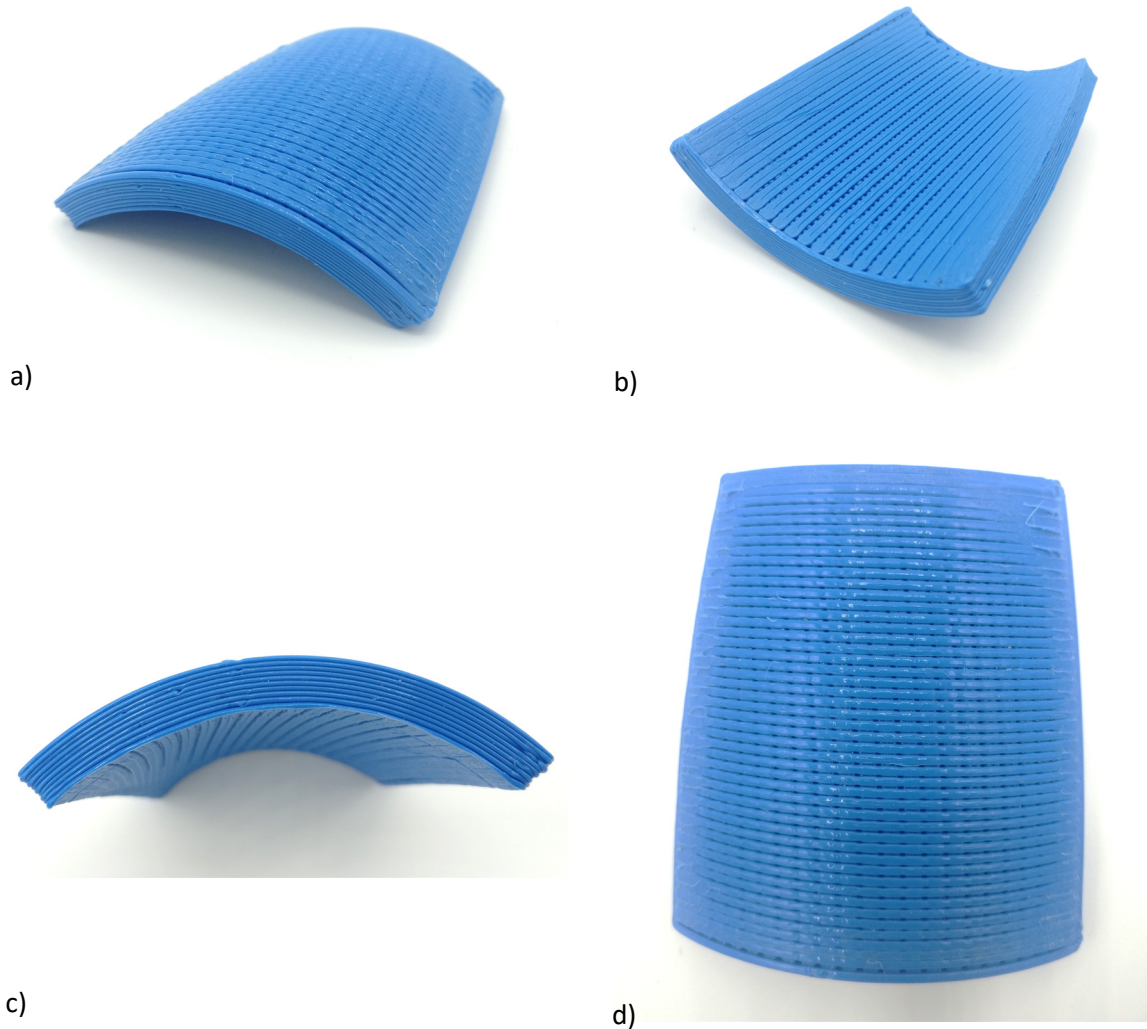
degrees around Y axes and  $\pm 13$  degrees around X axis. The dimensions, slicing, toolpaths and meso-structure simulation are shown in Figure 4.3 whereas different view of the finished object is shown in Figure 4.4. The manufacturing was done with an alternating toolpath orientation following the parametric  $U$  direction for all odd and  $V$  parametric direction for all even layers. Its completion was considered as a sufficient attestation of the framework's capacity to process part models of similar geometry for multi-axis ME, and the manufacturing system's capacity to execute it.



*Figure 4.3 Progressive steps through processing pipeline of the pilot case study: a) 3D model, b) Layers as outcome of slicing, c) Alternating toolpaths between red and blue orientation d) Simulation of extrudate (contours removed for clarity)*

Additionally, the pilot case study was also used to calibrate all of the process parameters and reach their final value as shown in Table 4.1, including distance between toolpaths and contours (walls), amount of retraction and compensation, extrusion multiplier, etc. The distance between adjacent toolpaths was selected to be  $1.5\text{mm}$  with a projected nominal filament deposition width of  $1.1\text{mm}$ . This was done to avoid over-extrusion issues present especially in the corners of the infill toolpath, presumably from the lowering of the actual manufacturing speed, or when inaccuracies in the physical system lead to a lower layer thickness in a certain zone of the layer. Seeing how this research looks into the topic of multi-axis slicing strategies, it prioritises the shape, topology and arrangement of layers rather than the precise percentage of infill or toolpath algorithm itself. The selected distance between

toolpaths lead to a repeatable and reliable manufacturing of objects with less than a 100% infill, limited localised over-extrusion and clearly identifiable toolpath directions.



*Figure 4.4 Several views of the Pilot case study printed with multi-axis software tools, framework and manufacturing system*

A certain extent of irregularities arising from the practical execution of the process can be noticed in Figure 4.4 e.g. slight variations between toolpaths distance (suspected as a result to further presence of backlash in the manufacturing system), extrusion of unwanted material local to points of initiation and finalisation of layers, or thermal degradation of material resulting in discolouring. While these imperfections were acknowledged - and given the practical nature of Material Extrusion technology to some extent expected - they were seen as marginal parameters that would not impede or hinder in any way the research as planned in this work, especially seeing how the core research element of layer arrangement and slicing strategy are clearly identifiable.

### 4.3. Assumptions and considerations

The conglomerate of processing framework described in Chapter 3 with all of its integrated algorithms and hardware aspects, from the manufacturing system and the selected processing parameters for multi-axis ME execution, describe the experimental environment in which the studies of this Doctoral Research have been done. It is worth noting that such combination of elements is neither the only possible composition nor the most optimal one according to a certain benchmark criterion, but rather one feasible alternative for implementation of multi-axis ME. Therefore, regardless of what the particular choice of processing framework, parameters and equipment for a specific study, it would seem inevitable that some level of assumptions are always made regarding its impact on obtained results. Some of these considerations are discussed here below:

#### *Hardware aspect.*

Multi-axis ME, at least in this research, is intended as the execution of ME in a setup of more than 3 axis, which translates in more than 3 degrees of freedom between the extruder head and a deposition substrate of a given manufacturing system. While analysis on kinematic chains of such manufacturing systems is clearly outside of the scope of this study, examining prior research done in this field has revealed various equipment used to practically execute the technology. For example, in one study [58] a parallel Stewart mechanism has been implemented with 6 degrees of freedom while in [99] a 5-axis machine with a tilt-and-turn table has been used. An increasing number of research also uses robotic setup for the execution of multi-axis ME, such as in [75] and [52]. Different equipment from these selected works is presented in Figure 4.5.

Since different manufacturing system pose different dimensional limitations on the workspace in terms of linear movements and rotations, it is assumed that the choice of it heavily affects the feasibility of multi-axis ME in terms of possible geometries, slicing strategies and freeform layer shapes that can be processed. Consequently, the use of the manufacturing system as described in Figure 4.1 has also impacted the possible shapes freeform layers can take in this study. However, it is supposed that within the realm of what is possible to be achieved with a given manufacturing system, the results are not affected by the particular kinematics of the apparatus as long as it is able to execute the process within nominal conditions as described by the processing framework.

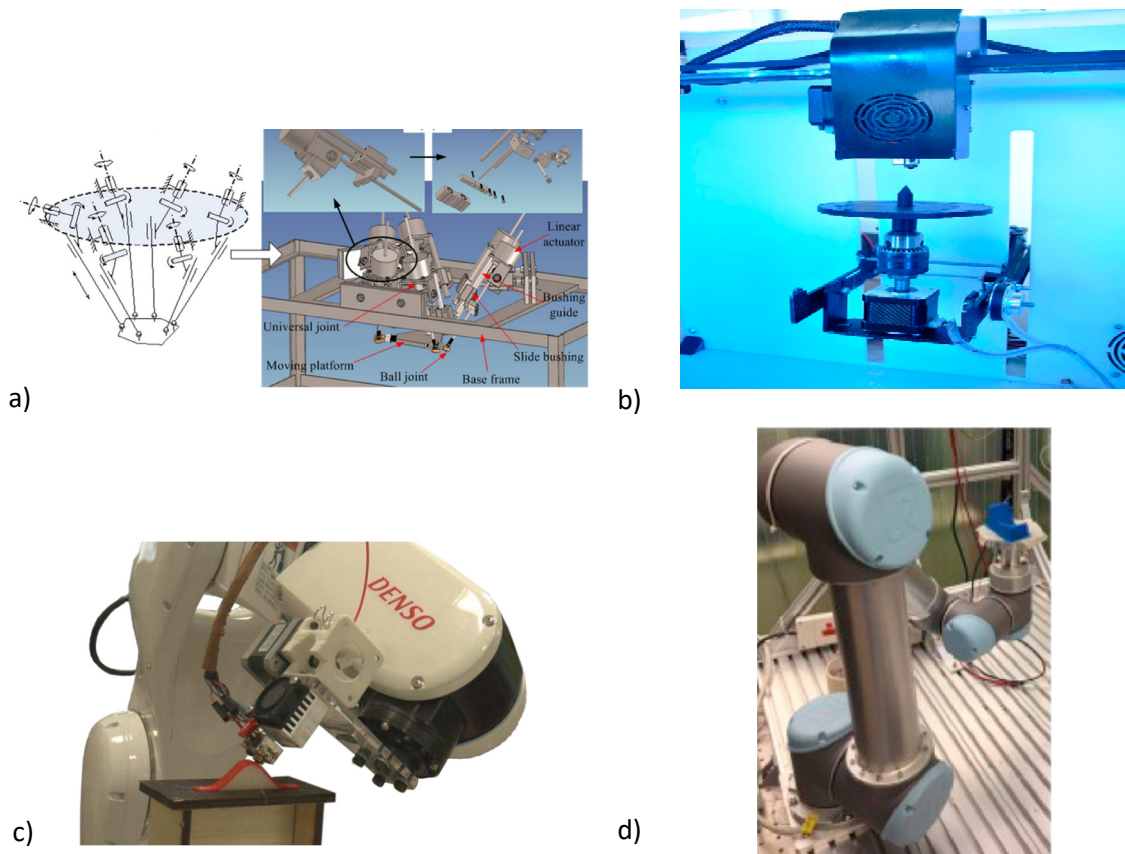


Figure 4.5 Examples of different manufacturing systems used in various prior art: a) Adopted from [58], b) Adopted from [99], c) Adopted from [75], d) Adopted from [52]

Another aspect that falls within the hardware design is the positioning of the extrusion system with respect to gravity. While in [75] and [76] the extruder head has been placed as an end effector of the robotic equipment, many other references have used a setup similar to [51], [52] where the robot has the deposition substrate as an end effector. This difference can be noted in Figure 4.5 c) and d). Yet another important factor often cited in previous studies such as [53] is the interference between the extruder and the layers in a multi-axis context. As this issue was considered critical since it directly impacts the feasibility of a given shape of a freeform layer, the risk of it occurring has been mitigated in this research by the implementation of the in-house designed extrusion nozzle as depicted in Figure 4.2 a). Clearly, many other designs can be adopted for improved clearance between extrusion nozzle and manufacturing piece during process execution.

#### *Software aspect.*

The major algorithms that form the processing framework implemented as a tool in this study have already been described in Chapter 3. However, implementing a multi-axis ME process

through the manufacturing equipment often involves the use of control software used to actuate the manufacturing system according to the process described in the instruction list (Figure 3.10). An example of parameters that could be affected by this software is the multi-axis motion control aspect of the process with its variable such as manufacturing velocity (feedrate). Some research has already been done on this point [77], that proposes toolpath smoothing and feedrate scheduling algorithms for robotic multi-axis ME which can lead to benefits of final quality on surface finish. In this study a nominal manufacturing speed of  $300\text{ mm/min}$  has been selected as it provided a good compromise between safe and smooth operation of manufacturing equipment and a fabrication process within reasonable timeframe. No effort was done in this study to measure the effective manufacturing speed of the process, maximise it or investigate its effect on parts made by multi-axis ME.

#### *Process execution.*

All case studies analysed in this Doctoral Research had their manufacturing phase executed according to the following protocol:

- Performing a homing sequence of the machine that provided for a repeatable starting point of each of its axis.
- Deposition of a support structure by a conventional 3-axis ME process, or a calibration with respect to an existing support structure.
- Purging of  $3\text{ m}$  of extrudate through extrusion nozzle in order to remove a potentially thermally degraded material from its melting chamber.
- Launch of instruction list comprising intra-layer toolpaths, inter-layer safety toolpaths, extrusion rate and extruder temperature, resulting in the finished part of each respective case study.
- Uncontrolled ambient cooling of  $30\text{ min}$  before proceeding with part removal from deposition substrate.

An additional step of material change was involved in the manufacturing of studies containing both build and conductive materials. This was done by inserting a pause in the printing of the part and integrating one change from build to conductive material and one change back from conductive to build material with steps of purging for avoiding contamination. A single nozzle was used for both of the materials.

The above described setup and processing parameters, together with the software tools developed in Chapter 3 and their defined sequence of data-flow as depicted in Figure 3.12, define a fixed chain of processing events that given a digital part model, result in a physically manufactured object according to a desired slicing strategy.

In an effort to decouple these processing events and selected equipment from the tests in the following chapters, the combination of elements discussed in Chapters 3 and 4 has been kept fixed throughout the studies. In other words, each of the multi-axis case studies regardless of the slicing objective or slicing strategy has been processed through the same pipeline in order to minimise any potential effect it has on final results. This characteristic enables for the same processing framework together with all hardware aspects to be used for both following Chapters of this research:

*Chapter 5:* analysis of slicing methods driven by accuracy.

*Chapter 6:* analysis of slicing methods driven by function.

# 5

## Non-planar Slicing Driven by Part Accuracy

The hypothesis in this Doctoral Research is that unlike conventional planar ME technology, the multi-axis extension enables a great number of possibilities when it comes to slicing, or otherwise defining a layer arrangement, many of them with a different effect on part quality.

What is investigated in Chapter 5 is the effect that different slicing strategies have on the accuracy of the obtained part, or in other words, how well the finished product approximates the desired digital geometry, by characterising the staircase effect. In accordance to methodology step *M2* established in Section 2.2.2, initial batch of case studies is done on *Part A* geometry used exclusively in Section 5.1. Then, in Section 5.2 the obtained results and conclusions are applied to *Part B* geometry for cross-comparison with slicing strategies aimed at different objective elaborated in Chapter 6. Through the case-study based analysis and results, observations and conclusions are made that help gain an understanding on how to guide the layer arrangement in order to optimise the accuracy of the finished product by minimising the impact of the staircase effect.

Section 5.3 then summarises the observations and forms conclusions considering a generic multi-axis slicing method aiming at optimising accuracy outcome as a part quality.

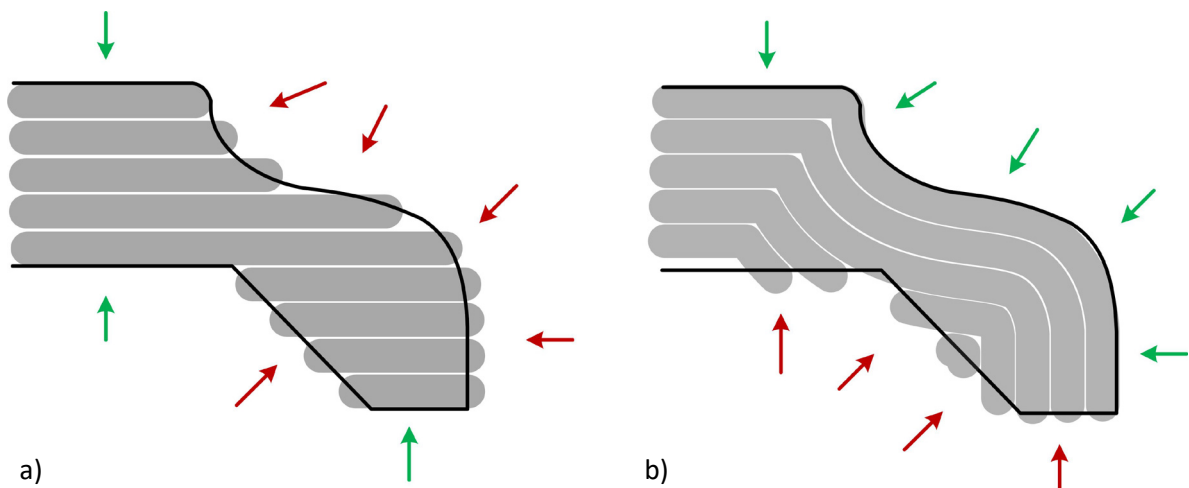
---

## 5.1. How to slice for improved accuracy

The objective of Section 5.1 is to correlate non-planar slicing with focus on the accuracy outcome (location and impact of the staircase effect) in the context of the entire geometry of a part's model, and establish a slicing method suitable for general application.

### 5.1.1. Introduction

As described in Section 1.2, one of the major shortcomings of AM in general and ME as a process in particular is the accuracy of the obtained parts. The accuracy issue, as identified in terms of the presence of the so-called staircase effect, or stepped surfaces, comes from the nature of AM itself where an ideal, desired digital geometry is being approximated by the successive placement or superimposition of layers. In conventional 3-axis ME, the problem is particularly evident in surfaces that are sloped, curved or otherwise inclined with respect to the horizontal direction. As shown in Figure 5.1a), the accuracy problem is not present in the case of horizontal surfaces due to the fact that the layers themselves are horizontal, so as long as deposition can take place at the required height, the staircase effect can be avoided on that surface, manufacturing it with a high degree of similarity with respect to the ideal part.



*Figure 5.1 Problem of accuracy with respect to the ideal geometrical shape in a case of a) planar and b) non-planar layers. Red arrows point presence (low accuracy) while green lack of staircase effect (improved accuracy)*

Some of the few parameters that are able to be controlled when defining the process and have a direct impact on the accuracy issue are the layer height and orientation of the part. Many



researchers have dedicated their work in understanding how to model, control or optimise them, leading to previous literature that is predominantly focused on either adaptive slicing methods [20] or orientation and surface angles as the controlled parameter [12]. For further information on this topic, reference can be made to additional and exhaustive reviews [123] and [124].

In the case of non-planar ME, besides the benefits obtained regarding the mechanical characteristics of the part, another highly quoted aspect has been the improvement of the obtained accuracy. These two parameters are the most commonly reported benefits of the use of non-planar layers that have been both theoretically hypothesised from the pioneering works on this topic [36] and practically supported later on [29], [30]. A common geometry selection used for demonstration purposes among such previous work [41], [114] especially related to the group of CLFDM terminology use, is a smooth doubly-curved surface, offset with a limited uniform thickness, at times being applied as a selected surface as well while the rest of the object is built in conventional flat layering. This could be due to the fact that thin, doubly curved uniform thickness objects are possibly the best examples of showing the potential advantages non-planar layer implementation could have on the strength and accuracy as qualities of a printed part. A replicate of such sample geometry has been used in Section 4.2, noted in this research as *Case\_Pilot* where the two principal curved surfaces are effectively an orthogonal offset of each other, so guiding the non-planar layer arrangement is quite intuitive since following both the bottom and top surfaces causes essentially the same slicing strategy that brings benefits throughout the majority of object's geometry. However, studying the effect of layer arrangement with respect to the entirety of the part, would require analysis on a more general geometrical topology with observations on the effects spanning across the whole product volume. This could indicate that even if an object is sliced with non-planar layers following a part of its geometry, staircase effect could still be present in other parts of the object as shown in Figure 5.1b).

### 5.1.2. Methodology

In order to investigate the effect that particular slicing strategy has on the accuracy of the part in a more general case, a part model containing two predominant doubly curved surfaces will be analysed. The analysis consists in processing the same object with different multi-axis ME slicing strategies and reporting on the effect they cause on the accuracy. The accuracy is then studied in both quantitative and qualitative approach. Quantitative analysis is done by simulating the volume of layers by creating a closed NURBS polysurface by normal offsetting of the layer surface by the layer height, which in turn gives an indication of the volume of the

staircase effect. In addition, the impact of the staircase is measured through its effect on the exterior surfaces in terms of surface area, providing a quantitative parameter that also takes in consideration the positioning of the staircase. Qualitative analysis consists in observing the presence of the staircase effect or the lack thereof, and its positioning with respect to the part model volume. Microscopy imaging metrology is used to relate digital, simulated data, to outcome of real physical samples. In addition to the reference of the location of the staircase effect, the layers' deposition conditions are also discussed as an important parameter of process execution.

The ultimate goal of Section 5.1 is to conclude statements regarding the correlation between non-planar slicing and presence of the staircase effect that can lead to the establishment of a general multi-axis slicing method applicable on various geometries. The observations are then categorised as observations from digital nature (parameters obtained throughout the slicing process) and practical nature (observations made from the practically manufactured samples).

### 5.1.3. Single surface slicing

A testing part model with increased geometrical complexity with respect to *Case\_Pilot* is designed for the scope of the study. It is composed of 6 surfaces, where the two surfaces with highest surface area are no longer a perpendicular offset of each other, creating so an object with a non-uniform thickness varying between 3mm at the edges and 6mm in the middle of the part. This new geometrical model, referred to as *Part A* throughout this research, has been obtained by modifying the top surface of *Case\_Pilot* and is presented in Figure 5.2. The curvature and positioning of the part are the following: the normal vectors from the top surface vary w.r.t. vertical gravity direction in a range of  $-14,03 \div 4,6$  degrees around *X* axis and  $+/- 46.62$  degrees around *Y* axis. Normal vectors from the bottom surface vary w.r.t. vertical gravity direction in a range of  $-13,34 \div 4,41$  degrees around *X* axis and  $+/- 45.08$  degrees around *Y* axis. *Part A* geometry is used to do an isolated analysis focused on establishing a slicing method aimed at optimising accuracy of printed part model, applicable to various geometries.

Unlike uniform thickness thin curved parts, such as *Case\_Pilot*, the slicing of *Part A* is not particularly intuitive due to the fact that top and bottom surface are no longer normal offsets of each other, which introduces a choice on how to guide the slicing process. Namely, either the top surface can be used to progress it towards the bottom, creating layers that are offset from the top surface (*Case\_Atop*), or conversely, the bottom one can be used to create layers

that would resemble the bottom most surface and would progressively be offset upwards (*Case\_Abot*) as shown in Figure 5.2b).

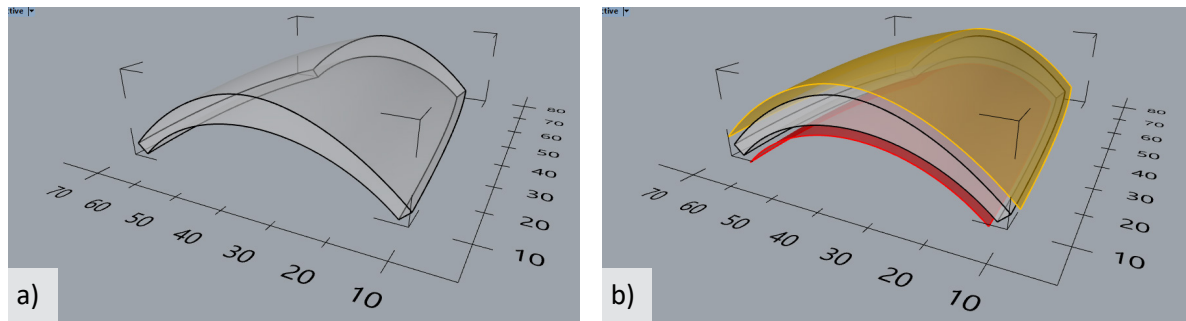


Figure 5.2 Part A geometry: a) Transparent model, b) the model with emphasised principle surfaces for different slicing: top (gold) surface propagated downwards or bottom (red) surface propagated upwards

Using the slicing algorithm described in Section 3.3, the two different cases were processed and non-planar layers surfaces were generated for both slicing strategies. The surface layers were then used to simulate enclosed volumes that indicate where material would be deposited during the subsequent manufacturing steps. Lastly, comparing the simulated layer volumes to the ideal part model provides an insight into the distribution and size of the staircase effect. Processing the case studies through the multi-axis ME framework as established in Chapter 3 enabled for the physical manufacturing of case studies samples. The full information tables for *Case\_Abot* and *Case\_Atop* are shown in Tables 5.1 and 5.2 respectively. Additional images of the case studies during manufacturing can be found in Appendix A.

Referring to Tables 5.1 and 5.2, it is evident that the selection of the layer arrangement has an impact over the location of the staircase effect and therefore the accuracy of the part. While in accordance with much of the previous work done from other studies, that non-planar slicing has the ability to improve the accuracy by avoiding the staircase effect, the case studies developed in this research support the idea that it is only so regarding one segment of the part: the surface coinciding to the direction of layers. These correspond to the top surface in *Case\_Atop* and the bottom one in *Case\_Abot*. Their counterpart surfaces however, have presented the staircase effect due to the difference between the slicing surface or their offsets and the surfaces that make up the object.

Geometry: A  
 Name: Case\_Abot  
 Layer Height: 0.6 mm  
 Num. of layers: 10

Slicing strategy: Entire part model sliced with bottom surface

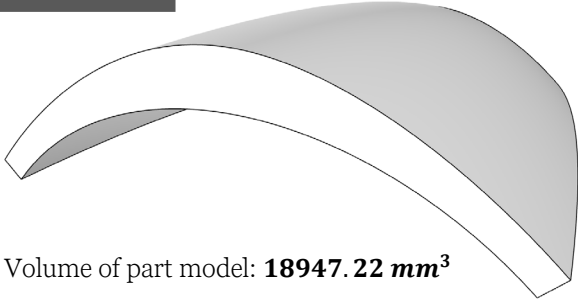
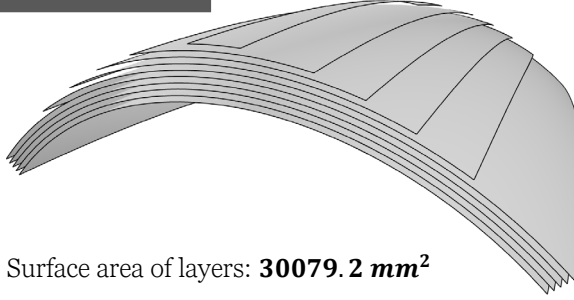
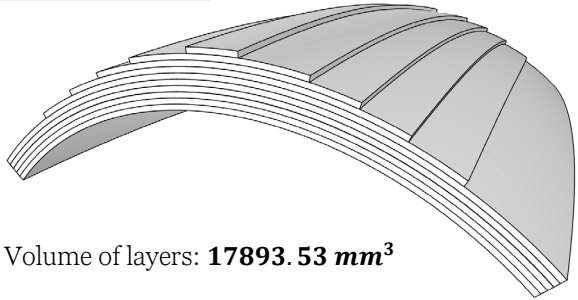
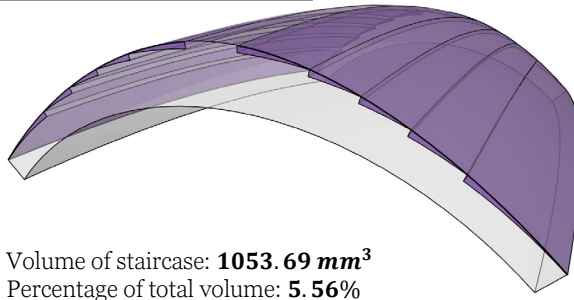
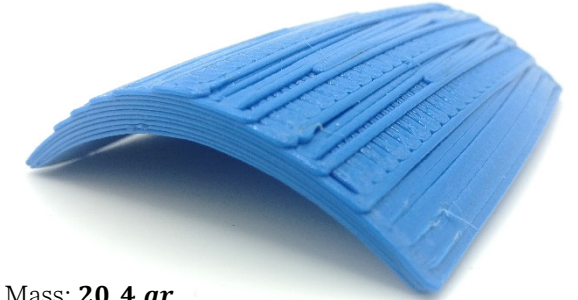

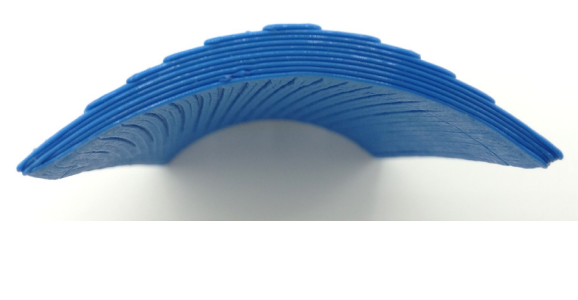

<p><b>Part model</b></p>  <p>Volume of part model: <b>18947.22 mm<sup>3</sup></b></p>	<p><b>Surface Layers</b></p>  <p>Surface area of layers: <b>30079.2 mm<sup>2</sup></b></p>
<p><b>Volume Layers</b></p>  <p>Volume of layers: <b>17893.53 mm<sup>3</sup></b></p>	<p><b>Staircase visualisation</b></p>  <p>Volume of staircase: <b>1053.69 mm<sup>3</sup></b>        Percentage of total volume: <b>5.56%</b>        Affects <b>93.87%</b> of top surface, <b>45.42%</b> of all exterior.</p>
<p><b>Isometric top view</b></p>  <p>Mass: <b>20.4 gr</b>        Total toolpath length: <b>21608.05 mm</b></p>	<p><b>Isometric bottom view</b></p> 
<p><b>Front view</b></p> 	<p><b>Top view</b></p> 

Table 5.1 Case\_Abot study info table

Geometry: A  
 Name: Case\_Atop  
 Layer Height: 0.6 mm  
 Num. of layers: 10

Slicing strategy: Entire part model sliced with top surface

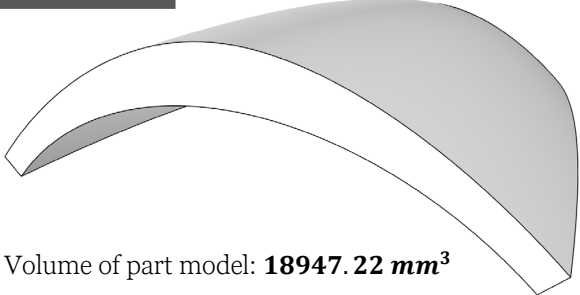
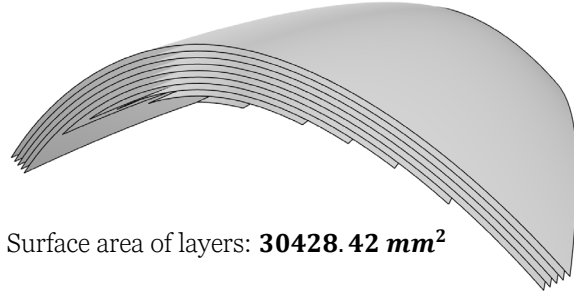
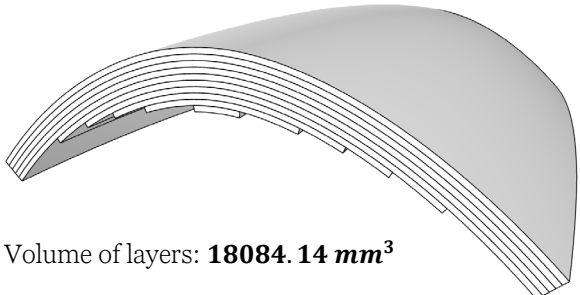
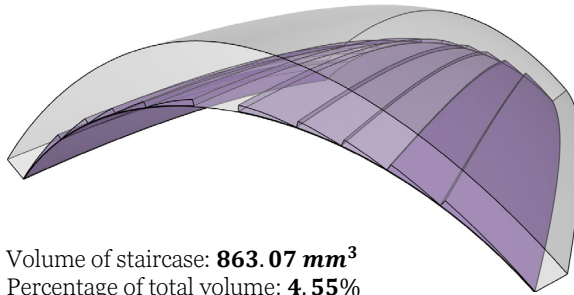
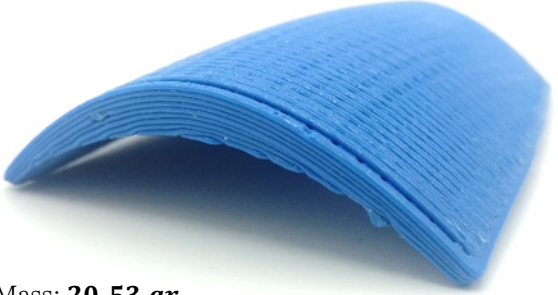
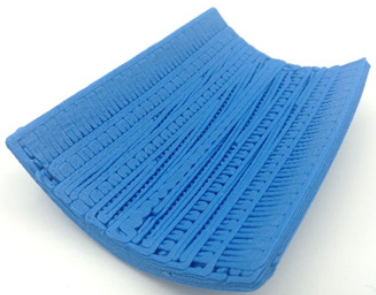


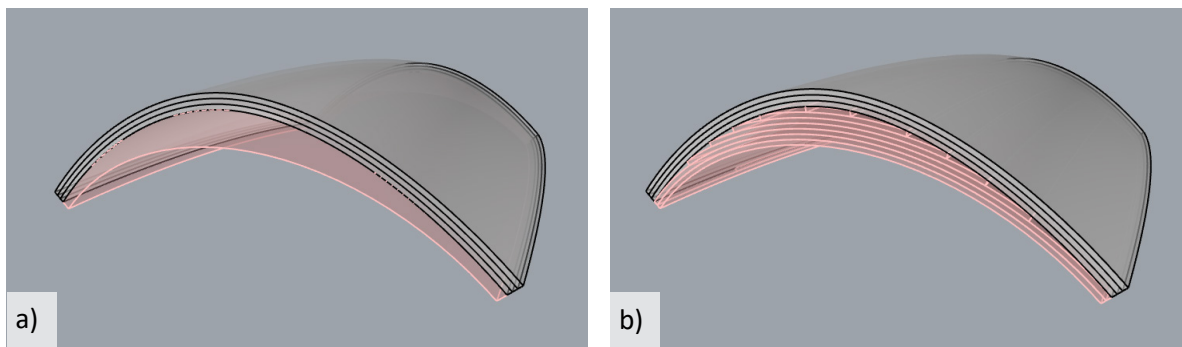
<p><b>Part model</b></p>  <p>Volume of part model: <b>18947.22 mm<sup>3</sup></b></p>	<p><b>Surface Layers</b></p>  <p>Surface area of layers: <b>30428.42 mm<sup>2</sup></b></p>
<p><b>Volume Layers</b></p>  <p>Volume of layers: <b>18084.14 mm<sup>3</sup></b></p>	<p><b>Staircase visualisation</b></p>  <p>Volume of staircase: <b>863.07 mm<sup>3</sup></b>      Percentage of total volume: <b>4.55%</b>      Affects <b>93.82%</b> of bottom surface, <b>39.74%</b> of all exter.</p>
<p><b>Isometric top view</b></p>  <p>Mass: <b>20.53 gr</b>      Total toolpath length: <b>21974.99 mm</b></p>	<p><b>Isometric bottom view</b></p> 
<p><b>Front view</b></p> 	<p><b>Top view</b></p> 

Table 5.2 Case\_Atop study info table

#### 5.1.4. Multiple surface slicing through volume sub-division

The selection of either top or bottom surface as a guide for the layer arrangement of the part has led to a different outcome with respect to the accuracy of the part: a partial improvement in accuracy with respect to the part model coinciding with the selected slicing surface. Therefore, with an objective of combining the benefit noted in both *Case\_Atop* and *Case\_Abot*, a third slicing approach named *Case\_Asan* was processed where both the top and bottom surfaces were used to slice the object following a ‘sandwich’ strategy. Namely, the layer arrangement processing was initiated by the creation of 3 layers that followed the top surface, as shown in Figure 5.3a). The sum volume enveloped by those 3 layers was then removed from the total volume of the parts geometry, and the remaining volume was then sliced following the shape of the bottom surface, resulting in 7 additional layers Figure 5.3b). The full information table regarding *Case\_Asan* is shown in Table 5.3 below, while supplementary images of the case study during manufacturing can be found in Appendix A.



*Figure 5.3 Combined slicing using both top and bottom surface: a) top 3 layers and remaining volume b) remaining volume sliced with bottom surface (right)*

The principle idea behind the multiple surface slicing concept through volume sub-division is that dedicated volume sections of the part model  $V_{1,2...k}$ , where  $\sum_{i=1}^k V_i = V_{total}$ , get sliced with different slicing surfaces or otherwise different slicing parameters, tuned according to a desired final outcome of the part. In Figure 5.3, this concept has been introduced through one of its most basic cases with only 2 sub-volumes defined from the total part volume, but various subdivision combinations can be made.

Geometry: A  
 Name: Case\_Asan  
 Layer Height: 0.6 mm  
 Num. of layers: 10

Slicing strategy (in that order):  
 i) 3 layers with top surface  
 ii) Remaining volume with bottom surface

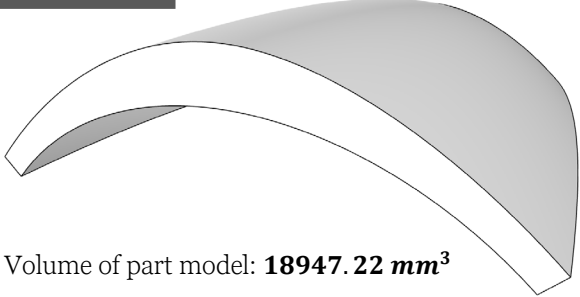
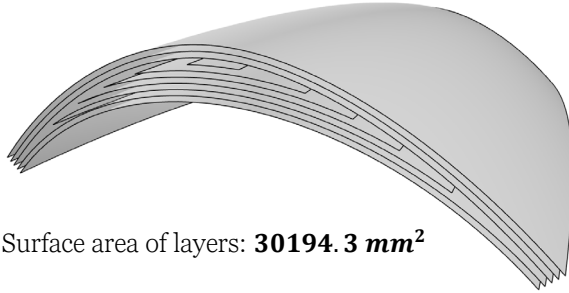
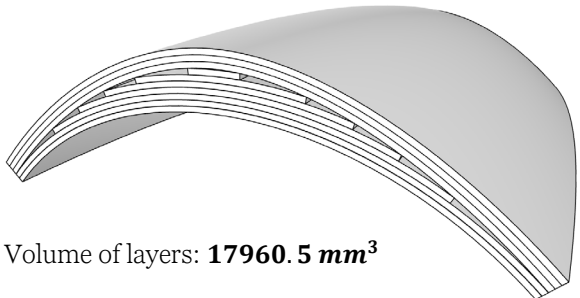
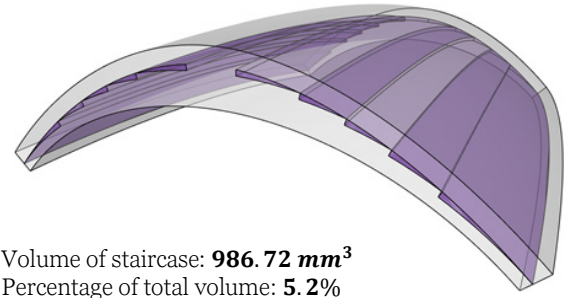
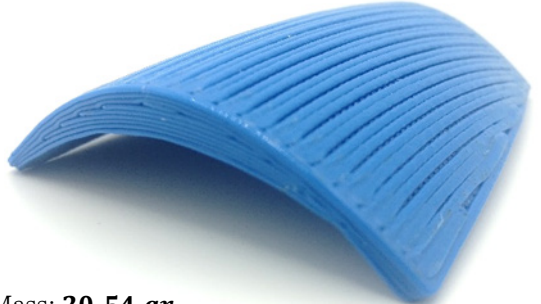
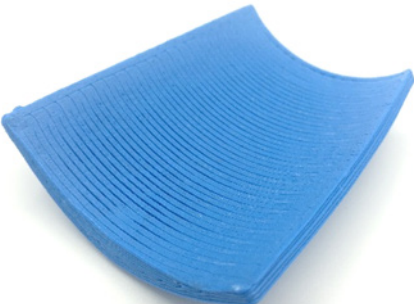

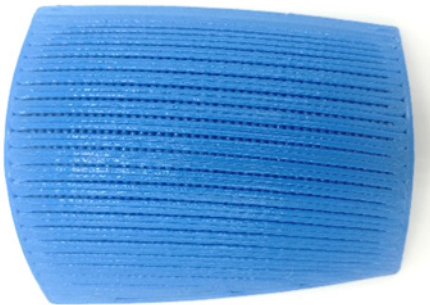
<p><b>Part model</b></p>  <p>Volume of part model: <b>18947.22 mm<sup>3</sup></b></p>	<p><b>Surface Layers</b></p>  <p>Surface area of layers: <b>30194.3 mm<sup>2</sup></b></p>
<p><b>Volume Layers</b></p>  <p>Volume of layers: <b>17960.5 mm<sup>3</sup></b></p>	<p><b>Staircase visualisation</b></p>  <p>Volume of staircase: <b>986.72 mm<sup>3</sup></b>        Percentage of total volume: <b>5.2%</b>        Affects <b>0%</b> of bottom/top surface, <b>0.32%</b> of all exterior.</p>
<p><b>Isometric top view</b></p>  <p>Mass: <b>20.54 gr</b>        Total toolpath length: <b>20968.34 mm</b></p>	<p><b>Isometric bottom view</b></p> 
<p><b>Front view</b></p> 	<p><b>Top view</b></p> 

Table 5.3 Case\_Asan study info table

The idea of subdividing the part volume has been previously discussed as the basis for many different slicing algorithms [124], also for technologies other than ME [125] with particular presence in the works of multi-orientation slicing algorithms [79]. However, the main goal of prior studies has been the avoidance of support material and in most of the cases the slicing surfaces are never modified from a planar to a freeform shape. Here instead, we look into the proposition of dividing the part model in slicing different sub-volumes with different freeform surfaces with the objective of analysing their effect on the part's properties, specifically the obtained accuracy.

Referring to Table 5.3, it can be observed that following this combined approach, an outcome was reached where the staircase effect was barely evident on the external geometrical boundaries of the object, but was rather repositioned towards the internal volume of the part's model.

#### 5.1.5. Results and conclusion

The slicing strategies, analysis and case studies preparation has generated data from both digital processing nature and practical nature by manufacturing the samples. While it comes earlier in the pipeline and does not represent the full scope of a multi-axis ME manufacturing, digital processing data has the characteristics of depending solely on a fixed orthogonal slicing algorithm and not on the toolpath generation algorithms and manufacturing systems. Therefore, such digital processing data provides more deterministic insight, decoupled from the specifics of further multi-axis ME implementation which can vary between studies. Practical samples on the other hand involve the whole multi-axis ME manufacturing process and systems, therefore dependency on all distinct operations and phases as elaborated previously in Chapter 3 and 4, such as: toolpath algorithm, manufacturing system, data format and process parameters. However, practical samples offer valuable insight into the still rare realisation of multi-axis ME technology and direct observation between what is digitally simulated and practically achieved. Considering this duality of data, the results are categorised in two groups of digital nature and practical nature.

##### 5.1.5.1. *Digital processing parameters*

A first initial assessment can be made by comparing the quantitative indications from the processing parameters resulting from the different slicing methods applied to a fixed geometry: *Part A*. The layer surface area is an indication of the 3D space in a form of freeform



surfaces where the processing framework has access to as a result of the slicing algorithm. It is exactly these surfaces that are used to generate the freeform toolpaths for infill and manufacturing of the part. The layers' simulated volume is an indication of the ideal amount of material that would be deposited by a processing framework. Since it is a volumetric measure, it offers the possibility to be compared to the ideal volume of the desired part model, that in turns generates an indication of the volume of the staircase effect, or rather, the volumetric portions where the processing framework has no control over. Another parameter that has been analysed are the portions of external surface area that are affected by the staircase, giving thus a quantitative indication that also depends on the location of the staircase with respect to the part model exterior surfaces.

Considering these two processing parameters provides deterministic quantitative insight in the different slicing strategies, without the disturbances of the specific algorithms used for toolpath development. In other words, the provided layer surfaces and volumes can subsequently be processed with any toolpath development algorithm, including some that might differ from the ones used in this study, extending thus the scope of validity of such data. These process parameters have been regrouped from the info tables of their respective case studies and are shown in Table 5.4.

	<i>Case_Abot</i> (single surface slicing method)	<i>Case_Atop</i> (single surface slicing method)	<i>Case_Asan</i> (multiple surface slicing method)
Part model volume:	18947.22 mm <sup>3</sup>		
Layer surface area:	30079.2 mm <sup>2</sup>	30428.42 mm <sup>2</sup>	30194.3 mm <sup>2</sup>
Layer volume:	17893.53 mm <sup>3</sup>	18084.14 mm <sup>3</sup>	17960.5 mm <sup>3</sup>
Staircase volume as % of part volume:	5.56 %	4.55 %	5.2 %
Position of staircase and impact on exterior surface:	Mostly towards external volumetric boundary. Affects 93.87% of top surface, 45.42% of all exterior surface	Mostly towards external volumetric boundary. Affects 93.82% of bottom surface, 39.74% of all exterior surface	Mostly contained within internal volume space. Affects 0% of bottom and top surface, 0.32% of all exterior surface

*Table 5.4 Accuracy data per case study extracted from digital processing parameters*

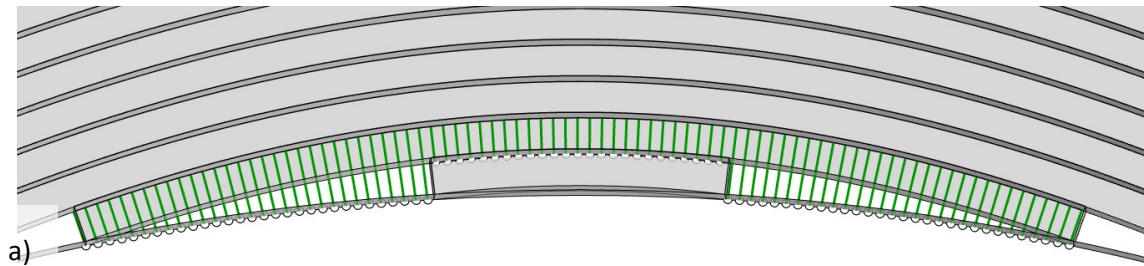
The three reported case studies performed on *Part A* manage to process a similar quantity of the ideal part volume, in a range between 4.55 % in *Case\_Atop* and 5.56 % in *Case\_Abot*. This

follows as a direct consequence of the slicing procedure, an intrinsic property of many AM technologies where an ideal geometry is approximated with a finite number of layers. It is presumed that these absolute values are directly dependent on the relation between the size of the object and the layer height used to do the slicing.

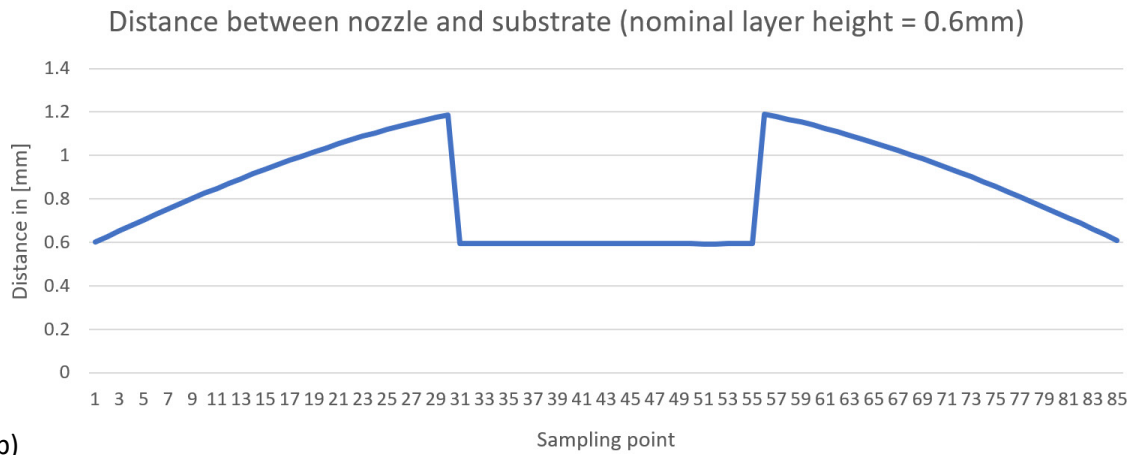
The relative similarity in the processed volume over the ideal one indicates that multiple surface slicing method implemented in *Case\_Asan* does not offer improvement in accuracy by bringing the quantity of digitally processed volume closer to the ideal one, but rather by displacing the staircase effect from the external volume boundaries of the part towards the internal zone. By doing so, freeform layers are generated that completely match the external surfaces of the part model. These provide access to the processing framework of guiding extrusion tool precisely along the part model geometry, greatly limiting the impact of the staircase effect on the external dimensions of the part. In fact, the exposure of the staircase effect to the cumulative exterior surface area of the part has been brought down from 45.42% for *Case\_Abot* and 39.74% for *Case\_Atop* to 0.32% in *Case\_Asan*. As a conclusion, the multiple surface slicing method using external part model surfaces for a two-step slicing strategy causes similar volumetric processing error in quantity as compared to the single surface slicing methods, but enables for a repositioning of the staircase effect towards the inside of the part model where it has marginal effect on external dimensions.

Another aspect that can be noted from the digital processing of different slicing strategies are the conditions under which deposition would take place during the manufacturing phase of the samples. In specific, in the *Case\_Atop* situation the layers are such that the initial phase of the manufacturing process is required to be executed under circumstances of non-perpendicular orientation and uneven layer height due to the difference in curvature between the first 6 layers and the deposition surface.

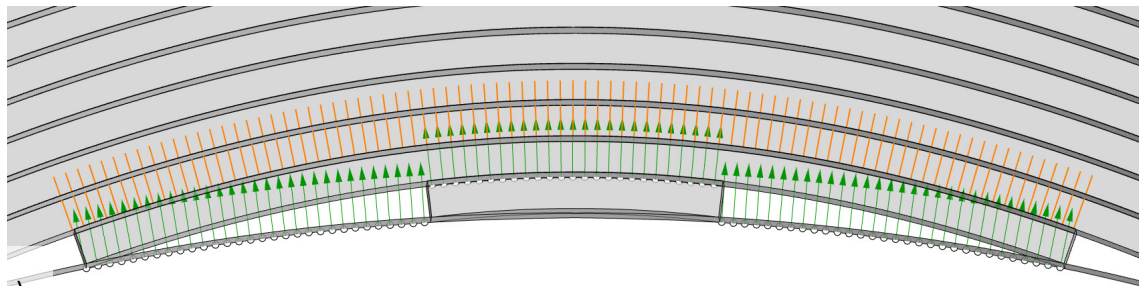
This leads to various process conditions to be sub-optimal such as: lowered correlation between extruded material and height of layer, lowered adhesion of layers to the substrate and increased probability of collisions between nozzle and support structure. An example of this is shown in Figure 5.4 where the process parameters of the deposition of the 2<sup>nd</sup> layer in *Case\_Atop* are looked into in detail. What can be noted is that the process parameters deviate from their nominal conditions in the areas where the staircase effect is present and they turn to their optimal values when depositing on top of the 1<sup>st</sup> layer. The deposition conditions of 2<sup>nd</sup> layer only are shown in Figure 5.4 for clarity, but the same phenomenon happens, at some point, with all of the first 6 layers that involve a direct deposition on the substrate instead of a previously deposited layer (Figure 5.4c)). Therefore, in *Case\_Atop*, all of the bottom surface footprint area has been deposited under sub-optimal process conditions at some point over the deposition of the first 6 layers.



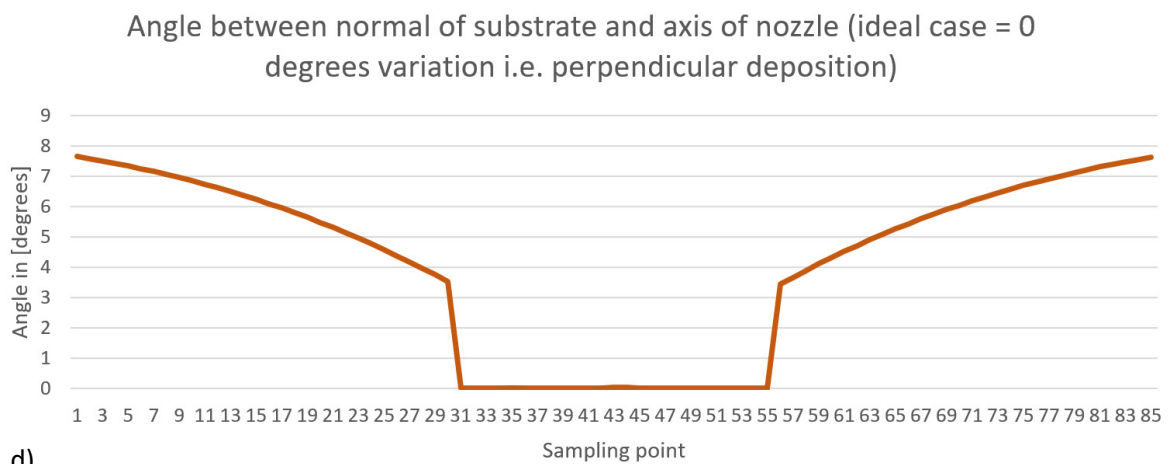
a)



b)



c)



d)

Figure 5.4 Mapping of process parameters during deposition: a) and b): Model and length distance variations of layer height; c) and d): Nozzle axis (orange lines) and normal vectors of substrate (green arrows) for angle angular deviation analysis

While similar suboptimal process conditions can be encountered also during the manufacturing process of *Case\_Asan* (Figure 5.5c) and d)), they occur between already deposited layers belonging to the part model itself, and a new layer. Besides the apparent advantage of repositioning of the staircase effect towards the internal volume of the part, another noted benefit during the practical manufacturing was improved layer adhesion since it now occurred between layers of the same build material rather than a substrate and build material. Also, contrary to *Case\_Atop*, *Case\_Asan* had only one initial layer that was deposited through optimal conditions of perpendicularity and consistent distance to the deposition substrate from the supporting structure, and only one layer executed under suboptimal conditions deviating from nominal ones.

In terms of deposition conditions, *Case\_Abot* was the only case study where there was no deviation from the nominal process parameters since the staircase effect is reported on the top surface, where no other deposition or contact to surfaces are present.

#### 5.1.5.2. *Physical samples*

With an intent to better measure and evaluate the staircase effect present in the different layer arrangements, magnified frontal views were taken by optical microscope using a *Leica DFC295* digital camera and are shown in Figure 5.5 and 5.6. Accuracy outcome along the thickness of the part model was not considered due to the small dimensions compared to the rest of the surfaces. All case studies involved normal multi-axis slicing with layer height of  $0.6\text{mm}$ . While the staircase effect in *Case\_Abot* (Fig 5.5e) and f) geometrically corresponds to the foreseen simulation obtained from the slicing, and was measured to be the same value as the layer height, *Case\_Atop* (Figure 5.5a) and b) and *Case\_Asan* (Fig 5.5c) and d) did not report the same measures, but rather a diminished staircase effect that was filled up by the flow of molten material. This is due to the semi-liquid material falling under gravity, infilling the empty space within the staircase feature within  $0.45\text{mm}$  in *Case\_Atop* and  $0.352\text{mm}$  in *Case\_Asan*, even if the simulated errors in accuracy are noted to be an order of magnitude larger. This phenomenon does not only influence the material infill of the staircase itself in what appears to be a positive effect, but impacts the shape of the freeform layers whose filaments fell under their own weight, since they now deviate from their nominal freeform surfaces. Consequently, the staircase effect is somewhat transferred to the above deposited layer, albeit in a rather diminished form. Very little information has been found regarding this issue in previous studies, limited only to the work of [126] where according to the described mathematical model for curved layer deposition on top of planar ones, the effect of material

sagging is drastically decreased with each successive layer deposition. However, no correlation with measurements on physical samples has been provided.

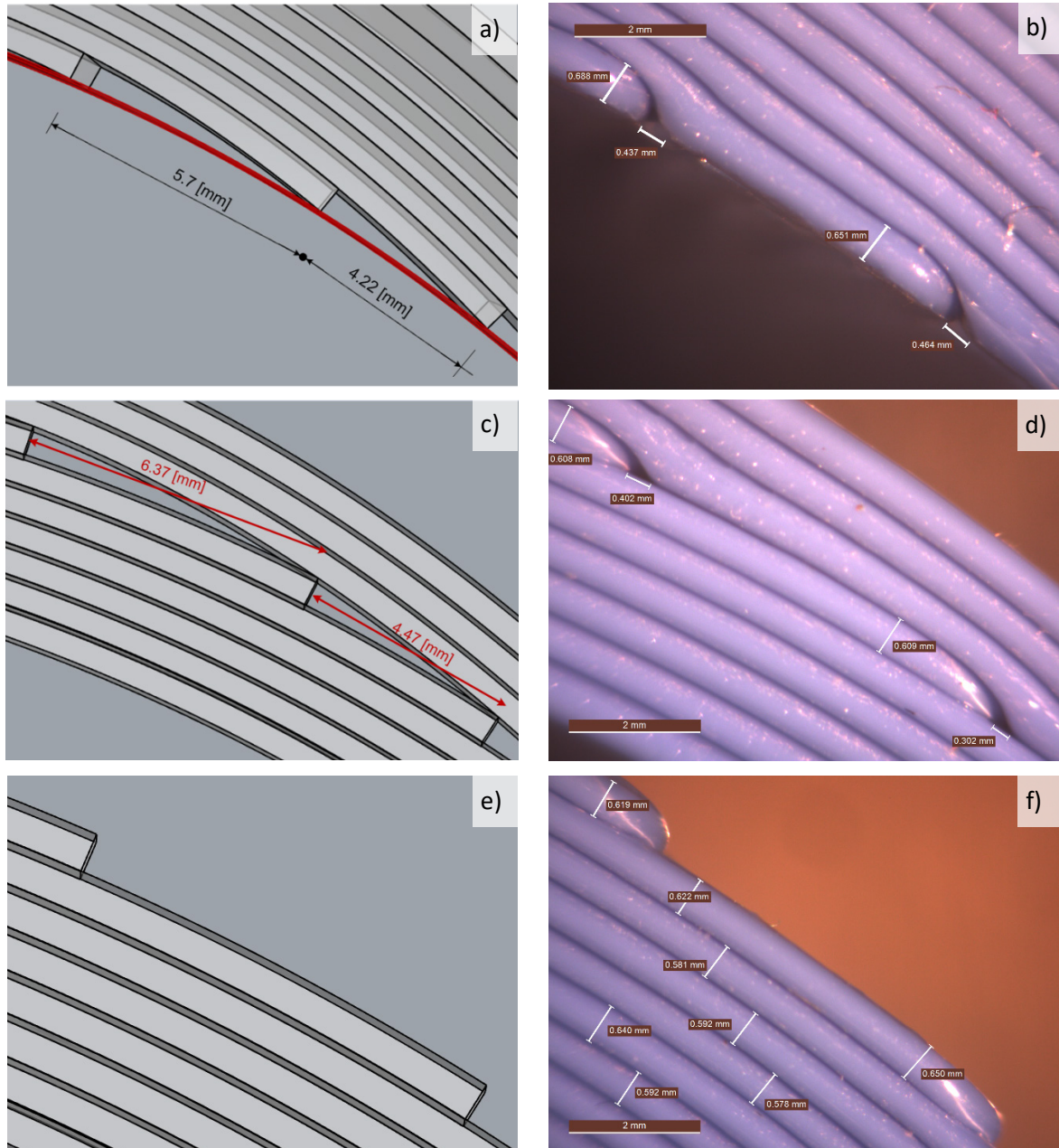


Figure 5.5 Simulated and experimental samples displaying varying staircase effect features as a result of varying layer arrangement: a) and b): Case\_Atop, c) and d): Case\_Asan, e) and f): Case\_Abot

Additional measurements of the material sagging are presented in Figure 5.6 where a front view of Case\_Atop and Case\_Asan is presented; the two slicing strategies which reported this phenomenon. An overlap of a magnified image of these case studies with their respective ideal layer shape (red) is shown with measures of deviation between the two. The measurements show a significant change between the bottom and top surface of a given freeform layer. In

*Case\_Atop*, the bottom surface of the first layer deviated in average  $0.43\text{mm}$ , or  $71.67\%$  of total layer height, while the top surface of the same layer reported a deviation of  $0.18\text{mm}$  or  $30\%$  of total layer height. The top surface of the second and third layer reported a further decrease of the staircase effect down to  $0.125\text{mm}$  or  $20.83\%$  and  $0.071\text{mm}$  or  $11.83\%$  of the layer height respectively. In *Case\_Asan*, the bottom surface of the first layer deviated in average  $0.5\text{mm}$ , or  $83.33\%$  of total layer height, while the top surface of the same layer reported a deviation of  $0.24\text{mm}$  or  $40\%$  of total layer height. The top surface of the second layer reported a further decrease of the staircase effect down to  $0.11\text{mm}$  or  $18.33\%$  of the layer height, while the deviation of top surface of third layer could not be effectively measured.

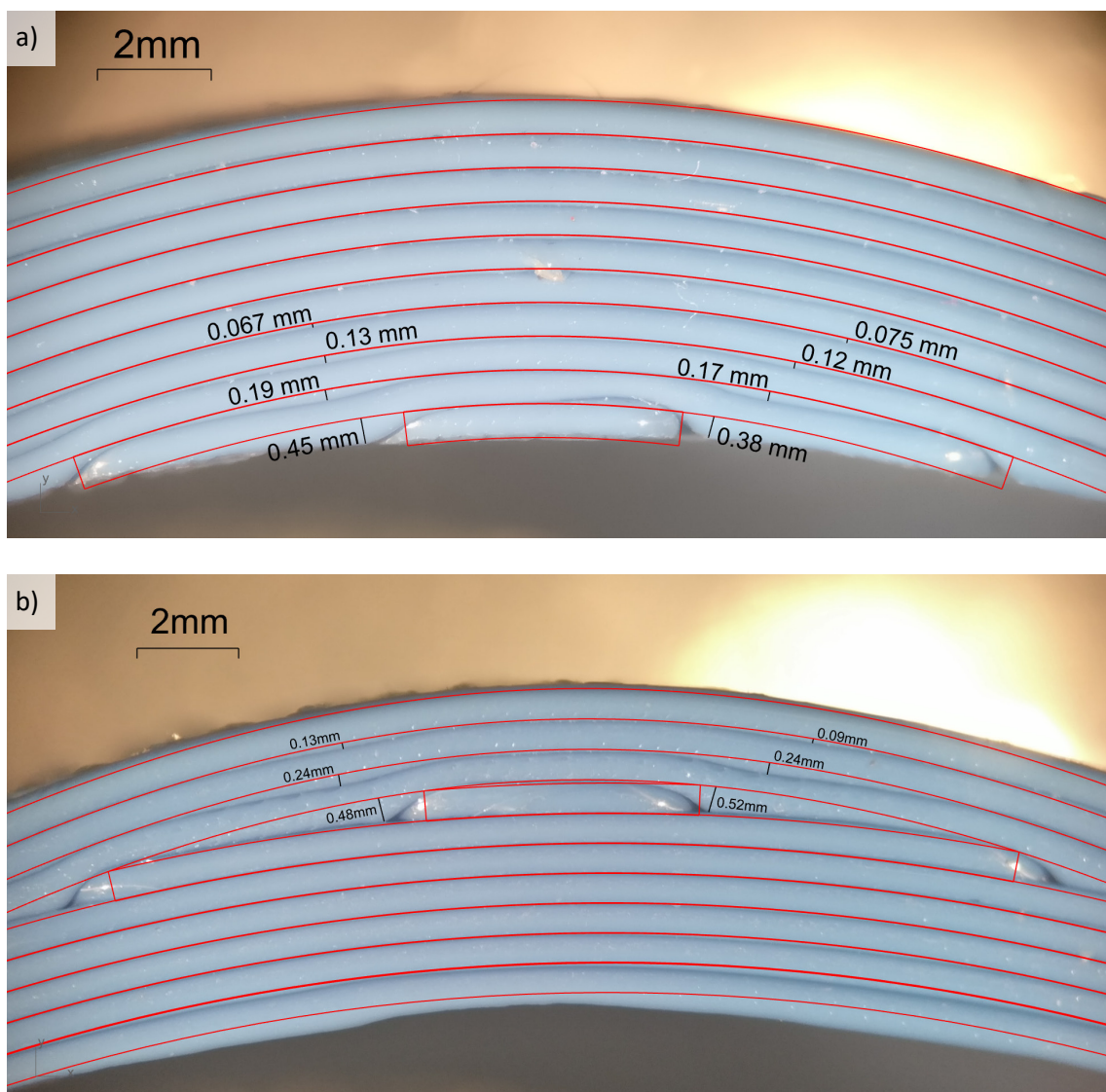


Figure 5.6 Deviations measurements between real and ideal layer formation due to fall of material under gravity: a) *Case\_Atop*, b) *Case\_Asan*

Some differences in the measurements between case studies was noticed: *Case\_Asan* for example reported higher initial deviations but they progressively decreased faster than *Case\_Atop*. This may be attributed to the slightly different curvature and shape of the layers of interest. According to the measurements, every newly deposited layer acts as a filter of the higher geometrical dynamics of the staircase, with its bottom surface reporting higher deviations while the top one is smoother, with 88.16% of the nominal layer height restored by the end of the third layer in *Case\_Atop*. These measurements indicate that some improvement in accuracy can be expected even with one layer that follows an external surface of the part, but the effect in attenuating the staircase errors may depend on other parameters, for instance, the number of layers applied or layer thickness. It is hypothesised also, this effect depends heavily on other factors too, such as: the orientation between the staircase feature and the gravity vector, extrusion temperature, type of material, localised cooling during manufacturing etc., making it challenging to predict its outcome. Additional work is required to understand how to account for it in slicing strategies and process execution.

From the above methods using simulated layers, physical realisation of specimen and imaging metrology, it can be observed that implementing a slicing method using multiple surfaces extracted from the part's model through volume sub-division could lead to benefits regarding accuracy of the part. This is obtained by repositioning of the staircase effect from the external volumetric boundaries towards the inside of the part where it has a more limited effect on the external dimensions. Results from microscopy measurements point to the high similarity in improved accuracy in both *Case\_Atop* and *Case\_Asan* slicing strategies due to the collapsing of the melted material under its own weight, reducing the staircase features. Nevertheless, the presence of the staircase effect in *Case\_Atop* can still be noticed due to the difference between the slicing surface and the encountering bottom surface of the part's model.

Weighing the above considerations concerning part outcome and process parameters, *Case\_Asan* is selected as a superior slicing strategy for obtaining better part accuracy when compared to both *Case\_Atop* and *Case\_Abot* slicing strategies applied on *Part A*. This multiple surface slicing strategy allows for re-positioning of the staircase effect away from the external geometry of the part's model and placing it towards the internal volume. Therefore, the multiple surface slicing strategy through volume sub-division is the established accuracy driven slicing method for further testing and cross comparison on a common geometry.

## 5.2. Applying multiple surface slicing method through volume sub-division

Given the apparent advantage of using multiple surfaces extracted from the part's model in order to avoid staircase effect on the external volumetric boundaries of the part, an additional geometry with increased complexity has been processed that will serve as a cross-comparative platform for different slicing strategies elaborated in this thesis. This digital geometry referred to as *Part B* exhibits an increased geometrical complexity w.r.t. *Part A* as it consists of 3 major surfaces, one of which is slightly concave, that form a closed polysurface of a total of 7 surfaces.

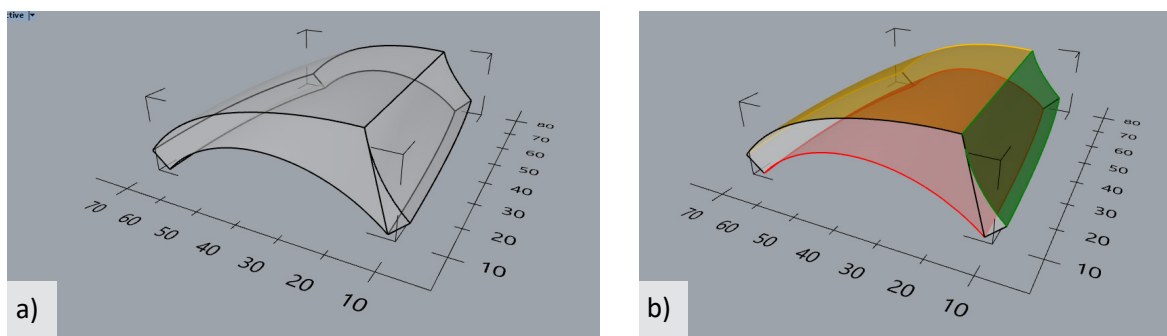


Figure 5.7 Part B geometry: a) Transparent model, b) the model with emphasised principle surfaces for different slicing: top surface (gold), side surface (green) and bottom surface (red). Dimensional units – [mm]

The bottom surface has been kept identical to *Case\_Pilot* and *Part A*, while the normal vectors from the top surface (yellow) vary w.r.t. vertical gravity direction in a range of  $-13,48 \div 4,42$  degrees around *X* axis and  $-13,88 \div 47,53$  degrees around *Y* axis. Normal vectors from the side surface (green) vary w.r.t. vertical gravity direction in a range of  $-27,2 \div 4,3$  degrees around *X* axis and  $-79,33 \div -39,66$  degrees around *Y* axis. *Part B* geometry is shown in Figure 5.7.

Besides the aim of generating case studies on common, comparative geometry, another goal of applying slicing with multiple surfaces on *Part B* is to examine the generality extent of the multi-surface slicing method through volume sub-division established in Section 5.1.4 where different volume sections whose sum complete the total part model are sliced with different surfaces for a combined benefit with respect to the accuracy of the final product, thus, serving as a platform to test its ability to reduce the staircase effect in more complex, generic shapes.

Three different volume sections using three slicing surfaces were used to develop layer arrangements with different order, referred to as *slicing operations*. *Case\_Btop* represents a layer arrangement where first 3 layers are sliced following the top surface, slicing a volume



$V_{top}$ . If the volume of the entire part is represented with  $V$ , the remaining volume  $V - V_{top}$  is then subjected to a second slicing operation with 5 layers following the side surface, enclosing a volume  $V_{side}$ . Finally, third slicing operation processes the remaining  $V_{bot}$  until exhausting the entirety of it, where  $V_{bot} = V - V_{top} - V_{side}$ .

Conversely, *Case\_Bside* changes the order of slicing operations by initiating first with 6 layers sliced with the side surface, followed by 5 layers of the top surface. The final slicing operation is similar in concept with the remaining volume being sliced with the bottom surface. The above described slicing operations are graphically represented in Figure 5.8. The full information tables of *Case\_Btop* and *Case\_Bside* are shown below in Tables 5.5 and 5.6 respectively. Additional images of their manufacturing process can be found in Appendix A.

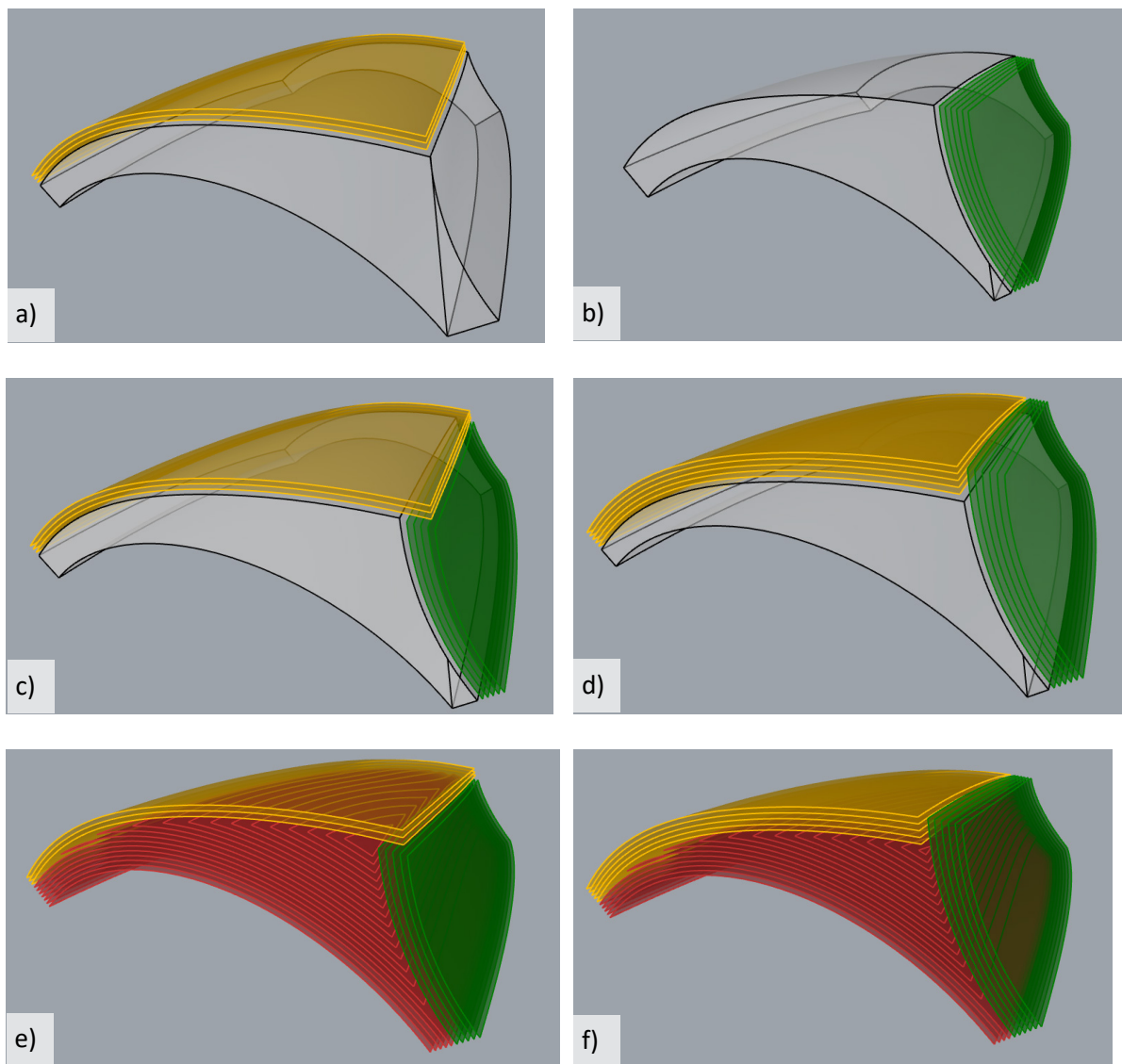


Figure 5.8 Slicing sequence of two different layer arrangements: a), c) and e) *Case\_Btop* and b), d) and f) *Case\_Bside*

Geometry: B  
 Name: Case\_Btop  
 Layer Height: 0.6 mm  
 Num. of layers: 29

Slicing strategy (in that order):  
 i) 3 layers with top surface  
 ii) Remaining volume with 5 layers with side surface  
 iii) Remaining volume with bottom surface

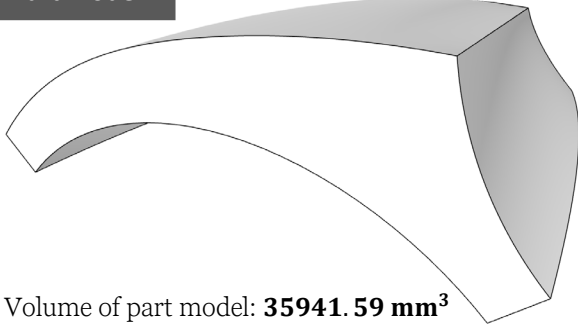
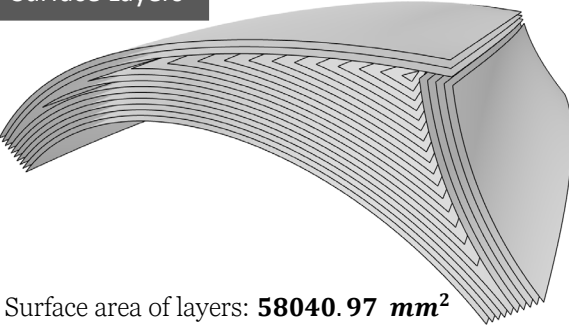
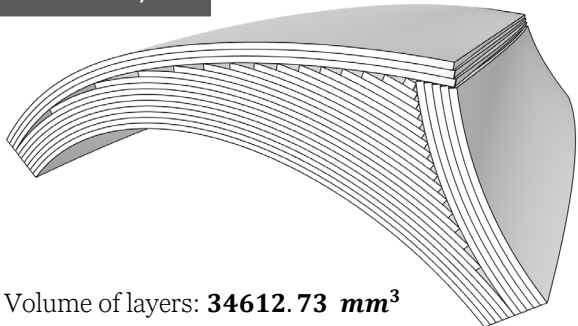
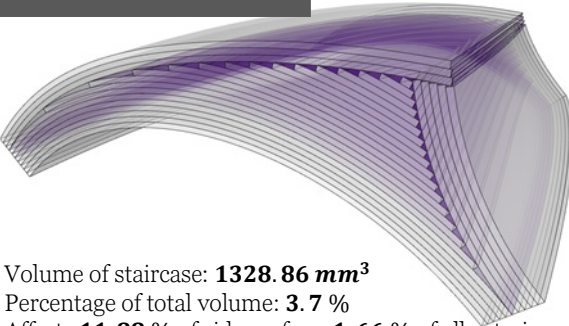
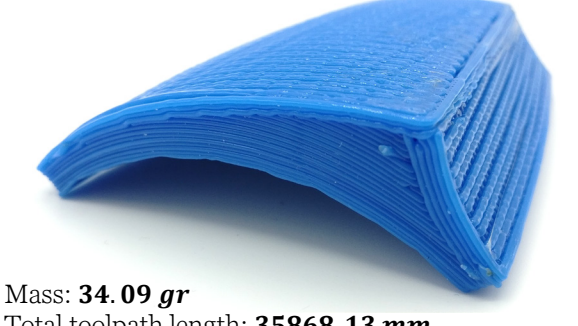

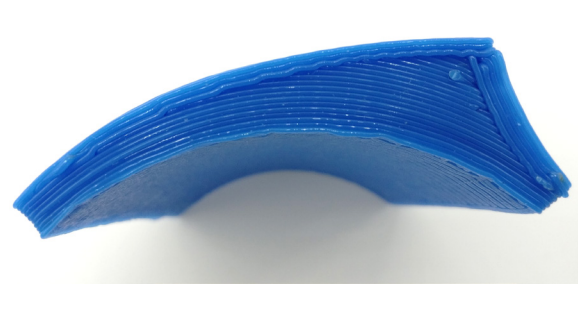

<p><b>Part model</b></p>  <p>Volume of part model: <b>35941.59 mm<sup>3</sup></b></p>	<p><b>Surface Layers</b></p>  <p>Surface area of layers: <b>58040.97 mm<sup>2</sup></b></p>
<p><b>Volume Layers</b></p>  <p>Volume of layers: <b>34612.73 mm<sup>3</sup></b></p>	<p><b>Staircase visualisation</b></p>  <p>Volume of staircase: <b>1328.86 mm<sup>3</sup></b>        Percentage of total volume: <b>3.7 %</b>        Affects <b>11.88 %</b> of side surface, <b>1.66 %</b> of all exterior</p>
<p><b>Isometric top view</b></p>  <p>Mass: <b>34.09 gr</b>        Total toolpath length: <b>35868.13 mm</b></p>	<p><b>Isometric bottom view</b></p> 
<p><b>Front view</b></p> 	<p><b>Top view</b></p> 

Table 5.5 Case\_Btop study info table

Geometry: B  
 Name: Case\_Bside  
 Layer Height: 0.6 mm  
 Num. of layers: 30

Slicing strategy (in that order):  
 i) 6 layers with side surface  
 ii) Remaining volume with 5 layers with top surface  
 iii) Remaining volume with bottom surface

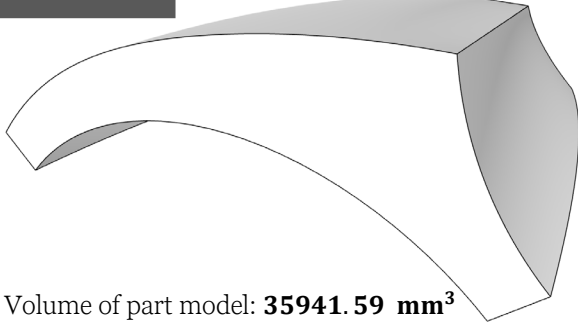
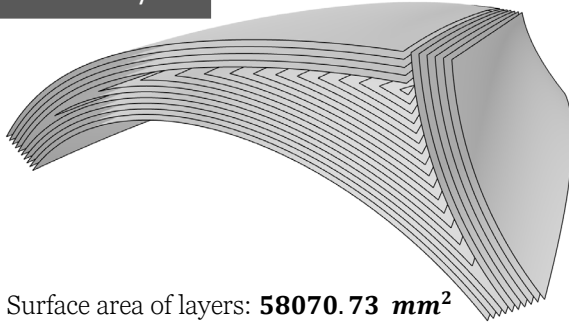
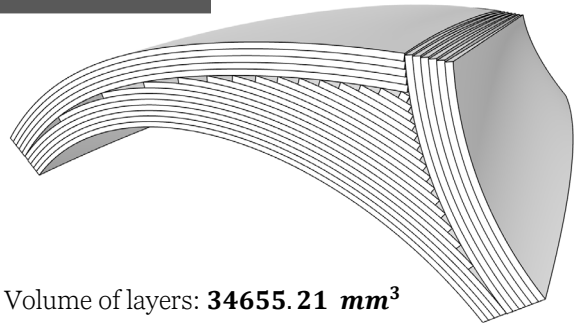
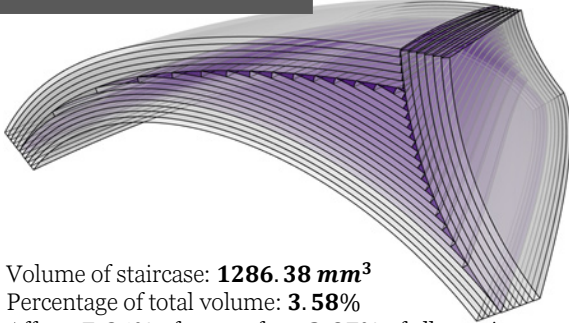
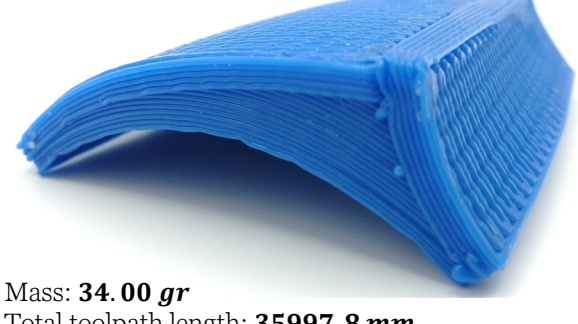

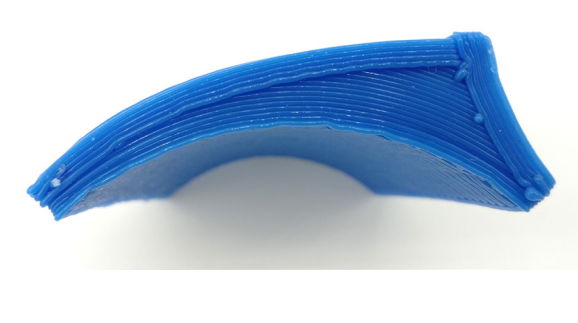

<p><b>Part model</b></p>  <p>Volume of part model: <b>35941.59 mm<sup>3</sup></b></p>	<p><b>Surface Layers</b></p>  <p>Surface area of layers: <b>58070.73 mm<sup>2</sup></b></p>
<p><b>Volume Layers</b></p>  <p>Volume of layers: <b>34655.21 mm<sup>3</sup></b></p>	<p><b>Staircase visualisation</b></p>  <p>Volume of staircase: <b>1286.38 mm<sup>3</sup></b>        Percentage of total volume: <b>3.58%</b>        Affects <b>7.36%</b> of top surface, <b>2.97%</b> of all exterior</p>
<p><b>Isometric top view</b></p>  <p>Mass: <b>34.00 gr</b>        Total toolpath length: <b>35997.8 mm</b></p>	<p><b>Isometric bottom view</b></p> 
<p><b>Front view</b></p> 	<p><b>Top view</b></p> 

Table 5.6 Case\_Bside study info table

Case studies *Case\_Btop* and *Case\_Bside* demonstrate that the multi-step slicing method using surfaces extrapolated from the part model has been successfully implemented on a more complex geometry that comes closer to a generic case when compared to *Part A*. The outcome is consistent with the studies from Section 5.1 in that both *Case\_Btop* and *Case\_Bside* have the majority of the staircase relocated towards the internal volume of the part model. The higher geometrical complexity has also provided the possibility to show the extent of the methodology to three slicing operations on the same part model, but it is hypothesised that this can extend and vary greatly depending on the choice of the slicing operations involved, the dynamics of the geometry of the part model and the capacity of processing framework to elaborate and physically manufacture each of the desired multi-axis operations.

Two different orders of the slicing operations led to a different outcome in terms of layer shape generating *Case\_Btop* and *Case\_Bside*. However, their processing parameters data show to a very similar layer surface, volume, location and size of staircase. *Case\_Btop* resulted in the staircase volume affecting 11.88% of the side surface, or 1.66% of the cumulative exterior surface area. *Case\_Bside* resulted in the staircase volume affecting 7.36% of the top surface, or 2.97% of the cumulative exterior surface area. While both of the layer arrangements contributed with major benefits in eliminating most of the staircase effect of the three major surfaces describing the part, there is an overlapping volume that is approximated differently due to the different slicing approaches. Namely, *Case\_Btop* does create a staircase effect on the side surface and *Case\_Bside* creates one on the top surface. It is assumed that the extent of the staircase effect and its impact on the external surfaces depends on the relationship between the curvature of the Top and Side surface, especially in the zone of mutual edge, and the number of layers for each slicing operation.

Due to the high similarity in outcome between *Case\_Btop* and *Case\_Bside*, both of them are considered a result from applying multi-surface slicing strategy through volume sub-division oriented towards optimising accuracy on *Part B* and will both be considered later on in the comparative analysis.

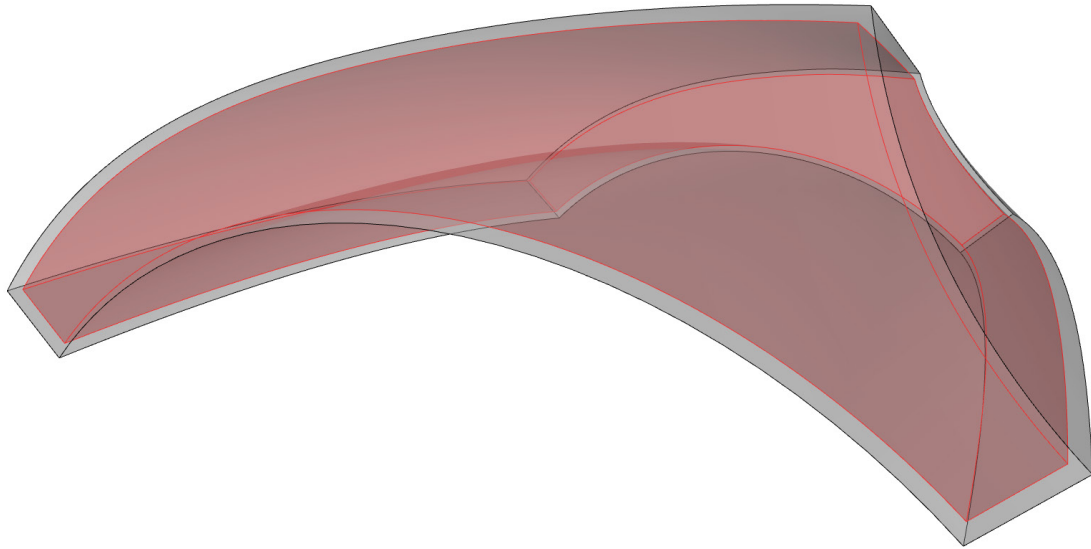
### 5.3. Accuracy driven non-planar slicing: observations and conclusions

What has been observed from 3 different case studies on *Part A* and 2 case studies on *Part B* is that multi-axis ME technology offers the means to provide different layer arrangements to a given part. The layer arrangements analysed in this chapter were all guided by surfaces

extracted from the geometry of the models themselves, in an effort to provide slicing that minimises the errors in accuracy and enables toolpaths to pass closely to the ideal digital geometry of the part. While this conclusion has been recreated and confirmed by the case studies here, in accordance with much of the previous studies in the field of CLFDM, depending on the geometry of the part, following one of its surfaces might not be enough to avoid the staircase effect throughout the entire part model. This seems evident in parts with geometry that is more complex than a uniform thickness part of one dominant doubly curved surface.

In such occasions, the case studies here have demonstrated that one possible method to approach the accuracy issue in non-planar ME would be to apply multi-surface slicing where different operations of non-planar slicing are involved to build up specific sections of the volume of the part, until its completion. Using this method, the majority of the inevitable approximation of a digital geometry by a uniform thickness layer approach in the form of the so-called staircase effect, has been brought towards the inside volume of the part, where its effect on external dimensions is minimised. Many factors are involved in the feasibility of this method: the geometry of the part itself, the ability to perform the required slicing, computational geometry and toolpath development calculations and the ability of the manufacturing system to deliver them in a controlled multi-axis ME process. Furthermore, applying this method requires the decision on which surfaces to use for the slicing of the part and the decision on how many layers to apply them for. For instance, *Case\_Btop* and *Case\_Bside* the top (yellow), side (green) and bottom (red) surfaces (Figure 5.6) have been used to slice *Part B*, but not the rest of the surfaces that have much more planar topology. Also, the number of layers involved in each slicing operation might lead to different outcomes noting the phenomenon of material falling under its own weight as discussed in Section 5.1.5. The combination of these decisions gives varying results, especially in the volume zones close to the edges that separate the slicing surfaces, which could be processed in multiple ways. For example, both the top and side surface could be merged into a single surface which would then be offset to slice and generate layers, but with potential difficulties in mathematically obtaining a correct offset of such surface, or a toolpath with desired characteristics. Seeing how the core concept of this slicing method is to follow the external geometrical topology in order to avoid layered approximations on the surface of the parts, it would seem logical that one potential candidate for optimal accuracy-based slicing would be to unify all part surfaces into one and offset it to create one single layer that would not create any staircase on any surface. A theoretical example of such layer, representing effectively an offset of the original geometric shape is shown in Figure 5.9. However, for such a case to be practically implementable, new methods for slicing and toolpath generations would need to be developed

as well as hardware solutions that would enable an extrusion tool to access the entire digital shape of the part in manufacturing.



*Figure 5.9 Concept for an ideal, theoretical layer spanning across entire part model for slicing strategy aimed at optimising accuracy*

It is presumed that the answer to the question: ‘How many different surfaces and which ones would suffice for a given part?’ is significantly complex and dependent on the complexity of the geometry (e.g. smooth continuous surfaces vs. high dynamics ones with delicate features), the capability of the software and hardware tools to realise the optimal case, assuming one such case exists, as well as process parameters such as the choice of build material or melting temperature. Regardless of these parameters that still remain unresearched, what seems apparent is that multiple surfaces could be used to generate an intricate form of non-planar slicing that can improve part’s quality in terms of external geometrical accuracy.

In conclusion, applying multiple slicing operations through volume sub-division using surfaces extracted from the part geometry, represents one possible method to apply towards reaching an objective of improved accuracy of a given object.

# 6

## Non-planar Slicing Driven by Functionality of Conductive Materials

Similarly to Chapter 5 where case studies were used to examine the effect of various slicing approaches on part accuracy, Chapter 6 will instead investigate the effect that slicing has on functionality of conductive materials.

It has been theorised yet not fully experimentally confirmed that by using multi-axis ME technologies, conductive materials can be deposited in a continuous way during the manufacturing phase of the part, which will affect their post-printing functionality [111]. Due to scarcity of experimental work in this field, in both planar and multi-axis context, the first phase elaborated in Section 6.1 deals with analysing the effect that slicing has on post-printing functionality in conductive materials. These findings then give the basis for the later phase in Section 6.2: a case study where slicing and layer arrangement of multi-axis ME are driven by the optimisation of the functionality of conductive materials, demonstrating a potential way on how using multi-axis ME can be beneficial for mutual use with conductive materials. Section 6.2 therefore uses common geometry (*Part B*) for cross-comparison of slicing strategies aimed at different objectives.

Lastly, Section 6.3 provides the results of a comparative analysis between different slicing strategies applied on equal geometry throughout this research. The obtained conclusions then trigger a final case study design that merges previous slicing strategies and demonstrates their combined use in a slicing strategy optimised for both functionality and accuracy.

---

## 6.1. How to slice for improved conductivity

Aiming to investigate if multi-axis ME can be used to the extent of improving post-printing functionality of conductive materials, an isolated experiment was done, where the goal is to understand the underlying principles that dictate the post-printing conductivity of conductive materials used within Material Extrusion. This experiment was conducted in 3-axis context due to current lack in literature concerning fundamental research in conventional, planar ME and due to the fact that experiment realisation requiring precise movements on a sub-millimetre level can be more tightly controlled in a planar setup than a freeform one. Therefore, a study was performed where planar conductive track samples with constant width and varying heights between  $0.4\text{mm}$  and  $0.8\text{mm}$  were prepared using two different commercial conductive materials in a single, double and triple layer strategy. Functional analysis was done by measuring the resistance of samples at different lengths and comparing it to their corresponding counterparts fabricated with different slicing. Physical characterisation on selected samples was done by measuring the surface area of their cross sections using microscope images and their mass. The conclusions of the study were then used as the basis for a case study investigating the effect of non-planar layer arrangements on functional materials.

### 6.1.1. Introduction

Part of ME's popularity in both research and application realms is due to the high diversity in materials that can be implemented with this process [127]. In a number of works, materials suitable for ME process with different functionality have been developed by dispersing particles in thermoplastic matrix [128]. One such functionality that is not otherwise exhibited to a high extent by a certain base polymer and has been obtained when different particles are added to the base polymer matrix is conductivity [129]. Similar works have been done on compounds involving acrylonitrile-butadiene-styrene (ABS) by [130] and polypropylene (PP) material by [131] resulting in a variety of materials, each with different mechanical, morphological and functional characteristics obtained with different process parameters. Common extrusion approaches include thermoplastic deposition [132] and inks or pastes extrusion [133] and [134] with some research involving hybrid methods across ME and other AM processes [102]. Their use in conjunction with ME process allows for the design of electronic components [135] or features that exhibit conductive characteristics embedded in an object, such as conductive tracks [136].



However, between the material specifications as its intrinsic property, and the final obtained functionality in terms of conductivity after the material has been used through the ME process, the object needs to be passed through the processing pipeline. As it has been noted in many cases in this work and regardless of the fact if the ME process is a 3-axis one or a non-planar, multi-axis one, this process pipeline consists of various steps such as slicing, toolpath generation and manufacturing [8]. Some studies such as [130] and [137] have analysed how the resistivity of conductive thermoplastic compounds changes after printing and its dependency of the building direction, but with geometric shapes that resemble a three-dimensional object rather than a conductive connection and with little detail on the processing parameters, particularly regarding the slicing.

The goal of Section 6.1 study is to understand the effects of slicing on the resistivity of single-line conductive tracks manufactured by ME process in order to be able to assess the potential of multi-axis ME to offer benefit when depositing functional materials or parts with embedded functional materials. Consequently, it serves as a validation of the need for guiding slicing for the purpose of affecting post-printing functionality. It aims at achieving this through a post-printing functional analysis by measuring the resistivity exhibited by conductive tracks of different slicing strategies in a first step of the study. With an objective of isolating the slicing as the only independent variable and maintaining high repeatability and accuracy required for the experiment, the primary phase has been done in a planar, 2-dimensional context. The experimental step was followed by a post-printing physical characterisation of the samples in terms of mass and cross sectional area, in order to verify the equivalence between compared samples, as some of these parameters have been closely related to the resistance of conductive tracks as noted in [132] and [129].

### 6.1.2. Post-printing functional analysis

The post-printing functional analysis represents the principle part of this study that focuses on examining the effect slicing strategy has on the post-printing functionality of the conductive tracks, analysed via the resistance exhibited by the samples after being 3D printed by ME. The resistivity is therefore regarded as an inverse proportional indicator of the conductivity, and consequently the functionality, of the conductive tracks.

### 6.1.2.1. Methodology and design of experiment

A single-line serpentine shape represented in Figure 6.1a), with constant outer dimensions of  $96\text{mm} \times 60\text{mm}$ , constant width of  $1.4\text{mm}$  and  $6\text{mm}$  of distance between the lines has been defined as a sample shape. The serpentine style was selected as an appropriate one due to its potential to maximise the length of the conductive track samples while minimising footprint and therefore lowering the possibility for an error due to a suboptimal calibration between the substrate and the printing nozzle of the 3D printer. Samples with  $0.4\text{mm}$ ,  $0.5\text{mm}$ ,  $0.6\text{mm}$ ,  $0.7\text{mm}$  and  $0.8\text{mm}$  of total height were fabricated in a single, double and triple layer strategy as illustrated in Figure 6.1b) and according to Table 6.1. The lowest implemented layer height was  $0.2\text{mm}$  while the highest one was  $0.8\text{mm}$ , in order to keep the layer heights used for the experiment within 20%-80% of the  $1\text{mm}$  nozzle diameter used for this study (Table 6.3). Therefore, triple layer strategies for samples with total height of  $0.4\text{mm}$  and  $0.5\text{mm}$  were omitted from the experiment.

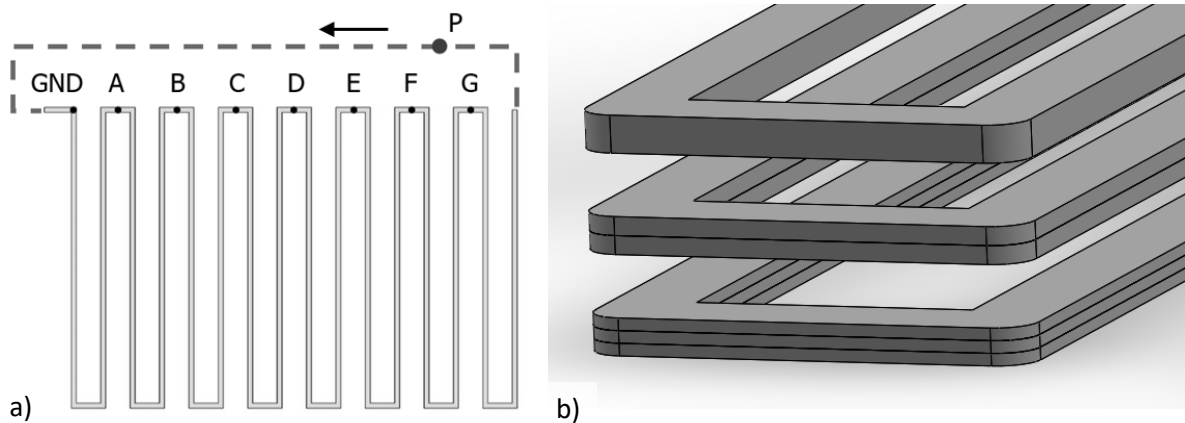


Figure 6.1 Design of sample shape for experiment: a) A schematics in top view, b) From the top: a CAD model of single, double and triple slicing strategy of a sample with an equal total height

All samples were initially manufactured in a closed-loop shape as shown in Figure 6.1a), with a starting/ending point  $P$  and a printing direction as indicated by the arrow, and were later brought to an open-loop serpentine shape by cutting out the segment represented with dashed line after removal from the print bed and before measurement. This was done in order to have a final sample made by a steady extrusion process, undisturbed by possible extrusion variations in the start of new samples or whenever the printing process involved a move in  $Z$  axis to proceed to a successive layer. Post-printing functionality was assessed by measuring the resistivity of the conductive tracks between 7 different segments of each of the samples ( $[GND - A]$ ,  $[GND - B]$ ,  $[GND - C]$  etc.) as depicted in Figure 6.1a).

Slicing Strategy	Total Sample Height				
	0.4mm	0.5mm	0.6mm	0.7mm	0.8mm
<b>Single</b>	1 layer of 0.4mm	1 layer of 0.5mm	1 layer of 0.6mm	1 layer of 0.7mm	1 layer of 0.8mm
<b>Double</b>	2 layers of 0.2mm	2 layers of 0.25mm	2 layers of 0.3mm	2 layers of 0.35mm	2 layers of 0.4mm
<b>Triple</b>	N/A	N/A	3 layers of 0.2mm	3 layers of 0.233mm	3 layers of 0.267mm

Table 6.1 Slicing Strategies applied to conductive tracks samples with different height

Two different PLA-based commercial conductive 3D printing filaments were used to fabricate the samples: a material referred to as *Conductive PLA Proto-Pasta* from the manufacturer *ProtoPlant, Inc.* [138] and a material referred to as *AlphaOhm* from manufacturer *FiloAlpha* [139]. Both of the materials were used in a filament form of 1.75mm diameter. Implementing the slicing strategies according to Table 6.1 led to 13 different batches of samples, with 3 samples per batch for a statistical significance for each of the materials, resulting in a total number of 78 conductive track samples. The samples were 3D printed by an in-house developed 3D printer shown in Figure 6.2 and with specifications shown in Table 6.2. Prior to the fabrication of the samples, a calibration process was done to bring the printing substrate and the tip of the nozzle as close as possible to a coplanar state, minimizing the variation in distance in Z axis between them when moving the extruder in XY plane.

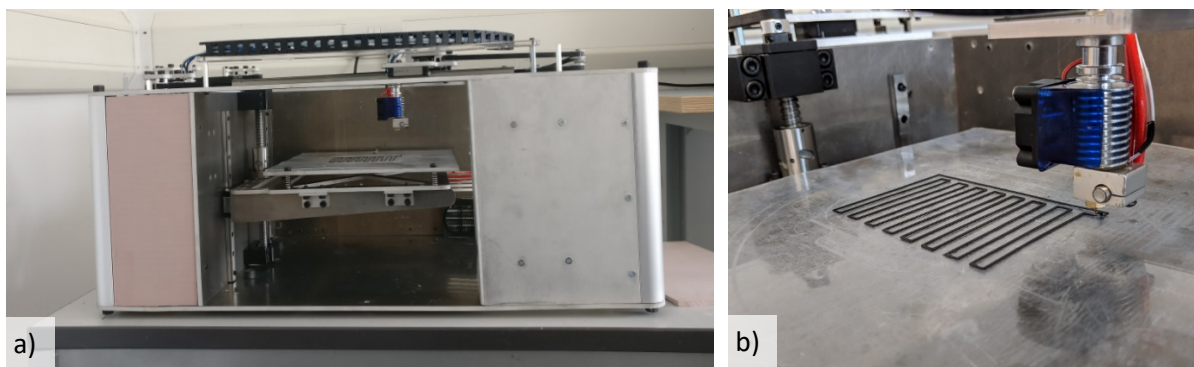


Figure 6.2 Images of the in-house 3D printer used to manufacture the samples: a) Front view of the 3D printer, b) A deposited sample of a conductive track

<b>3D Printer Specifications</b>			
<b>External Dimensions</b>	606mm x 345mm x 356mm	<b>Actuation Assemblies</b>	Nema 17 stp. motors, XY belt driven, Z ball screw driven
<b>Build Area</b>	120mm x 140mm x 215mm	<b>Connectivity</b>	WIFI, USB
<b>Extrusion System Type</b>	Bowden	<b>Max. Printing Speed</b>	Firmware limited to 100mm/s
<b>Max Extruder Temp</b>	280 °C	<b>Resolution</b>	XY 12,5µm, Z 1,25µm (x16 micro-stepping mode)

Table 6.2 3D Printer Specifications

The process parameters used for the manufacturing of the samples are shown in Table 6.3. The only variation in the process parameters between the different materials was the printing temperature that was selected according to the corresponding manufacturer's guidelines. Within each conductive material, the process parameters were kept constant in order to isolate the layer height and number of layers as the only independent variables in the experiment. *Simplify3D* software [140] was used to specify process parameters and generate the instruction lists (g-code).

<b>Process Parameter</b>	<b>Value</b>	<b>Process Parameter</b>	<b>Value</b>
<b>Nozzle Diameter</b>	1mm	<b>Manufacturing Speed</b>	10 mm/s
<b>Extrusion Temp.</b>	<i>ProtoPasta</i> : 225°C <i>AlphaOhm</i> : 220°C	<b>Road (Extrusion) Width</b>	1.4 mm
<b>Substrate Temp.</b>	Ambient (no heating)	<b>Heated Environment</b>	No

Table 6.3 Process Parameters applied throughout the experiment

#### 6.1.2.2. Experimental procedures and measured data

Conductive tracks samples were deposited according to the methodology described in section 6.1.2.1. The samples were then measured in 14 points. Actual height was kept within  $\pm 0.04\text{mm}$  and actual width was kept within  $\pm 0.08\text{mm}$ . Samples that did not satisfy

these constrains were discarded. Images of conductive track samples with and without magnification are shown in Figure 6.3.

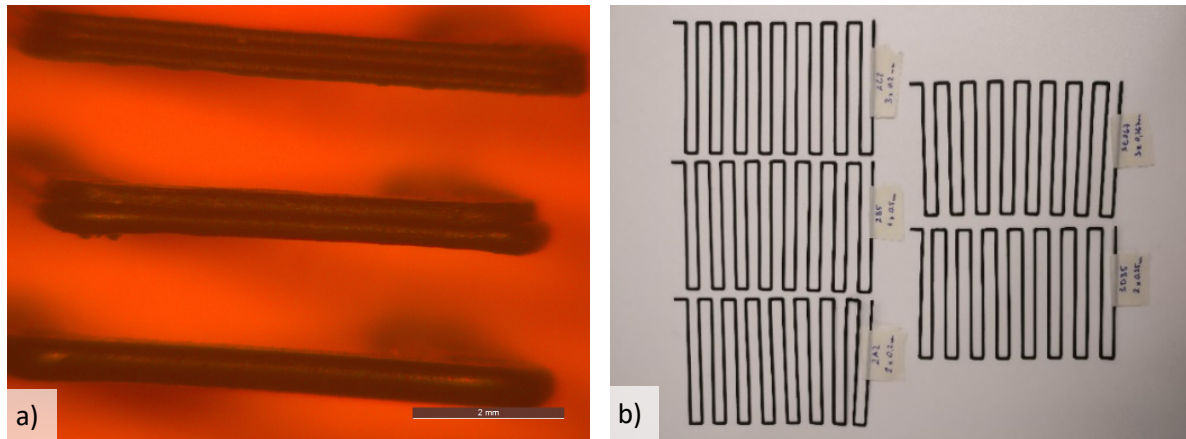


Figure 6.3 Images of deposited conductive tracks: a) Microscope image of 3 segments of 0.6mm conductive tracks with 3 different deposition strategies, b) Image of 5 samples used in the experiment

The post-printing functionality was accessed via measuring the resistance by placing two probes, one fixed on the “GND” position while the other was subsequently repositioned between points “A” and “G” as depicted in Figure 6.1a). *Hirschmann* safety probes were used for an enveloped contact along the entire profile of the samples and a constant contact force, while *Agilent 34405A* device was used to read the resistance. Figure 6.4 shows the equipment used and the measurement process.

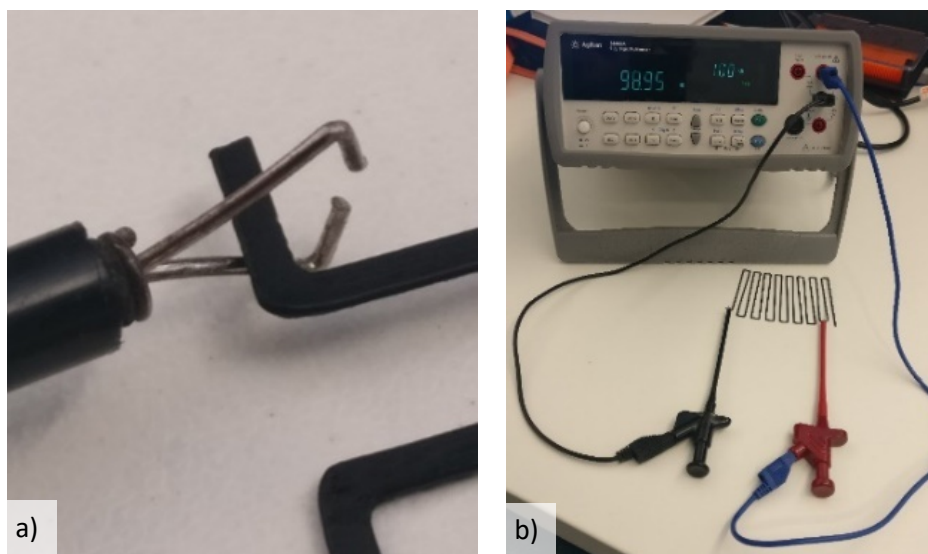


Figure 6.4 Resistivity measurements and equipment: a) Open Hirschmann safety probe prior to contact, b) Agilent device used to measure resistivity

The results of the measurements are reported in Table 6.4. For brevity and compactness, only the average resistance noted across the mid-length segment “GND-D” is shown as a reference point for the exhibited resistance. Complete measurements data can be found in Appendix B. In bold, the increase in resistance of double-layered samples when compared with single-layered ones, and the increase of triple-layered samples when compared with both double and single-layered counterparts from the same material. The final results in bold contain the analysis of the resistance measures across all 7 segments. The Relative Standard Deviation (RSD) was limited to 3.2% for *ProtoPasta* samples and 4.98% for *AlphaOhm* samples.

Total Height	Slicing Strategy	Material	Resistance of GND-D	Avg. Resist. Increase w.r.t 1 layer	Avg. Resist. Increase w.r.t 2 layers
0.4 mm	1 x 0.4 mm	<i>ProtoPasta</i>	75.04 [kΩ]	-	-
		<i>AlphaOhm</i>	36.86 [kΩ]	-	-
	2 x 0.2 mm	<i>ProtoPasta</i>	97.12 [kΩ]	<b>29.31 %</b>	-
		<i>AlphaOhm</i>	65.67 [kΩ]	<b>78.26 %</b>	-
0.5 mm	1 x 0.5 mm	<i>ProtoPasta</i>	58.36 [kΩ]	-	-
		<i>AlphaOhm</i>	25.92 [kΩ]	-	-
	2 x 0.25 mm	<i>ProtoPasta</i>	72.78 [kΩ]	<b>24.71 %</b>	-
		<i>AlphaOhm</i>	39.00 [kΩ]	<b>49.88 %</b>	-
0.6 mm	1 x 0.6 mm	<i>ProtoPasta</i>	50.08 [kΩ]	-	-
		<i>AlphaOhm</i>	21.98 [kΩ]	-	-
	2 x 0.3mm	<i>ProtoPasta</i>	59.70 [kΩ]	<b>19.03 %</b>	-
		<i>AlphaOhm</i>	29.07 [kΩ]	<b>32.83 %</b>	-
	3 x 0.2 mm	<i>ProtoPasta</i>	62.93 [kΩ]	<b>24.85 %</b>	<b>4.89 %</b>
		<i>AlphaOhm</i>	44.43 [kΩ]	<b>102.27 %</b>	<b>52.28 %</b>
0.7 mm	1 x 0.7 mm	<i>ProtoPasta</i>	41.55 [kΩ]	-	-
		<i>AlphaOhm</i>	16.52 [kΩ]	-	-
	2 x 0.35 mm	<i>ProtoPasta</i>	47.09 [kΩ]	<b>13.13 %</b>	-
		<i>AlphaOhm</i>	21.38 [kΩ]	<b>29.7 %</b>	-
	3 x 0.233 mm	<i>ProtoPasta</i>	51.61 [kΩ]	<b>24.06 %</b>	<b>9.66 %</b>
		<i>AlphaOhm</i>	30.61 [kΩ]	<b>84.87 %</b>	<b>43.13 %</b>
0.8 mm	1 x 0.8 mm	<i>ProtoPasta</i>	36.55 [kΩ]	-	-
		<i>AlphaOhm</i>	15.09 [kΩ]	-	-
	2 x 0.4 mm	<i>ProtoPasta</i>	39.35 [kΩ]	<b>7.80 %</b>	-
		<i>AlphaOhm</i>	18.63 [kΩ]	<b>23.23 %</b>	-
	3 x 0.267 mm	<i>ProtoPasta</i>	44.39 [kΩ]	<b>21.67 %</b>	<b>12.87 %</b>
		<i>AlphaOhm</i>	23.84 [kΩ]	<b>58.17 %</b>	<b>28.36 %</b>

Table 6.4 Measured and processed data from the functional analysis experiment

### 6.1.3. Post-printing physical characterisation

In a secondary part of this study, a physical characterisation of the cross sections has been done on the samples made by the *ProtoPasta* conductive material that showed lower

discrepancy in resistivity and lower RSD, in an effort to investigate if a possible variation in the cross sections' areas of samples produced with different slicing strategy could relate to the difference in the post-printing functionality. In addition, the mass of all samples was also measured in order to provide an additional physical indicator for the level of equivalence between sample batches of equal total height but different slicing strategy, as it could indicate a potential uneven extrusion, for example in a case of gas inclusions within the samples.

#### 6.1.3.1. Methodology

The process of measurement of the cross sections of conductive track samples indirectly introduced the challenge of revealing and analysing a cross section of an object as little as  $1.4\text{mm} \times 0.4\text{mm}$  made by thermoplastic compound, without affecting the geometry of the cross section itself. In order to avoid such an issue, in this study, a method was used where two random cross sections were cut from each sample made by *ProtoPasta* material, submerged in epoxy resin, and subsequently polished after hardening to an unaltered cross section of the conductive tracks sample before taking a microscopic image of the cross section for measurement and analysis. A sample holder was designed to receive 6 samples of each sample batch as illustrated in Figure 6.5.

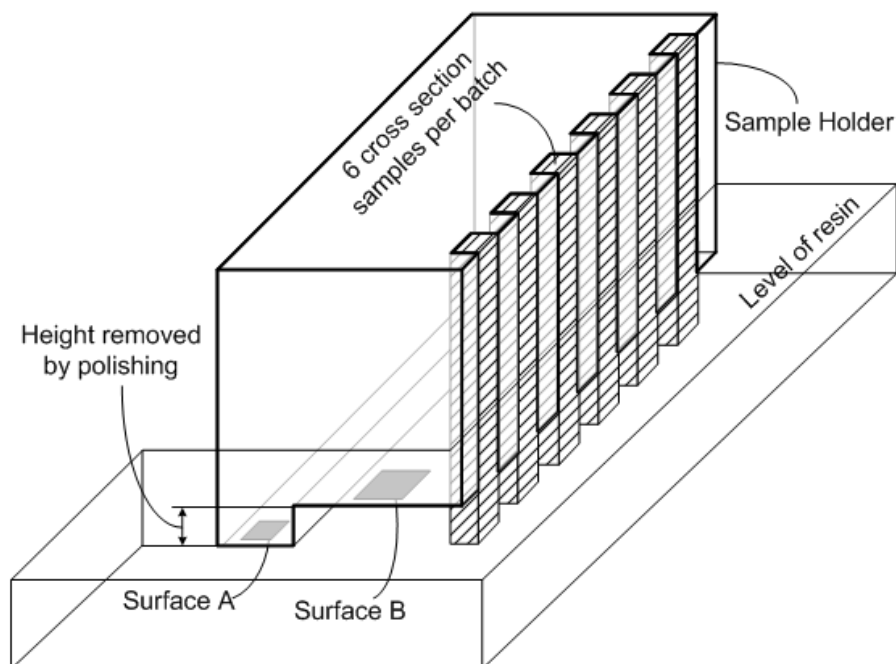


Figure 6.5 An illustration of the sample holder design with 6 cross sections mounted and submerged in resin

Random cross sections were cut away from the central zone of the samples as illustrated in Figure 6.6a) with example sections *T* and *Q*. 13 such sample holders were 3D printed by ME and together with 6 sections of the conductive tracks extending approximately to the length of surface *A* (Figure 6.5) were submerged in a mixture of *EpoxiCure*<sup>™</sup> 2 resin and hardener. After hardening, the samples were polished down with a P240 grade polishing paper until surface *B* was revealed through the resin, after which they were additionally polished with a P600 grade polishing paper for 5 minutes. This was done to ensure that the final cross section revealed after the polishing process is in an unaltered section of the conductive track. Images of the cross sections were then captured by an optical microscope using a *Leica DFC295* digital camera, in order to further measure their surface area of cross sections belonging to samples with different batches and compare it to their corresponding counterparts of equal total height but different slicing strategy. An image of a polished sample revealing 6 cross sections is shown in Figure 6.6b).

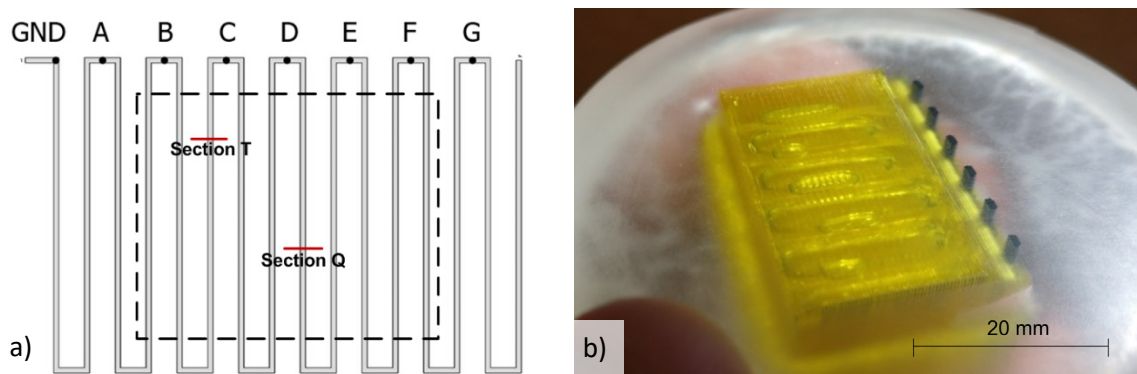


Figure 6.6 Sample preparation for cross section analysis: a) An example of two random sections cut away from the mid-zone of a conductive track sample b) a polished sample revealing 6 cross sections for microscopy imaging

### 6.1.3.2. Experimental procedures and measured data

*ImageJ* software was used in order to extract the contour of the cross section and measure its area. The images were converted to 32 bit grayscale type (Figure 6.7a)), their threshold adjusted until a clear distinction of the cross section was achieved, to lastly measure the area of the cross section by extracting the outline as shown in Figure 6.7b). Using this method, 6 cross sections per sample batch were analysed for a total of 78 images. The mass of the samples was also measured with *HR73 Halogen Moisture Analyzer*. The results of the cross sectional area analysis of samples made by *ProtoPasta* only, and the mass measurements and deviations of all samples are reported in Table 6.5.



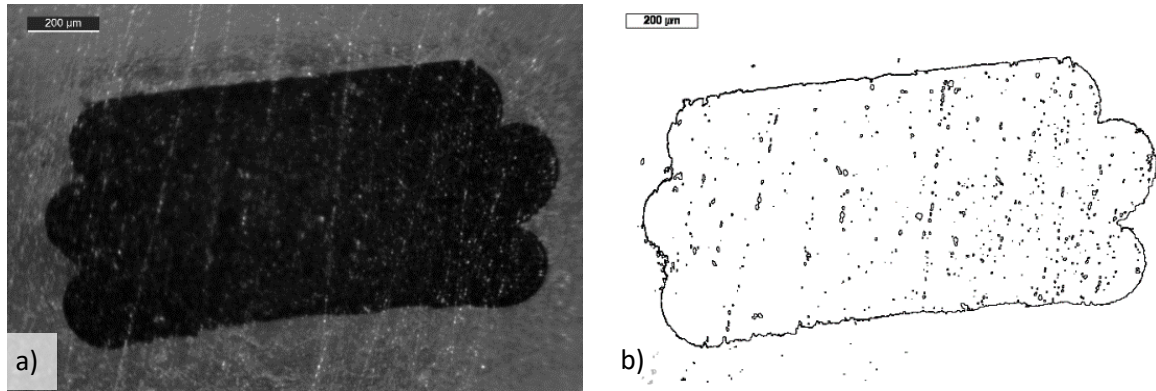


Figure 6.7 An example of image analysis process of one cross section of a conductive track sample with a total height of 0.7mm made by triple layer strategy: a) 32 bit grayscale image, b) extracted outline for surface area measurement

Total Height [mm]	Slicing Strategy [layers x mm]	Avg. area of cross section [mm <sup>2</sup> ]	Avg. difference w.r.t 1 layer	Avg. difference w.r.t 2 layers	Material	Measured Mass [gr]	Avg. difference w.r.t 1 layer
0.4	1 x 0.4	0.5167	-	-	ProtoPasta	0.694	
					AlphaOhm	0.758	
	2 x 0.2	0.4886	-5.44%	-	ProtoPasta	0.663	-4.46 %
					AlphaOhm	0.76	0.22 %
0.5	1 x 0.5	0.6434	-	-	ProtoPasta	0.847	
					AlphaOhm	0.935	
	2 x 0.25	0.605	-5.97%	-	ProtoPasta	0.806	-4.84 %
					AlphaOhm	0.947	1.25 %
0.6	1 x 0.6	0.7442	-	-	ProtoPasta	0.986	
					AlphaOhm	1.076	
	2 x 0.3	0.6951	-6.58%	-	ProtoPasta	0.928	-5.9 %
					AlphaOhm	1.139	5.95%
					ProtoPasta	0.980	-0.6 %
					AlphaOhm	1.147	6.6 %
0.7	1 x 0.7	0.8878	-	-	ProtoPasta	1.173	
					AlphaOhm	1.34	
	2 x 0.35	0.8817	-0.69%	-	ProtoPasta	1.148	-2.16 %
					AlphaOhm	1.28	-4.4 %
	3 x 0.233	0.8892	0.15%	0.85%	ProtoPasta	1.165	-0.68 %
					AlphaOhm	1.325	-1.1 %
0.8	1 x 0.8	0.9925	-	-	ProtoPasta	1.30	
					AlphaOhm	1.535	
	2 x 0.4	1.006	1.33%	-	ProtoPasta	1.335	2.69 %
					AlphaOhm	1.457	-5.04 %
	3 x 0.267	0.98	-1.24%	-2.58%	ProtoPasta	1.309	0.7 %
					AlphaOhm	1.511	-1.52 %

Table 6.5 Cross section analysis of ProtoPasta samples (left half) and mass measurements of all samples (right half)

#### 6.1.4. Results and conclusion

Referring to the results obtained from the post-printing functional analysis it can be noted that all samples made by double layered strategy exhibited increased resistance when compared to their single layered counterparts of equal height and material. Also, all samples made by triple layered strategy exhibited increased resistance when compared to both their single layered and double layered counterparts of equal height and material. In every occasion where the slicing strategy was increased by 1 layer in the experiment (either from 1 to 2 layers or from 2 to 3 layers) for samples with equal total height, the increase in resistance varied between 7.8% and 29.31% for the *ProtoPasta* samples, and between 23.23% and 78.26% for the *AlphaOhm* samples, despite the fact that *AlphaOhm* is the more conductive material of the two as it can be inferred from Table 6.4. Furthermore, multi-layer slicing increased the resistance by a higher amount in samples with a lower total height. This trend can be seen in both Figure 6.8 regarding data from *ProtoPasta* samples and Figure 6.9 regarding data obtained from *AlphaOhm* samples. One interesting phenomenon that can be noted is that the trend of resistance increase regarding the 2 Vs. 1 layer comparison, has a much more linear characteristics in the case of samples made by *ProtoPasta* material. Another interesting phenomenon can be observed in Figure 6.10 where data for both of the materials are shown regarding a comparison between 3 Vs. 2 layer strategies. Here it can be noted that while *ProtoPasta* samples exhibited an increasing trend with the increase of total sample height, *AlphaOhm* samples exhibited a decreasing one.

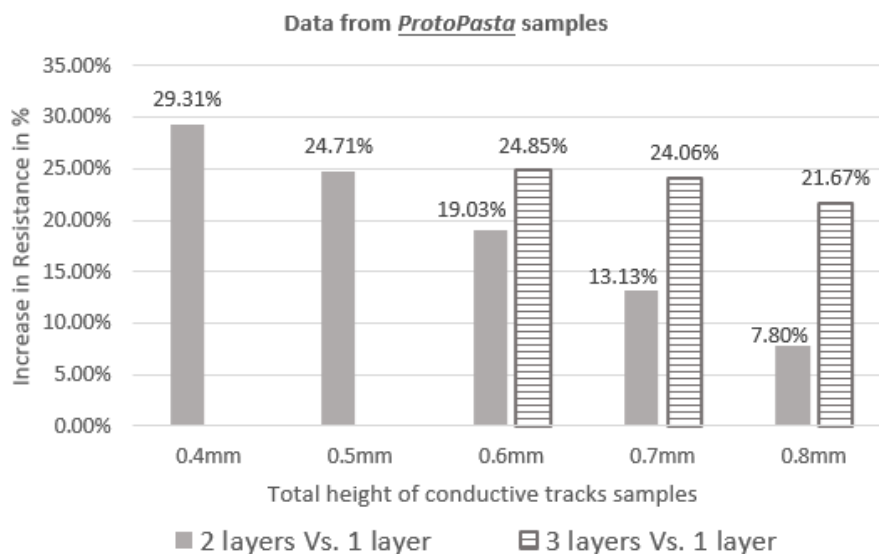


Figure 6.8 Increase in resistance between samples made by *ProtoPasta* material according to total sample height and number of layers used to fabricate the samples

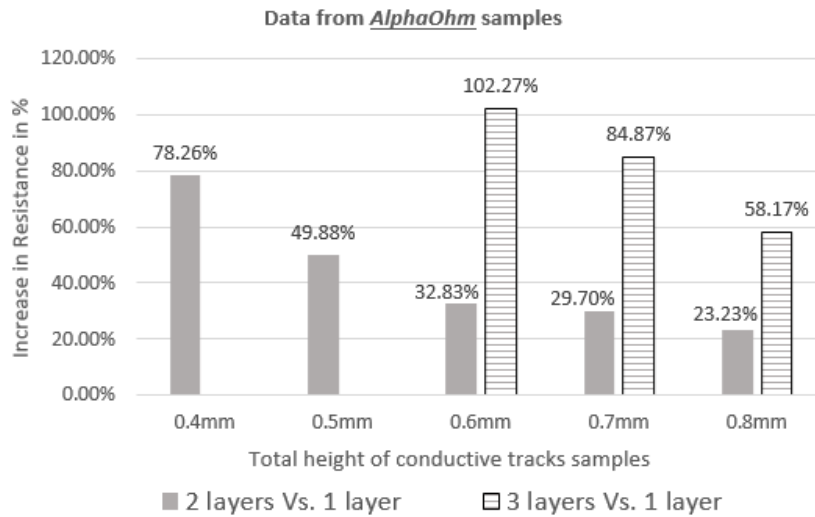


Figure 6.9 Increase in resistance between samples made by AlphaOhm material according to total sample height and number of layers used to fabricate the samples

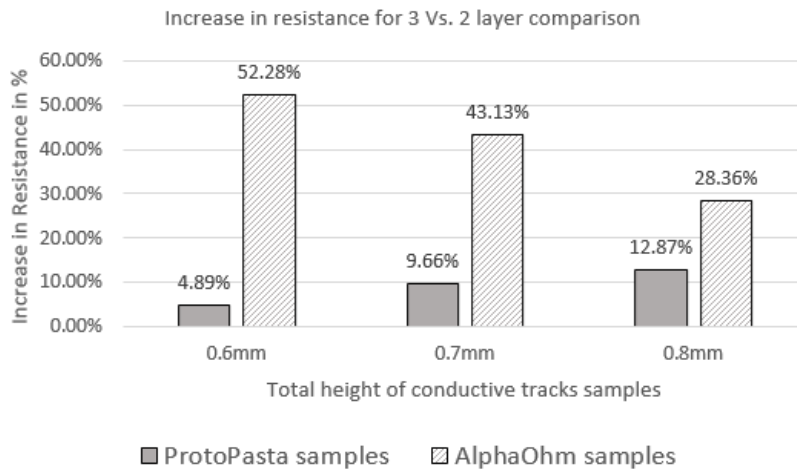


Figure 6.10 Increase in resistance between samples of equal height when comparing 3 Vs. 2 layer strategies

The highest discrepancy for equal height samples made by *ProtoPasta* material was 29.31% noted between double layered and single layered samples of total height of 0.4mm, while the highest discrepancy for the samples made by *AlphaOhm* material was 102.27% noted between triple layered and single layered samples of total height of 0.6mm. The lowest discrepancy for both of the materials was noted between double layered and single layered samples of a total height of 0.8mm, with an average increase in resistance of 7.8% for *ProtoPasta* and 23.23% for *AlphaOhm* material. In addition, the post-printing functional analysis confirmed the expected increase of resistance with the increase of sample's length, and decrease in resistance

with increase of their surface area which is consistent with data from previous research, such as [132] and [129].

A secondary aspect investigated by this study was the post-printing physical characterisation of the conductive track samples. With reference to the results of the mass measurement, all of the multi-layered samples from both of the materials remained within  $-5.9\%$  and  $6.6\%$  with respect to the mass reported by their single layered counterparts. The analysis of the surface area of cross sections extracted from multi-layered samples made by *ProtoPasta* material showed a discrepancy within the range of  $-6.58\%$  and  $1.33\%$  with respect to the surface area of their corresponding single-layered counterparts. Further to the quantitative study, Figure 6.11 gives an example of the different cross section shape that was reported by samples made with different slicing strategy and equal total height due to the difference in slicing.

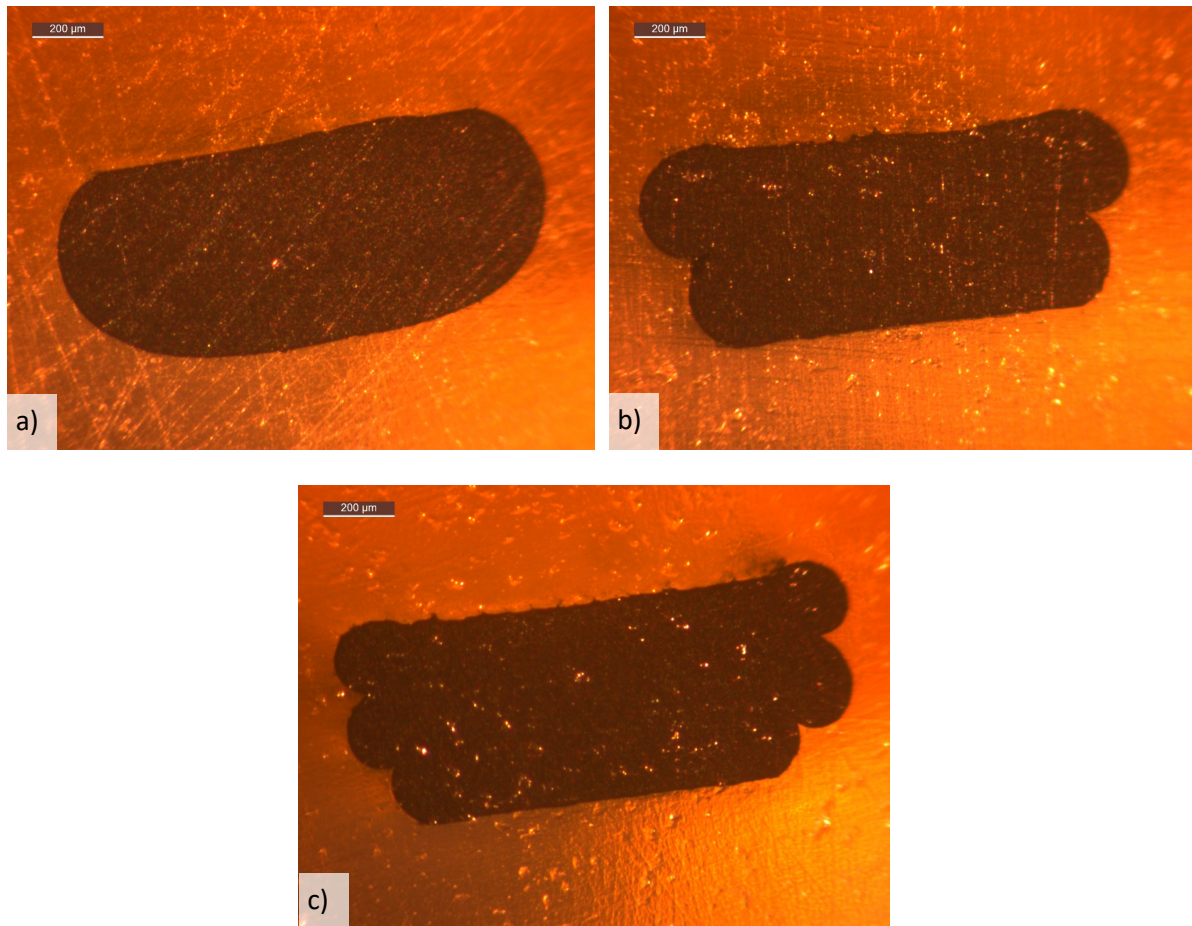


Figure 6.11 An example of shape of cross section according to different slicing in the case of 0.6mm height samples with greatest variation in surface area a) single layer strategy b) double layer strategy c) triple layer strategy

The sample batch represented in Figure 6.11 is the batch where greatest difference of  $-6.58\%$  in surface area between double layered and single layered samples was measured. The smallest amount of surface area variation maintained within a range of  $-0.69\%$  and  $0.85\%$  was reported by the sample batch with a total height of  $0.7\text{mm}$ . Comparing the variations between mass and surface area for samples made by *ProtoPasta* material, similar values can be noted, suggesting that either of the two measures can be regarded as potential indicators in the level of equivalence between samples from the same batch.

In conclusion, this study analysed the post-printing functional and physical characteristics of conductive track samples made by different slicing strategies and two different materials. It deduced that functionality decreases with the increase of number of layers needed to 3D print a conductive track of a given geometry. However, the quantity of increase in resistance, and hence, decrease in functionality, is highly affected by the material used and the manufacturing process. In this study we report an increase in resistance between  $7.8\%$  and  $78.26\%$  depending on the material, in every occasion where the number of layers constituting the track was increased by 1. It also reported increase in resistivity as high as  $102.27\%$  when comparing a triple-layered and single-layered conductive tracks of a total height of  $0.6\text{mm}$  when using *AlphaOhm* material. Furthermore, this increase in resistance is greater in the cases of lower total height of conductive track. Physical characterisation was also done by measuring the mass of all samples, and the surface area of samples made by *ProtoPasta* material only, in order to quantify the equivalence between conductive track samples with equal height but different slicing strategy, and possibly identify the cause of the decrease in functionality. Some of the batches noted higher surface area and mass variations within the range of  $-6.58\%$  to  $6.6\%$ , while in others, physical characterisation variations were well below  $1\%$ . While it is possible that these limited variations, resulting presumably from the non-ideal execution of the experiment, have contributed to the obtained results to some extent, it would seem very unlikely they represent the primary cause in the decrease of functionality according to the data of this study. In fact, referring to Table 7.5, several examples can be identified where samples that exhibited higher surface area and mass by as much as  $6.6\%$  than their counterparts, have nevertheless exhibited an increase in resistance by over  $100\%$  (for ex, 3 vs. 2 layers -  $0.6\text{mm}$  *ProtoPasta*, and 3 vs 1 layer -  $0.6\text{mm}$  *AlphaOhm*). Further work is necessary to understand the reasons behind the decrease in post-printing functionality. One reason could be a modified dispersion or interconnection of the filler particles either within the same layer of the thermoplastic compound or across different layers, as a consequence from the different slicing strategy.

### 6.1.5. Postulates for expansion in 3D space

Experimental data obtained from Section 6.1 is consistent with a theory that given a conductive track with certain geometry and height, its post-printing resistivity can be lowered by fabricating it with the least number of layers (ideally one), whose layer height is kept at maximum. Furthermore, repeatable results with low variance were shown across measurements of different lengths of conductive tracks, from where it can be concluded that this phenomenon is length-indifferent for a given fixed slicing. In this Doctoral Research, the concrete data gathered from experiments are used for providing the basis of two postulates:

P<sub>1</sub>. The same phenomenon occurs also in 3-dimensional, freeform shaped conductive tracks, regardless of the fact that experiments have been done with planar layers.

P<sub>2</sub>. The same phenomenon is valid, at least to some extent, in cases where multi-layer slicing strategy is employed only in a section of a conductive track instead of its entire length.

Further visual descriptions of the two postulates are provided in Figure 6.12 and Figure 6.13 accordingly. With  $R$ , the resistance of the corresponding conductive track model is denoted.  $P_1$  is based on the assumption that if a freeform conductive track would be cut with lines like  $L_1, L_2, L_3$  etc. represented in Figure 6.12, that are small enough distance apart, each cut-out section would resemble the planar samples that were experimentally tested.

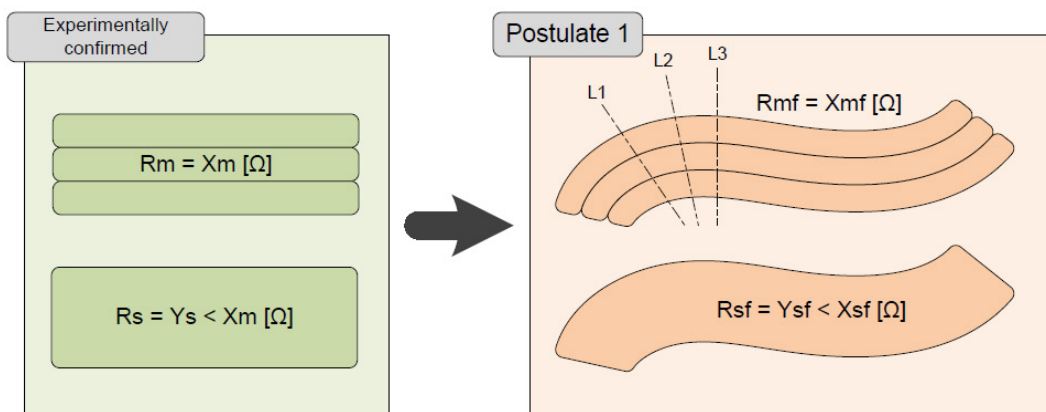


Figure 6.12 Visual description of Postulate 1 – freeform conductive tracks in space would exhibit the same phenomenon of resistance increase by multi-layered manufacturing instead of single-layer one

$P_2$  on the other hand is based on the assumption that any form of layer discontinuity in the manufacturing of a conductive track would result in a segment that could have otherwise been optimised by manufacturing it from a single layer while maintaining geometrical dimensions, as a direct consequence from the obtained results from the experimental phase of Section 6.1. Since the total resistance of the track is the sum of the resistances of all sections that constitute it, however divided, this would lead to an increase in the total resistance of the conductive track. This is particularly noticeable in the sections denoted with  $S_1, S_2, S_3...$  represented in Figure 6.13.

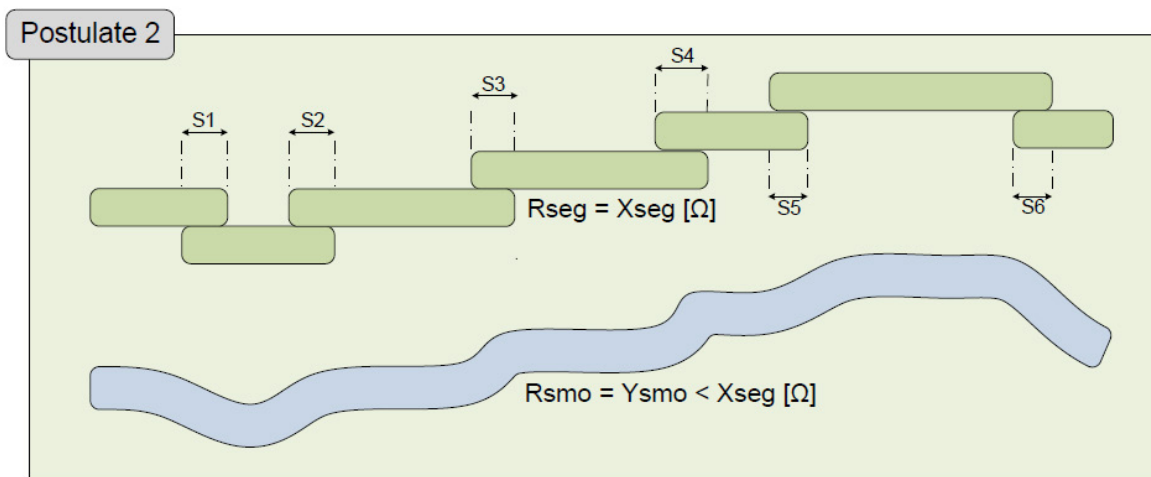


Figure 6.13 Visual description of Postulate 2 – smooth, continuous conductive track will have lower resistance than a counterpart with equal geometry constituting sections manufactured by multi-layer slicing

The above described postulates have been proposed based on theoretical assumptions due to limitations in both time and tools to experimentally test freeform conductive tracks with varying shape embedded into other parts. As such, they also set the basis for revealing the benefit that multi-axis ME brings towards inclusion of conductive tracks, by enabling their single-layer manufacturing in three-dimensional space and thus optimising their conductivity and design freedom. This will be demonstrated through the following case study elaborated in Section 6.2.

Selected work of section 6.1 is being published as a paper in the International Journal of Rapid Manufacturing with the following reference:

Chorbikj, M. and Cavallaro, M. (xxxx) (in press) 'Post-printing characterisation and design for additive manufacturing considerations for conductive tracks 3D printed by material extrusion', Int. J. Rapid Manufacturing, Vol. X, No. Y, pp.xxx–xxx.

The journal paper itself is a revised and expanded version of a paper entitled "Design for Additive Manufacturing Considerations for 3D Printing of Conductive Tracks Using Material Extrusion" presented at 16th Conference on Rapid Design, Prototyping & Manufacturing held at Brunel University, Uxbridge, on Thursday 4th and Friday 5th April 2019.

## 6.2. Applying single layer conductive tracks method

Experimental work in Section 6.1 has concluded that single layer approach offers optimal conductivity when manufacturing conductive tracks. The logic behind  $P_1$  and  $P_2$  postulates has provided the basis for processing a case-study where multi-axis slicing of an object containing conductive tracks is guided by the objective of optimising the conductivity of the conductive tracks. Such a case study will be done on the same *Part B* that was analysed in Section 5.2, with the difference that in this case we assume that there is a functional requirement involving conductive materials. Let us suppose that we need to manufacture *Part B* with 3 embedded conductive tracks that enable a conductive connection between edges  $M$  and  $T$ , while being exposed on the top surface (red) as represented in Figure 6.14.

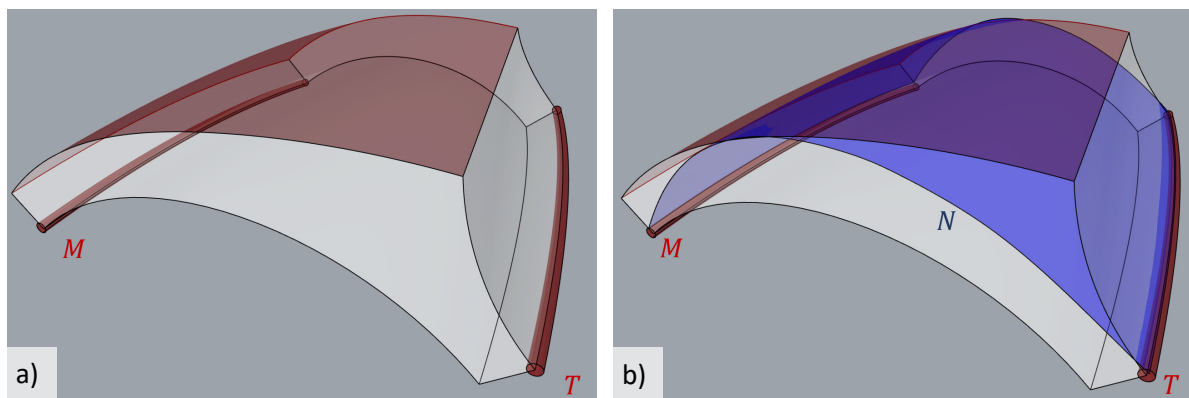


Figure 6.14 Design of case study with embedded conductive tracks: a) *Part B* with required functionality of 3 conductive tracks between edge  $T$ ,  $M$  and top surface; b) definition of a new surface  $N$  that could be used to guide slicing for optimised conductivity

Seeing the effect that slicing has on the functionality of conductive tracks, and assuming postulates  $P_1$  and  $P_2$  are true, one way to optimise the conductivity would be to deposit them in a single layer that would connect edges  $M$ ,  $T$  and at least some area of the top surface of *Part B*. In order to be able to do that, a surface was designed that would guide such slicing, since none of the surfaces belonging to the part can be directly used. This newly constructed surface,



which did not appertain from the model's geometry, is represented by the blue surface  $N$  in Figure 6.14b).

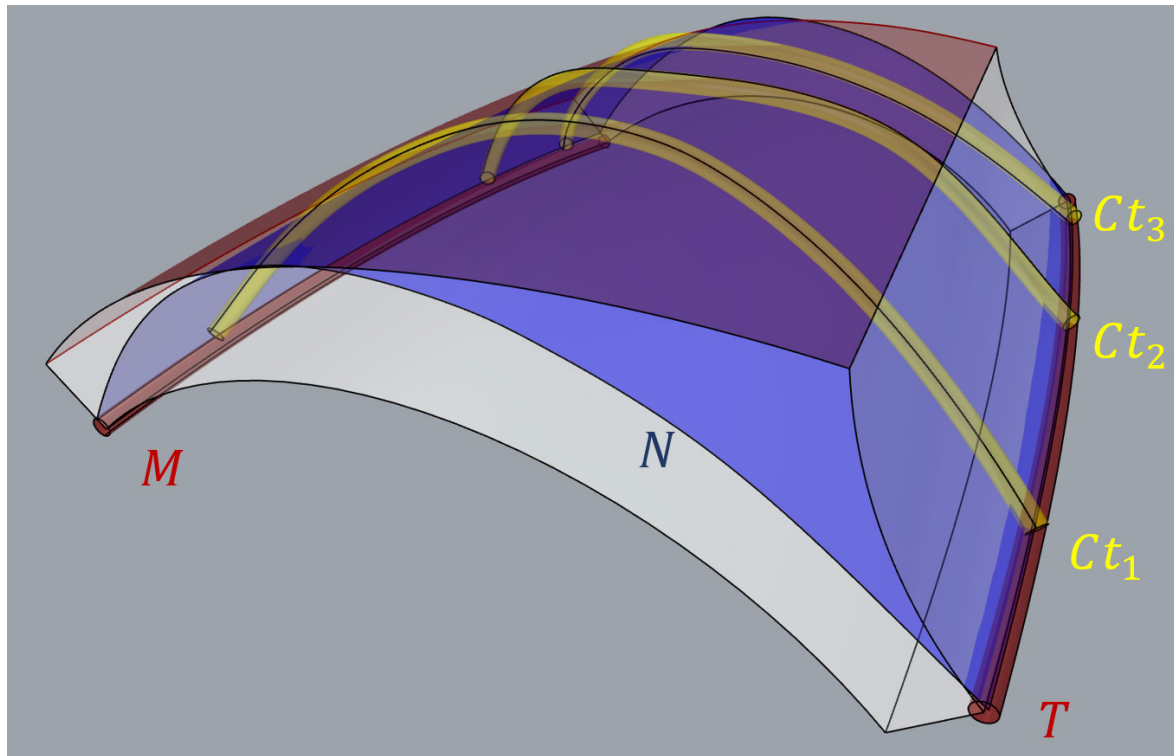


Figure 6.15 Creation of a new surface  $N$  that does not appertain from the part's model to guide slicing oriented towards optimised functionality of conductive tracks  $C_{t1}$ ,  $C_{t2}$  and  $C_{t3}$

Surface  $N$ , as a doubly curved freeform surface, spans across edges  $T$ ,  $M$  and the top surface and it was used to embed in it 3 conductive tracks  $C_{t1}$ ,  $C_{t2}$  and  $C_{t3}$  as shown in Figure 6.15. The rest of the model is then sliced up with that same surface that by manufacturing the desired conductive tracks in a single layer, optimises their post-printing functionality. Surface  $N$  itself was divided into 4 different segments to fill out the space between the conductive tracks. This case study is referenced as *Case\_Bcon*. A comparison between digital simulated slicing and physically printed test samples in different views are presented in Figure 6.16. The conductive material in the physical pieces on the right (black) is ProtoPasta.

An additional illustrative copy of *Case\_Bcon* sample was printed with the modification of inserting an adhesive paper tape between the conductive layer and the rest of the base of the parts, enabling for the creation of a split model to be used for visual confirmation of a single layer conductive tracks embedded into a one freeform layer. This demonstrator model in both assembled and split positioning is shown in Figure 6.17

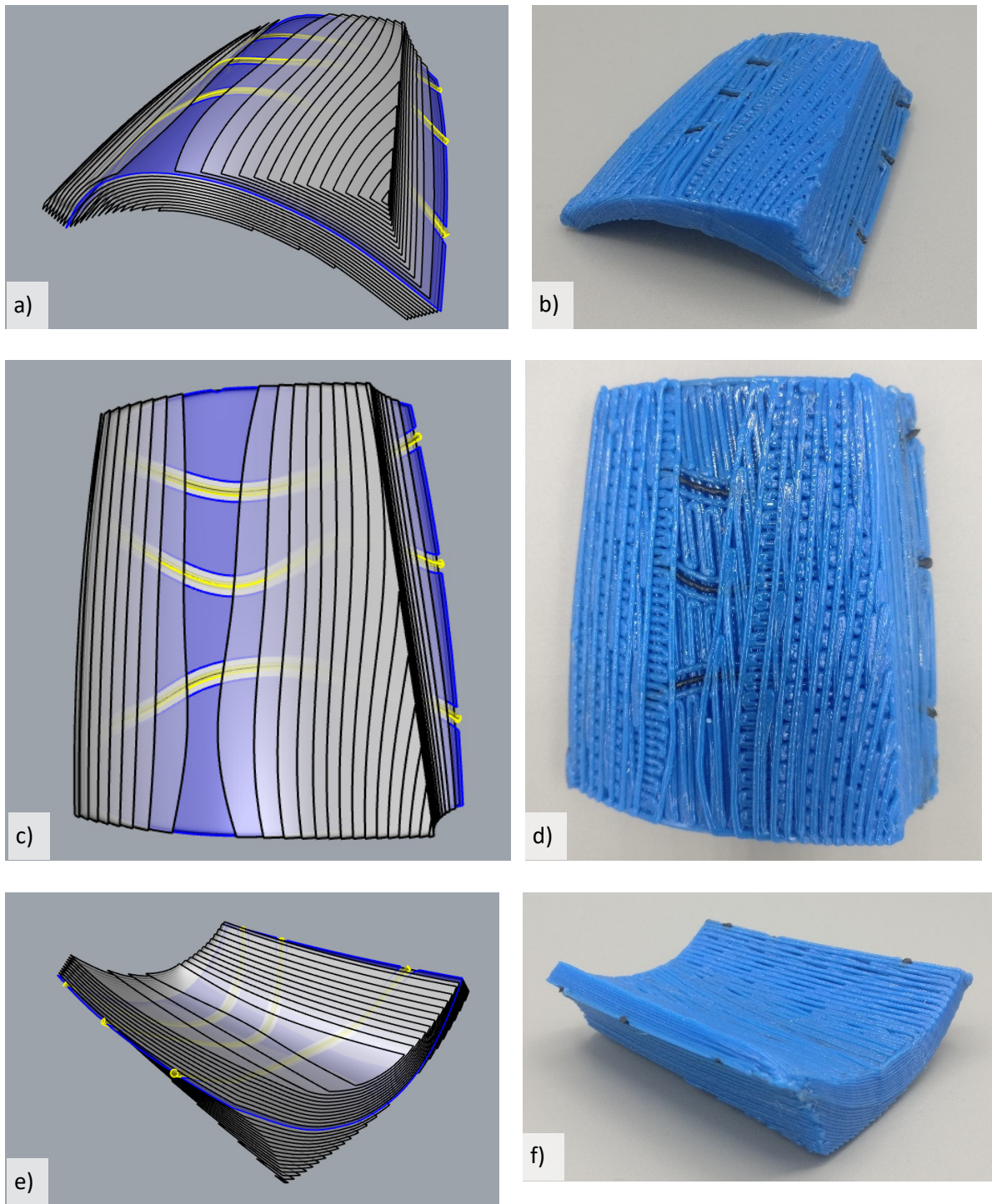


Figure 6.16 Different views of simulated transparent (a),c,e)) and physical (b),d,f)) printed samples with slicing for the purpose of embedding single-layer conductive tracks within a part

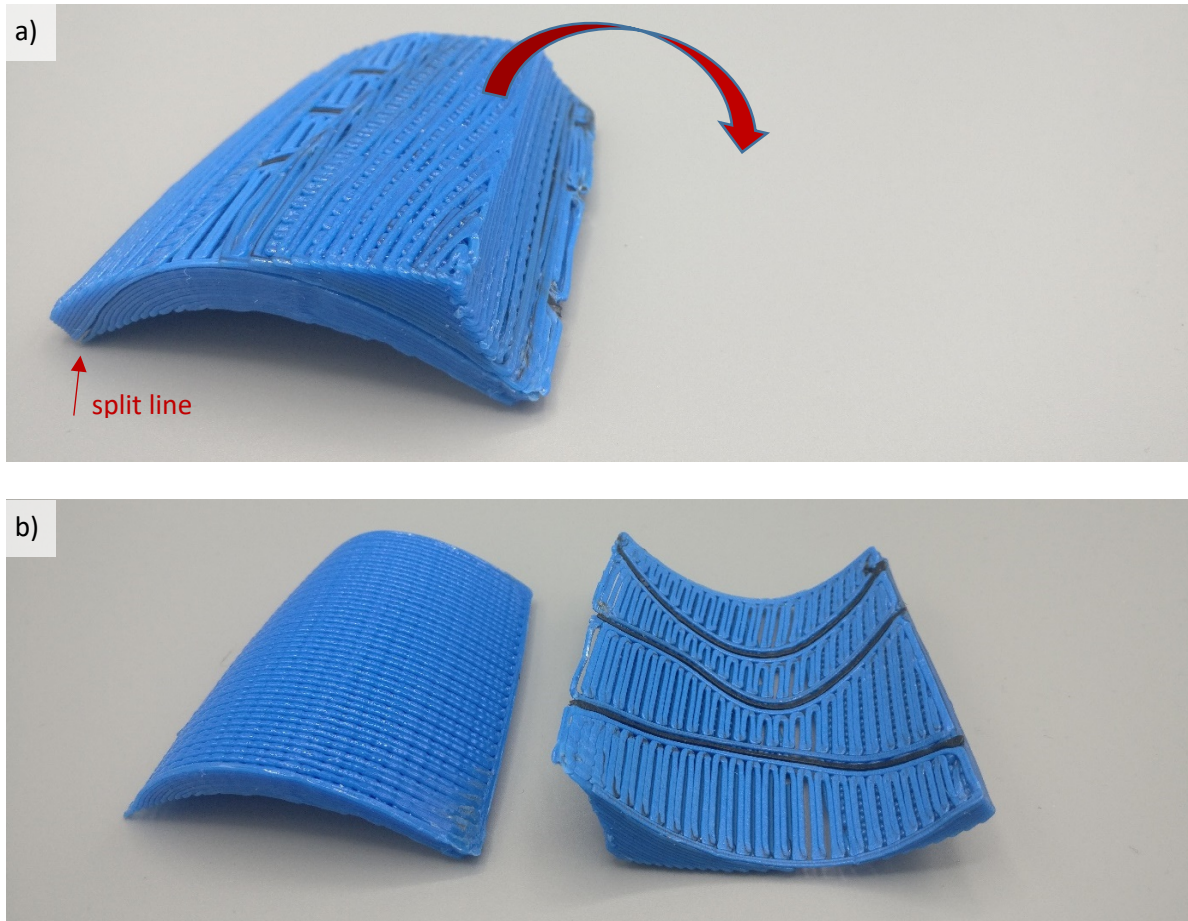


Figure 6.17 A split model for improved visual validation of the single-layered conductive tracks manufactured for optimised post-printing functionality

What can be noticed from Figures 6.16 and 6.17 is that the objective of a functionality driven slicing has been achieved. The layer arrangement of *Part B* has been guided by a user defined freeform surface as to enable the realisation of the desired conductive tracks  $C_{t1}$ ,  $C_{t2}$  and  $C_{t3}$  by one single layer, optimising so their conductivity. Also, all conductive tracks have been exposed to edges  $M$  and  $T$  and the top surface of the object as desired with the objectives for this study, in a doubly-curved freeform shape where conventional 3-axis slicing would be incapable of producing single layered conductive tracks, regardless of the selected printing orientation.

The full information table of *Case\_Bcon* is shown as Table 6.6. Further images of the sample during fabrication can be found in Appendix A.

Geometry: B  
 Name: Case\_Bcon  
 Layer Height: 0.6 mm  
 Num. of layers: 35

Slicing strategy: Entire volume with user defined surface spanning through edges N, T and top surface

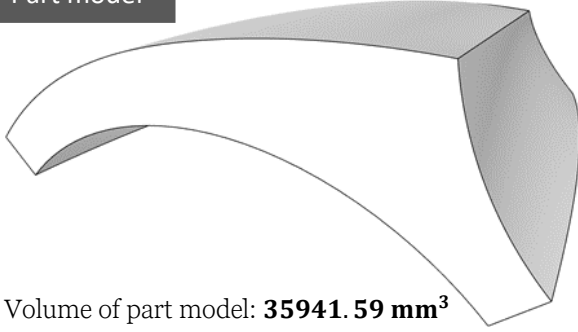
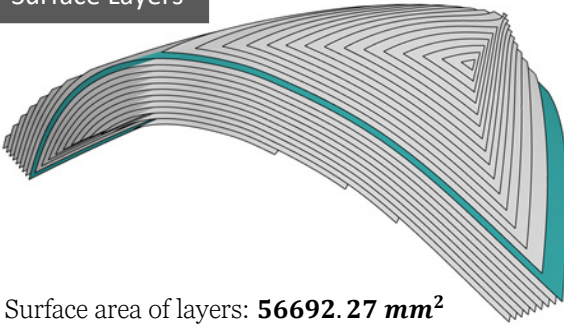
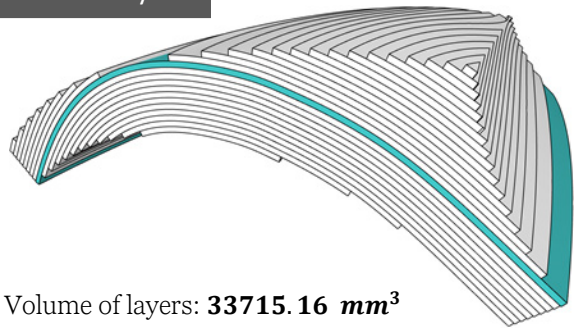
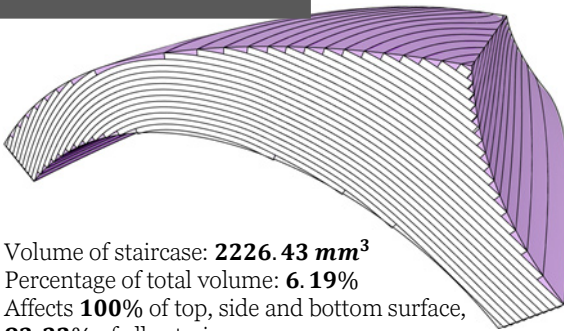
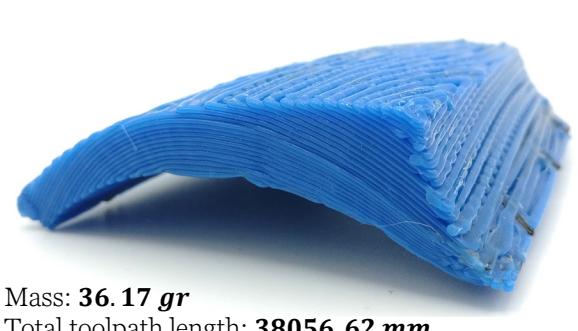
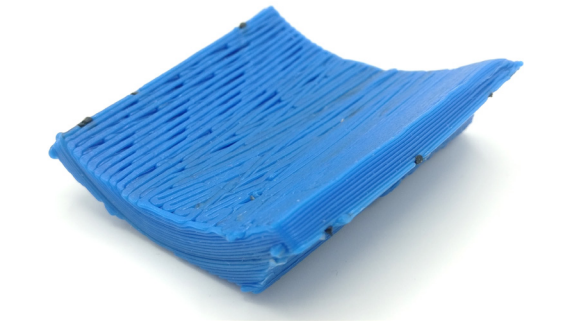

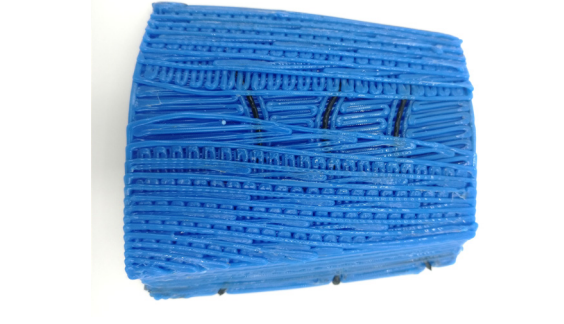
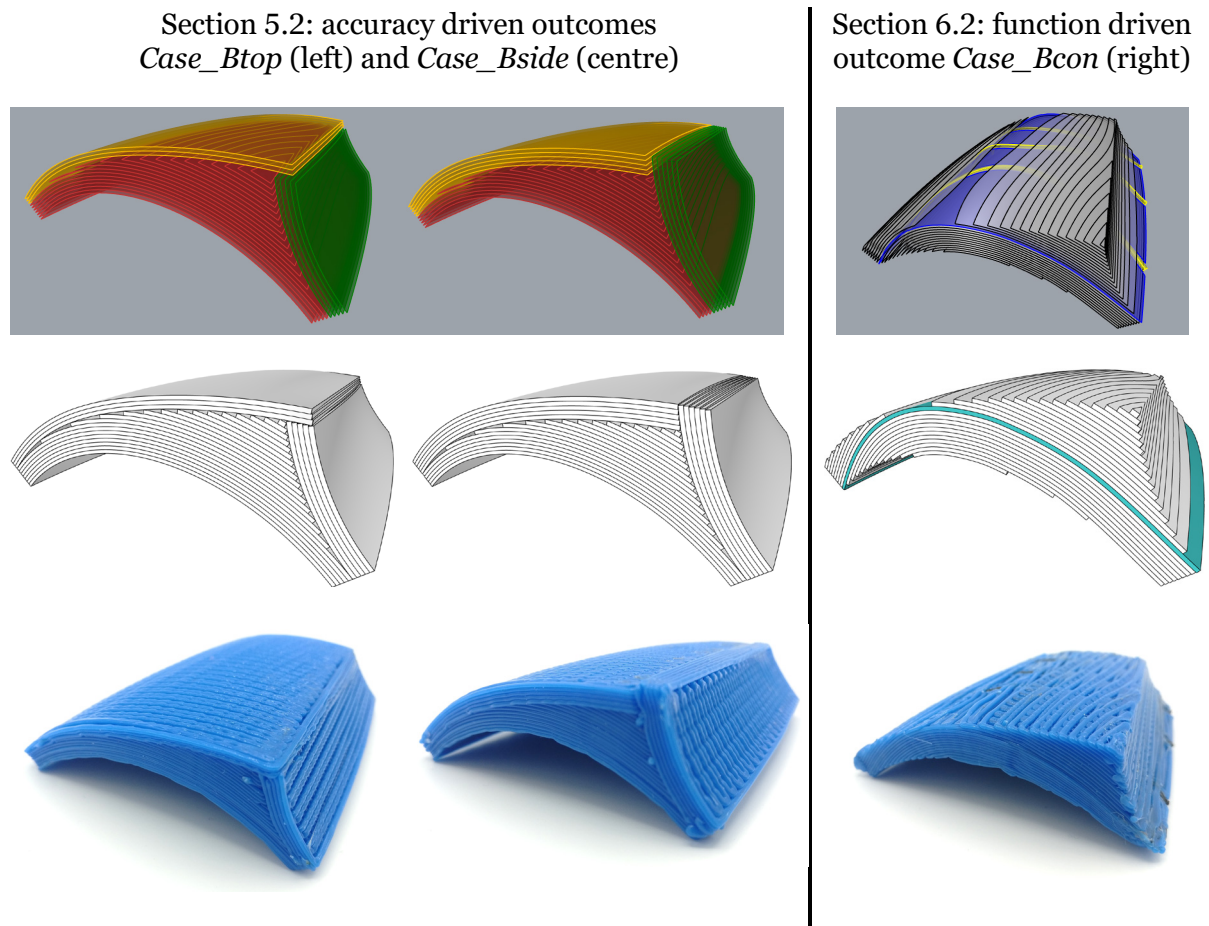
<p><b>Part model</b></p>  <p>Volume of part model: <b>35941.59 mm<sup>3</sup></b></p>	<p><b>Surface Layers</b></p>  <p>Surface area of layers: <b>56692.27 mm<sup>2</sup></b></p>
<p><b>Volume Layers</b></p>  <p>Volume of layers: <b>33715.16 mm<sup>3</sup></b></p>	<p><b>Staircase visualisation</b></p>  <p>Volume of staircase: <b>2226.43 mm<sup>3</sup></b>        Percentage of total volume: <b>6.19%</b>        Affects <b>100%</b> of top, side and bottom surface,  <b>83.32%</b> of all exterior.</p>
<p><b>Isometric top view</b></p>  <p>Mass: <b>36.17 gr</b>        Total toolpath length: <b>38056.62 mm</b></p>	<p><b>Isometric bottom view</b></p> 
<p><b>Front view</b></p> 	<p><b>Top view</b></p> 

Table 6.6 Case\_Bcon study info table

### 6.3. Comparing and combining function driven with accuracy driven slicing: results

Case studies from Section 5.2 have demonstrated outcomes where slicing is done using multiple surfaces extracted from the digital model of the part through volume sub-division, guiding so the layers to follow the ideal part's geometry and therefore optimise accuracy. Section 6.2 on the other hand applies a user defined freeform surface to process a slicing method that enables the embedding of single-layer conductive tracks, therefore, optimising their post-printing functionality, but with a rather poor outcome in terms of accuracy. In Figure 6.18, additional comparative views of accuracy guided slicing strategy from Section 5.2 with conductivity guided slicing strategy from Section 6.2 are presented.



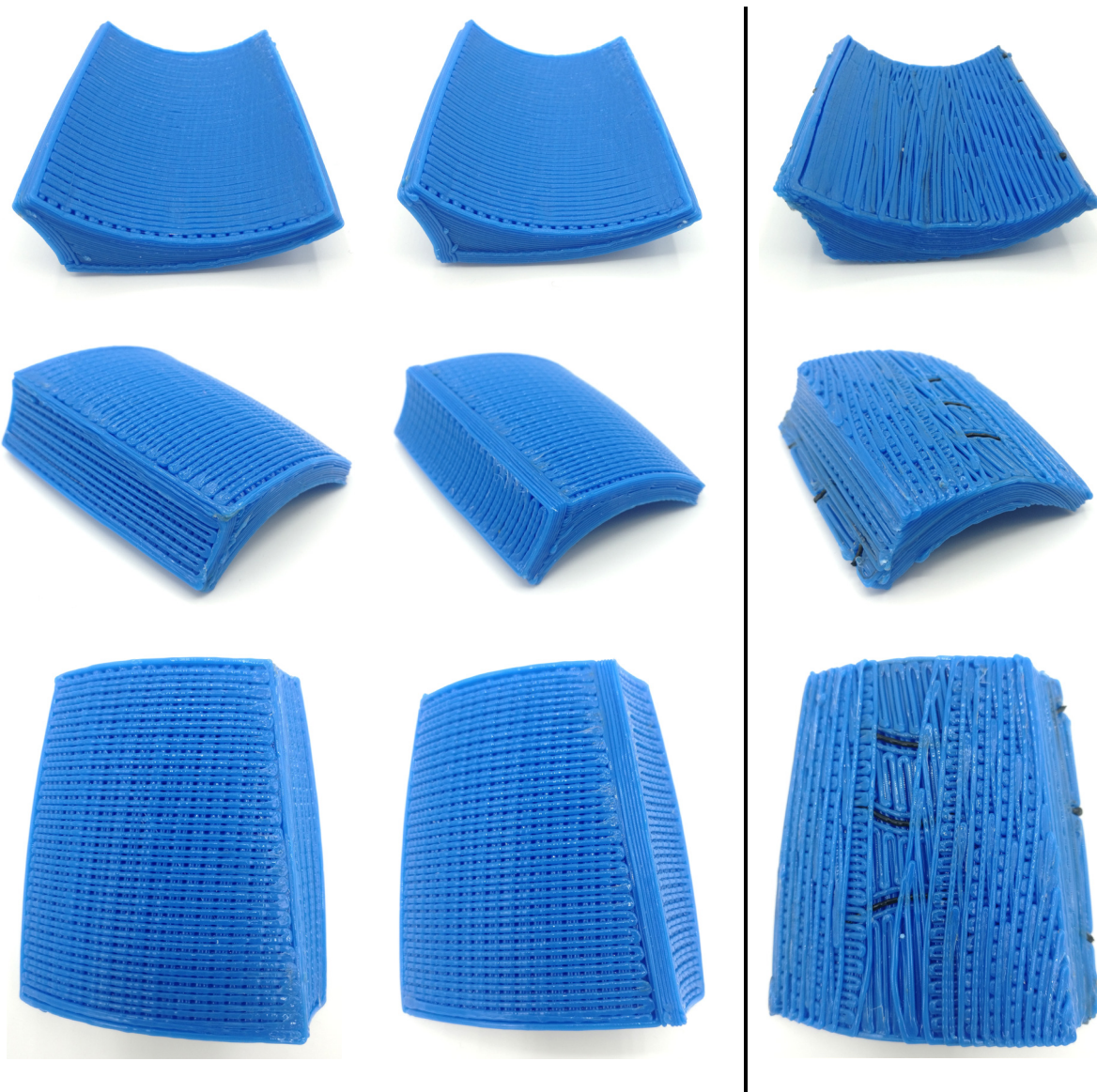


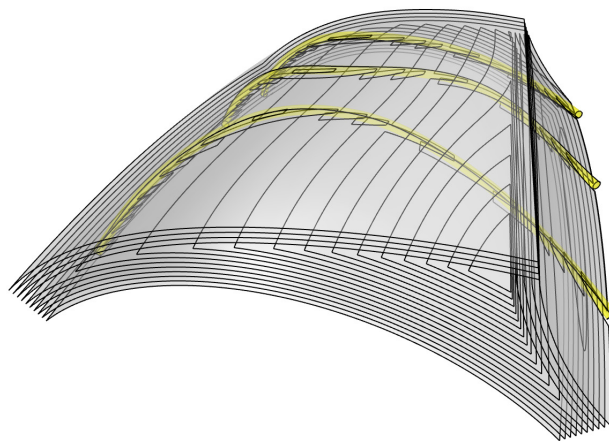
Figure 6.18 Comparison between accuracy driven slicing (left and centre) and function driven one (right)

The following distinct characteristics have resulted from an observational comparative analysis:

It is apparent from observation that there is significant difference in the accuracy of the same part manufactured by the two distinct slicing methods. This direct difference in the quality of the accuracy can be attributed to the fact that the multi-surface slicing method applied to process *Case\_Btop* and *Case\_Bside* follows the external surfaces that make up the object itself, with an objective to approximate them more accurately and reduce staircase. *Case\_Bcon* on the other hand puts a focus on slicing the object with a slicing surface defined by a user or a program, that would enable the freeform positioning of desired conductive tracks (or an arbitrary circuit) in a single layer according to their product design.

Referring to the quantitative data of case studies info Tables 5.5, 5.6 and 6.6 for *Case\_Btop*, *Case\_Bside* and *Case\_Bcon* respectively, we perceive an increase in the digital volumetric error that is obtained by slicing from 3.7% and 3.58% for accuracy driven slicing strategies to 6.19% for the function driven slicing strategy implemented in *Case\_Bcon*. More importantly then the quantity itself, and as noted in the studies in Chapter 5.1, the location of the staircase is mainly within the internal volume of the part in *Case\_Btop* and *Case\_Bside*, affecting 1.66% and 2.97% of the cumulative exterior surface area. Conversely to this, *Case\_Bcon* affects 100% of top, side and bottom surface or 83.32% of the cumulative exterior surface area, leading to poor accuracy in approximating the ideal part model. The crucial difference is the fact that accuracy driven slicing uses the external surfaces of the CAD model that define its volume, whereas the function driven slicing uses surfaces related to the internal functional design or multi-material composition of the part. Thus, it would appear that both of these slicing methods would only converge or overlap to a certain extent in a case where the desired conductive tracks are positioned along the external surfaces of the object itself, resulting in a slicing process that would generate results with benefits in both accuracy and functionality of conductive tracks.

While the difference in accuracy can be observed and measured digitally, the same comparison between the outputs of Sections 5.2 and 6.2 can also be made in terms of functionality. In other words, while it has been established that *Case\_Bcon* exhibits much lower accuracy compared to *Case\_Btop* and *Case\_Bside*, it is supposed that *Case\_Btop* and *Case\_Bside* would exhibit much lower functionality when compared to *Case\_Bcon*, had they contained the same conductive tracks.



*Figure 6.19 Simulated overview of Case\_Btop slicing strategy with cut-out sections for implementation of segmented conductive tracks*

Namely, if conductive tracks would be implemented following the layer arrangement of *Case\_Btop* or *Case\_Bside*, they would follow the direction of layers optimised for accuracy

and therefore inevitably result in segmented conductive tracks involving overlaps, thus increasing their resistance and lowering their functionality in accordance to the experimental data from Section 6.1. Unfortunately, the high number of material changes and overall complexity in managing the digital processing of such case study has inhibited its physical realisation. This in turn has inhibited the possibility to compare measured resistance of its conductive tracks to the resistance of conductive tracks from *Case\_Bcon*, leaving only the simulated digital form of such case study for discussion, presented in Figure 6.19.

The sum of studies performed in Chapters 5 and 6 is sufficient to come to a conclusion and provide feedback towards the initial hypothesis set forward in this Doctoral Research: a variety of slicing strategies can be applied on the same geometry using multi-axis ME technology, each one of them with a different quality outcome, pointing so to the conclusion that slicing can be tailored according to an a priori specified objective, consequently providing supportive evidence consistent with the hypothesis. However, due to the fact that accuracy based slicing uses the external geometry of the part while the function based slicing the internal part design and multi-material composition, a further question can be posed: could these slicing strategies be merged for a combined effect on part quality, both in terms of accuracy and functionality? In an effort to investigate this, a final case study is elaborated in this section that attempts to combine the slicing strategies from both Chapters 5 and 6.

In order for results to be easily comparable, the same geometry of *Part B* first introduced in Section 5.2 is used for this study as well. The goal is to demonstrate one possible slicing strategy that provides advantages in terms of both accuracy (as analysed in Section 5.2) and conductive materials functionality (as analysed in Section 6.2). Having the experience from previous case studies, the strategy involves slicing with the user defined surface N optimised for providing single-layered conductive tracks, while employing accuracy driven slicing for the rest of the part's model, through the step of sub-volume division. This resulted in an intricate slicing procedure composed out of 5 different slicing operations involving 4 different slicing surfaces, in a case study referred to as *Case\_Bx*. This slicing strategy is represented in Figure 6.20 with several phases subsequently adding layers from a different slicing operation, describing at the same time the manufacturing sequence in which the part was built in the study. The shape of the conductive tracks is maintained identical to the ones used in *Case\_Bcon*, providing an equal functionality parameter, while accuracy greatly improved due to the implementation of the multi-surface slicing strategy from Section 5.2, *Case\_Btop* in specific. The realisation of the piece has demonstrated that intricate slicing strategies applied on sub-volume level could be implemented that optimise the post-printing outcome of the parts in reference with more than one objective. The full information table for *Case\_Bx* is represented by Table 6.7, with additional manufacturing images in Appendix A.



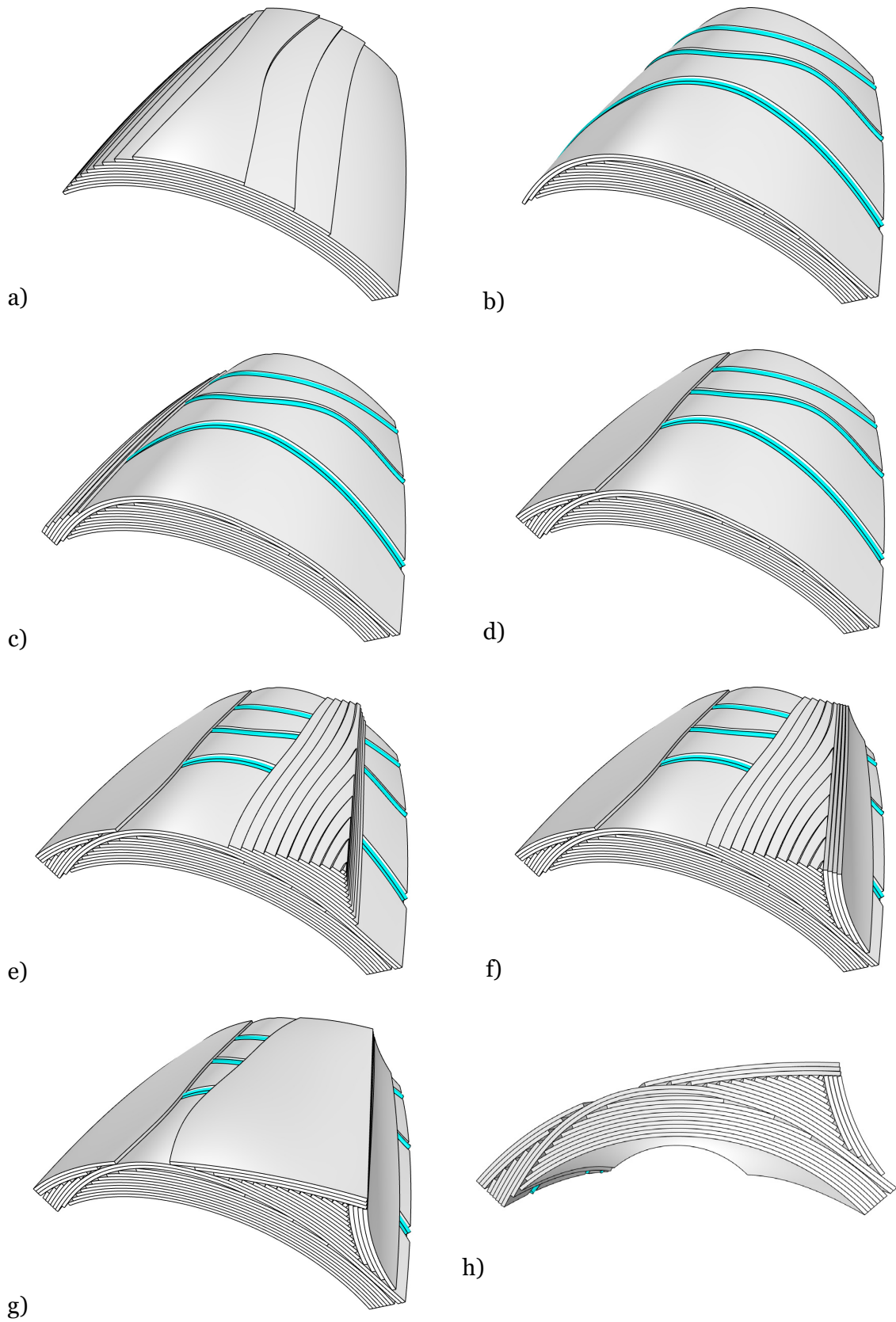


Figure 6.20 Case\_Bx slicing strategy: a)-g): ordered manufacturing steps for a multi-objective slicing aimed at benefiting both part's accuracy and the conductivity of embedded conductive tracks, h) frontal view

Geometry:	B	Slicing strategy	i) 2 layers with user defined surface
Name:	Case_Bx	(in that order):	ii) Top remaining volumes with 3 layers of top surface
Layer Height:	0.6 mm		iii) Top right remaining volume with 4 layers of side surface
Num. of layers:	38		iv) Top remaining volumes with 10 layers of user defined surface.
			v) Entire remaining volume with bottom surface.

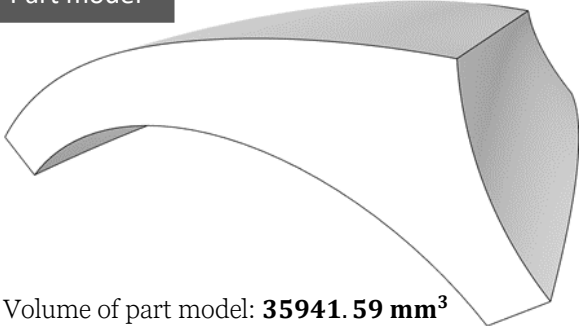
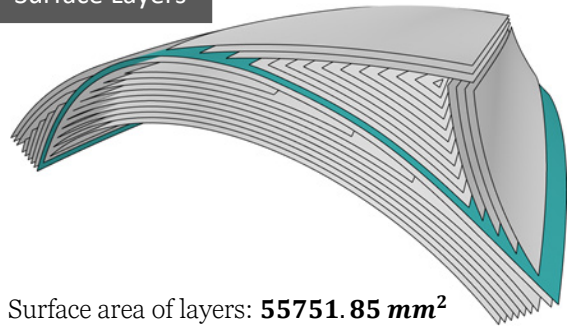
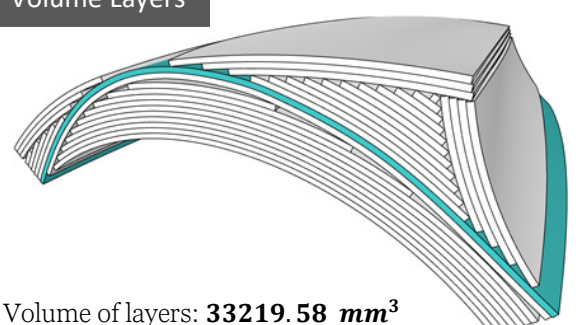
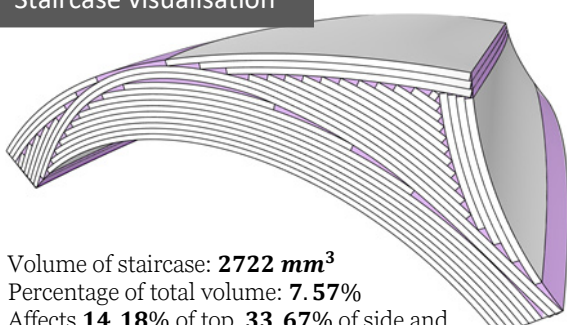
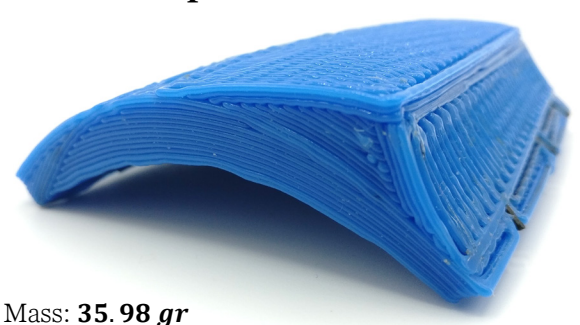
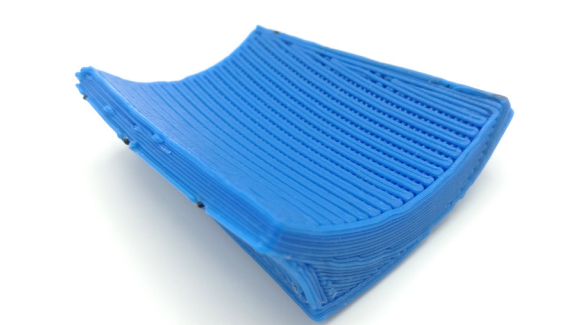
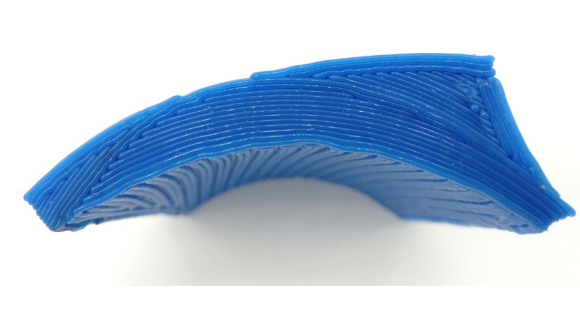

<p><b>Part model</b></p>  <p>Volume of part model: <b>35941.59 mm<sup>3</sup></b></p>	<p><b>Surface Layers</b></p>  <p>Surface area of layers: <b>55751.85 mm<sup>2</sup></b></p>
<p><b>Volume Layers</b></p>  <p>Volume of layers: <b>33219.58 mm<sup>3</sup></b></p>	<p><b>Staircase visualisation</b></p>  <p>Volume of staircase: <b>2722 mm<sup>3</sup></b>  Percentage of total volume: <b>7.57%</b>  Affects <b>14.18%</b> of top, <b>33.67%</b> of side and <b>6.71%</b> of bottom surface, <b>7.6 %</b> of all exterior surface.</p>
<p><b>Isometric top view</b></p>  <p>Mass: <b>35.98 gr</b>  Total toolpath length: <b>37643.36 mm</b></p>	<p><b>Isometric bottom view</b></p> 
<p><b>Front view</b></p> 	<p><b>Top view</b></p> 

Table 6.7 Case\_Bx study info table

The manufacturing of *Case\_Bx* provides a demonstration that both accuracy and functionality driven slicing approaches can be combined into an elaborate slicing strategy that brings benefits to both objectives. In the case of *Case\_Bx* functionality has still been given a priority by allowing an uninterrupted flow of the layer containing the conductive tracks and compromising with error in accuracy on the top surface of the model. However, while *Case\_Bcon* had staircase affecting 100% of side, top and bottom surfaces or 83.32% of all exterior surface area, in *Case\_Bx* 14.18 % of top, 33.67% of side and 6.71% of bottom surfaces have been affected, or 7.64% of all exterior surface area, which represents a great improvement over external accuracy while maintaining equal functionality.

*Case\_Bx* can also be seen as a demonstration that the initial hypothesis can also apply (or better, be re-formulated) on the level of sub-volume sections. In other words, different sub-volume sections of the same part can be sliced with varying slicing strategy, applied for optimising a certain objective. These sub-volume characteristics are then transferred to characteristics describing the entire part model.

#### 6.4. Function driven non-planar slicing: observations and conclusions

In order to analyse the potential benefit of non-planar slicing to the use of conductive materials, in the initial Section 6.1 of this chapter, a study investigating planar slicing and its effect on post-printing functionality in conductive materials has been done. Optimising the post-printing conductivity of such tracks is important because the conductivity of thermoplastic polymer blends is already much lower when compared to metallic materials. It deduced that the inclusion of higher number of layer for the manufacturing of a conductive track with given dimensions has a negative impact on the track's conductivity. Therefore, it concluded that conductive tracks are most conductive if manufactured in a single layer.

While realisation of planar single-layered conductive tracks might be possible in some product design specifications, it appears there is a very restrictive framework for parts made by conventional, planar Material Extrusion techniques: either the design of embedded electronics needs to be tailored to fit into a single planar layer, or accept the compromise in post-printing functionality, which will be lower than the one inherent by the material. Implementing multi-axis ME as a process, it is possible to provide a slicing strategy of the part that increases the freedom to design embedded features of functional materials, extending it to three-dimensional space. This is the emphasis of Section 6.2 and case study *Case\_Bcon*. Namely, freeform slicing was done not by the external surfaces defining part's volume, but by a surface resulting from the desired embedding of conductive tracks within the part. Thanks to the non-

planar slicing capability, the tracks were able to be printed in a single-layer fashion, thus optimising their conductivity.

Lastly, the results from the comparative analysis of function based to accuracy based slicing in Section 6.3, acknowledged the crucial difference between the two slicing methods, and in turn generated the design of combined slicing procedure in *Case\_Bx*, where besides maintaining optimised functionality, accuracy was also greatly improved. This demonstrated that slicing strategies with different objectives do not necessarily need to be applied on the whole part, but can also be combined on a sub-volume level, with their respective effect contributing towards the entire part's qualities.

One additional benefit that was noted through the realisation of *Case\_Bcon* and *Case\_Bx* is the following: due to the fact that the conductive materials are placed in a single freeform layer, change of material in the extrusion tool needs to take place only once. Conversely to this, if the conductive tracks are not placed in a single layer, as in simulated case study presented in Figure 6.19, the manufacturing system needs to change between build material and conductive material in more occasions, thus increasing manufacturing time and possibly compromising quality as it is often seen in conventional ME systems.

# 7

## Conclusions

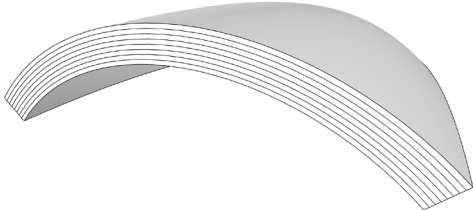
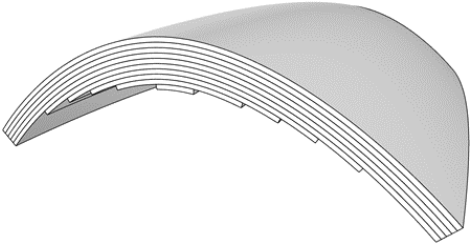
The last chapter concludes the work from this Doctoral Research and above all it relates it back to the very motive for doing it in first place: the Hypothesis and Research Questions from Section 2.2.1.

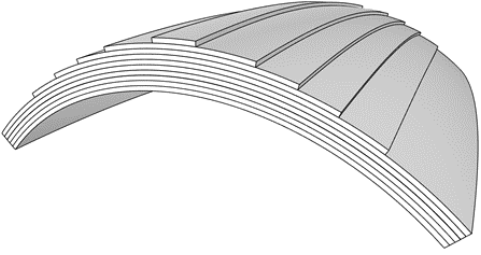

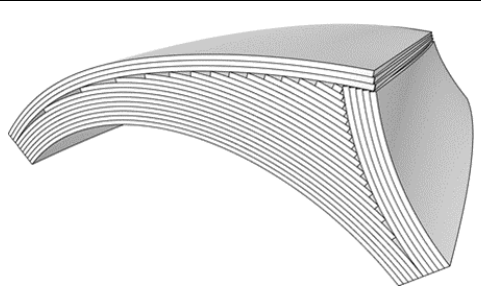
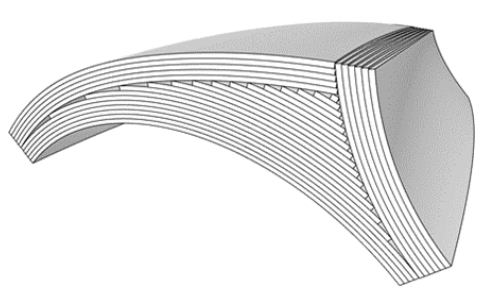
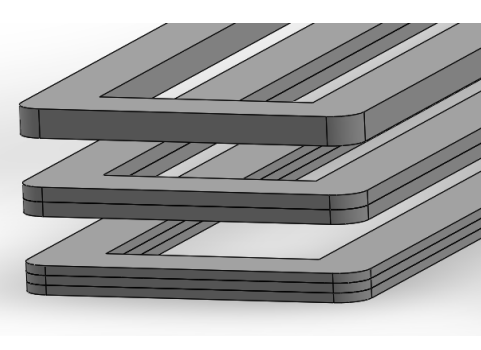
In addition, it also provides a summary and overview of the case studies, related contributions in terms of new knowledge brought towards understanding the technology and their relative connections with previous work done in the field. Lastly, discussions on various multi-axis ME aspects, including its limitations, and potential hypothesis expansion for future work are provided.

---

## 7.1. Summary, discussion and feedback to research questions

This Doctoral Research has implemented a combination of qualitative and quantitative research methods that has led to the design of experiments and case studies of non-planar ME application, supported by measured data. Each case study had a specific combination of geometry model and slicing strategy. Geometry models were selected in such a way that they sustain a gradual increase in complexity going through the Pilot geometry, *Part A* (geometry for isolated study of Section 5.1) and finally *Part B* which served as a cross-comparative geometry between chapters. Four of these case studies: *Case\_Btop*, *Case\_Bside*, *Case\_Bcon* and *Case\_Bx* involved *Part B* as the same geometry, leaving the slicing strategy as the only independent variable, thus generating a comparative platform for observations and conclusions with effects on the quality outcome of the part, defined in terms of geometric accuracy and functionality. The rest of the experiments or case studies instead led to the adoption of the accuracy and function driven slicing methods. Table 7.1 shows an overview of the analysis, case studies and crucial parameters of their design and process execution.

Reference, geometry and focus	Visual Representation	Slicing Strategy (in that order)	Peculiarities
<b>Objective: Pilot study for framework and manufacturing system verification (Section 4.2)</b>			
<p><i>Case_Pilot</i></p> <p>Geometry: Pilot</p> <p>focus: verify framework</p>		<p><u>Slicing surface:</u> top or bottom 10 layer x 0.6mm</p>	<p>Uniform thickness part from doubly curved surface. Top and bottom surface are orthogonal offsets, so non-planar slicing is intuitive with no staircase present. Served as a pilot case for framework testing and fit-for-purpose verification. High similarity to geometries from previous studies.</p>
<b>Objective: establish an accuracy driven slicing method (Section 5.1)</b>			
<p><i>Case_Atop</i></p> <p>geometry: <i>Part A</i></p> <p>focus: accuracy</p>		<p><u>Slicing surface:</u> top 10 layer x 0.6mm</p>	<p>Non-uniform thickness so slicing is not intuitive as a choice is present. Geometry A sliced from top. Improved staircase on top surface but still present on bottom surface. Suboptimal process execution: first 5 layers not always orthogonal nor equidistant to substrate. Less staircase than expected due to flow of extruded filament under gravity.</p>

<p><b>Case_Abot</b></p> <p>geometry: Part A</p> <p>focus: accuracy</p>		<p><u>Slicing surface:</u> bottom 10 layer x 0.6mm</p>	<p>Non-uniform thickness so slicing is not intuitive as a choice is present. Geometry A sliced from bottom. Improved staircase on bottom surface but still present on top surface. Easily noticeable staircase as simulated.</p>
<p><b>Case_Asan</b></p> <p>geometry: Part A</p> <p>focus: accuracy</p>		<p><u>1. Slicing surface:</u> top 3 layer x 0.6mm</p> <p><u>2. Slicing surface:</u> bottom 7 layer x 0.6mm</p>	<p>Non-uniform thickness geometry A sliced with both top and bottom surface. Improved accuracy on both top and bottom surface. New multi-surface method for eliminating staircase from external geometry towards inside of the part. Introducing slicing operations on various volume sections until exhaustion of model volume.</p> <p>Final outcome: established an accuracy driven slicing method – multi-surface slicing on sub-volume sections using external model surfaces.</p>
<p><b>Objective: apply accuracy driven slicing method to cross-comparative geometry (Section 5.2)</b></p>			
<p><b>Case_Btop</b></p> <p>geometry: Part B</p> <p>focus: accuracy</p>		<p><u>1. Slicing surface:</u> top 3 layer x 0.6mm</p> <p><u>2. Slicing surface:</u> side 5 layer x 0.6mm</p> <p><u>3. Slicing surface:</u> bottom 20 layer x 0.6mm</p>	<p>Cross-comparative geometry: Part B. Applied multi-surface slicing method from Case_Asan in the order top -&gt; side -&gt; bottom. Portion of side surface with staircase due to order of slicing.</p> <p>Final outcome 1 of applied accuracy driven slicing through sub-volume division.</p>
<p><b>Case_Bside</b></p> <p>geometry: Part B</p> <p>focus: accuracy</p>		<p><u>1. Slicing surface:</u> side 6 layer x 0.6mm</p> <p><u>2. Slicing surface:</u> top 5 layer x 0.6mm</p> <p><u>3. Slicing surface:</u> bottom 18 layer x 0.6mm</p>	<p>Cross-comparative geometry: Part B. Applied multi-surface slicing method from Case_Asan in the order side -&gt; top -&gt; bottom. Portion of top surface with staircase due to order of slicing.</p> <p>Final outcome 2 of applied accuracy driven slicing through sub-volume division.</p>
<p><b>Objective: establish a function driven slicing method for conductive tracks (Section 6.1)</b></p>			
<p><b>Cond. Tracks study</b></p> <p>geometry: serpentine lines</p> <p>focus: function</p>		<p><u>Slicing surface:</u> Planar (3-axis ME)</p> <p><u>Slicing strategy:</u> 5 batches single layer 5 batches double layer 3 batches triple layer</p>	<p>Single, double and triple layer slicing of equal geometry of serpentine conductive tracks. Effect of slicing on function measured by exhibited resistance of the conductive tracks. Concluded an inverse relationship between functionality (conductivity) of conductive track and the number of layers used to make it.</p>

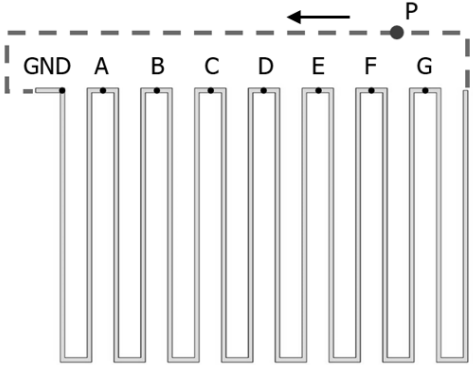
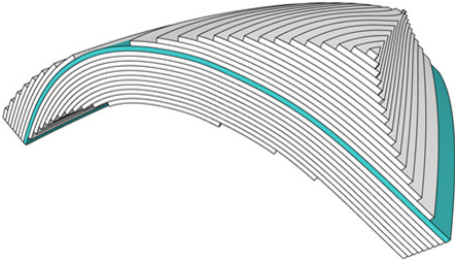
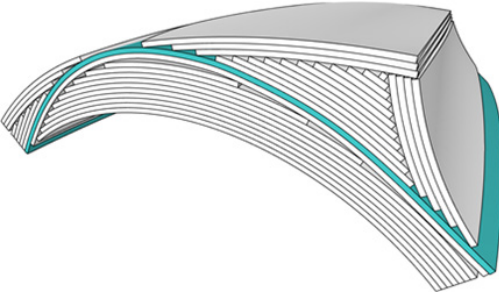
		<p>Final outcome: established a function driven slicing method – single layer conductive tracks.</p>
<p><b>Objective: apply function driven slicing method for conductive tracks to cross-comparative geometry (Section 6.2)</b></p>		
<p><i>Case_Bcon</i> geometry: <i>Part B</i> focus: function</p>		<p><u>1. Slicing surface:</u> user defined 36 layer x 0.6mm (1 containing conductive tracks, coloured green)</p> <p>Cross-comparative geometry: <i>Part B</i>. Slicing guided by a user-defined freeform surface not belonging to part's model. Surface designed according to assumed functionality design of embedded conductive tracks. Implemented single-layers conductive tracks, but poor accuracy, unlike <i>Case_Btop</i> or <i>Case_Bside</i>.</p> <p>Final outcome of applied function driven slicing.</p>
<p><b>Objective: combine both function and accuracy driven slicing methods to cross-comparative geometry (Section 6.3)</b></p>		
<p><i>Case_Bx</i> geometry: <i>Part B</i> focus: function and accuracy</p>		<p><u>1. Slicing surface:</u> user defined 2 layer x 0.6mm (1 containing conductive tracks, coloured green)</p> <p><u>2. Slicing surface:</u> top 3 layer x 0.6mm</p> <p><u>3. Slicing surface:</u> side 4 layer x 0.6mm</p> <p><u>4. Slicing surface:</u> user defined 10 layer x 0.6mm</p> <p><u>5. Slicing surface:</u> bottom 11 layer x 0.6mm</p> <p>Cross-comparative geometry: <i>Part B</i>. Combined slicing strategy for simultaneous optimisation of both functionality and accuracy. Functional slicing implemented from <i>Case_Bcon</i>, while accuracy from <i>Case_Btop</i>. Intricate part slicing composed of 5 different operations guided by 4 different slicing operations.</p> <p>Final outcome of combined function and accuracy driven slicing strategy on cross-comparative geometry through sub-volume division.</p>

Table 7.1 Summary of case studies and analysis conducted for this Doctoral Research

In addition to the 8 case studies where non-planar ME technology has been implemented, an additional in-depth study on the effect of slicing on post-printing functionality of conductive tracks has been done in Section 6.1 with an isolated geometry and its own design of experiment



leading to 13 different batches of conductive track samples, 3 different slicing strategies and 2 different materials. The findings from that isolated study have put the basis of non-planar slicing for optimised post-printing functionality.

In a short summary, this Doctoral Research has designed and developed a layer based, multi-axis ME framework, that was implemented to demonstrate different non-planar slicing strategies for the same geometrical object, oriented towards optimising two distinct post-printing characteristics of the finished part. By doing so, it has supported the initial hypothesis of tailoring a non-planar slicing of a part according to desired outcome, in a process of an objective-driven slicing in multi-axis ME technology. These characteristics were geometrical accuracy and post-printing functionality, each analysed in separate qualitative studies. Through such analysis and the above mentioned contributions, it has provided feedback to research questions R1 and R2 as set in Section 2.2.1:

R1: How do different non-planar slicing strategies affect the part's accuracy? Is there a slicing method that can be used to optimise the post-printing accuracy of the part?

Non-planar slicing has the ability to provide freeform layers that span in all three dimensions, so that they are able to follow a curved geometrical shape in an accurate manner. While this claim is well in line with previous research done in the field, it should be acknowledged that non-planar slicing following a single freeform layer shape, does not always results in accuracy benefits across the entire geometry of the part and for various part models. This research has analysed several different geometries with increasing complexity, pointing to the fact that non-planar slicing in non-trivial geometry shapes is accompanied by a choice on how to guide the layers that constitute the part. Namely, if layers are guided by the geometry of the part model, they do tend to eliminate staircase effect, but only to a section of the part that resembles the layer shape. The geometry of the object that is instead approximated by the thickness of the layer, still results in a formation of the staircase effect, similarly to the conventional, 3-axis ME technology. An example of this are case studies *Case\_Atop* and *Case\_Abot*. Noting this effect, this research established and implemented a method where the slicing was guided by multiple slicing surfaces extracted from the part model and applied on sub-volumes, that resulted in the staircase effect being re-positioned from the external part geometry towards the internal volume, optimising so the accuracy of the part after manufacturing. This method was then applied to a more complex, cross-comparative geometry, by varying the slicing operations and has given consistent results as one possible method for optimising non-planar slicing for post-printing part accuracy.

Referring to the second research question:

R2: How do different non-planar slicing strategies affect the part's conductivity? Is there a non-planar slicing method that can be used to optimise the post-printing functionality of conductive materials?

Unfortunately, the work organised in Section 6.1 did not manage to directly address different non-planar slicing strategies due to profound lack in literature of studies done in planar context. Therefore, the core founding concepts were first analysed in 3-axis environment through empirical qualitative work where experiment boundaries, realisation and precision could be controlled to a much greater extent. It was discovered that the slicing strategy has a high impact on the post-printing functionality of conductive tracks built by conductive polymer blends. Namely, higher number of layers tend to decrease the conductivity, thus functionality, of conductive tracks manufactured by ME.

Suspecting that the same phenomenon extends to the non-planar realm, this conclusion has given a base for the proposal and implementation of a multi-axis slicing method driven by the optimisation of conductivity of conductive tracks, by enabling for them to be printed in one single layer. It consists in defining a surface that does not necessarily belong to its geometrical model, but is rather guided by the single-layer realisation of the conductive tracks as designed, and slicing the entire, or a section of the part model, following said surface. In addition to the establishment of a single-layer slicing method for freeform embedding of conductive tracks, a physical characterisation was also done in Section 6.1 in order to investigate if potential decrease of the cross-sectional area is the reason for this phenomenon, but microscope imaging revealed that this was not the case. Hence, this research did not manage to find out why single layered conductive tracks have a lower resistance than multi-layered counterparts, but rather its presence as a phenomenon. It is hypothesised that this decrease in functionality might be due to the modified dispersion or interconnection of the filler particles either within the same layer of the thermoplastic compound or across different layers, as a consequence of the different slicing strategy, however further investigation would be necessary in order to conclude this.

Through the investigation of both accuracy driven and function driven slicing strategies explained above, supportive evidence has been provided towards the hypothesis that non-planar slicing has a great influence over the object's properties after its manufacturing through multi-axis ME technology. This conclusion was reached through demonstrating different slicing strategies applied on the same object that resulted in different quality outcome. The final case study of *Case\_Bx* also showed that different slicing strategies can be

merged into a complex slicing process that can result in combined benefits in more than one quality, transitioning the concept described in the hypothesis on a sub-volume level.

The liberty in managing the spatial arrangement of layers within the geometry of the part model was obtained through the ability to guide the slicing as desired, described in different slicing steps, each with different slicing parameters. For example, *Case\_Asan* involved 2 slicing procedures: one propagating the top surface downwards for 3 layers, followed by a second procedure where the remaining volume was sliced with the bottom surface until the entire part volume has been sliced. *Case\_Btop* and *Case\_Bside* took this concept a step further and implemented 3 slicing procedures, in different order and with different slicing parameters (number of layers) which resulted in a different part outcome. Ultimately, *Case\_Bx* applied 5 slicing operations, 1 aimed at optimising the functional characteristics of single-layered conductive tracks, and 4 other procedures aimed at maximising geometrical accuracy of the part. This idea of designating volume segments for different slicing is not novel, but in previous works it has been done predominantly for building an object without support. The case studies from this work demonstrate that multi-axis ME has an immense freedom in managing the slicing process, giving us the possibility to break free from conventional limitations of planar layers and some of the disadvantages related to it.

While full answers with complete in-depth comprehension of all aspects of the posed problematics have not yet been reached, this research has offered feedback that helps in understanding the full potential of multi-axis ME technology and how we can guide it. The initial assumption at the beginning of this Doctoral Research that we are just beginning to uncover multi-axis ME technology in its capacity, limitations and problems is again being reiterated here, after its completion. It appears that all of the great liberty offered by multi-axis ME in process design, definition of layers, tuning object parameters, material composition, capacity for intricate, functional object etc. is accompanied by a difficulty in understanding on how to limit this liberty, one example being the slicing strategy. In other words, if multi-axis ME really does offer all of this freedom in managing the layer arrangement of a part, how do we select which slicing strategy among the theoretically infinite number of possibilities? This Doctoral Research does not offer the full answer to this question, but provides supportive evidence towards one idea that maybe the slicing strategy could be selected according to the characteristics desired from the finished piece. Presumably, this can also be extended for possibly optimising other, more industrially oriented parameters such as production time or cost, that would generate their respective slicing strategies. In addition, the full implementation of the technology requires the successful integration of systems ranging from computational geometry, process management and execution via multi-axis manufacturing systems, ergo, more work is needed to understand all aspects of such a

conglomerate of interdisciplinary elements, and how they impact the implementability of theoretical slicing strategies.

Hopefully, this work will help inspire such future endeavours.

## 7.2. Contributions

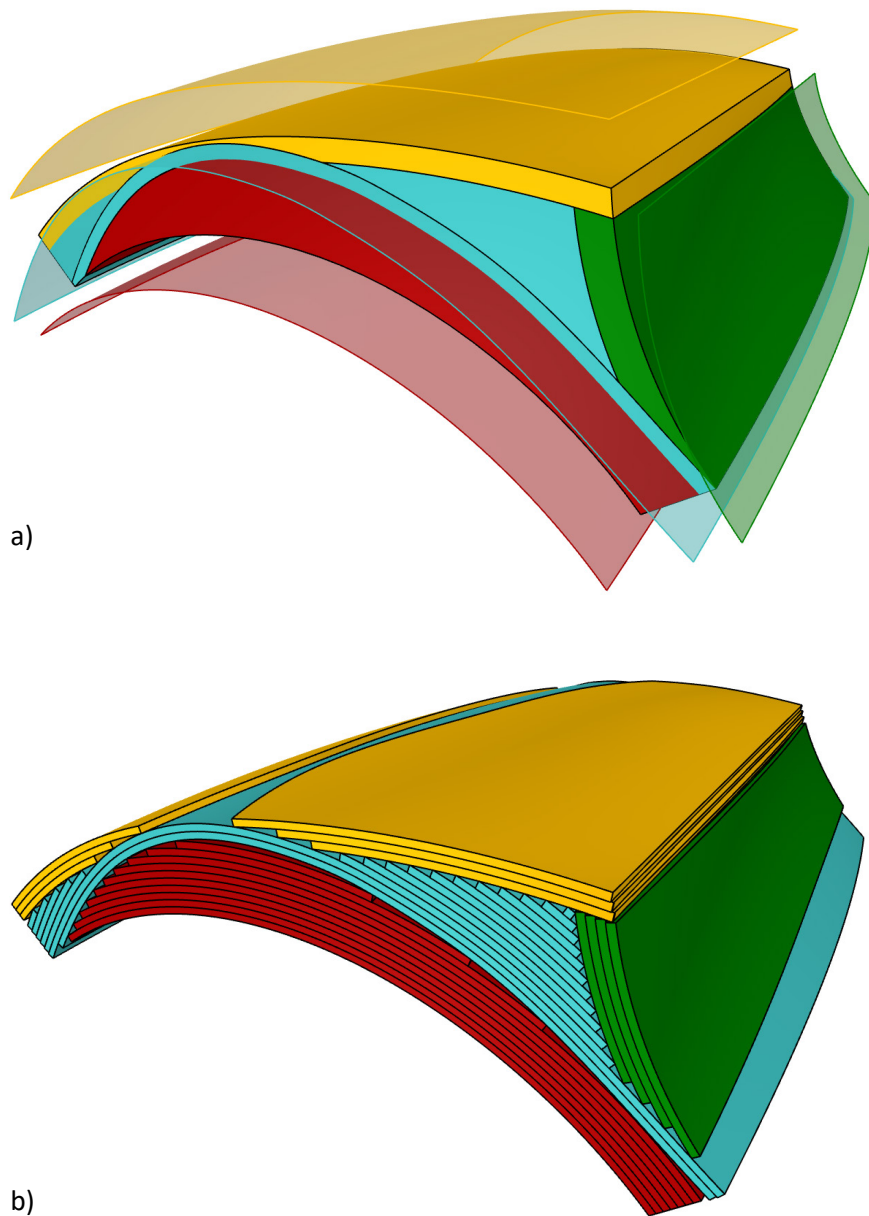
In this work, a variety of multi-axis ME process implementations have been developed, practically applied, their properties studied and analysed. Working through a multi-disciplinary field, different contributions have been made towards the advancement of multi-axis ME technology, its application, relation to functional elements and the freedom to control layer arrangement in parts. In the following, the major contributions brought forward by this Doctoral Research are discussed, categorised as contributions to knowledge and tools.

### 7.2.1. Contributions to knowledge

#### ***Sub-volume slicing method for multi-axis Material Extrusion***

One slicing method that resulted in an advantageous layer arrangement in *Case\_Asan* for the first time in this work and was repeatedly used later in *Case\_Btop*, *Case\_Bside* and *Case\_Bx* is the sub-volume slicing method for multi-axis ME. This method consists in combining different slicing operations on different sub-volumes of the part model  $V_{1,2...k}$ , where their sum  $\sum_{i=1}^k V_i = V_{total}$ , adds up to the total volume of the part model's geometry. Figure 7.1 below graphically represents the crucial concept behind this slicing method, using *Case\_Bx* as an example, the most elaborate case study developed in this thesis involving 4 different slicing surfaces, 5 slicing operations and 6 sub-volumes. The colours of the sub-volumes then relate to the colour of the respective slicing surface used for the required slicing operation.

The sub-volume slicing method allows for the freedom in arranging the freeform layers in various zones of the part – referred to as slicing operations - in order to result in a slicing that is optimal according to a desired characteristic in a part. An example of this is slicing peripheral sub-volumes with surfaces belonging to the part model, therefore increasing the final accuracy of the part, while slicing the internal sub-volumes with user-defined surfaces aimed at optimising functionality through inclusion of functional materials (blue coloured slicing operation, Figure 7.1).



*Figure 7.1 Sub-volume slicing method exemplified on Case\_Bx. a) colours relate sub-volumes with respective slicing surfaces b) obtained layers from slicing operations*

Sub-volume slicing method has been developed in this thesis and used in several variations through the design of specific case studies. Its application has enabled the slicing for improved accuracy of both *Part A* and *Part B*. It has also been used for an intricate layer arrangement of *Case\_Bx* where both functionality and accuracy driven slicing has been implemented, implying a high range of applicability in a general combination of geometry and desired part characteristics.

As mentioned in Section 5.1.4, the concept of volumetric division of a part model for guidance of slicing has been previously discussed and studied for over two decades [79], with a recent study involving sub-volume division and an exhaustive review of previous methods described in [141]. However, conversely to the major direction of prior work development that has focused on eliminating support material, the method developed in this work focuses instead on controlling the correlation between freeform slicing of different sub-volumes to the obtained characteristics of a finished part, specifically in terms of the duality between accuracy and functionality of conductive tracks. This method is also seen to be complementary to the extensive previous work done in terms of improving part accuracy by, for example, adaptive slicing as described in [20], or other slicing or toolpath generation methods as discussed in [124].

While the sub-volume slicing method has demonstrated how can the strong correlation between multi-axis slicing and part characteristics be managed, how it may be used to select an appropriate slicing for a part and has provided supportive evidence towards the hypothesis, it still requires further work. Namely, the method itself is highly impacted by the capacity of tools for computational geometry, the capacity of manufacturing systems for realisation of a given slicing strategy, the order of slicing operations for given sub-volumes and the choice of process parameters. Thus, additional work is required for its complete understanding.

### ***Impact of slicing on functionality of conductive tracks***

The work of Section 6.1 has discovered an inversely proportional relationship between post-printing functionality of conductive tracks and the number of layers used to make them, i.e. the more layers are used to manufacture a conductive track of given dimensions, the less conductive the track is. Post-printing physical characterisation did not reveal the cross-section of the conductive tracks as the reason behind this phenomenon, so further work is required as to understand why such behaviour occurs. One suspected reason could be a modified dispersion or interconnection of the filler particles. The conclusion has been based on a quantitative study composed of an experiment involving 78 conductive track samples done across two different conductive materials performed in a planar, 3-axis context. Low variance of data within the same conductive material has been seen as an indicator for an experiment done in a controlled and repeatable manner. Substantial variety of obtained results between different materials supports the idea that this phenomenon is heavily dependent on the type of material.

The impact of these findings spans in both 3-axis and multi-axis ME contexts. In planar, 3-axis ME they are used to provide Design for Additive Manufacturing guidelines that help position embedded conductive tracks in the design phase or select an appropriate slicing in the process phase. In multi-axis context, they provide the correlation between the span of freeform layers and the functionality of conductive materials, leading to the increased liberty in managing embedded conductive tracks or circuits manufactured in a single layer, that would otherwise be impossible to do with planar, 3-axis approach. This significant correlation between freeform layers and conductive materials has been suggested earlier in [42] and has been practically demonstrated in this research through the case studies *Case\_Bcon* and *Case\_Bx*.

In addition to the sub-volumes slicing method and the impact of slicing on conductive tracks, this Doctoral Research has contributed to the knowledge of multi-axis ME technology by forming and providing supportive digital and practical evidence of a hypothesis that freeform layer arrangement strongly relates to the final characteristics exhibited by a part manufactured with such technology. Further investigation is needed to fully understand the potential of freeform layer arrangement as a degree of freedom in process design of multi-axis ME technology.

### 7.2.2. Contributions to tools

#### ***Multi-axis ME processing tool and pipeline***

The work presented in Chapter 3 has presented the development of an integrated framework for multi-axis ME process. Using part geometry (or additional freeform surfaces) as an input, it is able to implement different slicing strategies, develop suitable toolpaths and formulate these process specifications into a g-code instruction list required for manufacturing of a desired part. Auxiliary operations, some of which scarcely researched by prior works, such as the need for additional geometrical information during the slicing process (Section 3.3), infill and safety inter-layer toolpaths (Section 3.4) have been developed, discussed and implemented. A verification of this framework in conjunction with a 5-axis manufacturing system has been done by printing a pilot case study, confirming it is fit-for-purpose for multi-axis

ME implementation. This validation was later re-iterated with the successful realisation of 7 other case studies using multi-axis ME process.

The development of such framework in this work was prompted by the current lack of multi-axis ME tools necessary for processing and implementation of this technology for the manufacturing of a given part. Therefore, its realisation has been supported by operational concepts and algorithms adopted from previous research works and conventional 3-axis slicers. The design of such framework does not reflect any optimisation procedure, academic or industry standard, nor it has been the result of a benchmark phase against other such frameworks or a given parameter, but rather follows from the necessity of having a tool for implementation of multi-axis ME technology and the slicing methods studied in this work. However, it is due to this rarity in such processing tools, that the framework design as discussed in Chapter 3 is considered one of the major contributions of this Doctoral Research. Together with the data transparency of multi-axis manufacturing system and processing parameters of Chapter 4, the framework represents one embodiment structure as tool for implementation of multi-axis ME technology, contributing towards the design and further improvement of other such frameworks in future research work. Moreover, its use in conjunction with the sub-volume slicing method implements the novel paradigm of *slicing operations* as steps of defining an overall slicing strategy for a given part. The final framework design with its major processing elements is depicted in Figure 7.2 below.

Additional aspect of the framework is its modularity in the sense that it can be utilised in a sub-complete form. For example, the slicing procedure (Figure 7.2, left) can be used with other technologies as well such as DED of metals, where the obtained layers could be used with a different algorithms of toolpath generation. Another example would be to use the framework in a context where no sampling of the toolpaths is done and therefore avoiding a step of approximation, or the data are sent through a more sophisticated file format. Therefore, it is assumed that the impact of the framework developed here can be extended beyond the scope of application, equipment and technology used in this study, thus contributing to development of multi-axis AM in general, in both academic and industrial sense. As such it can be improved through further work and possible implementation of other elements, such as for example a collision detection or toolpath ordering algorithm, or other elements that will augment its application capacity.



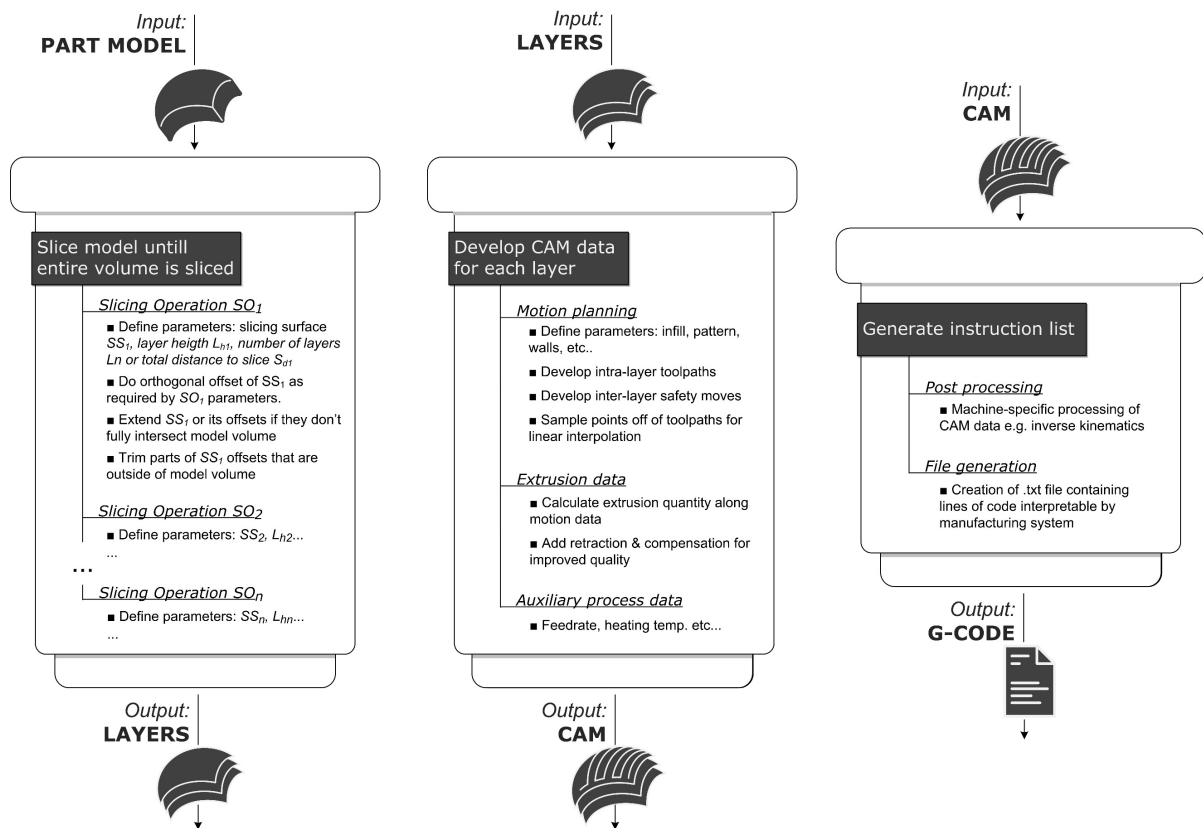


Figure 7.2 An overview of the processing framework and flow of information through it

### 7.3. Limitations and risks to validity

While a variety of slicing strategies have been implemented, measured, analysed and drawn conclusions upon, there is the inevitable presence of boundaries within which the studies described here have been done. This is especially true for non-planar ME technology, a field that being still in its infancy is yet to establish some standardised parameters as support. Therefore, it is of paramount importance to point out the limitations such boundaries pose to the generality of the presented work and potential risks they carry to the validity of observations and conclusions:

- *Uniform thickness layer based approach.*

The entire flow of logical reasoning, approach and scope of operation of the above studies have been guided by the core concept of making objects up by depositing of plurality of layers that, within the span of one single layer, the layer thickness does not change as a parameter. As noted in Section 2.1.2, there exist many other works that

instead look into concepts that challenge both the layered nature of Additive Manufacturing technologies [50] and the constant thickness paradigm [52]. Consequently, the contents of this work might not be as applicable in approaches where the step of slicing is by-passed or otherwise less present. However, it should be also noted that not just ME technologies but most of AM processes fall under the umbrella of uniform thickness layer based approach, therefore this is seen as limiting only to a certain extent.

- *A fixed framework.*

What was seen as a crucial element *E1* in Section 2.2.2. necessary for maintaining research integrity, rigour and repeatability, and one of the major contributions of this Doctoral Research, it is also present here as a limitation. Namely, all multi-axis ME studies in this work (therefore excluding isolated study described in Section 6.1) have been processed by a fixed dataflow and a set of tools developed or adapted specifically for this study: CAD format, slicing and toolpaths algorithm, extrusion model, material, processing parameters and manufacturing system. As explained in Chapter 3, the approach of developing such framework for the needs of this work was seen as unavoidable due to the lack of similar processing tools today, required for conducting the case studies. Nevertheless, the use of framework developed internally to the study bears certain constraints in generality and optimality of employed algorithms.

- *Inclusion of postulates.*

The core mechanism dictating how slicing impacts post-printing conductivity has been analysed in Section 6.1. Due to lack of experimental basis in prior literature and due to the possibility to better control the execution of an experiment in 3-axis context rather than a 5-axis one, the work in Section 6.1 was performed in a planar, 3-axis context. The extension into freeform realm was instead supported by posing two theoretical postulates P1 and P2. Consequently, the successive multi-axis slicing method is valid as long as the postulates are valid. However, similar assumptions have been made in previous work [42] providing the basis for relating freeform layers and benefit for conductive materials.

- *Processed geometries.*

The choice of geometries required to perform the case studies is yet another necessary choice done internally within this study. While their design was systematically justified

with respect to both previous research study and increase in complexity in turn leading to increase of generality of use, the geometries used in this study can clearly be even more complex. It should also be acknowledged however, that such additional complexity, possibly expressed by a high surface dynamics, could instead hinder the understanding of the technology by impeding its implementation, e.g. in the case of a surface too complex to have a well defined orthogonal offset.

#### 7.4. Research implications

The work presented in this thesis has been done in the field of non-planar ME technology with its own definition of processing framework and design of case studies for examination. As a research effort with limited resources within a context of a Doctoral Research, it was able to investigate the posed Hypothesis and Research Questions only to a certain extent, regardless of the topic's potential for future research. Here below is a list of particular broader aspects that could relate to the contents of this thesis:

- *Wider hypothesis outreach: part quality.*

The following hypothesis was analysed here: given part model can be sliced with different slicing strategies that give certain qualities to the part after it has been manufactured. If true, then it could mean that one may also tune the slicing process prior to the manufacturing process and according to what is expected from the part once manufactured. Two different slicing strategies, one driven by accuracy while the other driven by functionality provided supportive evidence of this hypothesis, but it is suspected that choice of slicing strategy in non-planar ME technologies could bear significance in other part qualities as well, such as: strength of parts, embedding of other functional materials besides conductive, accuracy of features, controlled fracture, process optimisation (cost, support, speed), improved meso-structure control, and/or others. Clearly, further work is necessary to investigate these possible effects.

- *Wider hypothesis outreach: scale and material.*

It can be acknowledged that with the exception of data present in Section 4.1 and figures depicting part models necessary for maintaining research integrity and repeatability, the case studies done in this Doctoral Research have little reference in terms of dimensions and process parameters such as layer height and nozzle diameter. In fact, most of the non-planar digital slicing or practical parts can be seen as oblivious

to scale and dimension, providing more of a sense of ratio between nozzle diameter, layer height and part dimensions, rather than absolute values. Also, the presence of multi-material aspect in Chapter 6 demonstrates the added value of being able to embed functional material within a product in a freeform way. Since ME is quite versatile with scale spanning from micro level to printing of buildings, and materials spanning from edible substances to composite polymer and cement, it is suspected that the contents of this thesis have validity in a scale and materials palette inherited directly from ME itself. However, additional research effort is needed to confirm this.

- *Role of manufacturing systems.*

Many of the non-planar slicing strategies consist of layers with a freeform topology involving high degree of curvature or dynamics, like some of the examples shown in Figure 3.5 or even more complex. While many studies can be done in a digital environment, clearly the three dimensional layers will need to be physically realised by manufacturing systems to bring utility of non-planar ME technology to practical context. As mentioned in Section 4.3, manufacturing systems can play a significant role in the practical implementation of non-planar ME as a direct result from machine's kinematics, available workspace and rotations, accuracy and precision, thermal management and the shape of the extrusion nozzle. Therefore, further research can be done relating a certain manufacturing system to what it can realistically deliver in terms of non-planar ME, so that such knowledge can be accounted for in the slicing phase.

- *Effect of slicing in planar context.*

What is seen as a potential limitation to validity in Section 7.3 referred to as "*Inclusion of postulates*" is here instead looked from the perspective of research impact in a wider context. Namely, the fact that Section 6.1 analysed the slicing effect in a conventional, 3-axis content, has lead to findings impacting the current state of ME technology. Therefore, results from Section 6.1 impact also the much larger field of planar, 3-axis Material Extrusion technology with implications in slicing and Design for Manufacturing.

- *Development of software tools and framework.*

One indicator pointing to the fact that non-planar ME is still in its infancy compared to its conventional 3-axis predecessor, is the current lack of processing tools and framework for this technology. As previously mentioned, this is the reason that prompted the development of such tools and framework within this research without

it being the primary topic of interest. Nevertheless, the shape and data-flow of the framework and tools established here represent one of the initial developments towards a more elaborate framework structure that could potentially be built and investigated for the needs of non-planar ME realisation.

## References

- [1] T. Wohlers and T. Gornet, “History of Additive Manufacturing,” 2014. doi: 10.31399/asm.hb.v24.a0006548.
- [2] I. Gibson, D. Rosen, and B. Stucker, *Additive manufacturing technologies: 3D printing, rapid prototyping, and direct digital manufacturing*, 2nd ed. 2014.
- [3] British Standards Institution, “BS ISO/ASTM 52900:2015 Additive manufacturing – General principles – Terminology,” 2015.
- [4] M. Khorram Niaki and F. Nonino, “Additive manufacturing management: a review and future research agenda,” *Int. J. Prod. Res.*, vol. 55, no. 5, pp. 1419–1439, 2017, doi: 10.1080/00207543.2016.1229064.
- [5] K. V. Wong and A. Hernandez, “A Review of Additive Manufacturing,” *ISRN Mech. Eng.*, vol. 2012, pp. 1–10, 2012, doi: 10.5402/2012/208760.
- [6] A. M. Platform, “Additive manufacturing: Strategic research agenda,” *AM SRA Final Consult. Doc.*, 2014.
- [7] British Standards Institution, “BS EN ISO 17296-2:2016 Additive manufacturing – General principles – Part 2: Overview of process categories and feedstock,” 2016.
- [8] M. Livesu, S. Ellero, J. Martínez, S. Lefebvre, and M. Attene, “From 3D models to 3D prints: an overview of the processing pipeline,” *Comput. Graph. Forum*, vol. 36, no. 2, pp. 537–564, 2017, doi: 10.1111/cgf.13147.
- [9] British Standards Institution, “BS ISO/ASTM 52915:2016 Specification for Additive Manufacturing File Format (AMF) Version 1.2,” 2016.
- [10] 3MF Consortium, “3D Manufacturing Format - Core Specification & Reference Guide,” 2015.
- [11] B. Starly, A. Lau, W. Sun, W. Lau, and T. Bradbury, “Direct slicing of STEP based NURBS models for layered manufacturing,” *CAD Comput. Aided Des.*, vol. 37, no. 4, 2005, doi: 10.1016/j.cad.2004.06.014.
- [12] M. Taufik and P. K. Jain, “Role of build orientation in layered manufacturing: A review,” *Int. J. Manuf. Technol. Manag.*, vol. 27, no. 1–3, pp. 47–73, 2013, doi: 10.1504/IJMTM.2013.058637.
- [13] S. Ahn, M. Montero, D. Odell, and S. Roundy, “Anisotropic material properties of fused deposition modeling ABS,” *Rapid Prototyp.*, vol. 8, no. 4, pp. 248–257, 2002, doi: 10.1108/13552540210441166.
- [14] I. International Organization for Standardization, “ISO 6983-1:2009 - Automation systems and integration -- Numerical control of machines -- Program format and definitions of address words -- Part 1: Data format for positioning, line motion and contouring control systems,” 2009.
- [15] S. Crump, “Apparatus and method for creating three-dimensional objects,” 1992.
- [16] J. F. Rodriguez, J. P. Thomas, and J. E. Renaud, “Characterization of the mesostructure of fused-deposition acrylonitrile-butadiene-styrene materials,” *Rapid Prototyp. J.*, vol. 6, no. 3, pp. 175–186, 2000, doi: 10.1108/13552540010337056.
- [17] C. Lee, S. Kim, H. Kim, and S. Ahn, “Measurement of anisotropic compressive strength of rapid prototyping parts,” *J. Mater. Process.*, vol. 187, pp. 627–630, 2007.

- [18] E. Sabourin, S. Houser, and J. Bohn, “Adaptive slicing using stepwise uniform refinement,” *Rapid Prototyp. J.*, vol. 2, no. 4, pp. 20–26, 1996, doi: 10.1108/13552549610153370.
- [19] D. Ahn, J. Kweon, S. Kwon, J. Song, and S. Lee, “Representation of surface roughness in fused deposition modeling,” *J. Mater. Process.*, vol. 209, no. 15–16, pp. 5593–5600, 2009, doi: 10.1016/j.jmatprotec.2009.05.016.
- [20] P. Pandey, N. Reddy, and S. Dhande, “Real time adaptive slicing for fused deposition modelling,” *Int. J. Mach.*, vol. 43, no. 1, pp. 61–71, 2003, doi: 10.1016/S0890-6955(02)00164-5.
- [21] H.-C. Song, N. Ray, D. Sokolov, and S. Lefebvre, “Anti-aliasing for fused filament deposition,” *CAD Comput. Aided Des.*, vol. 89, pp. 25–34, 2017, doi: 10.1016/j.cad.2017.04.001.
- [22] Y. Jin, Y. Wan, B. Zhang, and Z. Liu, “Modeling of the chemical finishing process for polylactic acid parts in fused deposition modeling and investigation of its tensile properties,” *J. Mater. Process. Technol.*, vol. 240, pp. 233–239, 2017, doi: 10.1016/j.jmatprotec.2016.10.003.
- [23] S. Rathee, M. Srivastava, S. Maheshwari, and A. N. Siddiquee, “Effect of varying spatial orientations on build time requirements for FDM process: A case study,” *Def. Technol.*, vol. 13, no. 2, pp. 92–100, 2017, doi: 10.1016/j.dt.2016.11.006.
- [24] B. Zhang, B. Seong, V. D. Nguyen, and D. Byun, “3D printing of high-resolution PLA-based structures by hybrid electrohydrodynamic and fused deposition modeling techniques,” *J. Micromechanics Microengineering*, vol. 26, no. 2, p. 025015, Jan. 2016, doi: 10.1088/0960-1317/26/2/025015.
- [25] A. Armillotta and M. Cavallaro, “Edge quality in fused deposition modeling: I. Definition and analysis,” *Rapid Prototyp. J.*, vol. 23, no. 6, pp. 1079–1087, 2017, doi: 10.1108/RPJ-02-2016-0020.
- [26] G. Kalmanovich, L. Dodin, and S. Tu, “Curved-layer laminated object manufacturing®,” *Proc. 7th Int. Conf. Rapid Prototyping, Univ. Dayt. Stanford Univ. 31 March–3 April*, pp. 51–59, 1997.
- [27] D. A. Klosterman *et al.*, “Development of a curved layer LOM process for monolithic ceramics and ceramic matrix composites,” *Rapid Prototyp. J.*, vol. 5, no. 2, pp. 61–71, 1999, doi: 10.1108/13552549910267362.
- [28] D. Chakraborty, B. Aneesh Reddy, and A. Roy Choudhury, “Extruder path generation for Curved Layer Fused Deposition Modeling,” *CAD Comput. Aided Des.*, vol. 40, no. 2, pp. 235–243, 2008, doi: 10.1016/j.cad.2007.10.014.
- [29] S. Singamneni, A. Roychoudhury, O. Diegel, and B. Huang, “Modeling and evaluation of curved layer fused deposition,” *J. Mater. Process. Technol.*, vol. 212, no. 1, pp. 27–35, 2012, doi: 10.1016/j.jmatprotec.2011.08.001.
- [30] R. J. A. Allen and R. S. Trask, “An experimental demonstration of effective Curved Layer Fused Filament Fabrication utilising a parallel deposition robot,” *Addit. Manuf.*, vol. 8, pp. 78–87, 2015, doi: 10.1016/j.addma.2015.09.001.
- [31] Ultimaker, “CURA,” 2019. <https://ultimaker.com/software/ultimaker-cura> (accessed Mar. 05, 2019).
- [32] M. Consortium, “MovAiD Project Website, 2017,” 2015. <http://www.movaid.eu/> (accessed Sep. 01, 2017).
- [33] R. L. Hope, P. A. Jacobs, and R. N. Roth, “Rapid prototyping with sloping surfaces,”

- Rapid Prototyp. J.*, vol. 3, no. 1, pp. 12–19, 1997, doi: 10.1108/13552549710169246.
- [34] M. Hayasi and B. Asisbanpour, “Conformed-to-CAD design sloped-edge adaptive slicing,” in *23rd Annual International Solid Freeform Fabrication Symposium - An Additive Manufacturing Conference, SFF 2012*, 2012, pp. 689–706.
- [35] S. Singamneni, A. Roychoudhury, O. Diegel, and B. Huang, “Modeling and evaluation of curved layer fused deposition,” *J. Mater. Process. Technol.*, vol. 212, no. 1, pp. 27–35, 2012, doi: 10.1016/j.jmatprotec.2011.08.001.
- [36] B. Huang and S. Singamneni, “Curved layer fused deposition modeling with varying raster orientations,” *Appl. Mech. Mater.*, vol. 446–447, pp. 263–269, 2014, doi: 10.4028/www.scientific.net/AMM.446-447.263.
- [37] H. W. Guan, M. M. Savalani, I. Gibson, and O. Diegel, “Influence of Fill Gap on Flexural Strength of Parts Fabricated by Curved Layer Fused Deposition Modeling,” *Procedia Technol.*, vol. 20, pp. 243–248, 2015, doi: 10.1016/j.protcy.2015.07.039.
- [38] B. Huang and S. Singamneni, “A mixed-layer approach combining both flat and curved layer slicing for fused deposition modelling,” *Proc. Inst. Mech. Eng. Part B J. Eng. Manuf.*, vol. 229, no. 12, pp. 2238–2249, 2015, doi: 10.1177/0954405414551076.
- [39] B. Huang and S. B. Singamneni, “Curved layer adaptive slicing (CLAS) for fused deposition modelling,” *Rapid Prototyp. J.*, vol. 21, no. 4, pp. 354–367, 2015, doi: 10.1108/RPJ-06-2013-0059.
- [40] Y. Jin, J. Du, Y. He, and G. Fu, “Modeling and process planning for curved layer fused deposition,” *Int. J. Adv. Manuf. Technol.*, vol. 91, no. 1–4, pp. 273–285, 2017, doi: 10.1007/s00170-016-9743-5.
- [41] T. Llewellyn-Jones, R. Allen, and R. Trask, “Curved Layer Fused Filament Fabrication Using Automated Toolpath Generation,” *3D Print. Addit. Manuf.*, vol. 3, no. 4, pp. 236–243, 2016, doi: 10.1089/3dp.2016.0033.
- [42] O. Diegel, S. Singamneni, B. Huang, and I. Gibson, “Curved layer fused deposition modeling in conductive polymer additive manufacturing,” *Adv. Mater. Res.*, vol. 199–200, pp. 1984–1987, 2011, doi: 10.4028/www.scientific.net/AMR.199-200.1984.
- [43] H. Prüß and T. Vietor, “Design for Fiber-Reinforced Additive Manufacturing,” *J. Mech. Des.*, vol. 137, no. 11, p. 111409, 2015, doi: 10.1115/1.4030993.
- [44] S. Doherty, W. De Backer, A. P. Bergs, R. Harik, M. Van Tooren, and I. Rekleitis, “Selective directional reinforcement of structures for multi-axis additive manufacturing,” in *CAMX 2016 - Composites and Advanced Materials Expo Conference Proceedings*, 2016.
- [45] J. C. S. McCaw and E. Cuan-Urquizo, “Curved-Layered Additive Manufacturing of non-planar, parametric lattice structures,” *Mater. Des.*, vol. 160, pp. 949–963, 2018, doi: 10.1016/j.matdes.2018.10.024.
- [46] E. Cuan-Urquizo *et al.*, “Elastic response of lattice arc structures fabricated using curved-layered fused deposition modeling,” *Mech. Adv. Mater. Struct.*, pp. 1–11, 2019, doi: 10.1080/15376494.2019.1682728.
- [47] J. C. S. McCaw and E. Cuan-Urquizo, “Mechanical characterization of 3D printed, non-planar lattice structures under quasi-static cyclic loading,” *Rapid Prototyp. J.*, vol. 26, no. 4, pp. 707–717, 2020, doi: 10.1108/RPJ-06-2019-0163.
- [48] I. Bin Ishak and P. Larochelle, “MotoMaker: a robot FDM platform for multi-plane



- and 3D lattice structure printing,” *Mech. Based Des. Struct. Mach.*, vol. 47, no. 6, pp. 703–720, 2019, doi: 10.1080/15397734.2019.1615943.
- [49] J. Etienne *et al.*, “Curvislicer: Slightly curved slicing for 3-axis printers,” *ACM Trans. Graph.*, vol. 38, no. 4, p. 11, 2019, doi: 10.1145/3306346.3323022.
- [50] B. Ezair, S. Fuhrmann, and G. Elber, “Volumetric covering print-paths for additive manufacturing of 3D models,” *CAD Comput. Aided Des.*, vol. 100, pp. 1–13, 2018, doi: 10.1016/j.cad.2018.02.006.
- [51] C. Dai, C. C. L. Wang, C. Wu, S. Lefebvre, G. Fang, and Y. J. Liu, “Support-free volume printing by multi-axis motion,” *ACM Trans. Graph.*, vol. 37, no. 4, p. 14, 2018, doi: 10.1145/3197517.3201342.
- [52] L. Chen, M. F. Chung, Y. Tian, A. Joneja, and K. Tang, “Variable-depth curved layer fused deposition modeling of thin-shells,” *Robot. Comput. Integr. Manuf.*, vol. 57, pp. 422–434, Jun. 2019, doi: 10.1016/j.rcim.2018.12.016.
- [53] K. Xu, Y. Li, L. Chen, and K. Tang, “Curved layer based process planning for multi-axis volume printing of freeform parts,” *CAD Comput. Aided Des.*, vol. 114, pp. 51–63, 2019, doi: 10.1016/j.cad.2019.05.007.
- [54] B. Huang, S. Singamneni, and O. Diegel, “Construction of a curved layer rapid prototyping system: Integrating mechanical, electronic and software engineering,” in *15th International Conference on Mechatronics and Machine Vision in Practice, M2VIP’08*, 2008, pp. 599–603, doi: 10.1109/MMVIP.2008.4749598.
- [55] J.-W. Choi *et al.*, “Development of a mobile fused deposition modeling system with enhanced manufacturing flexibility,” *J. Mater. Process. Technol.*, vol. 211, no. 3, pp. 424–432, 2011, doi: 10.1016/j.jmatprotec.2010.10.019.
- [56] H.-L. Li, C. G. Geisler, D. M. Wootton, and J. G. Zhou, “A new flexible and multi-purpose system design for 3-dimensional printing,” in *ASME 2011 International Manufacturing Science and Engineering Conference, MSEC 2011*, 2011, vol. 1, pp. 55–61, doi: 10.1115/MSEC2011-50176.
- [57] S. Lim, R. A. Buswell, P. J. Valentine, D. Piker, S. A. Austin, and X. De Kestelier, “Modelling curved-layered printing paths for fabricating large-scale construction components,” *Addit. Manuf.*, vol. 12, no. Part B, pp. 216–230, 2016, doi: 10.1016/j.addma.2016.06.004.
- [58] X. Song, Y. Pan, and Y. Chen, “Development of a low-cost parallel kinematic machine for multidirectional additive manufacturing,” *J. Manuf. Sci. Eng. Trans. ASME*, vol. 137, no. 2, p. 021005, 2015, doi: 10.1115/1.4028897.
- [59] W. C. Lee and S. C. Chung, “Design of a hybrid 5-axis machine tool with fused-deposition-modeling capability,” *Appl. Mech. Mater.*, vol. 446–447, pp. 640–644, 2014, doi: 10.4028/www.scientific.net/AMM.446-447.640.
- [60] S.-C. C. Wei-chen Lee, Ching-chih Wei, “Development of a hybrid rapid prototyping system using low-cost fused deposition modeling and five-axis machining,” *J. Mater. Process. Technol.*, vol. 214, no. 11, pp. 2366–2374, 2014, doi: 10.1016/j.jmatprotec.2014.05.004.
- [61] K. Kawagishi, S. Umetani, K. Tanaka, E. Ametani, Y. Morimoto, and K. Takasugi, “Development of four-axis 3D printer with fused deposition modeling technology,” *Int. J. Autom. Technol.*, vol. 11, no. 2, pp. 278–286, 2017, doi: 10.20965/ijat.2017.p0278.
- [62] H. Giberti, M. Strano, and M. Annoni, “An innovative machine for Fused Deposition

- Modeling of metals and advanced ceramics,” in *MATEC Web of Conferences*, 2016, vol. 43, p. 5, doi: 10.1051/matecont/20164303003.
- [63] M. Annoni, H. Giberti, and M. Strano, “Feasibility Study of an Extrusion-based Direct Metal Additive Manufacturing Technique,” *Procedia Manuf.*, vol. 5, pp. 916–927, 2016, doi: 10.1016/j.promfg.2016.08.079.
- [64] R. C. Luo, L. C. Hsu, T. J. Hsiao, and Y. W. Perng, “3D Digital Manufacturing via Synchronous 5-Axes Printing for Strengthening Printing Parts,” *IEEE Access*, vol. 8, pp. 126083–126091, 2020, doi: 10.1109/ACCESS.2020.3007772.
- [65] G. Q. Zhang, A. Spaak, C. Martinez, D. T. Lasko, B. Zhang, and T. A. Fuhlbrigge, “Robotic additive manufacturing process simulation-towards design and analysis with building parameter in consideration,” in *IEEE International Conference on Automation Science and Engineering*, 2016, vol. 2016-Novem, pp. 609–613, doi: 10.1109/COASE.2016.7743457.
- [66] G. Q. Zhang, W. Mondesir, C. Martinez, X. Li, T. A. Fuhlbrigge, and H. Bheda, “Robotic additive manufacturing along curved surface - A step towards free-form fabrication,” in *2015 IEEE International Conference on Robotics and Biomimetics, IEEE-ROBIO 2015*, 2016, pp. 721–726, doi: 10.1109/ROBIO.2015.7418854.
- [67] Z. Wang, J. K. Min, and G. Xiong, “Robotics-driven printing of curved 3D structures for manufacturing cardiac therapeutic devices,” in *2015 IEEE International Conference on Robotics and Biomimetics, IEEE-ROBIO 2015*, 2016, pp. 2318–2323, doi: 10.1109/ROBIO.2015.7419120.
- [68] K.-M. M. Tam, C. T. Mueller, J. R. Coleman, and N. W. Fine, “Stress Line Additive Manufacturing (SLAM) for 2.5-D shells,” *J. Int. Assoc. Shell Spat. Struct.*, vol. 57, no. 4, pp. 249–259, 2016, doi: 10.20898/j.iass.2016.190.856.
- [69] K. M. M. Tam and C. T. Mueller, “Additive Manufacturing Along Principal Stress Lines,” *3D Print. Addit. Manuf.*, vol. 4, no. 2, pp. 63–81, 2017, doi: 10.1089/3dp.2017.0001.
- [70] C. Gosselin, R. Duballet, P. Roux, N. Gaudillière, J. Dirrenberger, and P. Morel, “Large-scale 3D printing of ultra-high performance concrete - a new processing route for architects and builders,” *Mater. Des.*, vol. 100, pp. 102–109, 2016, doi: 10.1016/j.matdes.2016.03.097.
- [71] S. Keating and N. Oxman, “Compound fabrication: A multi-functional robotic platform for digital design and fabrication,” *Robot. Comput. Integr. Manuf.*, vol. 29, no. 6, pp. 439–448, 2013, doi: 10.1016/j.rcim.2013.05.001.
- [72] N. Oxman, J. Laucks, M. Kayser, E. Tsai, and M. Firstenberg, “Freeform 3D printing: Towards a sustainable approach to additive manufacturing,” in *Green Design, Materials and Manufacturing Processes - Proceedings of the 2nd International Conference on Sustainable Intelligent Manufacturing, SIM 2013*, 2013, pp. 479–483.
- [73] L. Mogas-Soldevila and N. Oxman, “Water-based engineering & fabrication: Large-scale additive manufacturing of biomaterials,” in *Materials Research Society Symposium Proceedings*, 2015, vol. 1800, pp. 46–53, doi: 10.1557/opl.2015.659.
- [74] J. R. Kubalak, A. L. Wicks, and C. B. Williams, “Exploring multi-axis material extrusion additive manufacturing for improving mechanical properties of printed parts,” *Rapid Prototyp. J.*, vol. 25, no. 2, pp. 356–362, 2019, doi: 10.1108/RPJ-02-2018-0035.
- [75] N. R. Fry, R. C. Richardson, and J. H. Boyle, “Robotic additive manufacturing system for dynamic build orientations,” *Rapid Prototyp. J.*, vol. 26, no. 4, pp. 659–667, 2020,

doi: 10.1108/RPJ-09-2019-0243.

- [76] L. Li, A. Haghghi, and Y. Yang, "A novel 6-axis hybrid additive-subtractive manufacturing process: Design and case studies," *J. Manuf. Process.*, vol. 33, no. May, pp. 150–160, 2018, doi: 10.1016/j.jmapro.2018.05.008.
- [77] F. Xie, L. Chen, Z. Li, and K. Tang, "Path smoothing and feed rate planning for robotic curved layer additive manufacturing," *Robot. Comput. Integr. Manuf.*, vol. 65, no. February, p. 101967, 2020, doi: 10.1016/j.rcim.2020.101967.
- [78] J. M. Flynn, A. Shokrani, S. T. Newman, and V. Dhokia, "Hybrid additive and subtractive machine tools - Research and industrial developments," *Int. J. Mach. Tools Manuf.*, vol. 101, pp. 79–101, 2016, doi: 10.1016/j.ijmachtools.2015.11.007.
- [79] P. Singh and D. Dutta, "Multi-Direction Slicing for Layered Manufacturing.," *J. Comput. Inf. Sci. Eng.*, vol. 1, no. 2, pp. 129–142, 2001, doi: 10.1115/1.1375816.
- [80] P. Singh, Y. Moon, D. Dutta, and S. Kota, "Design of a customized multi-directional layered deposition system based on part geometry," *Annu. Solid Free. Fabr.*, 2003, doi: 10.26153/tsw/5562.
- [81] H. Zhang, J. Jiang, H. Zou, and G. Wang, "Multi-axis path planning for hybrid plasma deposition and milling based on slicing characteristics," *Lect. Notes Comput. Sci. (including Subser. Lect. Notes Artif. Intell. Lect. Notes Bioinformatics)*, vol. 5314 LNAI, no. PART 1, pp. 225–234, 2008, doi: 10.1007/978-3-540-88513-9-25.
- [82] F. Liou, J. Ruan, and T. E. Sparks, "Multi-Axis Planning System (MAPS) for hybrid laser metal deposition processes," in *21st Annual International Solid Freeform Fabrication Symposium - An Additive Manufacturing Conference, SFF 2010*, 2010, pp. 592–605.
- [83] Y. Li and Y. Chen, "Five-axis manufacturing simulation based on normal arc mapping and offset volume computation," in *Proceedings of the ASME Design Engineering Technical Conference*, 2010, vol. 3, no. PARTS A AND B, pp. 391–403, doi: 10.1115/DETC2010-29051.
- [84] K. Lee and H. Jee, "Slicing algorithms for multi-axis 3-D metal printing of overhangs," *J. Mech. Sci. Technol.*, vol. 29, no. 12, pp. 5139–5144, 2015, doi: 10.1007/s12206-015-1113-y.
- [85] D. Ding, Z. Pan, D. Cuiuri, and H. Li, "Process planning for robotic wire and arc additive manufacturing," in *Proceedings of the 2015 10th IEEE Conference on Industrial Electronics and Applications (ICIEA)*, 2015, pp. 2000–2003, doi: 10.1109/ICIEA.2015.7334441.
- [86] D. Ding, Z. Pan, D. Cuiuri, H. Li, N. Larkin, and S. Van Duin, "Automatic multi-direction slicing algorithms for wire based additive manufacturing," *Robot. Comput. Integr. Manuf.*, vol. 37, pp. 130–150, 2016, doi: 10.1016/j.rcim.2015.09.002.
- [87] D. Ding, Z. Pan, D. Cuiuri, and H. Li, "A practical path planning methodology for wire and arc additive manufacturing of thin-walled structures," *Robot. Comput. Integr. Manuf.*, vol. 34, pp. 8–19, 2015, doi: 10.1016/j.rcim.2015.01.003.
- [88] D. Ding, Z. Pan, D. Cuiuri, H. Li, S. Van Duin, and N. Larkin, "Bead modelling and implementation of adaptive MAT path in wire and arc additive manufacturing," *Robot. Comput. Integr. Manuf.*, vol. 39, pp. 32–42, 2016, doi: 10.1016/j.rcim.2015.12.004.
- [89] D. Ding *et al.*, "Towards an automated robotic arc-welding-based additive manufacturing system from CAD to finished part," *Comput. Des.*, vol. 73, pp. 66–75,

- 2016, doi: 10.1016/j.cad.2015.12.003.
- [90] Y. Ding, R. Dwivedi, and R. Kovacevic, “Process planning for 8-axis robotized laser-based direct metal deposition system: A case on building revolved part,” *Robot. Comput. Integr. Manuf.*, vol. 44, pp. 67–76, 2017, doi: 10.1016/j.rcim.2016.08.008.
- [91] G. Zhao, G. Ma, J. Feng, and W. Xiao, “Nonplanar slicing and path generation methods for robotic additive manufacturing,” *Int. J. Adv. Manuf. Technol.*, vol. 96, no. 9–12, pp. 3149–3159, 2018, doi: 10.1007/s00170-018-1772-9.
- [92] H. Jee and M. Kim, “Spherically curved layer (SCL) model for metal 3-D printing of overhangs,” *J. Mech. Sci. Technol.*, vol. 31, no. 12, pp. 5729–5735, 2017, doi: 10.1007/s12206-017-1114-0.
- [93] J. Flores, I. Garmendia, and J. Pujana, “Toolpath generation for the manufacture of metallic components by means of the laser metal deposition technique,” *Int. J. Adv. Manuf. Technol.*, vol. 101, no. 5–8, pp. 2111–2120, 2019, doi: 10.1007/s00170-018-3124-1.
- [94] B. Xin, X. Zhou, and Y. Gong, “Surface based variable thickness slicing modeling for laser metal deposition,” *Int. J. Adv. Manuf. Technol.*, vol. 107, no. 1–2, pp. 463–474, 2020, doi: 10.1007/s00170-020-05023-4.
- [95] D. Ding, Z. Pan, D. Cuiuri, and H. Li, “Advanced Design for Additive Manufacturing: 3D Slicing and 2D Path Planning,” *New Trends 3D Print.*, pp. 1–23, 2016.
- [96] S. Mueller *et al.*, “WirePrint: 3D printed previews for fast prototyping,” in *UIST 2014 - Proceedings of the 27th Annual ACM Symposium on User Interface Software and Technology*, 2014, pp. 273–280, doi: 10.1145/2642918.2647359.
- [97] R. Wu, H. Peng, F. Guimbretière, and S. Marschner, “Printing arbitrary meshes with a 5DOF wireframe printer,” *ACM Trans. Graph.*, vol. 35, no. 4, 2016, doi: 10.1145/2897824.2925966.
- [98] W. Gao, Y. Zhang, D. C. Nazzetta, K. Ramani, and R. J. Cipra, “RevoMaker: Enabling multi-directional and functionally-embedded 3D printing using a rotational cuboidal platform,” in *UIST 2015 - Proceedings of the 28th Annual ACM Symposium on User Interface Software and Technology*, 2015, pp. 437–446, doi: 10.1145/2807442.2807476.
- [99] A. Avdeev *et al.*, “Strength increasing additive manufacturing fused filament fabrication technology, based on spiral toolpath material deposition,” *Machines*, vol. 7, no. 3, p. 57, 2019, doi: 10.3390/MACHINES7030057.
- [100] F. B. Coulter and A. Ianakiev, “4D Printing Inflatable Silicone Structures,” *3D Print. Addit. Manuf.*, vol. 2, no. 3, pp. 140–144, 2015, doi: 10.1089/3dp.2015.0017.
- [101] B. Khoda, “Build direction for improved process plan in multi-material additive manufacturing,” in *Proceedings of the ASME Design Engineering Technical Conference*, 2014, vol. 4, p. 7 pages, doi: 10.1115/DETC2014-35060.
- [102] T. Wasley *et al.*, “Enabling Rapid Production and Mass Customisation of Electronics Using Digitally Driven Hybrid Additive Manufacturing Techniques,” in *Proceedings - Electronic Components and Technology Conference*, 2016, vol. 2016-Augus, pp. 849–856, doi: 10.1109/ECTC.2016.187.
- [103] K. Izumi, Y. Yoshida, and S. Tokito, “Soft blanket gravure printing technology for finely patterned conductive layers on three-dimensional or curved surfaces,” *Jpn. J. Appl. Phys.*, vol. 56, no. 5S2, p. 05EA03, 2017, doi: 10.7567/JJAP.56.05EA03.
- [104] C. Kim, D. Espalin, and A. Cuaron, “Cooperative tool path planning for wire

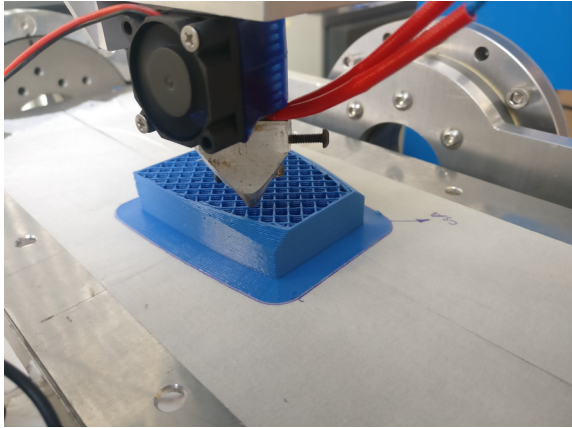
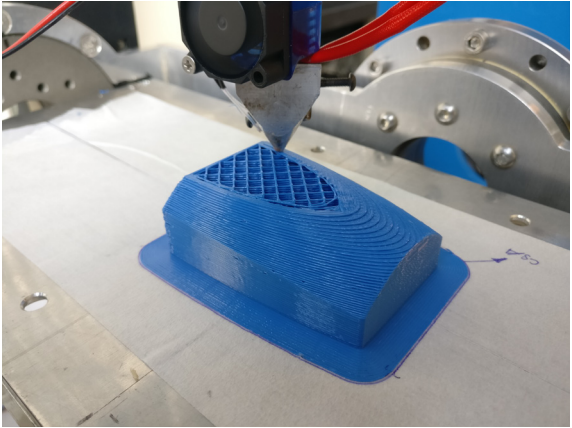
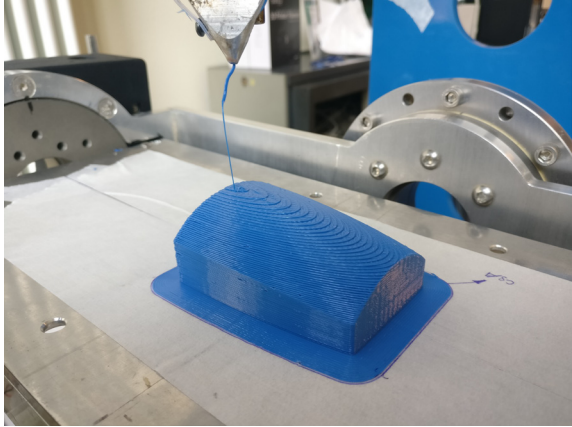
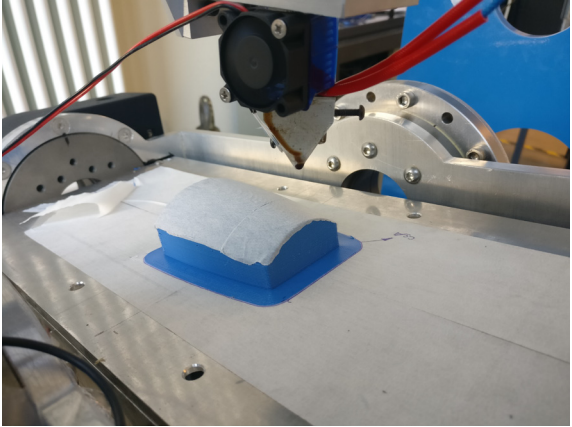
- embedding on additively manufactured curved surfaces using robot kinematics,” *J. Mech. Robot.*, vol. 7, no. 2, p. 021003, 2015, doi: doi.org/10.1115/1.4029473.
- [105] A. Panesar, I. Ashcroft, R. Wildman, and R. Hague, “A method for Bi-directional coupling of structure and system in the optimization of multi-functional components,” in *ECCOMAS Congress 2016 - Proceedings of the 7th European Congress on Computational Methods in Applied Sciences and Engineering*, 2016, vol. 2, pp. 3239–3248.
- [106] R. R. Ma, J. T. Belter, and A. M. Dollar, “Hybrid Deposition Manufacturing: Design Strategies for Multimaterial Mechanisms Via Three- Dimensional Printing and Material Deposition,” *J. Mech. Robot.*, vol. 7, no. 2, pp. 1–10, 2015, doi: 10.1115/1.4029400.
- [107] Y. Chen, C. Zhou, and J. Lao, “Additive manufacturing without layers: A new solid freeform fabrication process based on CNC accumulation,” in *21st Annual International Solid Freeform Fabrication Symposium - An Additive Manufacturing Conference, SFF 2010*, 2010, pp. 108–120.
- [108] Y. Chen, C. Zhou, and J. Lao, “A layerless additive manufacturing process based on CNC accumulation,” *Rapid Prototyp. J.*, vol. 17, no. 3, pp. 218–227, 2011, doi: 10.1108/13552541111124806.
- [109] Y. Pan, C. Zhou, Y. Chen, and J. Partanen, “Multitool and multi-axis computer numerically controlled accumulation for fabricating conformal features on curved surfaces,” *J. Manuf. Sci. Eng. Trans. ASME*, vol. 136, no. 3, p. 031007, 2014, doi: 10.1115/1.4026898.
- [110] X. Zhao, Y. Pan, C. Zhou, Y. Chen, and C. C. L. Wang, “R - An integrated CNC accumulation system for automatic building-around-inserts,” *J. Manuf. Process.*, vol. 15, no. 4, pp. 432–443, 2013, doi: 10.1016/j.jmapro.2013.05.009.
- [111] O. Diegel, S. Singamneni, B. Huang, and I. Gibson, “Getting Rid of the Wires: Curved Layer Fused Deposition Modeling in Conductive Polymer Additive Manufacturing,” *Key Eng. Mater.*, vol. 467, pp. 662–667, 2011, doi: 10.4028/www.scientific.net/KEM.467-469.662.
- [112] S. Raut, V. S. Jatti, N. K. Khedkar, and T. P. Singh, “Investigation of the Effect of Built Orientation on Mechanical Properties and Total Cost of FDM Parts,” *Procedia Mater. Sci.*, vol. 6, no. Icmpe, pp. 1625–1630, 2014, doi: 10.1016/j.mspro.2014.07.146.
- [113] I. Durgun and R. Ertan, “Experimental investigation of FDM process for improvement of mechanical properties and production cost,” *Rapid Prototyp. J.*, vol. 20, no. 3, pp. 228–235, 2014, doi: 10.1108/RPJ-10-2012-0091.
- [114] Y. Jin, J. du, Y. He, and G. Fu, “Modeling and process planning for curved layer fused deposition,” *Int. J. Adv. Manuf. Technol.*, pp. 1–13, 2016, doi: 10.1007/s00170-016-9743-5.
- [115] Y. Patel, A. Kshattriya, S. B. Singamneni, and A. R. Choudhury, “Application of curved layer manufacturing for preservation of randomly located minute critical surface features in rapid prototyping,” *Rapid Prototyp. J.*, vol. 21, no. 6, pp. 725–734, 2015, doi: 10.1108/RPJ-07-2013-0073.
- [116] Robert McNeel & Associates, “Rhinoceros,” 2020. <https://www.rhino3d.com/> (accessed Mar. 16, 2020).
- [117] L. Piegl and W. Tiller, *The NURBS book*, 2nd ed. 1997.
- [118] G. V. V. Ravi Kumar, K. G. Shastry, and B. G. Prakash, “Computing non-self-

- intersecting offsets of NURBS surfaces,” *CAD Comput. Aided Des.*, vol. 34, no. 3, pp. 209–228, 2002, doi: 10.1016/S0010-4485(01)00081-1.
- [119] RepRap, “G-code,” 2020. <https://reprap.org/wiki/G-code> (accessed Feb. 27, 2020).
- [120] X. W. Xu and S. T. Newman, “Making CNC machine tools more open, interoperable and intelligent - A review of the technologies,” *Comput. Ind.*, vol. 57, no. 2, pp. 141–152, Feb. 2006, doi: 10.1016/j.compind.2005.06.002.
- [121] K. Cheng, Ed., *Machining Dynamics : Fundamentals, Applications and Practices*. Springer London, Limited, 2008.
- [122] LinuxCNC, “LinuxCNC,” 2019. <http://linuxcnc.org/> (accessed May 23, 2019).
- [123] H. H. Nadiyapara and S. Pande, “A Review of Variable Slicing in Fused Deposition Modeling,” *J. Inst. Eng. Ser. C*, vol. 98, no. 3, pp. 387–393, 2017, doi: 10.1007/s40032-016-0272-7.
- [124] D. Zhao and W. Guo, “Shape and Performance Controlled Advanced Design for Additive Manufacturing: A Review of Slicing and Path Planning,” *J. Manuf. Sci. Eng. Trans. ASME*, vol. 142, no. 1, pp. 1–23, 2020, doi: 10.1115/1.4045055.
- [125] J. Xu, X. Gu, D. Ding, Z. Pan, and K. Chen, “A review of slicing methods for directed energy deposition based additive manufacturing,” *Rapid Prototyp. J.*, vol. 24, no. 6, pp. 1012–1025, 2018, doi: 10.1108/RPJ-10-2017-0196.
- [126] B. Huang, “Alternate Slicing and Deposition Strategies for Fused Deposition Modelling,” PhD Thesis. Auckland University of Technology, 2014.
- [127] B. Brenken, E. Barocio, A. Favaloro, V. Kunc, and R. B. Pipes, “Fused filament fabrication of fiber-reinforced polymers: A review,” *Addit. Manuf.*, vol. 21, pp. 1–16, 2018, doi: 10.1016/j.addma.2018.01.002.
- [128] R. C. Huber, C. Abert, F. Bruckner, M. Groenefeld, O. Muthsam, S. Schuschnigg, K. Sirak and D. S. Thanhoffer, I. Teliban, C. Vogler, R. Windl, “3D print of polymer bonded rare-earth magnets, and 3D magnetic field scanning with an end-user 3D printer,” *Appl. Phys. Lett.*, vol. 109, no. October 2016, p. 162401, 2016, doi: 10.1063/1.4964856.
- [129] R. H. Sanatgar, A. Cayla, C. Campagne, and V. Nierstrasz, “Morphological and electrical characterization of conductive polylactic acid based nanocomposite before and after FDM 3D printing,” *J. Appl. Polym. Sci.*, vol. 136, no. 6, p. 47040, 2019, doi: 10.1002/app.47040.
- [130] A. Dorigato, V. Moretti, S. Dul, S. H. Unterberger, and A. Pegoretti, “Electrically conductive nanocomposites for fused deposition modelling,” *Synth. Met.*, vol. 226, pp. 7–14, 2017, doi: 10.1016/j.synthmet.2017.01.009.
- [131] S. W. Kwok *et al.*, “Electrically conductive filament for 3D-printed circuits and sensors,” *Appl. Mater. Today*, vol. 9, pp. 167–175, 2017, doi: 10.1016/j.apmt.2017.07.001.
- [132] P. F. Flowers, C. Reyes, S. Ye, M. J. Kim, and B. J. Wiley, “3D printing electronic components and circuits with conductive thermoplastic filament,” *Addit. Manuf.*, vol. 18, pp. 156–163, 2017, doi: 10.1016/j.addma.2017.10.002.
- [133] M. Areir, Y. Xu, R. Zhang, D. Harrison, J. Fyson, and E. Pei, “A study of 3D printed active carbon electrode for the manufacture of electric double-layer capacitors,” *J. Manuf. Process.*, vol. 25, pp. 351–356, 2017, doi: 10.1016/j.jmapro.2016.12.020.
- [134] M. Almoqli, A. Aldalbahi, M. Rahaman, P. Govindasami, and S. Alzahly, “Influence of

- Biopolymer Carrageenan and Glycerine on the Properties of Extrusion Printed Inks of Carbon Nanotubes,” *Polymers (Basel)*, vol. 10, no. 10, p. 1148, 2018, doi: 10.3390/polym10101148.
- [135] V. Koncar, M. Lewandowski, and C. Dufour, “Design and Development of a Flexible Strain Sensor for Textile Structures Based on a Conductive Polymer Composite,” *Sensors*, vol. 7, no. 4, pp. 473–492, 2007.
- [136] S. J. Leigh, R. J. Bradley, C. P. Purssell, D. R. Billson, and D. A. Hutchins, “A Simple, Low-Cost Conductive Composite Material for 3D Printing of Electronic Sensors,” *PLoS One*, vol. 7, no. 11, p. e49365, 2012, doi: 10.1371/journal.pone.0049365.
- [137] D. Thaler, N. Aliheidari, and A. Ameli, “Electrical Properties of Additively Manufactured Acrylonitrile Butadiene Styrene/Carbon Nanotube Nanocomposite,” in *Proceedings of ASME 2018 Conference on Smart Materials, Adaptive Structures and Intelligent Systems*, 2018, p. V001T01A008, doi: 10.1115/smasis2018-8002.
- [138] “Proto-Pasta Conductive PLA,” 2019. <https://www.proto-pasta.com/pages/conductive-pla> (accessed Jan. 24, 2019).
- [139] “AlphaOhm,” 2019. <https://www.filoalfa3d.com/gb/special/171-292-alfaohm-8050327032354.html> (accessed Jun. 24, 2019).
- [140] “Simplify3D,” 2019. <https://www.simplify3d.com/> (accessed Jan. 24, 2019).
- [141] D. Zhao and W. Guo, “Mixed-layer adaptive slicing for robotic Additive Manufacturing (AM) based on decomposing and regrouping,” *J. Intell. Manuf.*, vol. 31, no. 4, pp. 985–1002, 2020, doi: 10.1007/s10845-019-01490-z.

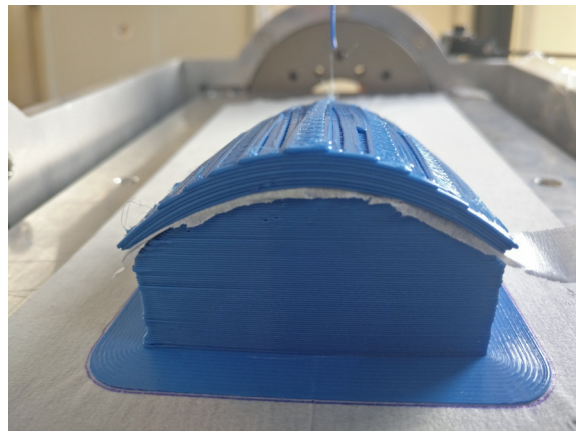
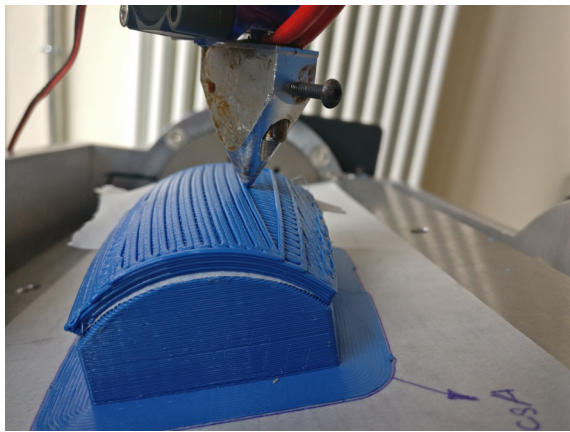
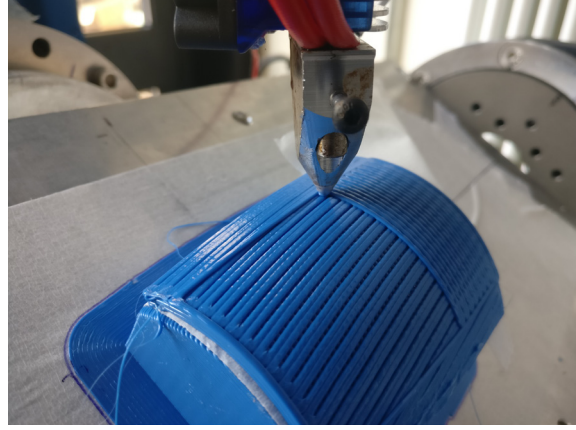
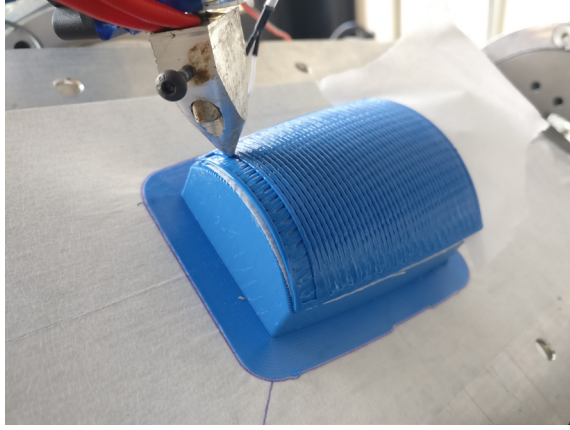
# Appendix A: Supplementary manufacturing images

Selected images from the manufacturing phase of each of the multi-axis ME case studies and the required support structure are reported here below:

<i>Support Structure</i>	
	
	
<i>Table A1: Images of the manufacturing of support structure by conventional, 3-axis ME</i>	

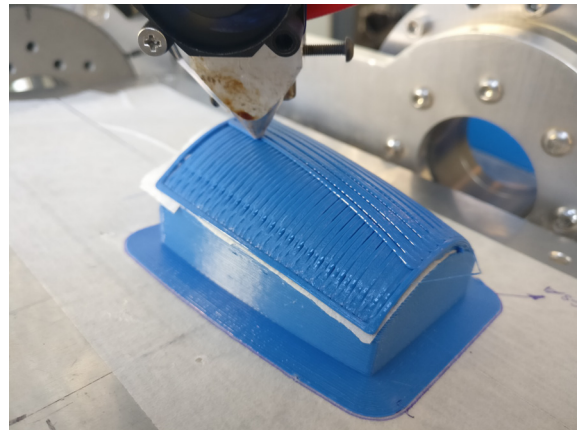
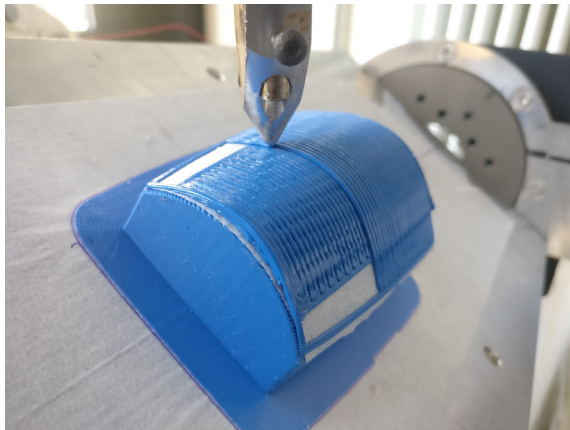
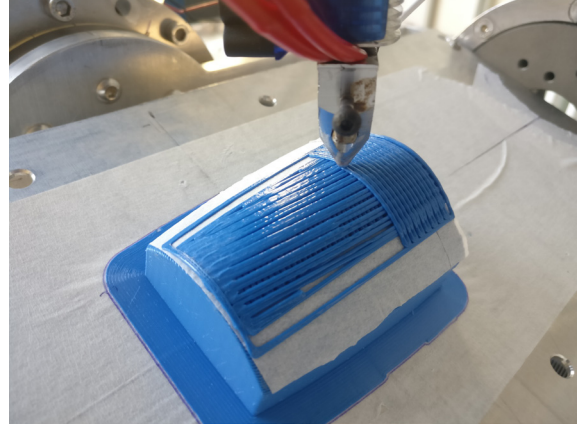
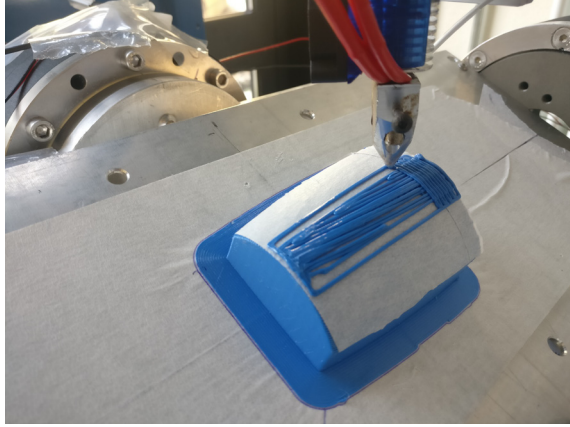


*Case\_Abot*



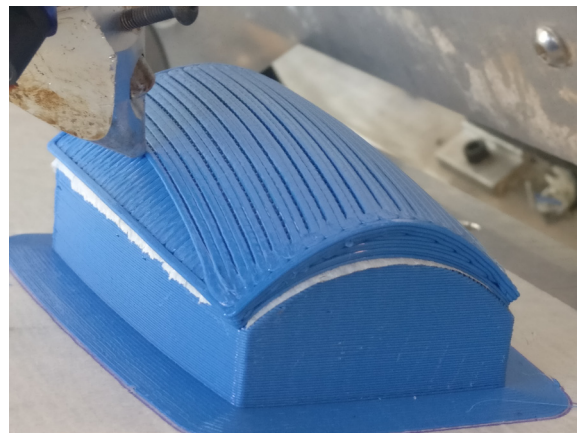
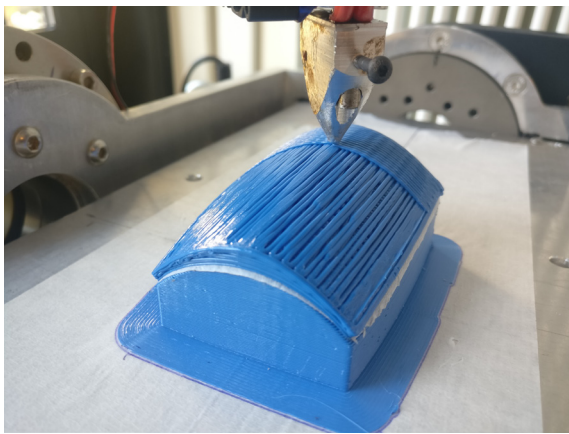
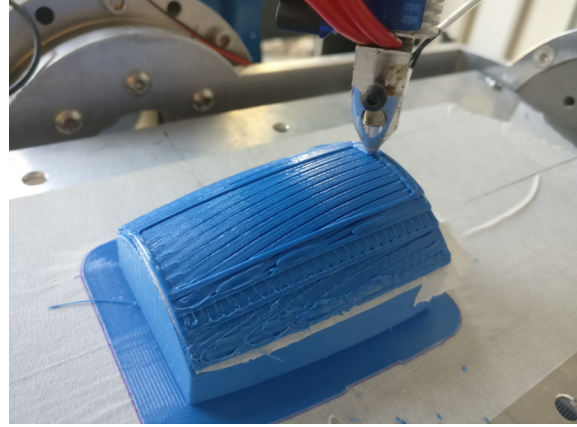
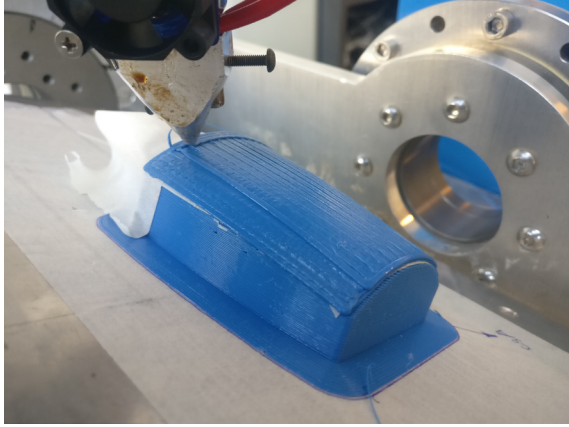
*Table A2: Images of manufacturing of Case\_Abot case study by multi-axis ME process*

*Case\_Atop*



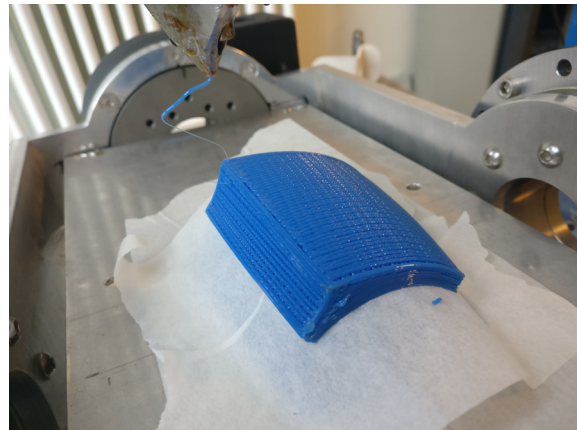
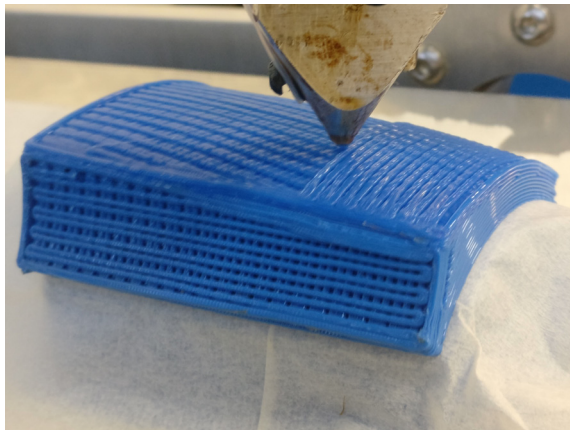
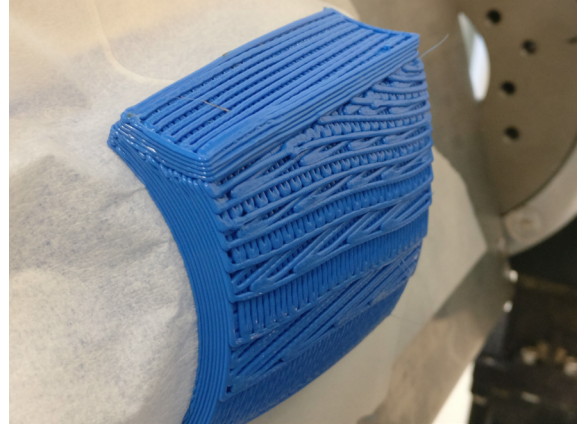
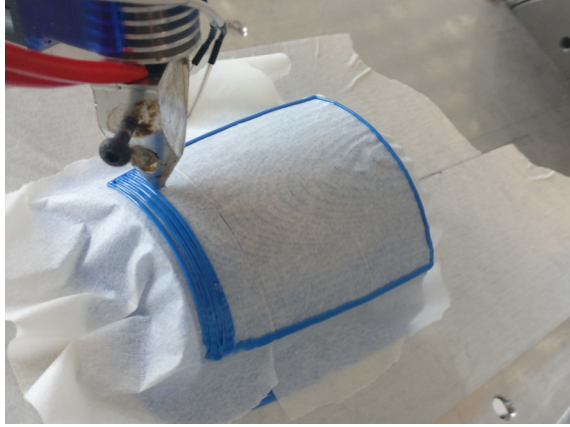
*Table A3: Images of manufacturing of Case\_Atop case study by multi-axis ME process*

*Case\_Asan*



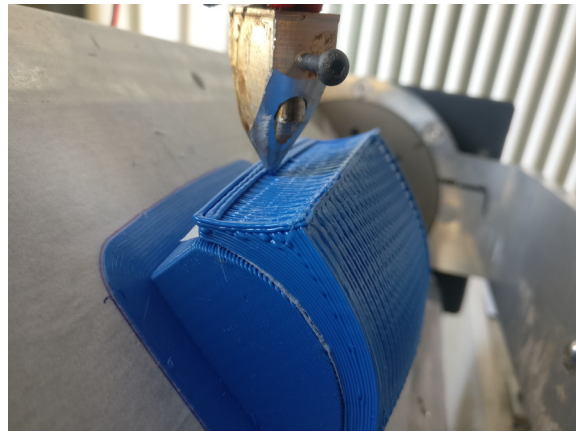
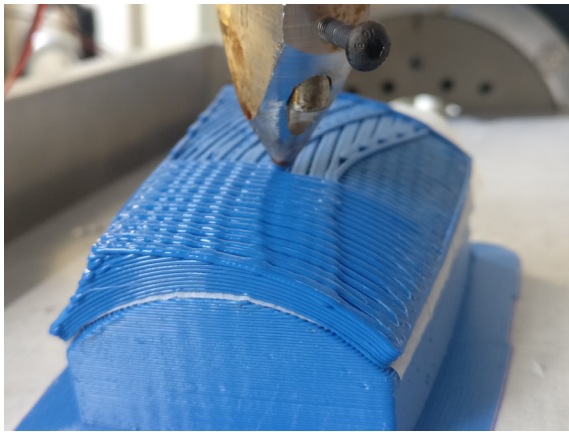
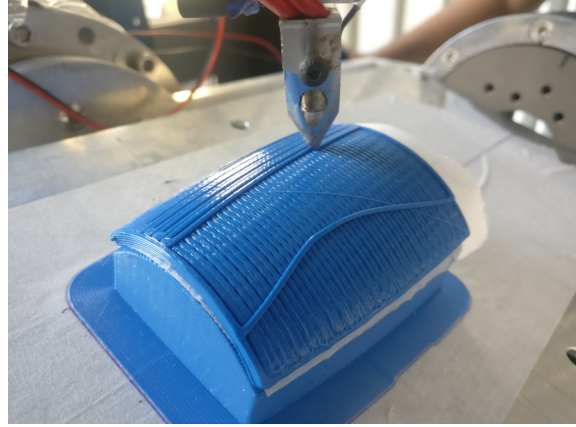
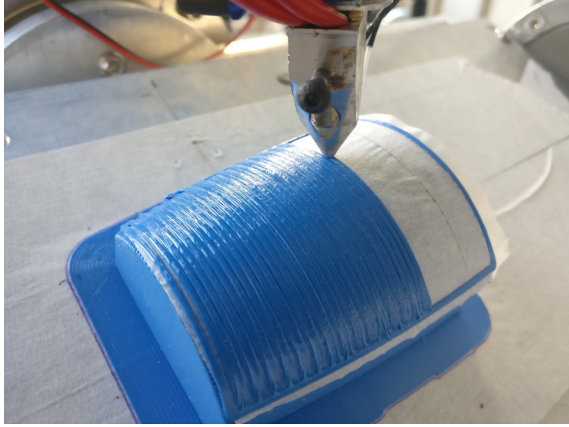
*Table A4: Images of manufacturing of Case\_Asan case study by multi-axis ME process*

*Case\_Btop*



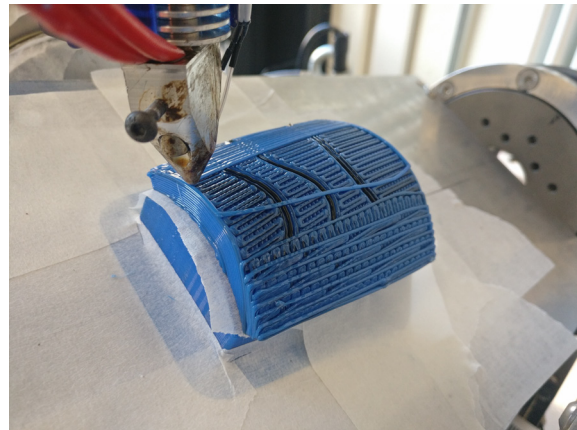
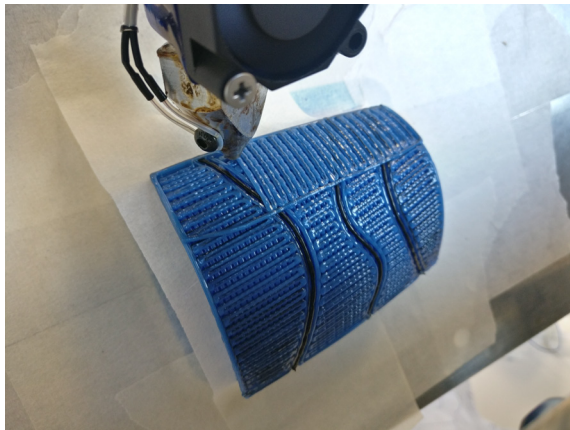
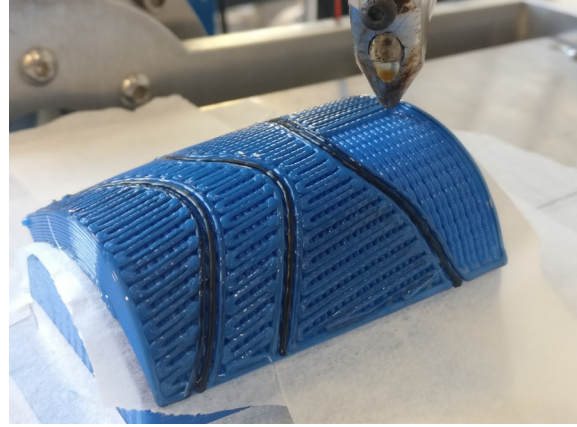
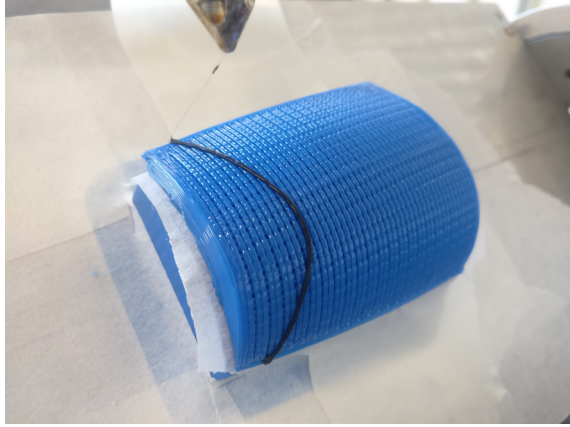
*Table A5: Images of manufacturing of Case\_Btop case study by multi-axis ME process*

*Case\_Bside*

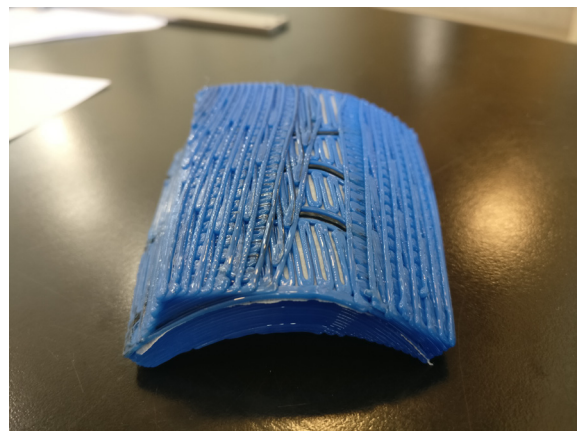


*Table A6: Images of manufacturing of Case\_Bside case study by multi-axis ME process*

*Case\_Bcon*

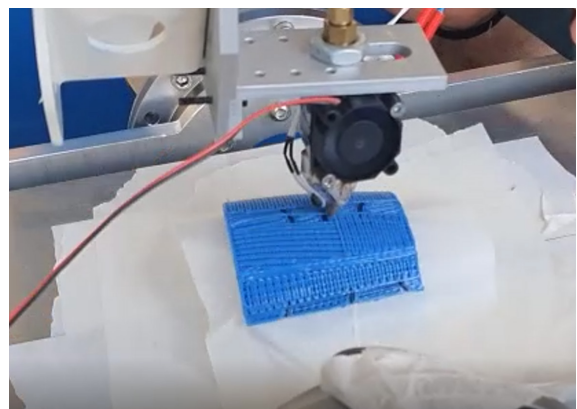
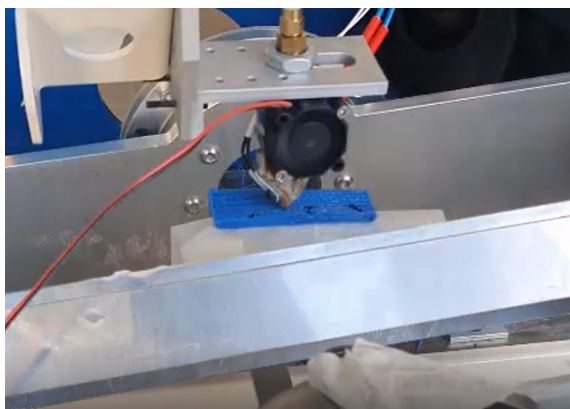
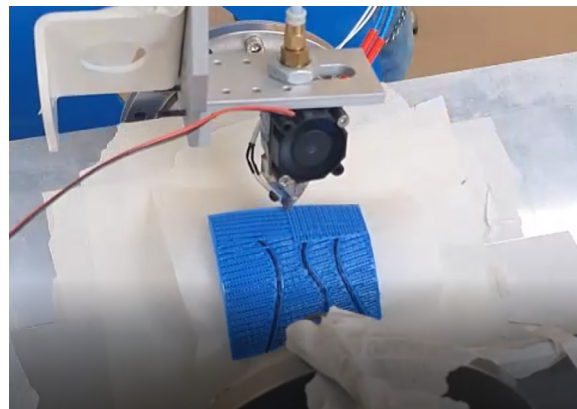
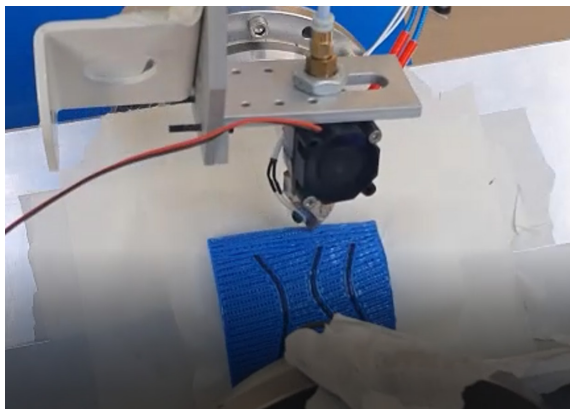
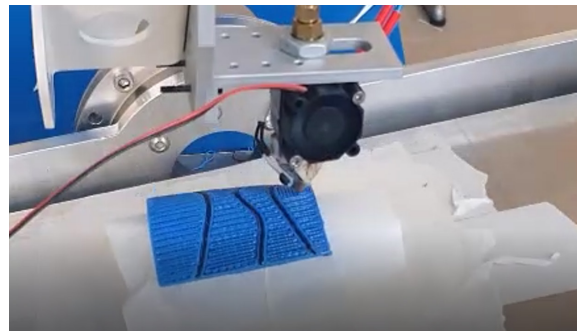
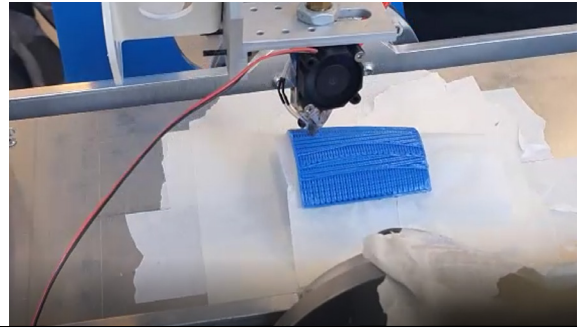
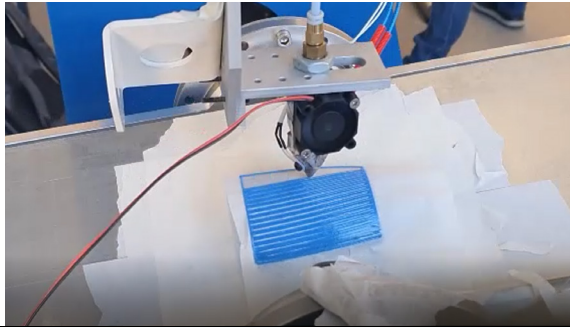


*Case\_Bcon – split model*



*Table A7: Images of manufacturing of Case\_Bcon case study by multi-axis ME process, both sample used for study and split model demonstrator presented in Figure 6.17.*

*Case\_Bx*



*Table A8: Images of manufacturing of Case\_Bx case study by multi-axis ME process*

## Appendix B: Complete data of resistivity measurements

Complete data regarding the resistivity measurements of conductive tracks required for the functionality analysis across all segments as reported in Figure 6.1 a) are supplied here below. Two distinct tables are provided for each of the materials used in the study.

Conductive material: <i>ProtoPasta</i>									
Total Height [mm]	Slicing Strategy	Data Type/Measure	Resistance between GND and Point X [kΩ] – Figure 6.1 a)						
			A - 129 [mm]	B - 261 [mm]	C - 393 [mm]	D - 525 [mm]	E - 657 [mm]	F - 789 [mm]	G - 921 [mm]
0.4	1 x 0.4	Average	18.60	37.25	56.12	75.04	93.91	112.71	131.54
		Average	24.24	47.99	72.53	97.12	121.27	145.39	169.92
	2 x 0.2	Res. Increase w.r.t 1x0.4	<b>30.34 %</b>	<b>28.83 %</b>	<b>29.24 %</b>	<b>29.42 %</b>	<b>29.14 %</b>	<b>29.00 %</b>	<b>29.18 %</b>
0.5	1 x 0.5	Average	14.55	29.10	43.63	58.36	72.92	87.51	102.30
		Average	18.18	36.19	54.42	72.78	91.04	109.21	127.45
	2 x 0.25	Res. Increase w.r.t 1x0.5	<b>24.90 %</b>	<b>24.35 %</b>	<b>24.72 %</b>	<b>24.72 %</b>	<b>24.86 %</b>	<b>24.80 %</b>	<b>24.59 %</b>
0.6	1 x 0.6	Average	12.54	24.98	37.51	50.08	62.61	75.19	87.91
		Average	14.83	29.68	44.71	59.70	74.68	89.63	104.80
	2 x 0.3	Res. Increase w.r.t 1x0.6	<b>18.23 %</b>	<b>18.84 %</b>	<b>19.21 %</b>	<b>19.20 %</b>	<b>19.27 %</b>	<b>19.21 %</b>	<b>19.21 %</b>
		Average	15.52	30.66	46.57	62.93	78.77	94.77	110.55
	3 x 0.2	Res. Increase w.r.t 1x0.6	<b>23.76 %</b>	<b>22.77 %</b>	<b>24.16 %</b>	<b>25.66 %</b>	<b>25.81 %</b>	<b>26.04 %</b>	<b>25.75 %</b>
Res. Increase w.r.t 2x0.3	<b>4.68 %</b>	<b>3.30 %</b>	<b>4.14 %</b>	<b>5.42 %</b>	<b>5.48 %</b>	<b>5.73 %</b>	<b>5.48 %</b>		
0.7	1 x 0.7	Average	10.46	20.79	31.12	41.55	51.97	62.31	72.86
		Average	11.77	23.48	35.24	47.09	58.84	70.55	82.56
	2 x 0.35	Res. Increase w.r.t 1x0.7	<b>12.59 %</b>	<b>12.96 %</b>	<b>13.26 %</b>	<b>13.35 %</b>	<b>13.23 %</b>	<b>13.21 %</b>	<b>13.31 %</b>
		Average	12.90	25.77	38.64	51.61	64.60	77.43	90.42
	3 x 0.233	Res. Increase w.r.t 1x0.7	<b>23.40 %</b>	<b>23.96 %</b>	<b>24.19 %</b>	<b>24.23 %</b>	<b>24.30 %</b>	<b>24.25 %</b>	<b>24.10 %</b>
Res. Increase w.r.t 2x0.35		<b>9.60 %</b>	<b>9.74 %</b>	<b>9.65 %</b>	<b>9.60 %</b>	<b>9.78 %</b>	<b>9.75 %</b>	<b>9.52 %</b>	
0.8	1 x 0.8	Average	9.11	18.24	27.39	36.55	45.72	54.87	64.15
		Average	9.86	19.68	29.47	39.35	49.27	59.12	69.00
	2 x 0.4	Res. Increase w.r.t 1x0.8	<b>8.27 %</b>	<b>7.91 %</b>	<b>7.62 %</b>	<b>7.68 %</b>	<b>7.77 %</b>	<b>7.75 %</b>	<b>7.57 %</b>
		Average	11.20	22.21	33.29	44.39	55.56	66.53	77.71
	3 x 0.267	Res. Increase w.r.t 1x0.8	<b>22.99 %</b>	<b>21.77 %</b>	<b>21.56 %</b>	<b>21.47 %</b>	<b>21.52 %</b>	<b>21.26 %</b>	<b>21.15 %</b>
Res. Increase w.r.t 2x0.4		<b>13.59 %</b>	<b>12.84 %</b>	<b>12.95 %</b>	<b>12.81 %</b>	<b>12.77 %</b>	<b>12.53 %</b>	<b>12.63 %</b>	

Table B1: Measurements data conducted on samples made by ProtoPasta conductive material



**Conductive material: *Alpha Ohm***

Total Height [mm]	Slicing Strategy	Data Type/Measure	Resistance between GND and Point X [kΩ] – Figure 6.1 a)						
			A - 129 [mm]	B - 261 [mm]	C - 393 [mm]	D - 525 [mm]	E - 657 [mm]	F - 789 [mm]	G - 921 [mm]
0.4	1 x 0.4	Average	9.21	18.43	27.62	36.86	46.14	55.37	64.73
		Average	16.19	32.45	49.05	65.67	82.63	100.13	116.70
	2 x 0.2	Res. Increase w.r.t 1x0.4	<b>75.79 %</b>	<b>76.02 %</b>	<b>77.62 %</b>	<b>78.19 %</b>	<b>79.09 %</b>	<b>80.85 %</b>	<b>80.28 %</b>
0.5	1 x 0.5	Average	6.46	13.00	19.46	25.92	33.73	39.01	45.80
		Average	9.96	19.67	29.52	39.00	48.78	58.26	67.62
	2 x 0.25	Res. Increase w.r.t 1x0.5	<b>54.05 %</b>	<b>51.32 %</b>	<b>51.71 %</b>	<b>50.48 %</b>	<b>44.62 %</b>	<b>49.34 %</b>	<b>47.62 %</b>
0.6	1 x 0.6	Average	5.49	10.98	16.53	21.98	27.44	32.93	38.39
		Average	7.43	14.85	21.94	29.07	36.26	43.22	50.21
	2 x 0.3	Res. Increase w.r.t 1x0.6	<b>35.36 %</b>	<b>35.26 %</b>	<b>32.76 %</b>	<b>32.26 %</b>	<b>32.15 %</b>	<b>31.25 %</b>	<b>30.79 %</b>
		Average	11.31	22.42	33.65	44.43	55.20	66.03	76.00
	3 x 0.2	Res. Increase w.r.t 1x0.6	<b>106.14 %</b>	<b>104.25 %</b>	<b>103.59 %</b>	<b>102.18 %</b>	<b>101.19 %</b>	<b>100.53 %</b>	<b>97.99 %</b>
		Res. Increase w.r.t 2x0.3	<b>52.29 %</b>	<b>51.01 %</b>	<b>53.36 %</b>	<b>52.87 %</b>	<b>52.25 %</b>	<b>52.78 %</b>	<b>51.37 %</b>
0.7	1 x 0.7	Average	4.20	8.33	12.42	16.52	20.66	24.75	28.81
		Average	5.71	11.38	16.99	22.57	28.08	33.66	39.23
	2 x 0.35	Res. Increase w.r.t 1x0.7	<b>35.98 %</b>	<b>36.63 %</b>	<b>36.80 %</b>	<b>29.47 %</b>	<b>35.91 %</b>	<b>36.01 %</b>	<b>36.16 %</b>
		Average	7.48	15.02	22.72	30.61	38.64	46.70	55.19
	3 x 0.233	Res. Increase w.r.t 1x0.7	<b>78.24 %</b>	<b>80.34 %</b>	<b>82.93 %</b>	<b>85.31 %</b>	<b>87.00 %</b>	<b>88.69 %</b>	<b>91.55 %</b>
Res. Increase w.r.t 2x0.35		<b>31.07 %</b>	<b>32.00 %</b>	<b>33.73 %</b>	<b>43.13 %</b>	<b>37.59 %</b>	<b>38.73 %</b>	<b>40.68 %</b>	
0.8	1 x 0.8	Average	3.76	7.55	11.33	15.09	18.91	22.71	26.53
		Average	4.63	9.28	13.94	18.63	23.29	28.05	32.71
	2 x 0.4	Res. Increase w.r.t 1x0.8	<b>23.16 %</b>	<b>22.97 %</b>	<b>23.10 %</b>	<b>23.45 %</b>	<b>23.17 %</b>	<b>23.50 %</b>	<b>23.27 %</b>
		Average	5.94	11.92	17.87	23.84	29.94	36.02	42.03
	3 x 0.267	Res. Increase w.r.t 1x0.8	<b>58.12 %</b>	<b>57.95 %</b>	<b>57.80 %</b>	<b>57.95 %</b>	<b>58.37 %</b>	<b>58.60 %</b>	<b>58.42 %</b>
Res. Increase w.r.t 2x0.4		<b>28.39 %</b>	<b>28.45 %</b>	<b>28.19 %</b>	<b>27.94 %</b>	<b>28.59 %</b>	<b>28.43 %</b>	<b>28.52 %</b>	

*Table B2: Measurements data conducted on samples made by AlphaOhm conductive material*

## Acknowledgements

---

There are a number of people who have supported me throughout this Doctoral Research in one way or another, and to whom I would like to express my sincere gratitude. First and foremost, I would like to thank my principle supervisor, Dr Marco Cavallaro for his continuous support, supervision and insight. His restless and creative mind will continue to be an inspiration for me for years to come. I would also like to thank my second supervisor Prof Karnik Tarverdi for revealing realms of material science previously unknown to me and guiding me through the experiments.

I am grateful to the College of Engineering, Design and Physical Sciences and the Department of Design in specific for supplying working space, facilities and materials that have enabled me to carry out this work. Particular gratitude towards Brunel University for awarding me a PhD Studentship which provided partial support for me to conduct this research.

I am thankful to the Institute of Intelligent Industrial Technologies and Systems for Advanced Manufacturing of the National Research Council of Italy, to Eng. Andrea Ballarino and Eng. Fabrizio Silva in specific, for letting me be a guest at their facilities, for allowing me to use their labs and equipment and making me feel welcomed.

Special thanks to all of my friends and fellow researchers with whom I shared ideas, workspace and many unforgettable experiences throughout my PhD journey, especially Tommaso, Giacomo and Rikesh.

As always, I am forever indebted to my fiancé Izabela, my parents Miroљub and Suzana, and my sister Biljana for their unconditioned love and support in all that I choose to do in my life. Thank you for being an inextinguishable source of motivation for me to keep moving forward.

Marko Chorbikj  
October, 2020